Final Report
to the
Office of Naval Research

BIOMECHANICS OF THE ACOUSTICO-LATERALIS SYSTEM IN FISH

[Navy Contract No. N00014-84-K-0164]

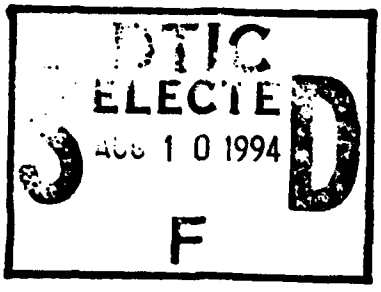

submitted by

Georgia Institute of Technology
College of Engineering

Principle Investigator

Peter H. Rogers
Neely Professor
George W. Woodruff
School of Mechanical Engineering

July 27, 1994

Table of Contents

List of Figures

List of Tables

List of Symbols

a_0 = nominal radius

c_c = critical damping constant

c_{eq} = equivalent damping constant for a 1 d.o.f. system

c_w = speed of sound in water

$d_{1,2}$ = distance between the centers of two bubbles

f_h = ultrasound frequency, Hz

$F(t)$ = forcing function

F_0 = magnitude of the forcing function

h_0 = thermal diffusivity of air at 1 atm

H = damping factor

I_{inc} = incident acoustic intensity

I_s = scattered acoustic intensity

k = acoustic wave number

k_{eq} = equivalent spring stiffness for a single degree of freedom system

l = distance between pressure measurement planes

m_{eq} = equivalent mass for a single degree of freedom system

m_f = mass of fish

p, p_{inc} = incident acoustic pressure

p_0 = ambient pressure

p_{xs} = excess internal pressure

Q = damping factor at resonance (quality factor)

r = range

s = surface tension

SNR = signal to noise ratio

t = time

v_{sb} = velocity of swim bladder surface

V_{sb} = total swim bladder volume

w = acoustic energy density

x = displacement

Greek

α_a = thermal diffusivity of air

γ = specific heat ratio (c_p/c_V)

ζ = damping ratio

η_{bf} = bulk viscosity

η_f = viscosity parameter

η_{sf} = shear viscosity

κ_a = thermal conductivity of air

Π_s = scattered acoustic power

μ_1 = real part of the complex shear modulus

μ_2 = imaginary part of the complex shear modulus

ξ = displacement

ξ_{inc} = incident acoustic particle displacement

ξ_{sb} = radial displacement of the swim bladder surface

ρ_f = density of fish

ρ_w = density of water

σ_s = scattering cross-section

ϕ = phase angle

ω = acoustic frequency, rad/sec

ω_0 = resonance frequency, rad/sec

Chapter 1

Introduction

The perception of auditory space is thought to be of greater biological significance than the ability to communicate by vocalization, since all vertebrates have adaptations for spatial hearing, whereas only a few have found the ability to vocalize (Fay, 1988b). Fay suggests that the primary function of the auditory system in most animals is to help form a three-dimensional image of the local environment. Perceiving objects in the environment involves separating their stimuli from the surroundings.

In order to survive, fish must be able to detect, classify, and localize relevant objects underwater in the presence of ambient noise (Rogers and Cox, 1987). These objects include aquatic animals that can be friend (conspecifics for schooling and mating) or foe (predators or prey). Rogers (1986) has presented a hypothesis that one fish could perceive nearby fish by recognizing the scattering of the ambient noise by the others' swim bladders. The swim bladder, acting like an air bubble, resonates in the ambient noise field, scattering significant amounts of acoustic energy. This characteristic scattered noise could allow for the detection and identification of the scatterer by the receiver.

In fish, a complex passive system has evolved for the detection of acoustic pressure and particle motion. Since the frequency range of best sensitivity for the fish occurs where ambient noise is high [Figure 1-1], it may be assumed that the fish is using ambient noise to its advantage.

Behavioral studies have shown that fish are able to discriminate differences in sound source location in three-dimensional space. It has been demonstrated in the cod (*gadus morhua*) that (1) a fish can be conditioned to discriminate between sound sources with a minimum audible angles ranging from 8 to 20 degrees in azimuth or elevation (Chapman and Johnstone, 1974; Hawkins and Sand, 1977), (2) the otolithic organs of the ear are probably responsible for this behavior, (3) fishes are capable of sound source discrimination (Schuijf and Hawkins, 1983), and (4) they can solve back-front and left-right (180 degree) ambiguity (Schuijf and Buwalda, 1980; Popper and Fay, 1984).

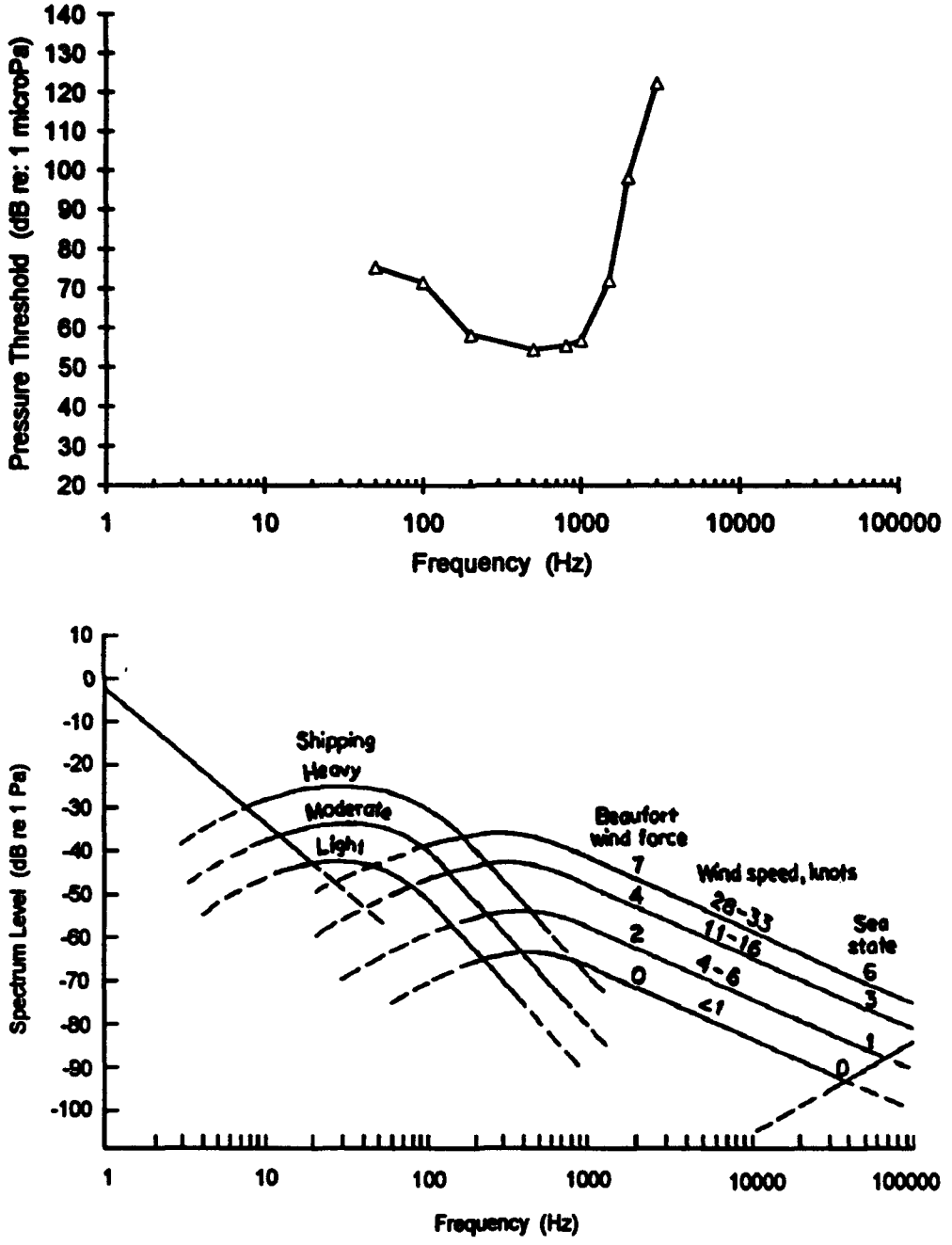

Figure 1-1. Sound pressure audiogram for the goldfish (top) and average deep water noise spectra characterized by sea state (Knudsen curves) and shipping density (bottom). Audiogram is from Jacobs and Tavolga (1967). Noise spectra are from Urick (1967).

Solution to the 180 degree ambiguity demonstrates the ability of the fish ear to use both acoustic pressure and particle motion information.

Noise ultimately determines the detectability of any signal to which fish responds (Fay, 1974). In a noisy environment, signal detection becomes a complex discrimination problem. Decreased sensitivity below ambient noise levels are not as crucial to signal detection as are mechanisms for complex processing and analysis of the signals received.

Behavioral and electrophysiological research has demonstrated and quantified some of the complex auditory processing ability of goldfish (*Carassius auratus*), including absolute detection thresholds, frequency discrimination, intensity discrimination, directional discrimination, temporal summation, complex spectral discrimination, temporal discrimination resolution, and auditory filter functions (see Hawkins, 1981). This research indicates that the capacity for auditory information processing, the detection of signals in noise, and the simultaneous and successive analysis of frequency by the fish auditory system do not differ significantly from those of the mammalian systems (Fay, 1978). Therefore, some of the mechanisms responsible for the analysis may be the same in fishes and mammals even though the form of their ears are completely different. More is known about the function of the complex and specialized structure of the cochlea that about the relatively simple acoustic receptor in fish (Tavolga, 1974).

Acoustic identification of conspecifics has been demonstrated in one species of vocalizing fish, which shows habituation to the presence and activities of neighbors within its territorial boundaries. Males of the bicolor damselfish (*Pomacentrus partitus*) were able to recognize individuals solely through identification of the characteristics of their neighbors' vocal sounds (Myrberg and Riggio, 1985). Proper sound source direction was also found to be important in recognition, indicating the ability to spatially map acoustic information. The question remains whether any non-vocalizing fish can detect others through acoustic means.

The purpose of this research was to determine the capacity of a fish to detect the scattering of ambient noise by another fish from the other's resonant swim bladder. The first task was to measure the characteristics of the acoustic signal scattered by the swim bladder of a fish. Next, the typical scattered signal was synthesized in the laboratory

aquarium. The last task involved determining the ability of a fish to detect this scattered ambient noise signal.

Although not conclusive, the results of this research may help shed light on the biological relevance of hearing in fish. The more an animal knows about its environment, the better are its chances for biological success (Kamil, 1988). This research will only verify the ability of a fish to *sense* another through scattered ambient noise. The fish *knows* other fish are around if, after sensing, it is able to change its behavior upon identification by exhibiting the proper response (fleeing from predators, for example). If fish know more about their surroundings through input from their auditory system, then hearing is biologically relevant.

The results of this research may also prove useful to others who need to detect, identify, and localize relevant objects in the undersea environment. The fish's ability to extract acoustic information in the presence of ambient noise using its tiny sensors is unrivaled. Equally impressive may be their prowess in finding resonant structures underwater.

Chapter 2

The Sense of Hearing in Fish

The underwater environment includes a complex composition of fluid motions and pressure perturbations, only a few of which result from the propagation of sound waves. Fish, evolving underwater, have specialized receptor organs to detect water motion and pressure disturbances. There are, however, no clear lines separating the detection of acoustic particle motion and acoustic pressure from the other mechanical disturbances and there is no definite delineation of which organs are responsive to which stimuli.

Sound detection in fishes is thought to involve both the inner ear and the lateral line. The lateral line detects the spatial and temporal patterns of relative motion between the water environment and the surface of the fish (Platt *et al.*, 1989). Its bandwidth spans from below 1 Hz to above 250 Hz (Popper, 1983). The lateral line is responsive to pure hydrodynamic water motions as well as those caused by a true sound source. However, since its threshold for motion detection is much higher than the inner ear's, the lateral line's contribution to hearing is thought to be relatively unimportant and was ignored for this research.

The first question for researchers to answer was whether or not fish could hear. Bigelow (1904) was the first to show that goldfish respond in a definite manner to sound vibrations in water, disputing an earlier assertion that the fish could not hear. In his experiments, Bigelow observed the response of normal goldfish to sound in an aquarium. Then he surgically severed the fifth and seventh nerves, the lateral line nerves and the spinal cord close to the medulla, effectively desensitizing the skin and the lateral line. These fishes responded to sound the same as normal fish. In other fishes, only the eighth nerve (leading to the ear) was cut, and they didn't respond to sound at all. Therefore, he concluded that goldfish could hear and that the inner ear was probably responsible.

The Fish Ear

Among the more than 20,000 species of fish, there is considerable structural and functional diversity in the inner ear and its peripheral accessories (Platt and Popper, 1981;

Popper, 1983). Although there is no typical fish ear, a few basic morphological and ultra structural patterns repeat in diverse fish groups (Popper and Coombs, 1982). The superorder Otophysi (= ostariophysi in previous literature), for example are distinguished by their specialized auditory structure, the Weberian ossicles [Figure 2-1]. The ossicles are a linkage of bones mechanically coupling the swim bladder to the fluid system of the inner ear. Nonotophysans may or may not have other special connections between the swim bladder and the ear.

The fish ear serves many purposes. The inner ear has evolved to function in controlling posture, locomotion, and eye stabilization as well as in the detection, analysis, and localization of underwater sounds (Platt *et al.*, 1989). The otolith end organs of the inner ear respond to static tilt and to vibrations and sound from 0.1 to more than 5000 Hz in some fish species (see Popper and Fay, 1984; Sand and Karlsen, 1986). The swim bladder also has various functions in different fish. It can serve in respiration, in the provision of buoyancy in the detection of pressure changes, including sounds, and in sound production (Alexander, 1966).

The fish ear is a paired membranous system of contiguous fluid filled ducts and sacs consisting of two parts, the *pars superior* and the *pars inferior* [Figure 2-2]. The *pars superior* consists of the utricle, the semicircular canals and their associated ampullary regions, and the macula neglecta. In most species the *pars superior* is thought to only be involved with the detection of gravity and linear and angular acceleration (Lowenstein, 1971). An exception to this occurs in the clupeids where the utricle was shown to be the major hearing organ (Blaxter *et al.*, 1981).

The *pars inferior* consists of the other two otolithic organs, the saccula and the lagena. There is considerable interspecific variability in the general shapes of the two organs, the interconnections between the saccula and lagena, and the size and shape of the otoliths (Fay and Popper, 1980). Each otolith is a calcium carbonate stone that is three times as dense as water. The saccular otoliths have complex and distinct species-specific shapes, while the lagenar otoliths are more simply and commonly shaped (Popper, 1977). The functions of the individual organs are determined by their connections to the peripheral auditory structures, the physical characteristics, shape, and location of the otolith and sensory epithelia, hair cell orientation patterns, and ciliary bundle length (Schellart and Popper, 1992).

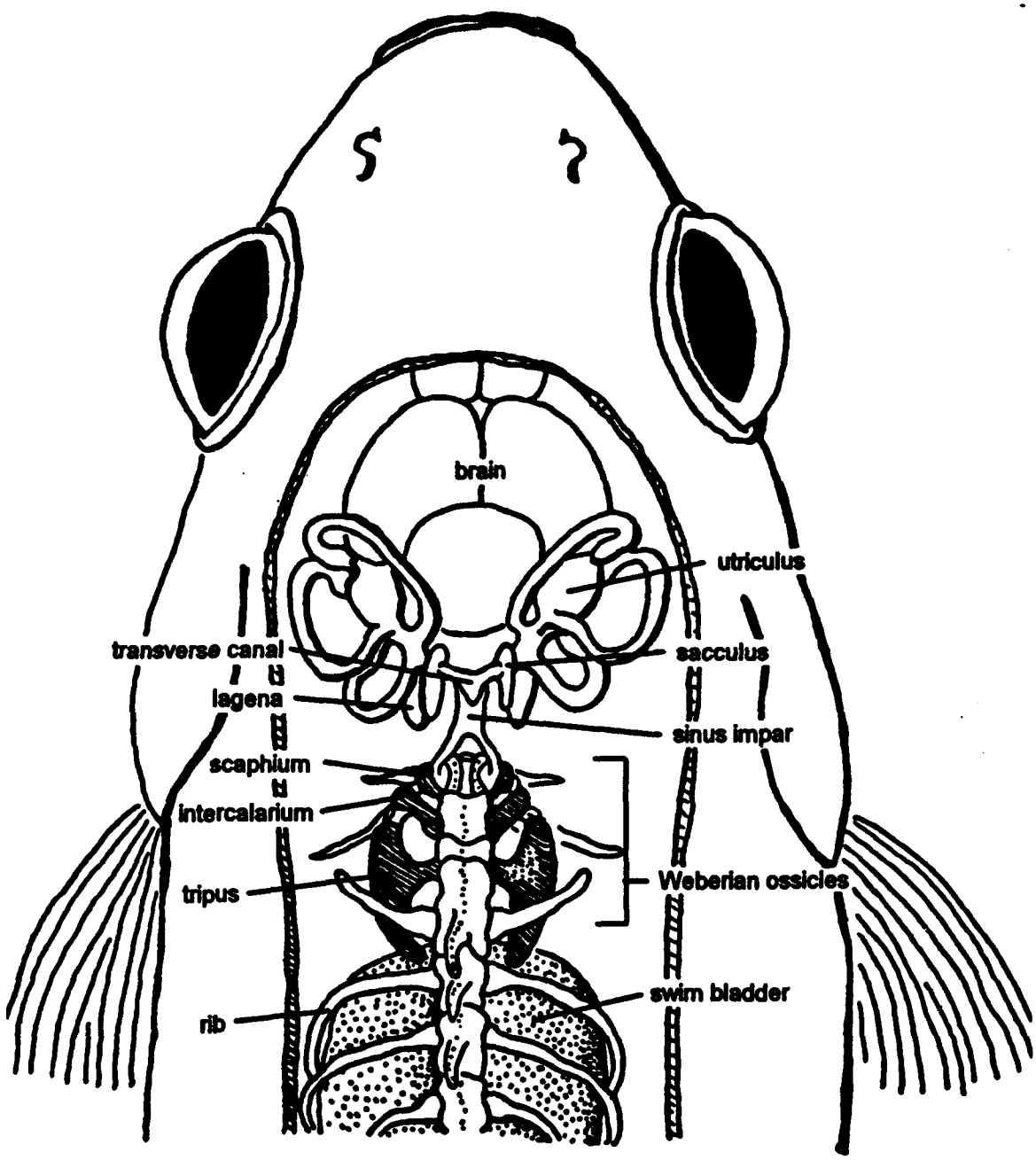

Figure 2-1. The layout of the swim bladder, Weberian ossicles, and the inner ear in an otophysan fish. (From Popper and Coombs, 1980.)

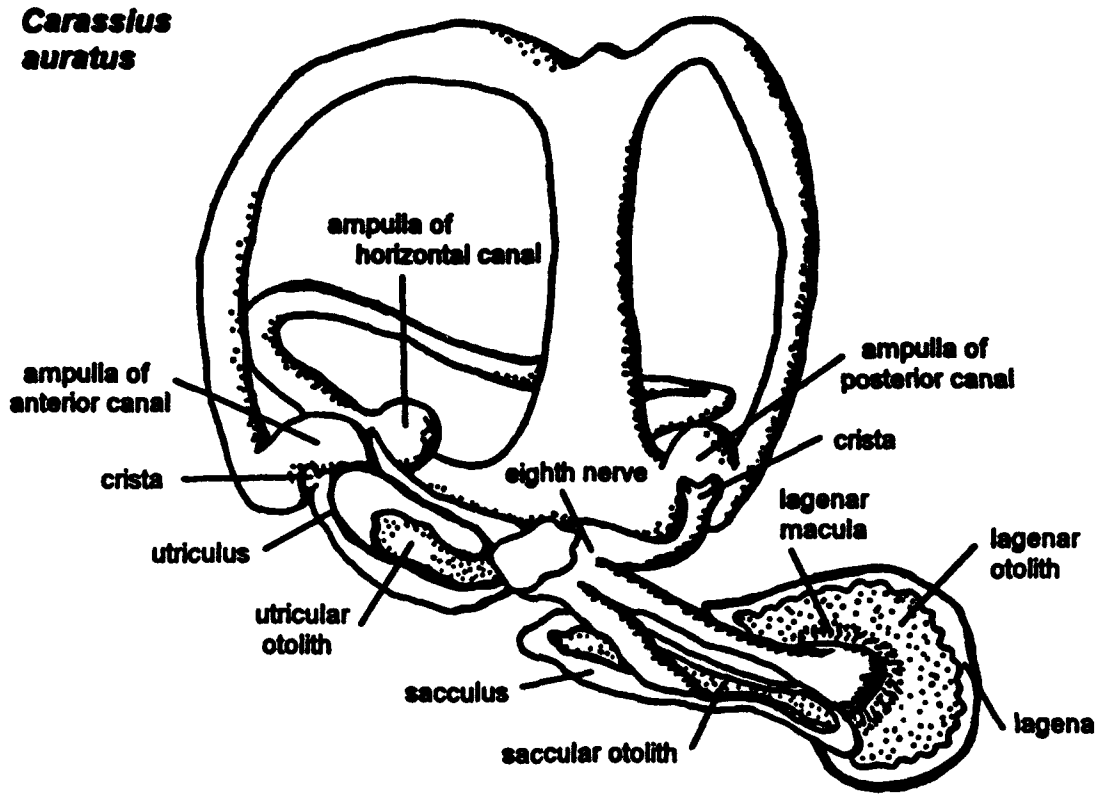

Figure 2-2. The inner ear of the goldfish. (From Popper and Coombs, 1980.)

The sensory epithelium of the otolithic organs, the macula, is overlaid with sensory and supporting cells. Some parts of the macula may be covered by the otolith within a gelatinous membrane, while other parts may be covered by only the membrane (Platt, 1977). The membrane is thought to act as an elastic coupling between the otolith and the sensory cells on the macula (Rogers and Cox, 1988).

The basic receptor element on the macula of the inner ear is the mechanosensory hair cell (Platt, 1983). Extending into the membrane from the surface of each hair cell is a bundle of microscopic hair-like processes. This bundle contains 20 to 80 processes called stereocilia and one true cilium, the kinocilium [Figure 2-3]. The adequate stimulus for response from individual hair cells is related to the bending of the cilia and is highly directional. Bending of the cilia triggers changes in the polarization of the cell: toward the kinocilium causes maximum depolarization, away causes hyperpolarization, and

Figure 2-3. Scanning electron micrograph of the apical surface of the lagenar macula from the goldfish. The K points to the kinocilium of an individual hair cell and the S to the stereocilia. The open arrows point in the direction of orientation for some hair cells. (From Popper *et al.*, 1988.)

orthogonal to this axis yields no response [Figure 2-4]. Bending off axis results in a cosine function response (Flock, 1971). This directional response results in changes in spike activity in the connecting afferent nerve fibers.

Hair cell orientation maps of the otolithic organs of the goldfish show that the macula has two oppositely oriented cell groups that can be separated by an unbroken line, as shown in Figure 2-5 (Platt, 1977). Typically, the hair cells in nonotophysan saccule macula are divided into four orientation groups (Popper and Coombs, 1982; Saidel and Popper, 1983). The anterior region of the macula has two horizontally opposed groups, one directed anterior and one posterior. The other two groups on the posterior region are oriented vertically, opposed dorsal and ventral. Other similarly structured patterns exist in other species of fish (Popper *et al.*, 1982).

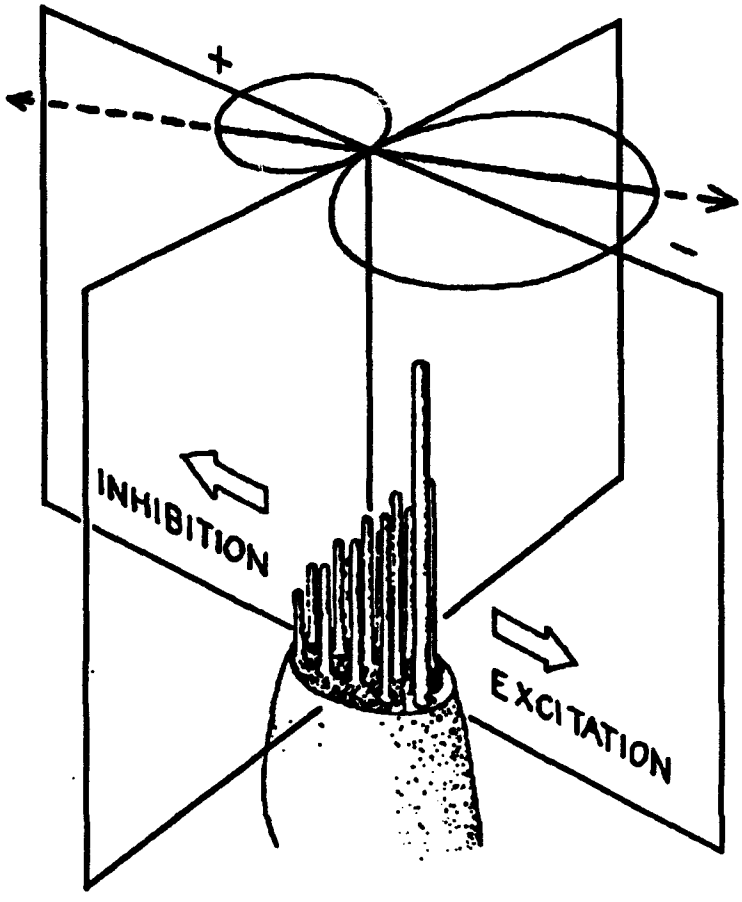

Figure 2-4. The directional sensitivity of the individual hair cell. The kinocilium is the longest of the cilia. (From Flock, 1971.)

Similar regionalization is shown in the innervation of the saccular sensory epithelium by the eighth nerve (Saidel and Popper, 1983). The posterior saccular branch innervates the mid-region and the caudal end of the macula where the vertically oriented hair cells are located. The anterior saccular branch innervates the rostral region where the horizontally opposed hair cells lie. Each branch of the eighth nerve divides many times before it reaches the epithelial region. Individual axons terminate on several hair cells.

Sound is detected in most fish by the inner ear; but other peripheral structures may respond to sound and transfer acoustic energy to the ear. Von Frisch (1938) was the first to point out that the swim bladder in many fish could function as an accessory hearing

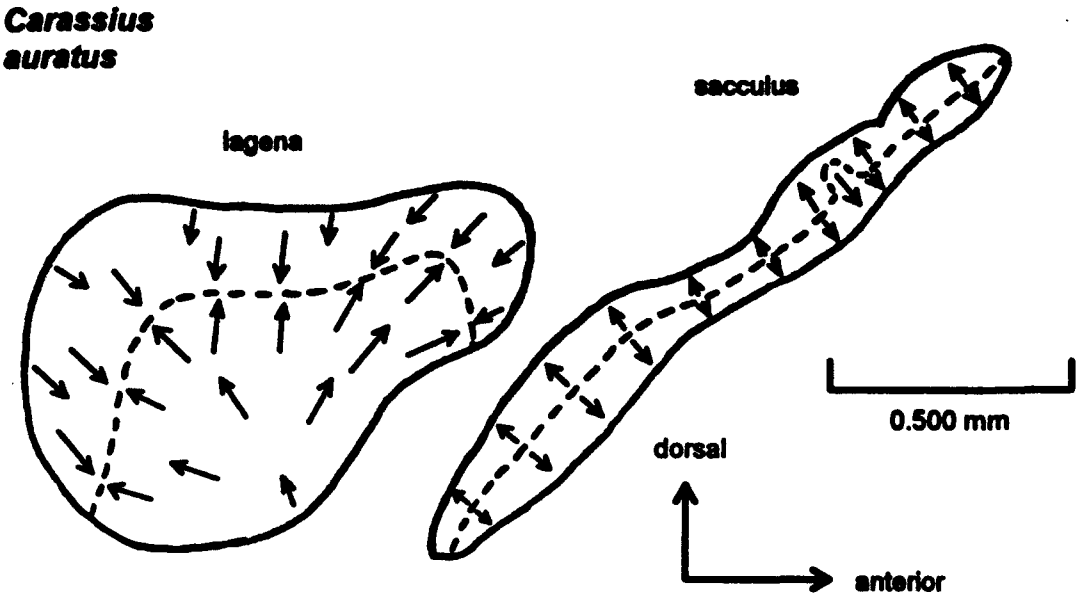

Figure 2-5. Orientation patterns of the hair cells on the lagena and the sacculus of the goldfish. Although shown in two dimensions, the macula are actually curved. The arrows indicate the direction of orientation of the kinocilium. (From Platt, 1977.)

organ, scattering incident sound energy, producing locally higher acoustic particle motions.

The Swim Bladder

The swim bladders of fish can be classified as one or the other of two main types; the open or physostomatous, which opens into the foregut through a pneumatic duct, and the closed or physoclistous, in which the pneumatic duct does not function or exist (Jones and Marshall, 1953). The pneumatic duct is typically a long, thick-walled tube with a narrow lumen, connecting the swim bladder to the dorsal or lateral wall of the esophagus.

In the physostomatous groups the swim bladder is single-chambered except in the Chanidae and the Otophysi. In the goldfish, the swim bladder consists of anterior and posterior chambers connected by a narrow neck, the ductus communicans (Alexander,

1966). Physoclistous fish usually have a single-chambered swim bladder, although in some the swim bladder may be divided by a constriction or a diaphragm with a central aperture (Jones and Marshall, 1953). The oscar is physoclistous with a single-chambered swim bladder.

Typically, the swim bladder wall is in two layers; the tunica externa and the tunica interna. The outer layer (tunica externa) is formed from an outer capillary network which overlies connective tissue consisting of a tough outer laminated section of collagenous fibers and elastic fibers, which merges into an inner, thicker section of fine collagenous fibers (Jones and Marshall, 1953). The inner layer (tunica interna) consists of smooth muscle fibers and an inner lining of pavement epithelium. Separating the two layers is a network of oily connective tissue, allowing the layers to slide freely over one another (Alexander, 1966). In the cyprinids (goldfish), only the anterior chamber is constructed with two layers. The tunica interna is whole while the tunica externa has a longitudinal slit in it.

In the cyprinids, smooth muscle cells form two lateral bands in the walls of the posterior chamber, and a single band in the floor of the anterior chamber continues upward to the roof posterior (Jones and Marshall, 1953). Each chamber has a well defined sphincter of smooth muscles close to the duct which joins them together. The function of the bands of smooth muscles is thought to maintain a sufficient excess internal pressure within the swim bladder to allow proper working of the Weberian ossicles (Jones and Marshall, 1953).

The volume of the swim bladder is adjusted by the addition or removal of gas. In physostomes, the excess gas can be released quickly through the pneumatic duct by a process called 'Gasspuckreflex' (Alexander, 1959c). In physoclists, gas escapes by diffusion across the oval, a modified region of the posterior end of the swim bladder wall (Jones and Marshall, 1953). Physostomes can replace gas through the pneumatic duct by swallowing air at the surface. Physoclists, and some physostomes, are able to secrete gas into the swim bladder. As a general rule, the anterior part of the bladder wall is specialized for gas secretion and the posterior half for gas diffusion. In physostomes with chambered swim bladders, however, gas transfer is confined to the posterior chamber. The pneumatic duct connects to the antero-ventral wall of the posterior chamber in these fish.

Weberian Ossicles

Dijkgraaf (1960) considered the Otophysi (the goldfish, catfish, minnows, and relatives) sound specialists due to the presence of their Weberian ossicles. The Weberian ossicles (tripus, intercalarium, and scaphium) are derived from the anterior vertebrae (Alexander, 1966). The tripus is the most posterior, attaching to the tunica externa at the edge of the slit. Next is the intercalarium and then the scaphium, all connected by a series of ligaments. When the swim bladder expands during the rarefaction phase of an acoustic wave (negative acoustic pressure), the tunica interna stretches, but the tunica externa does not, because of the slit. The edges of the split move apart and the ossicles rotate forward due to the tension in the connections from the ossicles to the vertebrae (Popper, 1971b). This action is illustrated in Figure 2-6. As the swim bladder contracts, the ossicles rotate back as the edges of the slit are moved together by the elastic recoil of ligaments which connect the tripodes to processes of the fourth vertebra.

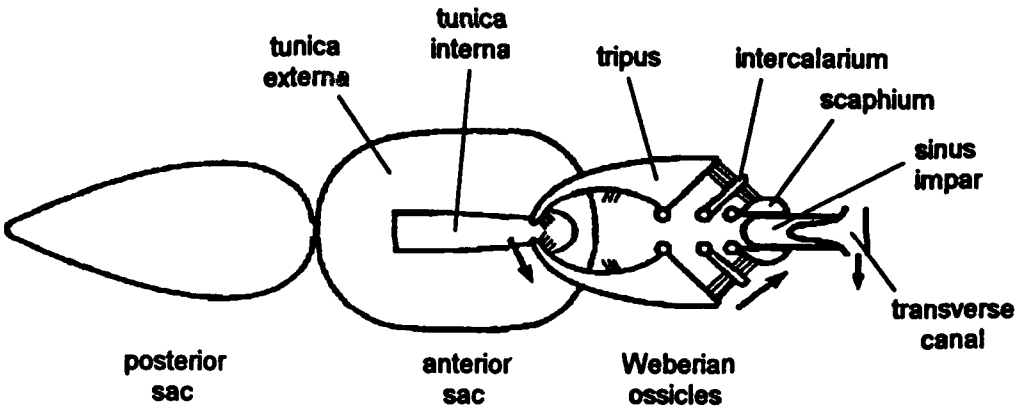

Figure 2-6. Diagram showing the function of the swim bladder and Weberian ossicles of the goldfish. Arrows indicate the direction of motion due to the rarefaction phase of an acoustic wave. (From Alexander, 1966.)

The scaphia are incorporated in the walls of the central fluid-filled cavity, the sinus impar (Alexander, 1966). The sacculi of the two ears are connected by a transverse canal. A posterior diverticulum of this canal, the sinus endolymphaticus, projects into the cavity of the sinus impar. It has a very thin wall. When the ossicles move forward, the scaphia

press on the sinus impar, driving the fluid in it forward, compressing the sinus endolymphaticus and displacing fluid from it into the sacculi. This is possible because there is a flexible region in the saccular wall. The saccular otoliths bear wing-like projections which lie in the path of the endolymph movements caused by the Weberian ossicles. Therefore, motion of the ossicles due to the passage of sound waves causes movements of the saccular otoliths and thus stimulates the saccular hair cells.

In general, species in which the swim bladder and the inner ear are closely coupled seem to perform 'better' than other species without such coupling in a number of auditory tasks, including simple sound detection and more complicated tasks related to frequency analysis. While some of these capacities are related to the pressure-transduction properties of the air filled swim bladder, others may not be (see Coombs and Popper, 1982).

Acoustic Stimulation

The passage of an acoustic wave can be characterized by a change in state variable (pressure, density, temperature) or a motion variable (displacement, velocity, acceleration) and can be completely described by the field of any one (Rogers and Cox, 1988). These variables are coupled by conservation of mass, momentum, and energy and an equation of state for the medium involved. The detection of at least one of these variables through either direct or indirect methods allows a fish to hear. It is now believed that the otoiithic organs respond directly to the particle motion associated with sound waves and that many fish with swim bladders or other air filled structures can indirectly sense the pressure fluctuations. The Weberian ossicles are thought to improve the coupling of the swim bladder to the inner ear, improving the sensitivity to acoustic pressure.

Fay and Popper (1974) calculated that for the goldfish the particle displacement at behavioral threshold is between 2 and 50 Angstroms. They determined that for 'natural' situations, the fish would respond to sound pressure impinging upon the swim bladder before the particle motion vibrating the head. Without the swim bladder, however, the only functional mechanism for stimulation is particle motion.

For the goldfish, it seems that information about the axis of particle motion is better represented in the profile of most active fibers within the lagena rather than in the

saccule or utricle (Fay, 1988b). The distribution of stimulus direction for best neural response in the saccule correlates well with the axis of the scattered pressure wave from the swim bladder. By recording microphonic potentials, Sand (1974) also demonstrated this in a nonotophysine, the perch (*Perca fluviatilis*).

Van Bergeijk (1967) referred to the swim bladder as a secondary source of sound, radiating its own pressure and displacement fields when subjected to sound pressure. The resonant swim bladder amplifies the particle motion in the nearfield of the scattered sound around its resonance frequency.

To examine the relationship of the pressure stimulus to the velocity stimulus, Buwalda and van der Steen (1979) performed experiments on cod using four opposing underwater sound projectors in a cylindrical tank. By manipulating the direction of the particle motion in the horizontal and vertical planes and the ratio of the pressure to velocity, they demonstrated that at a low p/v ratio (high velocity), the sensitivity of the anterior part of the saccular macula was similar to the results from Sand (1974), but at higher ratios, the response was omnidirectional. These results indicate the ability of the pressure signal to overwhelm the directional velocity signal.

Poggendorf (1952) found that the threshold sound pressure of the otophysan bullhead (*Ictalurus nebulosus*) increased by 30 to 40 dB after removal of the tripus of the Weberian ossicles, although the shape of the auditory curve remained the same. He concluded that the amplitude of vibration in the labyrinth constituted the adequate stimulus for the sensory cells of the saccula and lagena. This vibration was due to the swim bladder, so that the shape of the threshold curve depends on the resonance characteristics of the swim bladder.

Many species of fish have shown the ability to discriminate frequencies (Hawkins, 1981), although no mechanism for frequency discrimination is obvious in the form of the ear. Fay and Ream (1985) found that individual saccular nerve fibers of the goldfish can be grouped into four categories based on tuning and best frequency; (1) untuned, (2) low frequency (<120 to 290 Hz), (3) mid-frequency (330 to 670 Hz), (4) high frequency (790 to 1770 Hz). The frequency selectivity of these fibers act as bandwidth filters reducing broadband noise to lower detection thresholds for narrow band signals. The dynamic

range for best sensitivity of separate saccular fibers is over 55 dB within individual goldfish.

An interesting model of the processing of the acoustic signals in fish has been presented (Popper *et al.*, 1988; Rogers *et al.*, 1988). Their hypothesis assumes that the response of the saccule and the lagena to direct and indirect acoustic motion can be decomposed into the directional information on the direct particle motion and pressure information [Figure 2-7]. This signal processing is thought to occur in the wiring of the eighth nerve fibers to the hair cells.

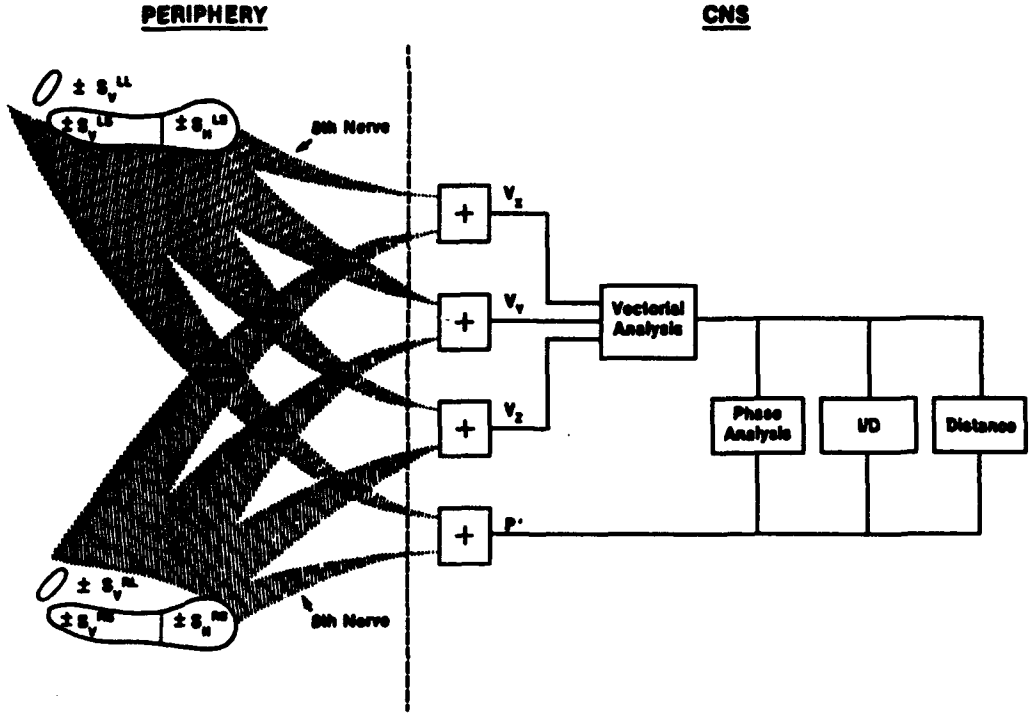

Figure 2-7. Theoretical model for auditory processing in fishes. Input is from the two saccules (LS and RS) and lagenae (LL and RL) via the eighth nerve. Vectorial analysis is determined from v_x, v_y, and v_z. Phase analysis, frequency discrimination, and distance determination are performed using pressure input as well. (From Rogers *et al.*, 1988.)

Swim Bladder Resonance

Most of the previous work on the scattering of sound by the swim bladder has been concerned with the measurement of acoustic target strength for the estimation of quantity, size, and species of fish by commercial fishermen and marine biologists using sonar or echo-sounders. Others have made direct measurements of the motion of the swim bladder due to sound waves to study its effect on a fish's own hearing. As a damped air bubble, the swim bladder resonates at a characteristic frequency and bandwidth based on its size, shape, and the characteristics of the surrounding tissue.

Experimental studies on the scattering by the swim bladder in fishes include the work of McCartney and Stubbs (1971), Sand and Hawkins (1973), and Lovik and Hovem (1979), who used ring hydrophones to measure the resonant behavior of the swim bladder for various species and sizes of fish. In all of those experiments, it was shown that the resonance frequency and the broadness of the resonance curve (as characterized by Q, the quality factor) were significantly different than those of a similarly sized air bubble in water; the resonance frequency of the swim bladder was higher and the Q lower. The majority of the scattered sound by intact fish was attributed to only the anterior portion of the swim bladder since the wall of the posterior sac is very much less extensible than that on the anterior sac (Alexander, 1959a).

Using a photocell, Poggendorf (1952) directly measured the oscillations from the anterior swim bladder of a minnow (*Phoxinus laevis*) that had been dissected out from the body. These excised swim bladders were found to have resonant frequencies coincident with those of similarly sized air bubbles with only a slight increase in damping.

By leaving the swim bladder in an anesthetized fish, Tavolga (1964) reported finding much higher damping using a contact microphone but cited only minimal data. Popper (1974) measured the response of the swim bladder by inserting a 0.5 mm probe coupled to a microphone into the anterior chamber of a dead goldfish. Results showed that the response of the swim bladder was flat from 50 to 2000 Hz, indicating extremely high damping. Both of these results were compromised due to the addition of the transducer to the swim bladder.

Cox and Rogers (1986, 1987) developed a technique to measure *in vivo* the motion of the swim bladder noninvasively using ultrasound. A comparison of *in vivo* and *post mortem* frequency response curves from early results showed the necessity of working with live subjects.

Masking

The underwater environment is characterized by levels of natural and man-made noise. Any signal to be detected underwater will be masked by this ambient noise, raising its threshold of audibility. Determining the physical parameters that affect masking may explain functional aspects of the fish ear.

Using classical heart rate conditioning, Buerkle (1968) measured the pure tone threshold of the cod to a background noise field of an octave band of noise centered around the test frequency. Up to 283 Hz, the signal-to-noise thresholds were constant (around 20 dB) at different background noise levels and different frequencies. Later (Buerkle, 1969), noise maskers centered around frequencies above and below the signal frequency were shown to be less effective than maskers of the same intensity at the signal frequency. This indicated the existence of auditory filters in the hearing of the cod. Similar results were later obtained for other species of fish: the goldfish (Fay, 1974; Tavolga, 1974), the pin fish, *Lagondon rhomboides* (Tavolga, 1974), the African mouth breeding cichlid, *Tilapia macrocephala* (Tavolga, 1974), and the blue-striped grunt, *Haemulon sciurus* (Tavolga, 1967).

Masked tone detection is determined by the characteristics of auditory filters centered on the signal frequency. Bandwidths for the goldfish are significantly wider than those determined for man (Fay, Yost, and Coombs, 1983).

Masking is a linear function of masker level, and grows approximately 3 dB per octave with signal frequency. The value of the S/Ns at threshold (or the critical masking ratio, CR) is thought to be determined in part by the bandwidths of hypothetical filters used in signal detection. In estimating these bandwidths from CR values, two assumptions are usually made: (1) a rectangular band of noise centered on the tone frequency is responsible for the masking, and (2) the power of the noise in the effective band is equal to the power of the signal at masked threshold (Fay and Coombs, 1983).

The level of masking changes when signal and masker come from different directions (Chapman and Johnstone, 1974; Popper, 1983). For angular separations between tone and noise sources greater than 10 degrees, there was a significant decrease in the mean signal-to-noise ratio of about 7 dB. The same masking level differences were obtained for all angles between 45 and 180 degrees. This is an example of the cocktail party effect in fish, showing its ability to use directional information to differentiate signals from noise when the source of the signal is spatially separated from the source of the noise (Fay, 1988b).

Chapter 3

Swim Bladder Resonance

The first task of this thesis was to determine how the swim bladder responds to the ambient noise field. As a first approximation, the swim bladder was thought to scatter sound like a resonant air bubble. Since the wavelength of sound in the hearing range of a fish is much greater than any characteristic length of the swim bladder, the swim bladder responds to the oscillations of acoustic pressure by uniform volume contraction and expansion, scattering sound in all directions. By measuring the radial displacement of the swim bladder, the scattered sound field can be determined.

The swim bladder's displacement was measured directly using the NIVAMS (Non-Invasive Vibration Amplitude Measurement System). This system was developed to measure the motion of the internal organs of the peripheral auditory system in goldfish (Cox and Rogers, 1986, 1987; Cox, 1987).

NIVAMS transmits low power continuous wave ultrasound to probe *in vivo* the body of a fish. The gas-filled swim bladder, having a much lower specific acoustic impedance than the surrounding watery fish tissue, reflects the ultrasound. Since this reflecting surface is moving in response to low frequency sound stimulus, the length of the path that is traveled varies sinusoidally and the reflected ultrasound is phase modulated. The frequency spectrum of the reflected ultrasound consists of the original transmitted frequency plus sidebands at the sum and difference of the ultrasound and the low frequency stimulus. The energy from the carrier is shifted to the sidebands. After measuring the relative amplitude of these sidebands to the carrier, the radial displacement of the reflecting surface can be calculated (Cox and Rogers, 1987).

This system was used to measure the swim bladder response of goldfish and oscars. The data from this experiment was then generalized and compared to the resonant ideal air bubble model and to the swim bladder models of Andreeva (1964) and Love (1978). Next, the effect of the coupling between the two chambers of the goldfish's swim bladder was examined using the models of Shima (1971) and Zabolotskaya (1984).

Experimental Method - NIVAMS

Initial experiments were performed using the equipment set-up and procedure as described in Chapter IV of Cox, 1987. Modifications were later made that increased the reliability of the measurements. Details of the final set-up are given here.

NIVAMS consists of three subsystems (ultrasonic measurement, target positioning, and low frequency stimulus) linked by computer control. A General Purpose Interface Bus connects the system instruments to an IBM-PC running BASICA programs. The final equipment configuration for NIVAMS is shown in Figure 3-1 and described here.

The Hewlett-Packard 3585A spectrum analyzer generates a spectrally pure 10 MHz signal which was used as the high frequency source for the ultrasonic measurement system. This signal was reduced by 20 dB using a Wavetek A151 RF attenuator before being amplified by 50 dB with an EIN 325LA RF power amplifier, yielding approximately 32 V rms. Identical Panametrics Videoscan immersion transducers (model V373) were used for both the ultrasound transmitter and receiver. These transducers (0.64 cm diameter element and 3.18 cm nominal focal length) were set up in the test tank as described in Cox (1987) with their focal regions aligned to the same point in space.

The output of the ultrasonic receiver was connected directly into the 1 M Ohm input of the spectrum analyzer. The computer collected data from the spectrum analyzer by recording the amplitudes of the carrier, $v_{carrier}$, and sidebands, $v_{sideband}$. The amplitude of displacement of the target, ξ_t, could be calculated directly from this data as

$$\xi_t = \left(\frac{v_{sideband}}{v_{carrier}}\right)\frac{c_w}{2\pi f_h} \qquad (3\text{-}1)$$

where the first term is the relative amplitude, c_w is the speed of sound in water, and f_h is the ultrasound frequency, 10 MHz (Cox and Rogers, 1987). With the nominal 80 dB dynamic range of the spectrum analyzer, the minimum detectable displacement was on the order of 24 Angstroms. Cox (1987) and the early experiments for this thesis used 20 MHz ultrasound. This was changed for three reasons. First, the Wavetek 178 used as the high frequency source became unreliable. Second, the added spatial resolution at the higher frequency was actually a hindrance, as the larger focal region using 10 MHz

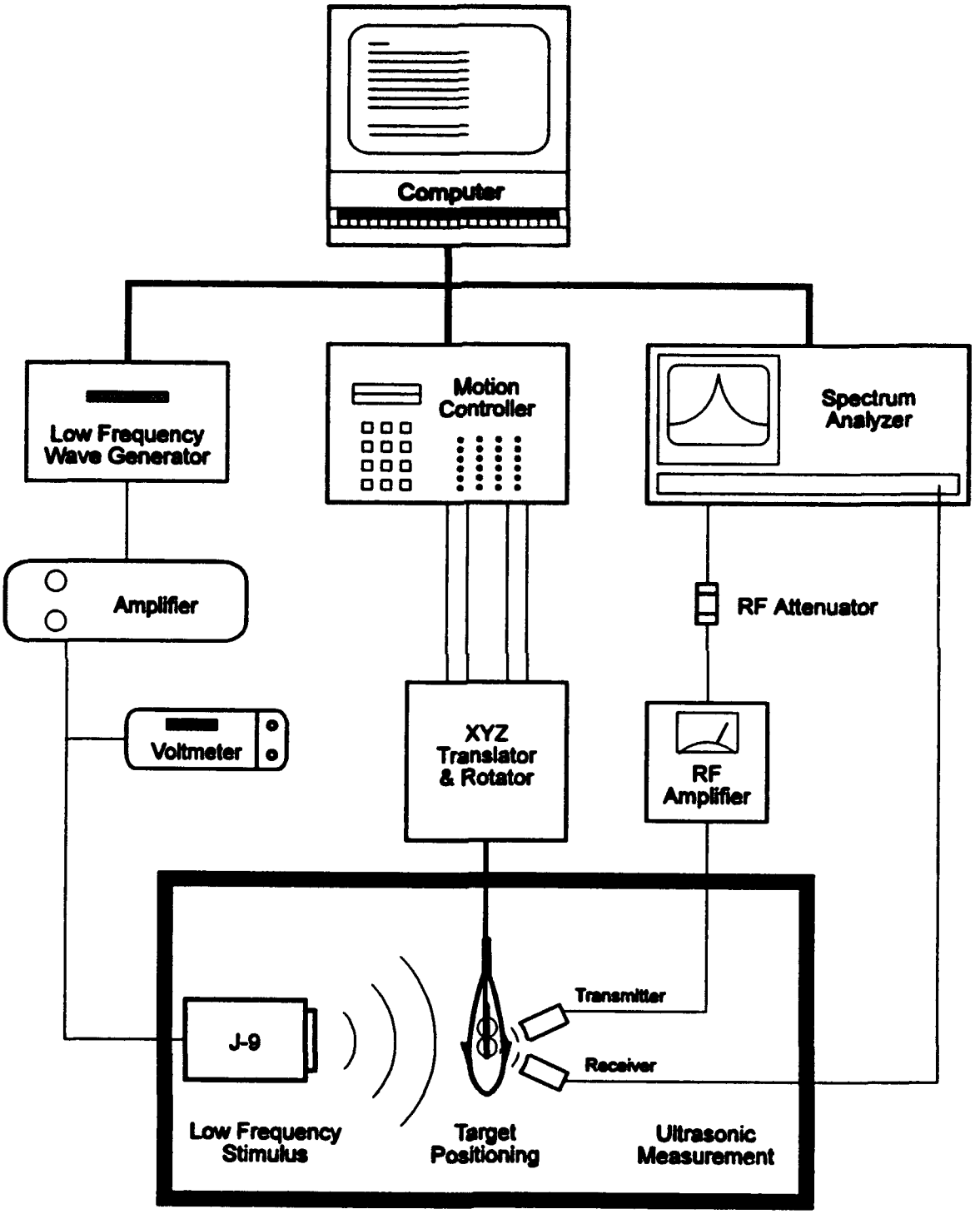

Figure 3-1. Non-invasive vibration amplitude measurement system (NIVAMS).

tolerated more incidental movement of the target. Third, the swim bladder motions are large compared to the minimum detectable displacement at 10 MHz, the added sensitivity at higher frequencies was unnecessary.

Since the focal point of the measurement system was fixed, the target needed to be moved to that point in space. Targets (fish) were located using a packaged Aerotech positioning system. A Unidex XI programmable 4 axis motion controller interfaced to the IBM-PC over a RS-232-C serial line. Stepper motored linear translators allowed motion in the three orthogonal axes with a stepper motored rotator as the final stage. The whole assembly was inverted so that the rotator table cantilevered over the test tank. The minimum step size along each linear axis was 10 microns. This system was unchanged from Cox (1987).

The low frequency stimulus was provided by a Wavetek 275 waveform generator. The output was amplified by a Carver TFM-6C power amplifier. The output voltage of the amplifier was monitored using a Hewlett-Packard 3435A digital multimeter. This signal drove the USRD J-9 underwater sound projector in the test tank, providing the low frequency sound stimulus for the fish. The computer controlled the output frequency and voltage of the waveform generator. The Carver amplifier replaced the McIntosh used before, but was functionally equivalent.

The test tank was a glass-walled 190 liter aquarium (0.91 m x 0.46 m x 0.46 m) filled with conditioned water to a depth of 0.43 m. Four air-spring isolators (4.10/3.50 - 5 butyl inner tubes) underneath decoupled the test tank from ground vibrations. The sound projector, transducers and focal point were positioned as shown in Figure 3-2.

The sound pressure level in the tank was measured using a B&K 8103 hydrophone and the spectrum analyzer. Measurements were made at 15 points in the tank, including the focal point of the transducers and 14 points forming a 25 mm cube around the focal point (Cox, 1987). The first sweep (200 to 2000 Hz) was made with the input to the J-9 at a constant 5 Volts. From these pressure measurements, voltage inputs were calculated to yield a relatively constant pressure stimulus, since acoustic pressure drives the oscillation of the swim bladder. Sound pressure levels were then measured again using the variable input voltages. This produced an averaged pressure frequency response as shown

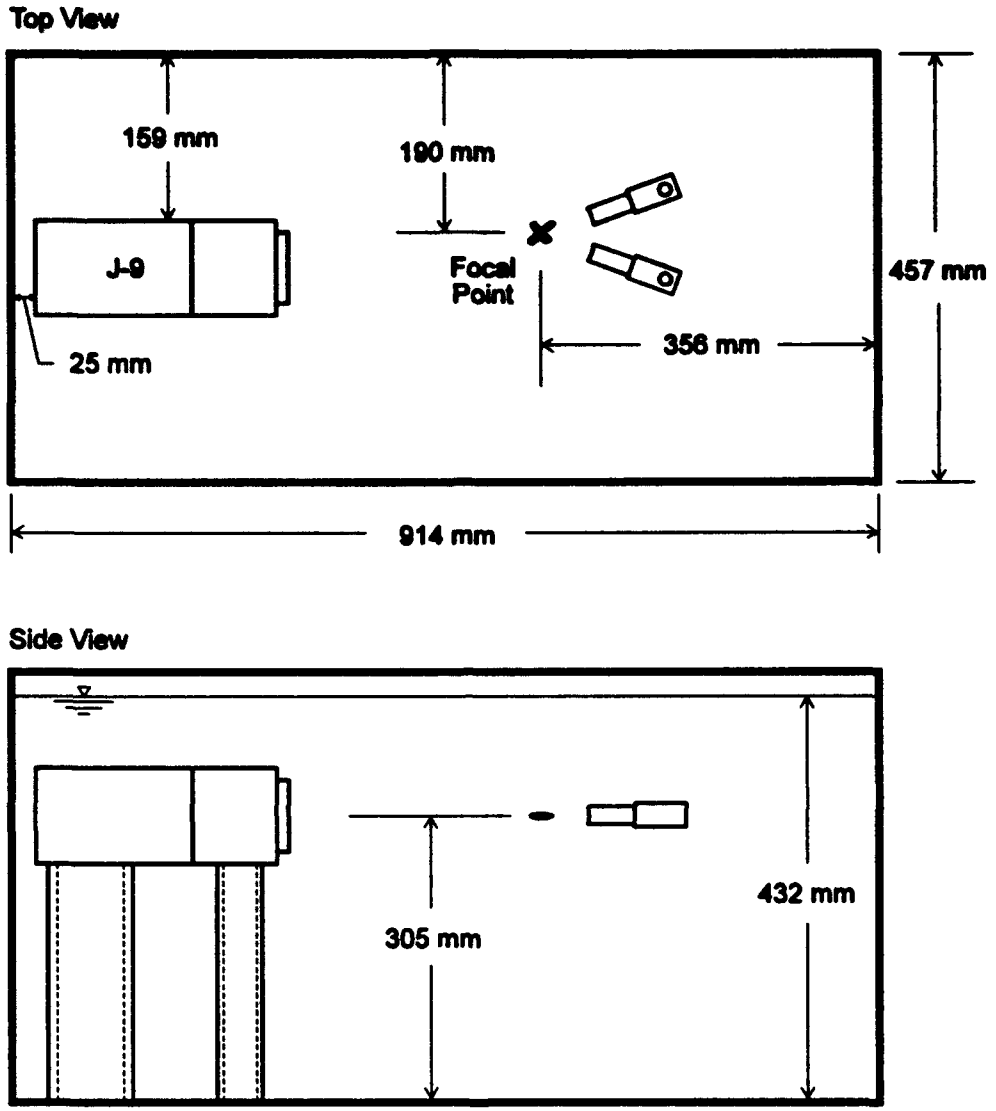

Figure 3-2. Position of transducers and focal point in test tank.

in Figure 3-3. These sound pressure levels were approximately 50 to 80 dB above hearing thresholds of the goldfish.

The test subject was first anesthetized in a solution of MS-222 (0.20 g/l for the goldfish and 0.40 g/l for the oscars) until respiration ceased. Sutures were then inserted through the tissue at two places dorsal to the spinal cord, usually anterior and posterior to the base of the dorsal fin. The ends of the sutures were attached to a threaded post with a

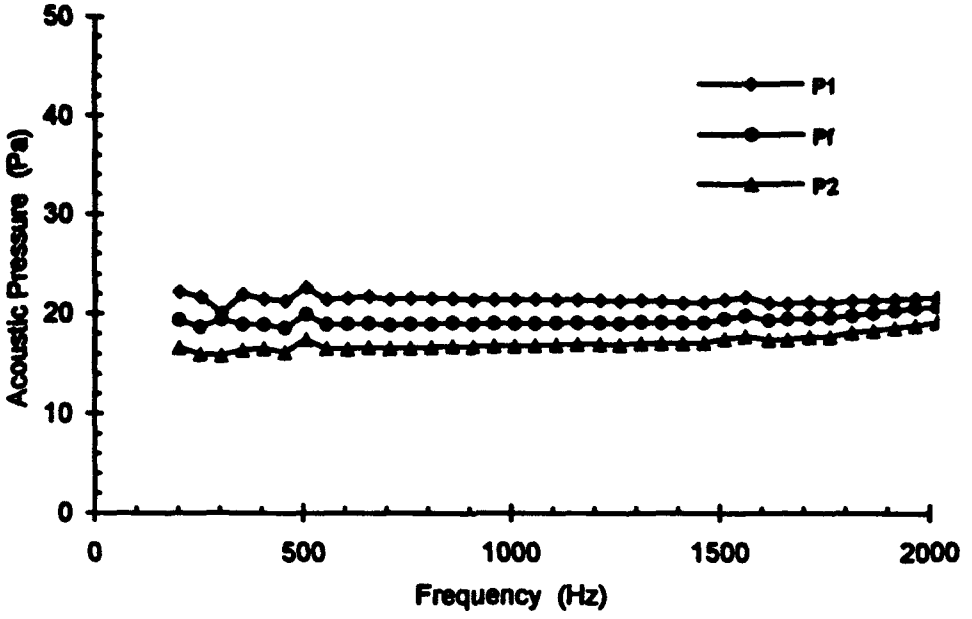

Figure 3-3. Measured acoustic pressure in the vertical planes nearest the J-9 (p1), at the focal point (pf), and furthest from the J-9 (p2).

rubber band. Since the subjects had a tendency to float when anesthetized, an anchor consisting of a loop of suture holding paper clips was hung around the fish between the sutures. The number of paper clips used was varied to provide just enough weight to prevent the subject from floating.

The subject was then immersed in fresh water until steady respiration resumed. Ventilation was assisted when necessary by stroking the ventral side between the gill edges and the mouth to pump water through the gills. The subject was then transferred to the test tank by attaching the post to the inverted table of the positioner.

The trick to this experiment was keeping the subject still in the water. As the focal point actually consisted of a volume (based on 3 dB attenuation) of about 0.32 mm in diameter by 0.85 mm deep, any significant motion by the subject would reduce the reflected signal. So the test tank was filled with a solution of MS-222 (0.0075 % for goldfish and 0.0150 % for oscars) and adjusted as necessary for the individual subject.

When the correct solution was found, data could be taken for up to 12 hours without apparent harm to the subject.

The subject was then positioned such that the region of the focal point was on the surface of the swim bladder. This was identified as the position of maximum received signal on the spectrum analyzer, since the swim bladder was the largest reflector of sound. Visual observation was used to confirm the general location. Then the computer program was run that set the frequency and amplitude of the low frequency stimulus and determined the response by measuring the amplitude of the carrier and the sidebands. The low frequency stimulus was then changed to the next frequency of interest. A frequency sweep was typically from 200 to 2000 Hz in 50 Hz steps.

Multiple frequency sweeps could be made in the same session, either by simply rerunning the program or moving to another point on the swim bladder and rerunning. The session ended prematurely when the subject showed no signs of respiration movement. The sutures were then removed and the subject revived in freshwater.

Measurement Validation

The results of several experiments are shown in Figure 3-4. The data is presented as the measured displacement of the target divided by the acoustic pressure of the low frequency stimulus. Shown are response curves for similarly sized goldfish and oscar. For a given size, the oscar has a much lower resonance frequency. To compare this data to the models, an estimation of the size of the swim bladders of goldfish and oscars was required.

The goldfish has a swim bladder divided into approximately equal anterior and posterior chambers of almost spherical form, so two equally sized spherical chambers were initially assumed. Since the sum of the volumes of both swim bladders is approximately 8% of the goldfish's total volume (Alexander, 1959b), an estimate of their size was made as

$$V_{sb} = (\%\text{vol})\frac{m_f}{\rho_f} = 2\left[\frac{4\pi}{3}a_0^{\,3}\right] \qquad (3\text{-}2)$$

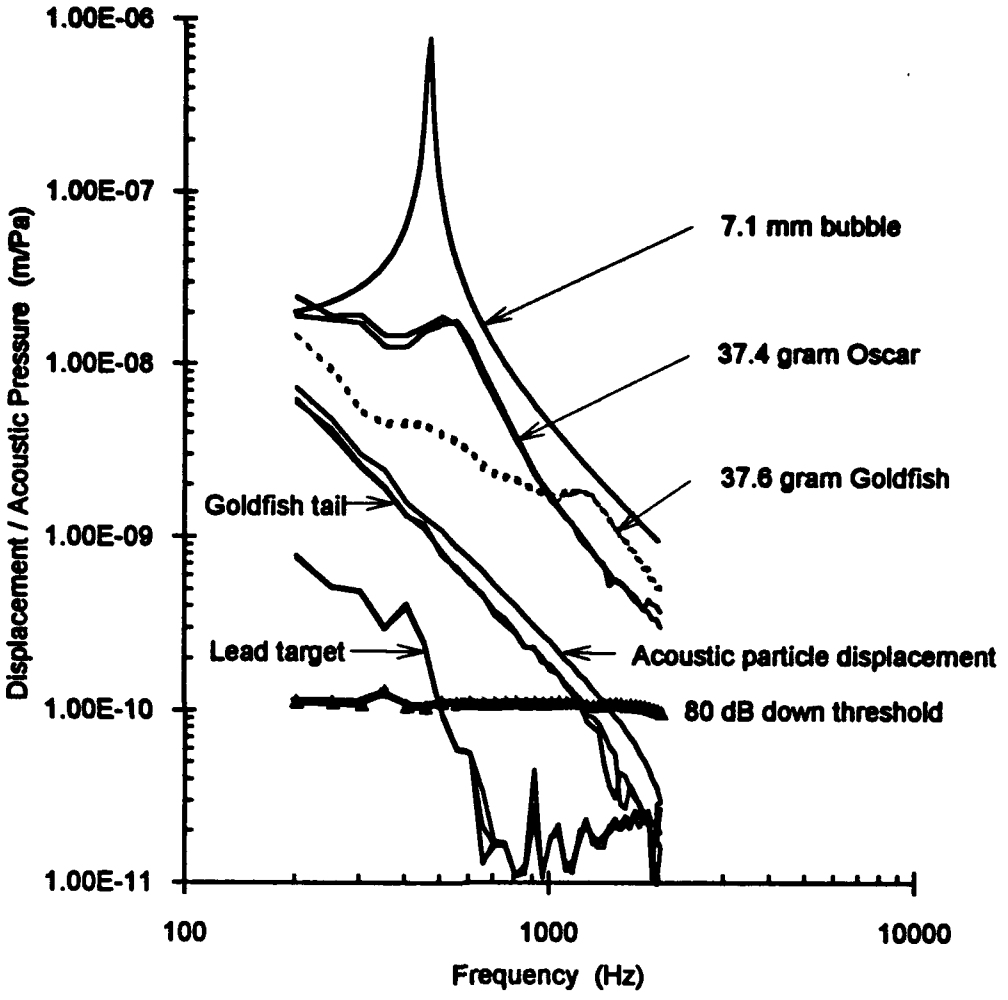

Figure 3-4. Comparison of measured target displacements to calculated theoretical values. See text for detailed explanation.

where V_{sb} is the total swim bladder volume, % vol is the volume percentage of the swim bladder for the fish, m_f is the mass of the fish, ρ_f is its density, and a_0 is the radius of the chamber. For a 37.6 gram goldfish, the effective swim bladder radius is 7.1 mm.

Although the form of the oscar's swim bladder is a single chamber of a more cigar shape, the spherical assumption was again used. This was reasonable since Strasberg (1953) and Weston (1967) have shown that the resonance frequency of spheroidal bubbles

is only slightly higher than spherical bubbles of equal volume. For a prolate spheriod with minor-to-major axis ratio of 0.25 (measured for the oscar from an X-ray), the resonance frequency would be about 8.7 % higher. The assumption of 8 % volume of the swim bladder was again made, since there was no available data for the oscar. This calculated to a_0 = 8.9 mm for the 37.4 gram oscar. For oscars and goldfish of identical weight, their effective swim bladder radii differ by 26 %.

The top curve in Figure 3-4 is the calculated response of an ideal air bubble (a_0 = 7.1 mm) from the equation

$$\frac{\xi_b}{p_{inc}} = \frac{1}{\rho_w a_0} \frac{1}{\sqrt{\left(\omega^2 - \omega_0^2\right)^2 + \left(\omega^2 (k a_0)\right)^2}} \tag{3-3}$$

where ξ_b is the displacement of the bubble surface, p_{inc} is the incident acoustic pressure, ρ_w is the density of water, ω is the incident frequency, ω_0 is the resonance frequency, and k is the wave number (ω / c_w), of the incident frequency. The resonance frequency was calculated from

$$\omega_0 = \frac{1}{a_0} \sqrt{\frac{3\gamma p_0}{\rho_w}} \tag{3-4}$$

where γ is the specific heat ratio and p_0 is the static ambient pressure (Minnaert, 1933). The resonance frequency and damping coefficient are much lower than that measured for either fish.

The line immediately below the fish data in Figure 3-4 illustrates the acoustic particle displacement generated by the low frequency stimulus. Since the focal point was in the nearfield region of the J-9, the low frequency sound field was assumed to consist of spherical progressive waves. The incident acoustic particle displacement, ξ_{inc}, was calculated from

$$\xi_{inc} = \frac{1}{\omega} \sqrt{\left(\frac{p_{inc}}{\rho_w c_w}\right)^2 + \left(\frac{\Delta p_{inc}}{\rho_w \omega \ell}\right)^2} \tag{3-5}$$

where p_{inc} is the measured incident pressure at the focal point, c_w is the speed of sound in water, Δp_{inc} is the difference in measured incident pressure in planes on each side of the

focal point along the x-axis (see Figure 3-3), and ℓ is the distance between the pressure measurements. The first term under the radical represents the true "sound" while the second represents the incompressible flow. Although it is noted that acoustics of small tanks is complex (Parvulescu, 1967), this assumption of propagating waves yielded reasonable results.

The assumption was made that since the fish is mainly water, the sound waves propagate through it. To test this, the response of fish tissue was compared to the acoustic particle displacement. The goldfish tail response in Figure 3-4 indicates the measured response of the flesh of a goldfish. This was made by positioning the tail of the goldfish in the focal region. Naturally, the echo was much lower than when the swim bladder reflected the ultrasound. The response of the fish tissue follows that of the particle displacement with only a slight decrease in amplitude.

The lead target response in Figure 3-4 indicates the motion of a chunk of lead to the low frequency stimulus. Cox (1987) used this test to measure the amplitude of the relative motion of the ultrasonic transducers. Since the density of lead is much higher than that of water, the lead should have been comparatively stationary, so any measured response indicates transducer motion. As this total was much less than the measured swim bladder motion, this correction was ignored.

The 80 dB down threshold can be thought of as the accuracy limit for the NIVAMS. The HP 3585A claims a dynamic range of greater than 80 dB, and the measurement scale displays 100 dB. The function used to measure the amplitudes of the carrier and the sidebands requires 20 dB signal-to-noise to be accurate. By setting the peak of the carrier signal to the top of the measurement scale, the 80 dB dynamic range could be obtained. Therefore, measured data below this line were not as accurate.

In summary, Figure 3-4 validated the measurement method by showing that: 1) the motion of the swim bladders of the goldfish and the oscar could be detected, 2) this motion differed significantly from the motion of the fish tissue (which moves like the water), 3) the motion of the ultrasonic transducers was not of significant concern, and 4) the measured displacements were significantly greater than the theoretical minimum of the NIVAMS.

Data Reduction

Figure 3-5 shows the data for the 37.6 gram goldfish and the 37.4 gram oscar expressed in terms of scattering cross-section. This parameter was chosen to allow direct comparison to existing theoretical models and the experimental results of others. Total scattering cross-section, σ_s, for an omnidirectional scatterer is defined as

$$\sigma_s \equiv \frac{\Pi_s}{I_{inc}} = \frac{4\pi a_0^2 I_s}{I_{inc}} \tag{3-6}$$

where Π_s is the total power scattered by an object, I_s is the scattered intensity, and I_{inc} is the incident intensity (Clay and Medwin, 1977). This can be rewritten in the form

$$\sigma_s I_{inc} = 4\pi a_0^2 I_s \tag{3-7}$$

to illustrate that scattering cross-section is an equivalent size for a cross-sectional area that scatters the incident wave.

The low frequency acoustic pressure drives the motion of the swim bladder, so the incident acoustic intensity was

$$I_{inc} = \frac{p_{inc}^2}{\rho_w c_w}. \tag{3-8}$$

The scattered intensity was determined by assuming the scattered waves to be spherical waves reradiated from a spherical source. Therefore,

$$I_s = \rho_w c_w v_{sb}^2 \left[1 + \left(\frac{1}{ka_0}\right)^2\right]^{-1} \tag{3-9}$$

where v_{sb} is the velocity of the motion of the swim bladder. For sinusoidal motion,

$$v_{sb}^2 = \omega^2 \xi_{sb}^2. \tag{3-10}$$

All of this was combined to calculate the scattering cross-section for each data point as

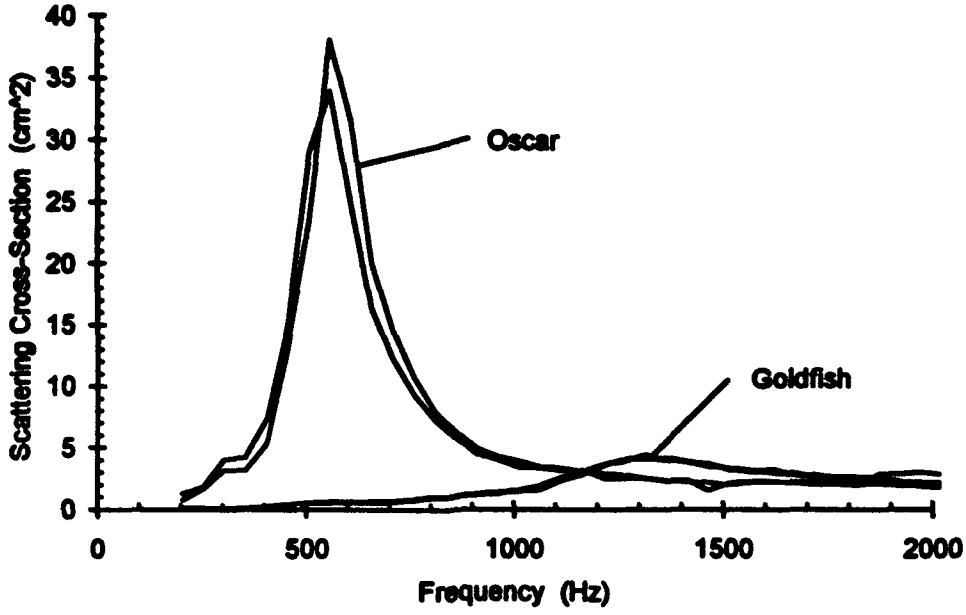

Figure 3-5. Scattering cross-section of a 37.6 gram goldfish and a 37.4 gram oscar. Data shown is 4 frequency sweeps for the goldfish and 2 for the oscar.

$$\sigma_s = \frac{4\pi a_0^{\,2}(\omega \xi_{ab})^2}{\left(\frac{p_{inc}}{\rho_w c_w}\right)^2 \left[1 + \frac{1}{(ka_0)^2}\right]}. \tag{3-11}$$

The data points indicate that the swim bladders of these fish scatter sound like a damped harmonic oscillator. To examine this, the data was compared to a generalized curve for scattering cross-section,

$$\sigma_s = \frac{4\pi a_0^{\,2}}{\left[\left(\frac{\omega_0}{\omega}\right)^2 - 1\right]^2 + \left[\frac{1}{Q}\frac{\omega_0}{\omega}\right]^2} \tag{3-12}$$

where Q is the quality factor at resonance. A three parameter (a_0, ω_0, and Q) non-linear least squares curve fit of this equation was made to the data. Curve fit results for two frequency sweeps along with the individual data points are shown in Figure 3-6.

This method of data presentation differs from that used before (Cox, 1987; Lewis *et al.*, 1991) which gave results in terms of relative motion. It can be shown (Appendix A) that the scattering cross-section is proportional to relative motion squared.

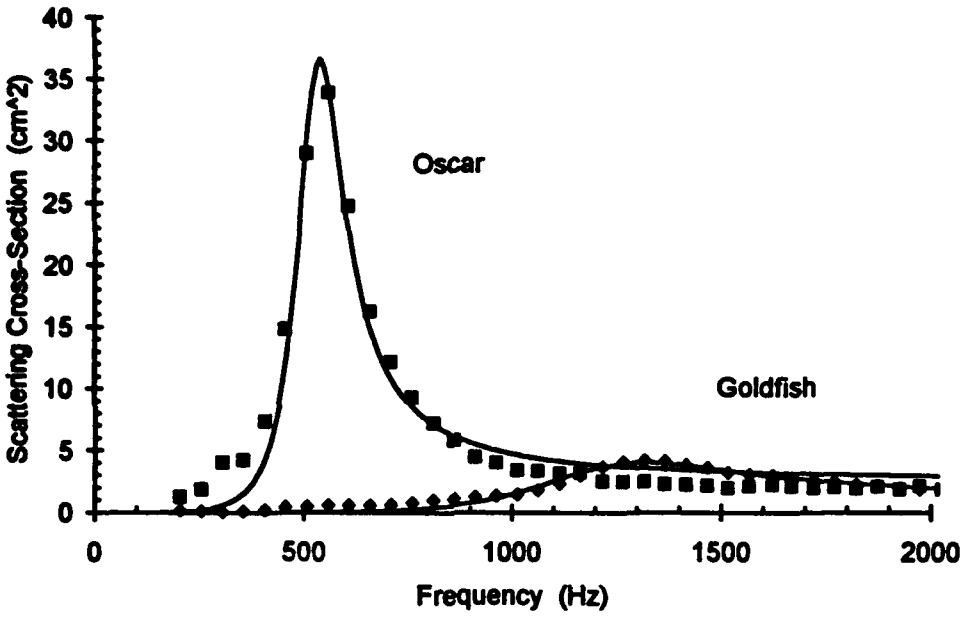

Figure 3-6. Three parameter curve fit of swim bladder data for a 37.6 gram goldfish and a 37.4 gram oscar to the generalized scattering cross-section formula (Equation 3-12). Symbols represent data points and the lines are calculated.

Experimental Results

Data was taken on the anterior swim bladders of 22 different goldfish, most with multiple sweeps per session, and half on more than one day, for a total of 107 sweeps. All of this data appears in Appendix B. Most of these sweeps were fit to the scattering cross-section function, Equation 3-12, with varying success. Repeated sweeps on a given day typically produced similar measurements (see Figure 3-5 for an example) although data on the same fish on different days may not (compare the data on the 57.1 gram goldfish in

Figures B-22 and B-23). Therefore, the curve fit parameters were averaged for data of a given fish for a given session. These daily individual averages and standard deviations for the anterior swim bladder data are shown in Table 3-1 and plotted in Figure 3-7.

Some of the data taken was not included in Table 3-1 and Figure 3-7 for one of several possible reasons. First, for the smallest goldfish (2.2 grams) the resonance peak appeared to be above the highest measured frequency (Figure B-1). Second, some responses were inconsistent between sweeps (22.6 gram - Figure B-4). Third, the data may not have followed the general shape of the resonance curve (see 26.1 gram - Figure B-6 for an extreme example). Fourth, and most interesting, two goldfish (48.9 and 58.8 gram) showed twin peaks in their resonance curves (Figure 3-8). This is a reasonable response, since the anterior and posterior swim bladder chambers are not always equal in size, and therefore may resonate at different frequencies. The twin peaks phenomenon, first reported in Lewis *et al.* (1991), was later investigated in this lab by others (Zhou, 1992).

The first step in the twin peaks investigation was to measure the frequency responses of both the anterior and posterior swim bladders of a goldfish. Figures 3-9, 3-10, and 3-11 show the response of both swim bladders of five goldfish. Although none of these fish showed twin peaks response of the anterior swim bladders, the response of the posterior swim bladder didn't always mimic that of the anterior. It was interesting to note that the magnitude of the posterior response was always smaller by factors ranging from 3 to 10.

Data was also taken on the swim bladders of 32 different oscars, ranging in size from 6.2 to 184.4 grams. All subjects were tested once on a given day, with a maximum of three sweeps in a day, for a total of 46 sweeps. This data comprises Appendix C. All of these sweeps were fit to the scattering cross-section function, with varying success. From this, 40 sweeps from 30 subjects were analyzed. Again daily averages and standard deviations were computed and are shown in Table 3-2 and plotted in Figure 3-12.

Comparison to Models

The data from this experiment was compared to three single degree of freedom lumped parameter models of increasing complexity for swim bladder response: 1) the

Table 3-1 Goldfish anterior swim bladder daily averages and standard deviations for resonance frequency and quality factor, Q, from the data in Appendix B.

Mass (gr)	# pts.	RF avg. (Hz)	RF s.d.	Q avg.	Q s.d.
14.8	1	1244.4		1.870	
14.8	2	1216.9	3.5	2.510	0.103
14.8	1	1226.1		4.018	
14.8	2	1158.8	90.3	2.246	0.953
19.4	3	1320.1	28.7	1.616	0.189
28.4	5	1017.3	205.9	1.016	0.254
32.1	2	1144.2	149.3	1.648	0.205
32.2	3	1043.6	4.3	2.608	0.058
33.1	3	1323.2	91.3	1.374	0.092
33.1	2	1079.1	8.4	2.731	0.343
33.1	1	1258.2		2.378	
33.1	1	1289.3		1.970	
35.0	1	1395.0		1.994	
35.0	1	1381.9		1.324	
35.0	4	1288.5	155.3	2.592	0.834
35.0	2	1020.7	3.3	2.653	0.395
35.0	1	1268.0		2.357	
36.0	1	1019.1		1.733	
36.0	3	955.4	52.7	1.644	0.187
36.0	2	973.1	20.6	2.033	0.372
36.0	2	1127.5	15.6	2.134	0.048
37.6	4	1225.8	9.6	1.850	0.093
39.5	1	992.4		2.001	
39.8	1	717.6		2.975	
39.8	2	973.5	96.6	1.225	0.209
43.1	4	1134.7	63.9	2.711	0.322
43.1	4	1253.4	72.8	2.441	0.327
46.5	1	623.5		1.477	
48.9	1	706.0		1.543	
50.0	5	968.4	11.7	1.800	0.058
52.0	1	622.8		2.088	
52.0	1	723.2		4.128	
52.0	1	794.3		2.240	
52.0	3	909.3	11.7	3.479	0.663
52.0	1	783.7		2.925	
57.1	1	833.4		2.516	
57.1	3	511.0	17.6	2.764	0.291
99.0	3	675.4	29.8	2.430	0.236

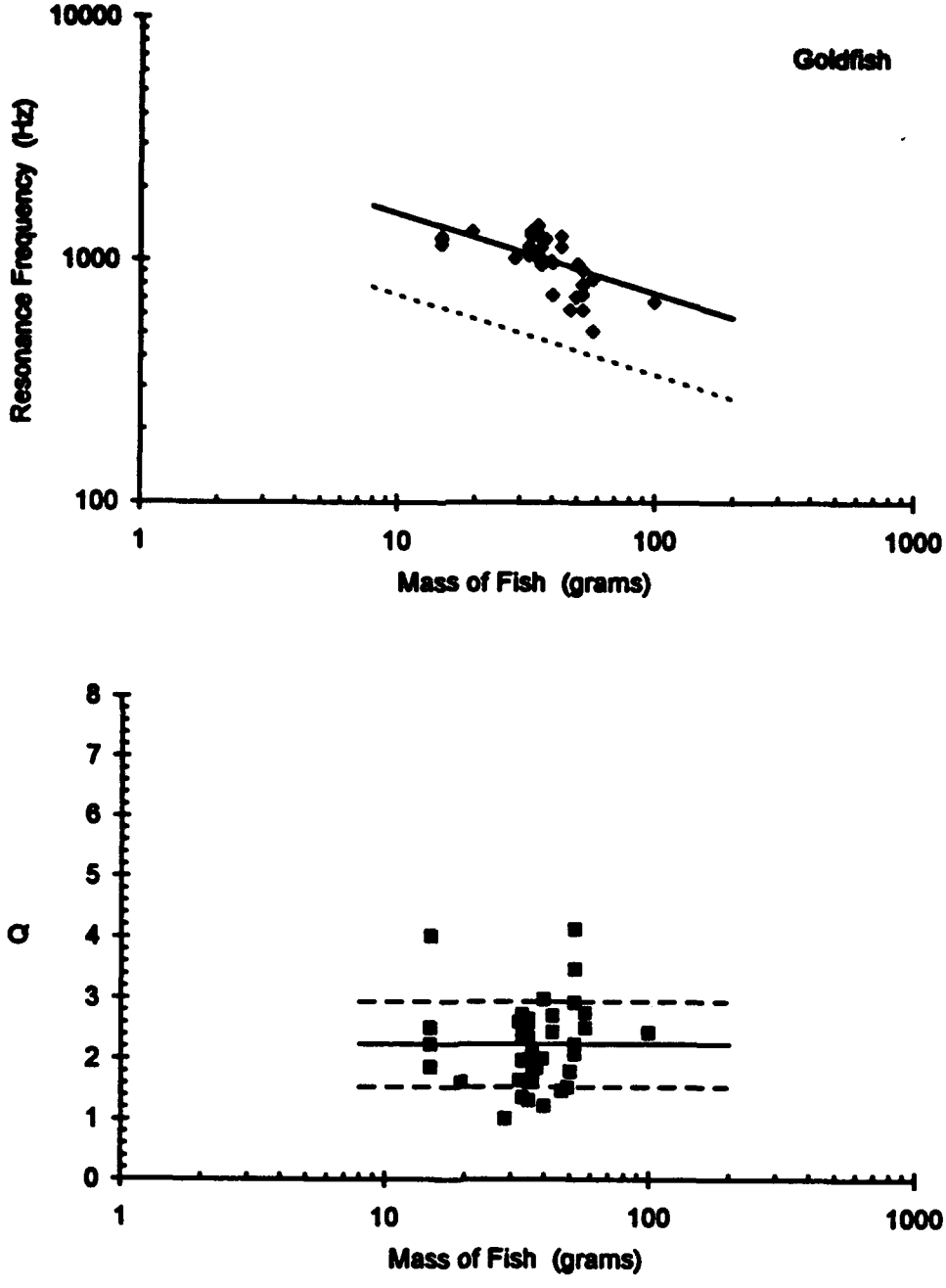

Figure 3-7. Resonance frequency vs. mass (top) and quality factor vs. mass (bottom) in the goldfish. In the top graph, the solid line represents the best fit to a cubic function ($R = 0.60$) and the dashed line represents the ideal air bubble model. In the bottom graph, the solid line represents the average and the dashed lines shows the upper and lower standard deviation ($Q = 2.24 \pm 0.70$).

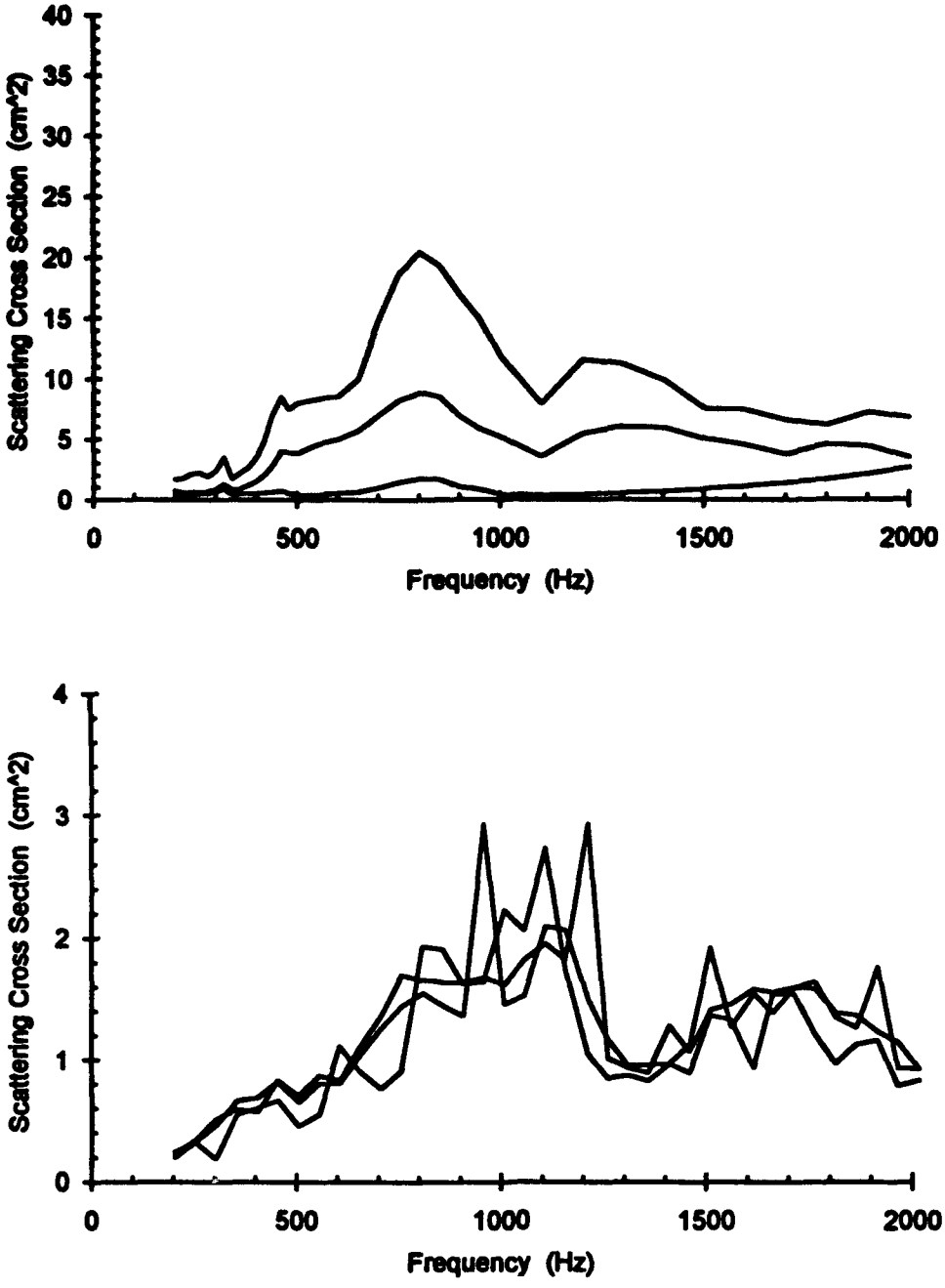

Figure 3-8. Twin peaks in the frequency response of the anterior swim bladders of a 48.9 gram (top) and a 58.8 gram (bottom) goldfish.

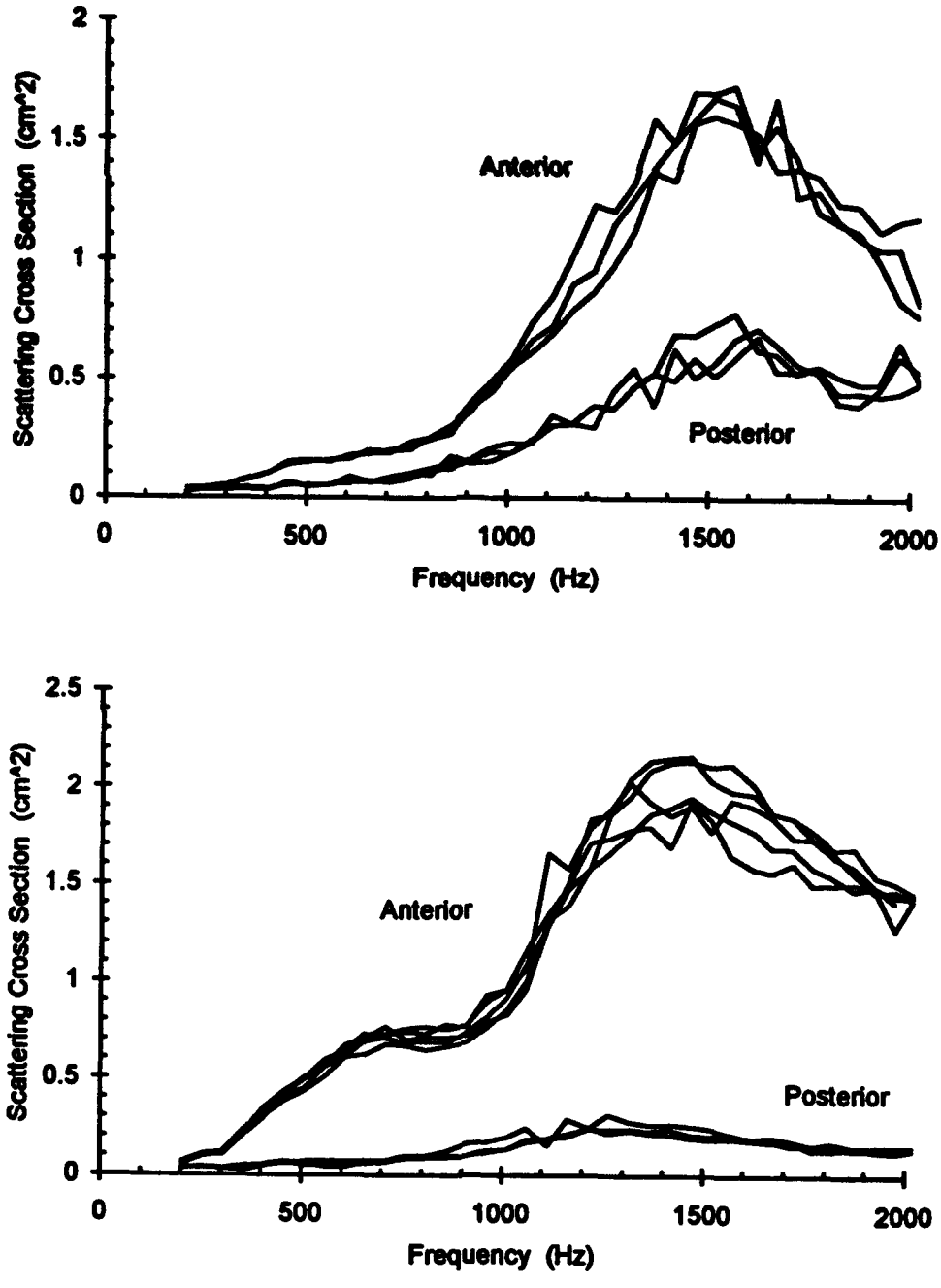

Figure 3-9. Frequency response of the anterior and posterior swim bladders of a 19.4 gram (top) and a 28.4 gram (bottom) goldfish.

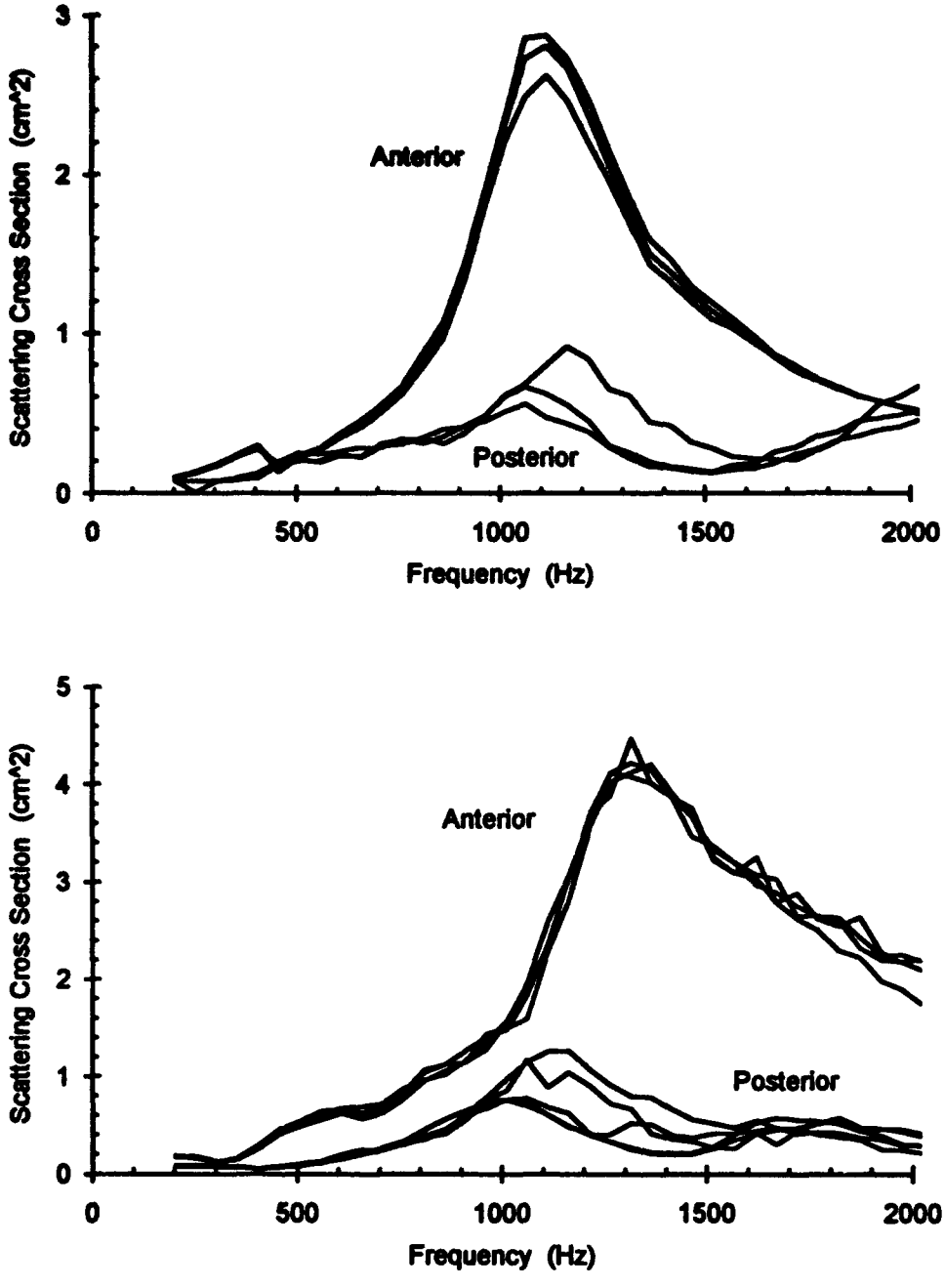

Figure 3-10. Frequency response of the anterior and posterior swim bladders of a 32.2 gram (top) and a 37.6 gram (bottom) goldfish.

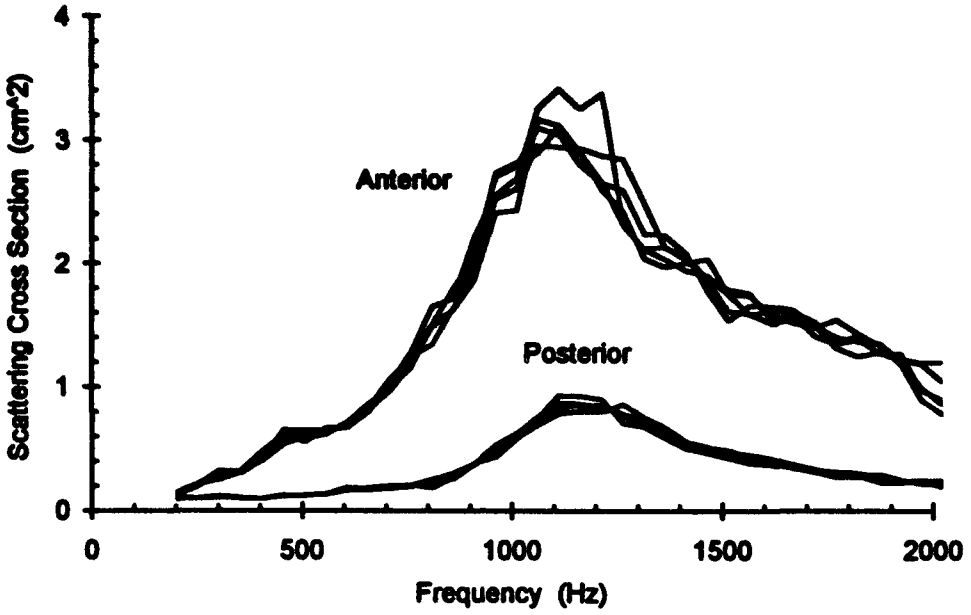

Figure 3-11. Frequency response of the anterior and posterior swim bladders of a 50.0 gram goldfish.

resonant ideal air bubble, 2) Andreeva's (1964) model of an air bubble in a viscoelastic matrix, and 3) Love's (1978) model of an air bubble surrounded by a small spherical fluid shell that supports a surface tension. All of these models can be related to the physics of a simple spring-mass-damper system.

The equation of motion for the viscously damped spring-mass system shown in Figure 3-13 can be obtained using Newton's second law:

$$m_{eq}\ddot{x} + c_{eq}\dot{x} + k_{eq}x = F(t) \qquad (3\text{-}13)$$

where m_{eq} is the equivalent mass of the object vibrating, c_{eq} is the equivalent damping constant, k_{eq} is the equivalent spring stiffness, F(t) is the forcing function, and x(t) is the displacement of the mass with time. (The dots over the displacement variable indicate derivatives with respect to time.) In simple ideal systems, these parameters are constants. In real systems, however, these parameters can be, and often are, complex functions of the motion variables (displacement, velocity, or acceleration) and time (frequency). The

Table 3-2. Oscar swim bladder daily averages and standard deviations for resonance frequency and quality factor, Q, from the data in Appendix C.

Mass (gr)	# pts.	RF avg. (Hz)	RF s.d.	Q avg.	Q s.d.
6.20	1	894.8		4.168	
6.45	1	791.2		4.353	
6.72	1	745.1		4.388	
6.86	1	750.6		5.022	
7.49	1	781.8		3.535	
7.83	1	750.7		4.888	
9.08	1	705.1		4.437	
11.43	1	625.4		4.164	
12.33	1	673.4		3.745	
12.90	2	601.8	0.1	3.241	0.175
13.81	2	624.4	25.2	3.602	0.240
14.14	1	545.2		2.530	
15.40	2	663.2	25.9	3.704	0.153
16.06	1	569.1		4.180	
16.87	1	565.9		4.236	
21.89	1	567.3		4.189	
25.00	1	526.2		3.682	
27.23	1	539.1		4.332	
34.26	2	444.1	7.4	4.237	0.146
35.42	1	498.3		3.067	
37.40	2	539.8	15.1	3.807	0.086
38.00	1	502.7		2.964	
41.69	2	568.4	14.0	3.397	0.308
42.91	1	438.7		3.071	
45.43	1	444.2		3.791	
48.62	1	389.6		5.002	
53.84	3	394.6	11.7	4.663	0.716
57.53	3	393.4	8.3	3.513	0.285
63.30	1	475.6		3.713	
184.40	1	258.9		3.891	

object of the models was to determine how these parameters - m_{eq}, c_{eq}, and k_{eq} - relate to the real system, the actual fish.

Each parameter represents physical quantities in the real system. When the swim bladder expands and contracts, the nearby fish tissue and surroundir g water moves with it.

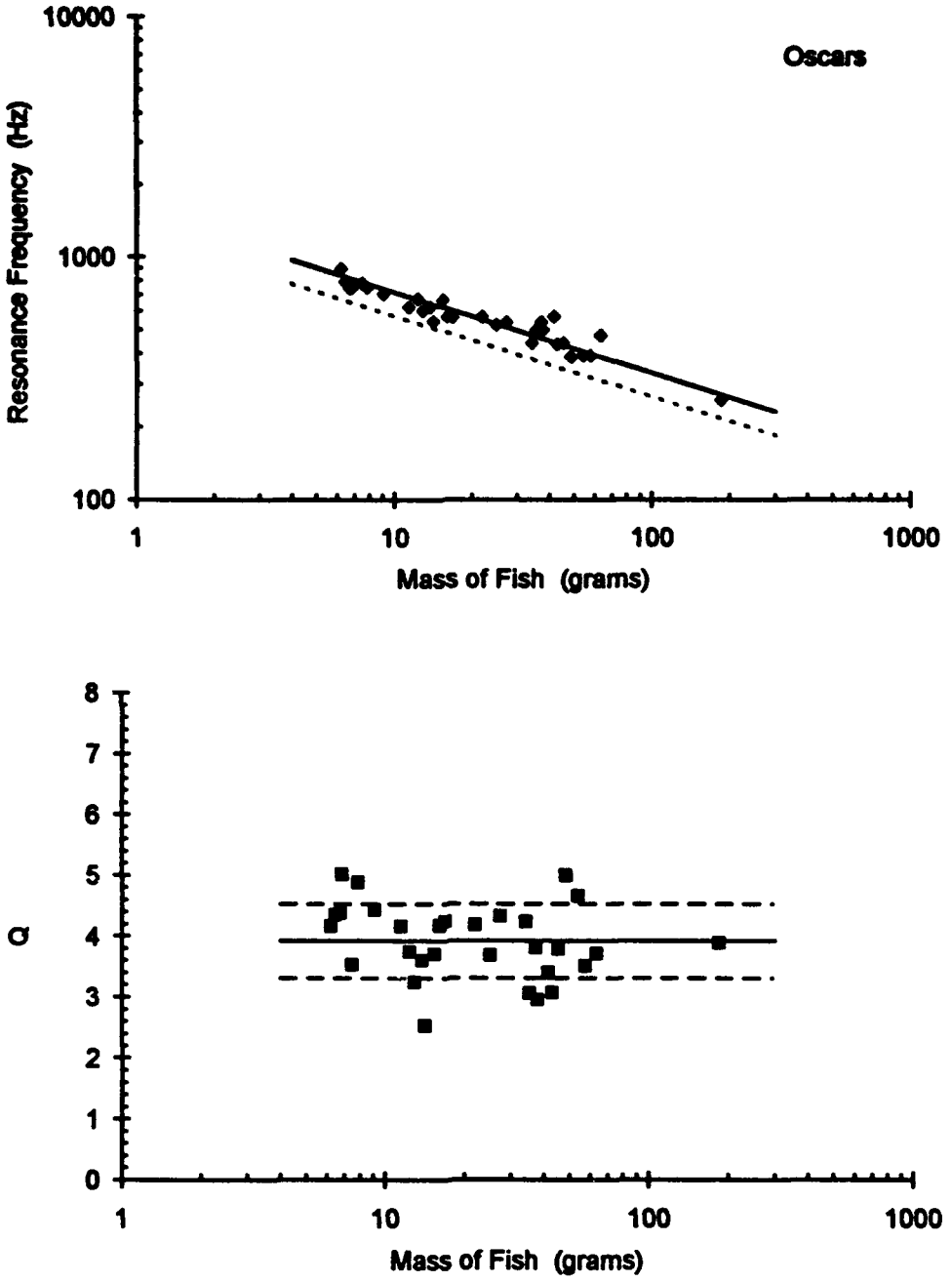

Figure 3-12. Resonance frequency vs. mass (top) and quality factor vs. mass (bottom) in the oscar. In the top graph, the solid line represents the best fit to a cubic function ($R = 0.95$) and the dashed line represents the ideal air bubble model. In the bottom graph, the solid line represents the averaged oscar data and the long dashed lines shows the standard deviation ($Q = 3.92 \pm 0.61$).

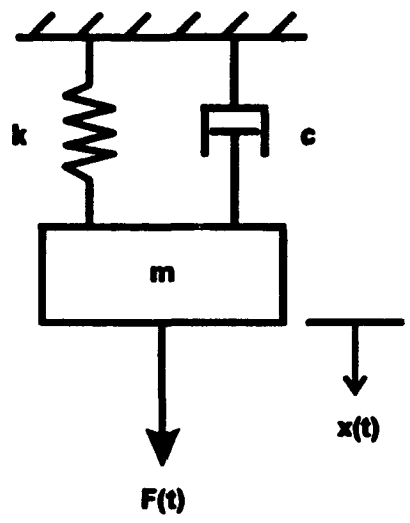

Figure 3-13. A spring-mass-damper system.

The mass term quantifies this. The spring term is identified with the elasticity of this moving tissue and the swim bladder wall as well as the compliance of the gas inside the swim bladder. The damping constant represents all forms of energy dissipation. As the motion of the swim bladder distorts the surrounding fluid elements, viscous forces dissipate energy. Thermal dissipation occurs since heat is lost to the surrounding tissue as the air in the swim bladder is compressed. Dissipation is inherent in elastic elements - there are no lossless springs. The reradiation of sound is also energy lost to the vibrating system.

The undamped resonance frequency for this system is

$$\omega_0 = \sqrt{\frac{k_{eq}}{m_{eq}}} \tag{3-14}$$

so it is only dependent on the stiffness and mass of the system. The quality factor, defined as

$$Q = \frac{\sqrt{k_{eq} m_{eq}}}{c_{eq}}, \tag{3-15}$$

is dependent on all three parameters.

The motion of the system in response to a sinusoidal forcing function can be obtained from the steady-state solution to Equation 3-13,

$$x(t) = \frac{F_0}{\left[(k - m\omega^2)^2 + (c\omega)^2\right]^{1/2}} \cos(\omega t - \phi) \tag{3-16}$$

where F_0 is the magnitude of the forcing function and ϕ is the phase angle between the forcing function and the displacement response. (The "eq" subscripts have been dropped for simplification.) Taking two time derivatives and using Equation 3-14 gives

$$\ddot{x}(t) = \frac{\frac{F_0}{m}}{\left\{\left[\left(\frac{\omega_0}{\omega}\right)^2 - 1\right]^2 + \left[\frac{2c}{2\sqrt{km}}\frac{\omega_0}{\omega}\right]^2\right\}^{1/2}} \cos(\omega t - \phi). \tag{3-17}$$

The term in the denominator, $2\sqrt{km}$, is equal to the critical damping constant, c_c, and the ratio of the damping constant to critical damping constant is the damping ratio, ζ. Therefore, the magnitude of the acceleration is

$$|\ddot{x}| = \frac{\frac{F_0}{m}}{\left\{\left[\left(\frac{\omega_0}{\omega}\right)^2 - 1\right]^2 + \left[2\zeta\frac{\omega_0}{\omega}\right]^2\right\}^{1/2}}. \tag{3-18}$$

The forcing function for this system is the acoustic pressure. This is thought to act uniformly at any given time over the entire surface of the swim bladder, so that the forcing function is the product of the acoustic pressure and the surface area of the swim bladder. The motion variable is the radial displacement of the swim bladder, ξ_{sb}. Since the forcing function is sinusoidal, the response is also sinusoidal, so the magnitude of the radial acceleration is the displacement times frequency squared. The effective mass is the radiation mass of a pulsating sphere, which is three times the displaced mass (the volume of the swim bladder times the density of the surrounding water). The term in the denominator, 2ζ, is equal to the inverse of the quality factor. Thus

$$\omega^2 \xi_{sb} = \frac{\frac{p_{inc}(4\pi a_0^2)}{3\rho_w(\frac{4}{3}\pi a_0^3)}}{\left\{\left[\left(\frac{\omega_0}{\omega}\right)^2 - 1\right]^2 + \left[\frac{1}{Q}\frac{\omega_0}{\omega}\right]^2\right\}^{\frac{1}{2}}}. \quad (3\text{-}19)$$

Squaring and multiplying both sides by the surface area of the swim bladder yields

$$\left[4\pi a_0^2\left(\frac{\rho_w a_0}{p_{inc}}\right)\right](\omega^2 \xi_{sb}) = \frac{4\pi a_0^2}{\left[\left(\frac{\omega_0}{\omega}\right)^2 - 1\right]^2 + \left[\frac{1}{Q}\frac{\omega_0}{\omega}\right]^2} \quad (3\text{-}20)$$

which, from Equations 3-11 and 3-12, is the scattering cross-section, σ_s. This single degree of freedom system can be used to model the response of the swim bladder to sound, and by measuring the response, the parameters of the model can be ascertained.

A Resonant Air Bubble

The first model considered was the ideal resonant air bubble. The radial motion of an ideal air bubble in water is a balance of the incident pressure with the compressibility of the enclosed air and the liquid mass moved by the bubble as it pulsates (Clay and Medwin, 1977). The resonance frequency for this model is

$$\omega_0 = \frac{1}{a_0}\sqrt{\frac{3\gamma p_0}{\rho_w}}. \quad (3\text{-}21)$$

The spring term in the numerator under the radical represents the compliance of the air within the bubble. Since the term under the radical is constant at a given depth, the resonance frequency is inversely proportional to the radius of the swim bladder. Using Equation 3-2 to relate the mass of the fish to the size of the swim bladder,

$$\omega_0 = \frac{1}{\sqrt[3]{m_f}}\left[\frac{\sqrt{\frac{3\gamma p_0}{\rho_w}}}{\sqrt[3]{\frac{\%\,vol}{2\rho_f \frac{4}{3}\pi}}}\right] = \frac{980.4}{\sqrt[3]{m_f}} \quad (3\text{-}22)$$

for the goldfish and $2^{-1/3}$ times this for the oscar. The resonance frequency for this model is simply a constant divided by the cube root of the mass of the fish. The resonance frequency versus fish mass using this model is shown in Figures 3-7 and 3-12. The measured resonance frequency of the swim bladder of the goldfish was about 115 percent higher on average than an equivalent ideal air bubble, while for the oscar, the measured resonance frequency was 32 percent higher.

For the ideal air bubble, the scattering cross-section is

$$\sigma_s = \frac{4\pi a_0^2}{\left[\left(\frac{\omega_0}{\omega}\right)^2 - 1\right]^2 + (ka_0)^2} \tag{3-23}$$

(Brekhovskikh and Lysanov, 1982). Comparing this to Equation 3-12, then

$$Q = \frac{\omega_0}{\omega k a_0} . \tag{3-24}$$

The damping in this model is entirely due to acoustic radiation resistance. At resonance ($\omega = \omega_0$),

$$Q = \frac{1}{k_0 a_0} = \frac{c_w}{\omega_0 a_0} = c_w \sqrt{\frac{\rho_w}{3\gamma p_0}} = 72.1 \tag{3-25}$$

For the ideal air bubble, the damping at resonance is independent of the size of the air bubble. This calculated value was much higher than any measured value, which ranged from 1.0 to 4.1 for the goldfish and 2.5 to 5.0 for the oscar.

For the oscar, the air bubble model predicts the trends well (inverse cube function for resonance frequency and constant Q) but not the magnitudes. For the goldfish, the correlations are not as good.

Andreeva's Bubble in a Visco-elastic Matrix

The second model considered was proposed by Andreeva (1964). In this model, the swim bladder of a fish was assumed to be a spherical air bubble with the fish's body a visco-elastic matrix characterized by a complex shear modulus $\mu = \mu_1(1 + i\mu_2)$, where μ_1

is the real part of the shear modulus and μ_2 is the loss factor in shear. This leads to the following equation for the resonance frequency (Andreeva, 1964):

$$\omega_0 = \frac{1}{a_0}\sqrt{\frac{3\gamma p_0 + 4\mu_1}{\rho_w}}. \tag{3-26}$$

The added term corresponds to an additional parallel spring element due to the elasticity of the surrounding fish tissue.

The quality factor for this model can be calculated from (Andreeva, 1964)

$$\frac{1}{Q} = \frac{1}{c_w}\sqrt{\frac{3\gamma p_0 + 4\mu_1}{\rho_w}} + 3(\gamma - 1)\sqrt{\frac{\alpha_a p_0 \rho_w \omega_0}{2p_0(3\gamma p_0 + 4\mu_1)}} + \frac{4\mu_1\mu_2}{3\gamma p_0 + 4\mu_1} \tag{3-27}$$

where α_a is the thermal diffusivity of the gas at standard ambient pressure p_0 (1 atm). The first term represents the radiation damping, the second thermal damping inherent in the cyclical compression of the air inside the swim bladder, and the third viscous damping in the surrounding tissue. Since the measurements were taken at a shallow depth, the static pressure was approximately equal to the ambient air pressure. By using Equation 3-26 and the relation between thermal diffusivity and thermal conductivity, this becomes

$$\frac{1}{Q} = \frac{\omega_0 a_0}{c_w} + \frac{3(\gamma - 1)}{\omega_0 a_0}\sqrt{\frac{\kappa_a \omega_0}{2\rho_a c_{pa}}} + \frac{4\mu_1\mu_2}{\rho_f \omega_0^2 a_0^2} \tag{3-28}$$

where κ_a is the thermal conductivity of air. Typically, the radiation and thermal losses were much smaller than the viscous loss. Figure 3-14 shows the contribution of each to the total.

The difficulty in using this model is in the accurate determination of the shear modulus. Andreeva (1964) presented tentative measurements of $\mu_1 = 10^5$ to 10^6 Pa, and $\mu_2 = 0.2$ to 0.3 with no additional comment. Lebedeva (1965) measured directly the complex shear modulus of muscle tissue specimens for one freshwater and several saltwater fish, demonstrating that although it was similar for different species, the shear modulus is a strong function of specimen fiber orientation and frequency. The data for the three saltwater fish in the 1.5 to 10 kHz range is shown in Figure 3-16. This tissue data correlates well to lines of slope equal to 2 ($\mu_1 \propto \omega^2$).

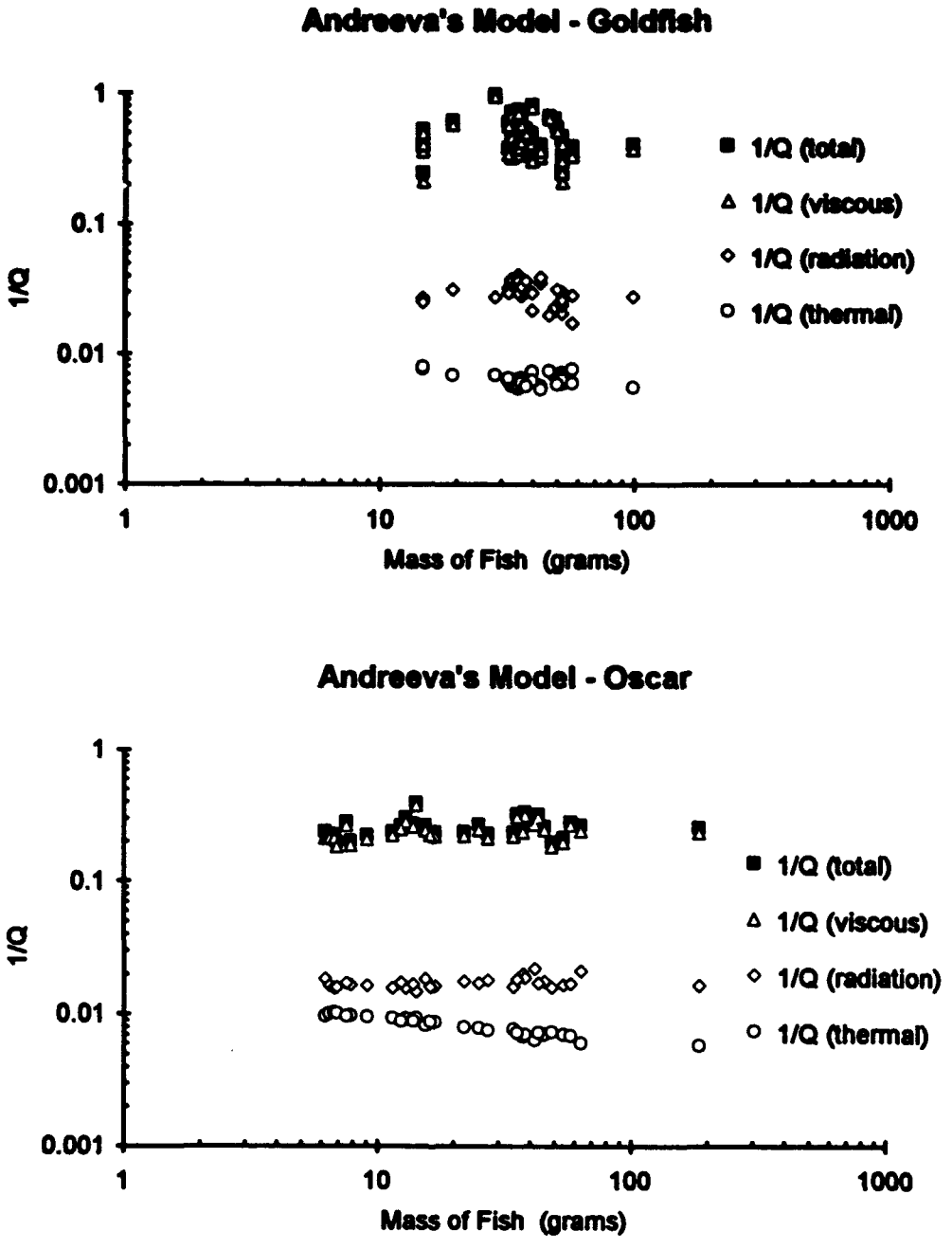

Figure 3-14. Contributions of viscous, radiation, and thermal damping to the quality factor using Andreeva's model.

By inverting Equations 3-26 and 3-28 and using the measured values for ω_0 and Q, estimates for the shear modulus, μ_1, and the loss factor in shear, μ_2, were made. These are also shown in Figure 3-15. For the goldfish, the results for μ_1 fit well to the square function, but were higher by at least two orders of magnitude. The data for the oscars, though, was not correlated with frequency.

Although reasonably correlated (R = 0.83), having the shear modulus as a function of frequency squared in the goldfish poses some potential difficulties. Assume that the shear modulus is a quadratic function of frequency,

$$\mu_1(\omega) = \mu'_1 \omega^2, \tag{3-29}$$

where μ'_1 is the best fit to the data. Inserting this into Equation 3-26 yields

$$\omega_0 = \frac{1}{a_0}\sqrt{\frac{3\gamma p_0 + 4\mu'_1 \omega_0^2}{\rho_w}}. \tag{3-30}$$

Collecting frequency terms

$$(\rho_w a_0^2 - 4\mu'_1)\omega_0^2 = 3\gamma p_0$$

and solving for resonance frequency gives

$$\omega_0 = \frac{1}{a_0}\sqrt{\frac{3\gamma p_0}{\rho_w - \frac{4\mu'_1}{a_0^2}}}. \tag{3-31}$$

Therefore, there is a critical size below which the resonance frequency becomes imaginary. This occurs when the denominator is less than zero, when

$$a_0 \leq \sqrt{\frac{4\mu'_1}{\rho_w}}. \tag{3-32}$$

For the goldfish data, $\mu'_1 = 0.00959$ (kg/m), so with the assumption that the shear modulus is proportional to frequency squared, for

$$a_0 \leq 0.62 \text{ (cm)}$$

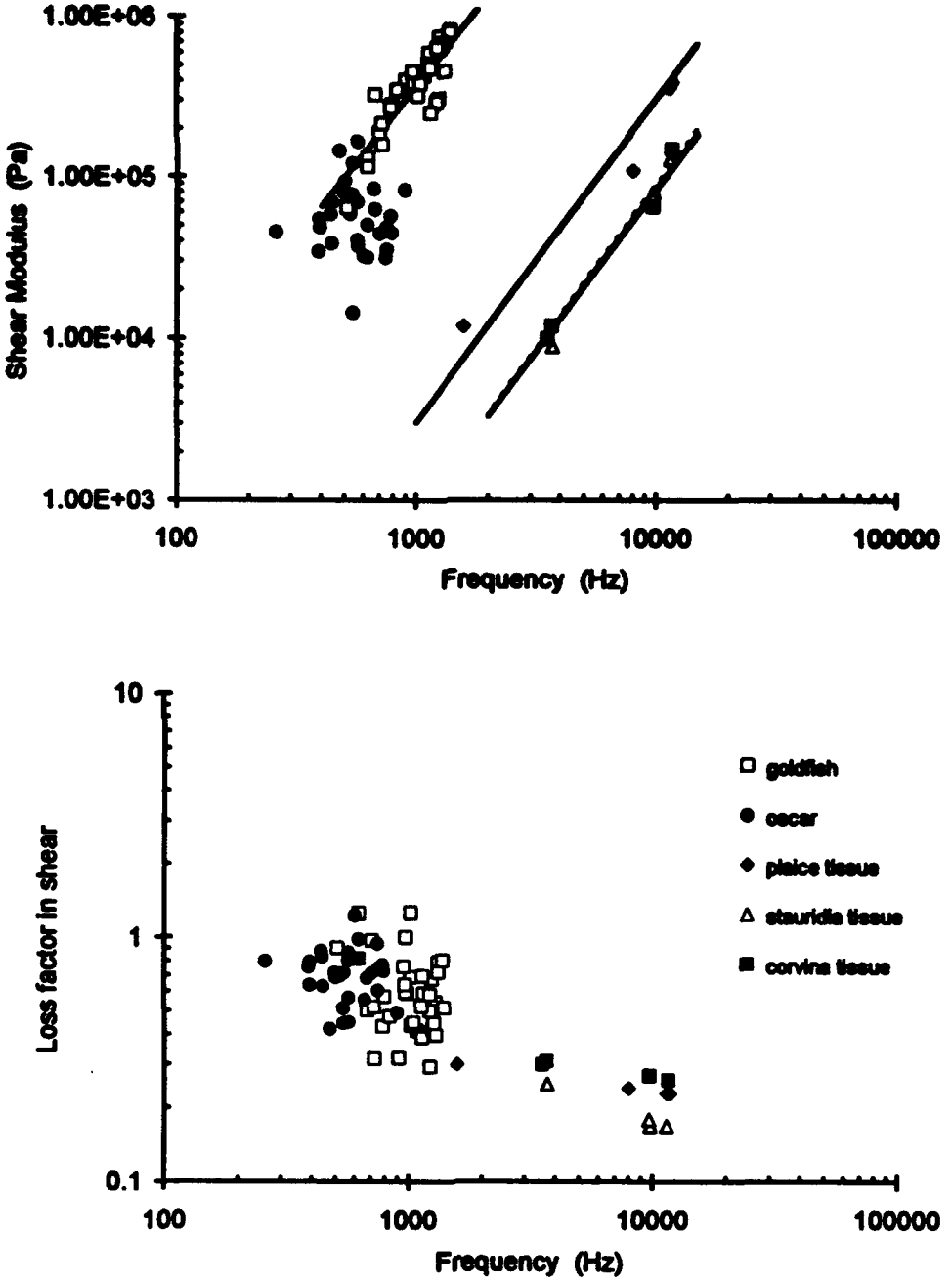

Figure 3-15. Calculated shear modulus of fish tissue, $\mu = \mu_1(1 + i\mu_2)$, from the model of Andreeva (1964) and measured values for three species (plaice, stauridia, and corvina) from Lebedeva (1965). Lines in top graph are fits to frequency squared function for the goldfish and the fish tissue. Symbols are the same for both.

there is no real resonance. Using Equation 3-2, this corresponds to a 25 gram goldfish. This curve is plotted in Figure 3-16. The most obvious problem with this result occurs when comparing with data collected for goldfish weighing less than 25 grams (see Figures A-1 to A-4).

Another approach used the power function that fits best to the goldfish data,

$$\mu(\omega) = \mu''_1 \omega_0^{n} \tag{3-33}$$

which was determined to be $\mu''_1 = 0.02623$ and $n = 1.8806$ ($R = 0.84$) Again this function was inserted into Equation 3-26 and using the relation $\omega_0^{1.8806} = \omega_0^{2}\omega_0^{-.1194}$,

$$\omega_0 = \frac{1}{a_0}\sqrt{\frac{3\gamma p_0}{\rho_w - \frac{4\mu''_1}{a_0^{2}\omega_0^{0.1194}}}}. \tag{3-34}$$

This function cannot be solved explicitly for the resonance frequency, but specific values can be determined implicitly using an iterative predictor-corrector technique. The curve for this is also shown in Figure 3-16. Although this formulation avoids having a singularity, it still doesn't fit the data well at smaller fish sizes.

For the oscars, there was no apparent correlation for the shear modulus with frequency, with an average and standard deviation of $\mu_1 = 61{,}900 \pm 33{,}900$ Pa (Figure 3-15). Using this average value for shear modulus in Equation 3-26 and using the relationship between oscar swim bladder size and mass gives

$$\omega_0 = \frac{1}{\sqrt[3]{m_f}}\left[\frac{\sqrt{\frac{3\gamma p_0 + 4\mu_1}{\rho_w}}}{\sqrt[3]{\frac{\%vol}{\rho_f \frac{4}{3}\pi}}}\right] = \frac{975.7}{\sqrt[3]{m_f}}. \tag{3-35}$$

This equation is the best fit of the oscar swim bladder data to the cubic function ($R = 0.95$) as shown in Figure 3-12.

For both the goldfish and the oscars, the loss factor, μ_2, was not well correlated with frequency. These values are shown in Figure 3-15. For the goldfish, the average and standard deviation were calculated to be $\mu_2 = 0.61 \pm 0.24$, and for the oscars,

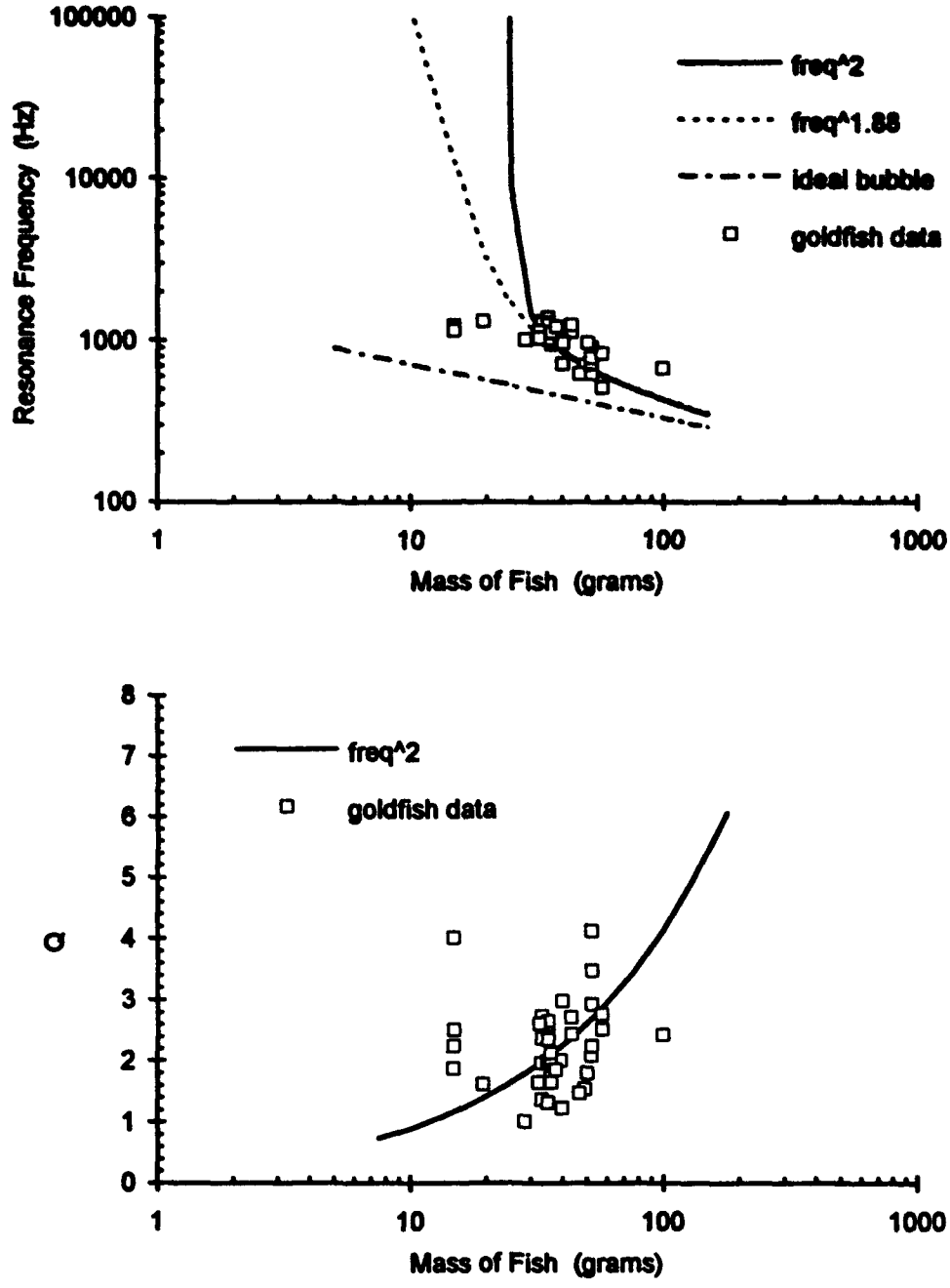

Figure 3-16. Theoretical resonance frequency vs. fish mass and quality factor vs. fish mass in the goldfish using Andreeva's model.

$\mu_2 = 0.72 \pm 0.18$. These values are a factor of two to three times higher than those of the tissue data in Lebedeva (1965). As shown in Figure 3-14, the viscous term dominates in determination of the quality factor:

$$Q \approx \frac{\rho_f \omega_0^2 a_0^2}{4\mu_1\mu_2}. \tag{3-36}$$

Inserting the resonance frequency gives

$$Q \approx \frac{3\gamma p_0 + 4\mu_1}{4\mu_1\mu_2}, \tag{3-37}$$

therefore, Q is dependent on the form of μ_1 and μ_2.

For the goldfish, if $\mu_1(\omega) = \mu'_1 \omega^2$ and μ_2 is constant, then

$$Q \approx \frac{3\gamma p_0}{4\mu'_1 \omega_0^2 \mu_2} + \frac{1}{\mu_2}. \tag{3-38}$$

Substituting in Equation 3-31 and 3-2 yields

$$Q \approx \frac{\rho_w a_0^2}{4\mu'_1 \mu_2} \tag{3-39}$$

$$\approx \left[\frac{\rho_w}{4\mu'_1 \mu_2}\left(\frac{\%\text{vol}}{2\rho_w \frac{4}{3}\pi}\right)^{\frac{2}{3}}\right] m_f^{\frac{2}{3}}. \tag{3-40}$$

This function is shown in Figure 3-16.

For the oscars, however, both μ_1 and μ_2 appear from the data to be independent of frequency, so the quality factor is also independent of frequency and equal to the average of the measured data, Q = 3.92. This is the solid line shown in Figure 3-12.

In summary for Andreeva's model, the addition of the elasticity of the tissue surrounding the swim bladder appears in the resonance frequency equation as an added spring and in the quality factor equation as viscous damping. By using constant values for this parameter, the model can be used to predict ω_0 and Q for the oscars. For the goldfish, however, the best fit for the shear modulus parameters does not allow reasonable

predictions for ω_0 and Q. Also all calculated values for μ_1 and μ_2 were much higher than the data in the literature.

Love's Spherical Fluid Shell

The third model considered was proposed by Love (1978) and consists of a small, spherical fluid shell enclosing an air cavity, in water. The shell, representing the fish body, was chosen to be made of a viscous, heat-conducting Newtonian fluid with the physical properties of fish tissue. A viscosity parameter, η_f, defined as

$$\eta_f = \tfrac{4}{3}\eta_{sf} + \eta_{bf} \tag{3-41}$$

where η_{sf} is the shear viscosity for the fish and η_{bf} is the bulk viscosity, characterizes the shell fluid. The swim bladder was modeled as a membrane of zero thickness, so that the tension in the membrane represents a surface tension. This surface tension, presumably under the fish's control, provides the increase in stiffness that causes variations in resonance frequency.

From this model, the resonance frequency was

$$\omega_0 = \frac{1}{a_0}\sqrt{\frac{3\gamma p_0 + (3\gamma - 1)\frac{2s}{a_0}}{\rho_f}} \tag{3-42}$$

where s is the surface tension. Again, the added term corresponds to an additional spring constant due to the surface tension, since it allows the swim bladder wall to support excess internal pressure. Since the surface of the swim bladder is curved, a force balance shows that there is a pressure difference across the wall (White, 1986)

$$p_{xs} = \frac{2s}{a_0} \tag{3-43}$$

where p_{xs} is the excess internal pressure. This is illustrated for a spherical membrane in Figure 3-17.

Love's model presents a damping factor H defined as

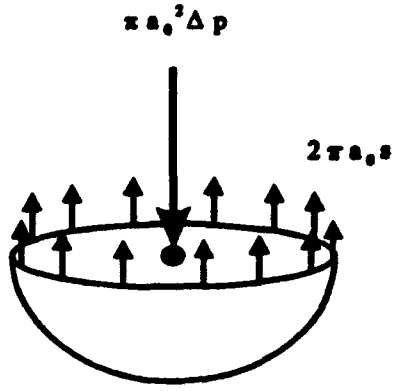

Figure 3-17. Relationship between internal pressure and surface tension..

$$\frac{\omega_0}{\omega H} = \frac{\rho_w \omega a_0}{\rho_f c_w} + \frac{3(\gamma-1)}{\omega a_0}\sqrt{\frac{\omega \kappa_s}{2\rho_s c_{ps}}}\left(1 + \frac{2s}{\rho_f \omega^2 a_0^3}\right) + \frac{2\eta_f}{\rho_f \omega a_0^2}. \qquad (3\text{-}44)$$

At resonance, $\omega = \omega_0$ and H = Q, and assuming $\rho_f \approx \rho_w$, then

$$\frac{1}{Q} = \frac{\omega_0 a_0}{c_w} + \frac{3(\gamma-1)}{\omega_0 a_0}\sqrt{\frac{\kappa_s \omega_0}{2\rho_s c_{ps}}}\left(1 + \frac{2s}{\rho_f \omega_0^2 a_0^3}\right) + \frac{2\eta_f}{\rho_f \omega_0 a_0^2}. \qquad (3\text{-}45)$$

Comparing with Equation 3-27, the first term represents radiation damping, the second thermal damping, and the third viscous damping. Figure 3-18 shows the contribution of each to the total. As with Andreeva's model, the viscous term dominates, so

$$Q \approx \frac{\rho_f \omega_0 a_0^2}{2\eta_f}. \qquad (3\text{-}46)$$

Again, the difficulty in using this model is in the precise determination of the new parameters. In his paper, Love discusses measurements of excess internal pressures in live, unanesthetized freshwater fish that correspond to surface tensions of 6 to 70 N/m (from Gee *et al.*, 1974). Alexander (1959c) presented data, shown in Table 3-3, on excess internal pressure for anaesthetized goldfish. This corresponds to surface tension data ranging from 6.5 to 17.7 N/m.

For the viscosity parameter, η_f, Love uses one set of data from direct measurements on animal tissue, while data from three other types of measurements were used to determine the viscosity indirectly. One of these was the complex shear modulus

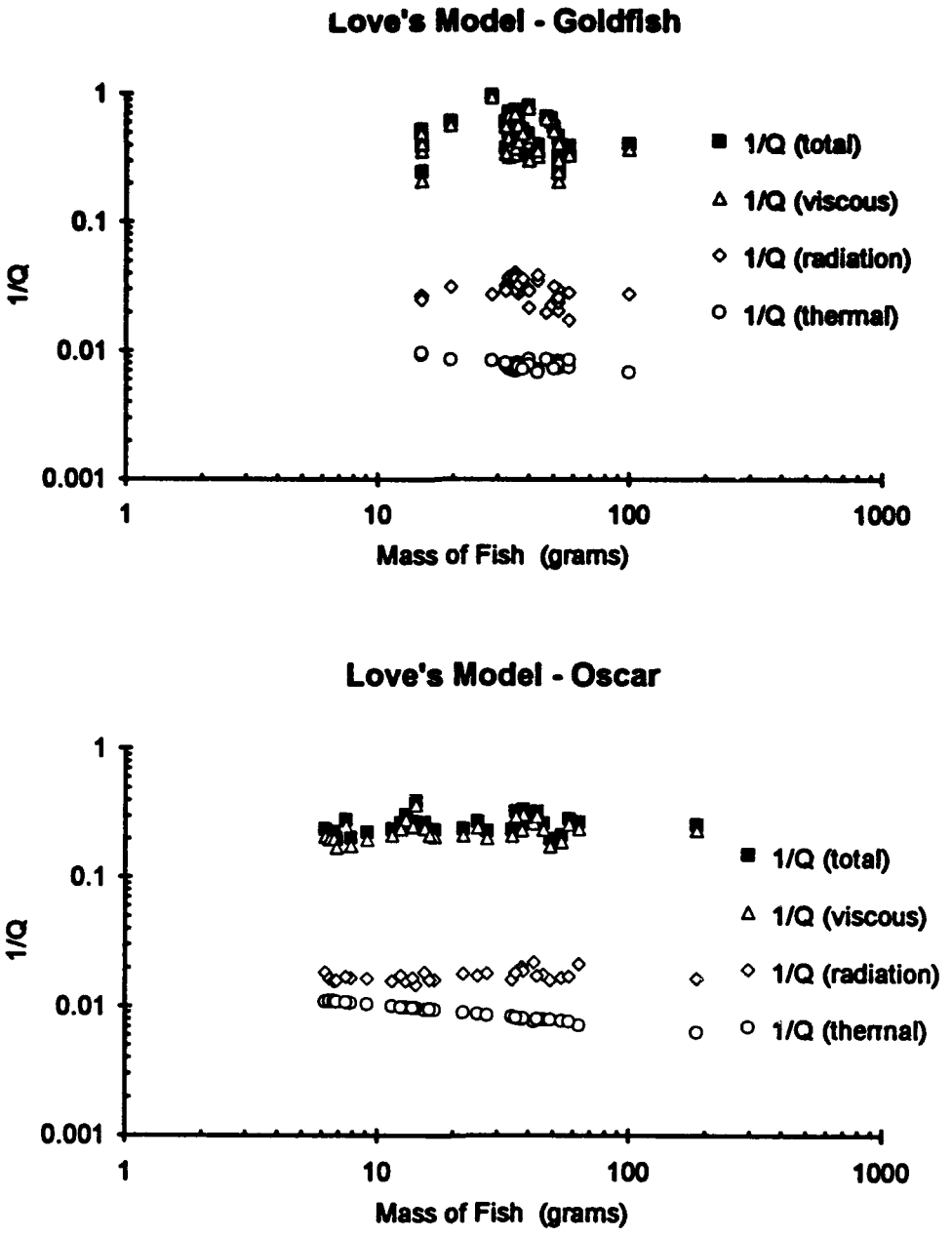

Figure 3-18. Contributions of viscous, radiation, and thermal damping to the quality factor using Love's model.

measurements of Lebedeva (1965) discussed earlier. From these, Love determined a likely range for the viscosity parameter of 5 to 200 Pa·s.

Table 3-3. Measured excess pressure, Pxs, in the swim bladders of goldfish from Alexander (1959). The first three columns are from that paper. The values of a (swim bladder radius) are calculated from Equation 3-2 and s (surface tension) from Equation 3-44.

mass (grams)	Pxs (cm Hg)	% vol.	Pxs (Pa)	a (m)	s (N/m)
35	1.8	8.9	2400	0.00719	8.6
35	3.7	8.9	4933	0.00719	17.7
40	2.8	6.3	3733	0.00670	12.5
26	1.6	7.3	2133	0.00610	6.5

By inverting Equations 3-42 and 3-45 and using the measured values for ω_0 and Q, estimates for the surface tension, s, and the viscosity parameter, η_f, were made. These are shown in Figure 3-19. For the goldfish, the values for the surface tension range from 326 to 3543 N/m and for the viscosity parameter from 22 to 148 Pa·s. For the oscars, the values of the surface tension range from 58 to 967 N/m and for the viscosity parameter from 10 to 44 Pa·s. These values for surface tension are at least an order of magnitude higher than those discussed above, while the viscosity parameter is within the likely range.

By comparing Equations 3-26 and 3-42 for the resonance frequencies and Equations 3-28 and 3-45 for the quality factor, the differences between Andreeva's model and Love's model can be noted. Andreeva's model adds stiffness in terms of a shear modulus for the tissue surrounding the swim bladder, $4\mu_1$. In Love's model, the additional stiffness can be thought of as a surface tension in the wall, $(3\gamma - 1)2s/a_0$, or as excess pressure inside the swim bladder, $(3\gamma - 1)p_{xs}$. Therefore, what was said about μ_1 is also true for p_{xs} and the plot for excess pressure is identical to the plot for shear modulus (Figure 3-15) with a change of scale by 1.25. The calculated excess pressure from this model ranges from 18,000 to 207,000 Pa for the oscars and 80,000 to 1,021,000 Pa for the goldfish. Again, these are much higher than any directly measured values.

Love effectively replaces the lossy effect of the shear modulus - $4\mu_1\mu_2$ - with a frequency dependent term - $2\eta_f\omega$. For the oscars, this translates to an inverse dependence for viscosity with frequency. But this violates the initial assumption for this model of a Newtonian fluid.

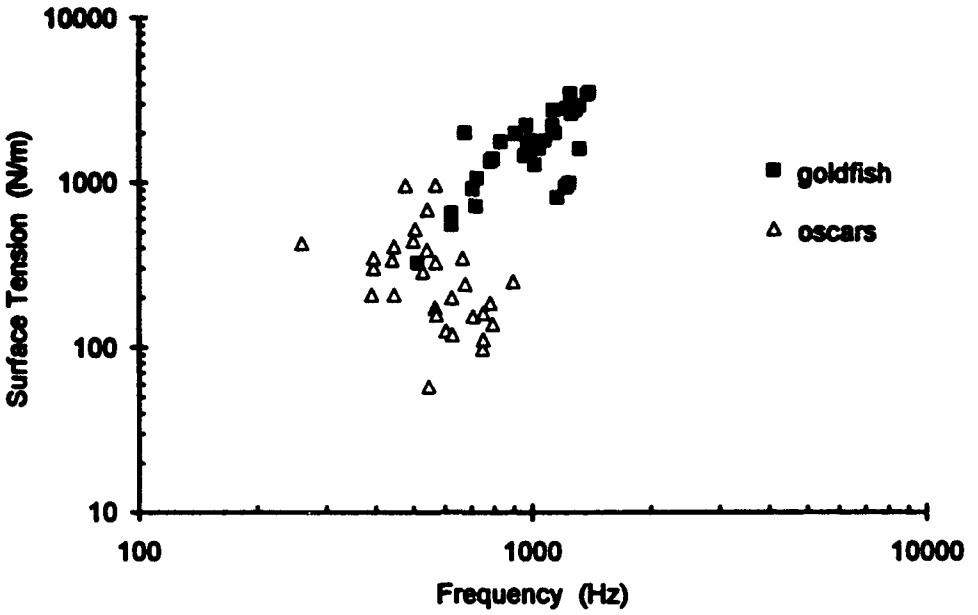

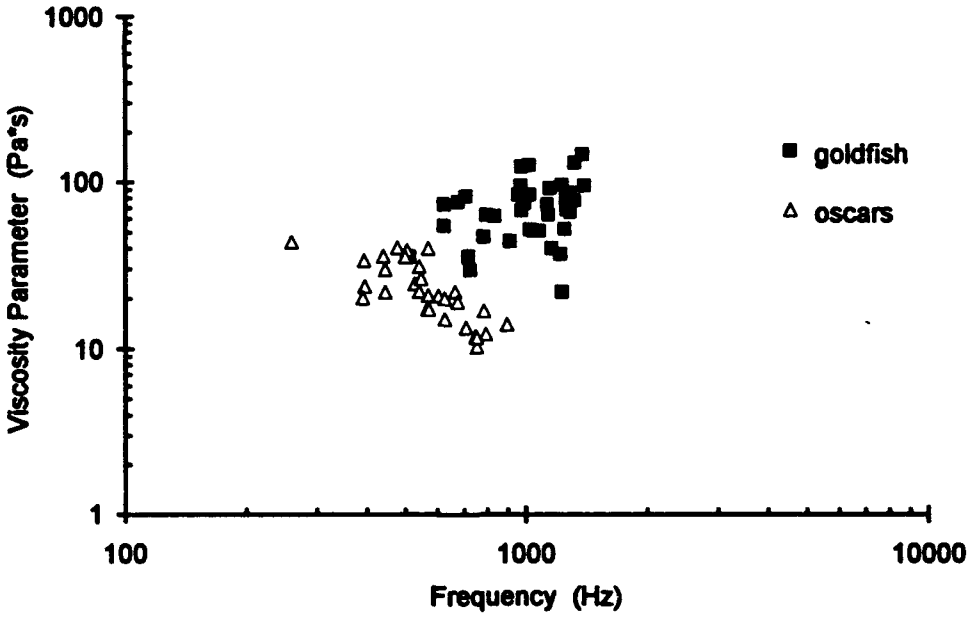

Figure 3-19. Calculated surface tension, s, and viscosity parameter, η_f, using the swim bladder resonance data and Love's model.

In summary for Love's model, the addition of the surface tension adds a spring in the form of excess pressure inside the swim bladder, which effectively raises the resonance frequency. But, the excess pressure levels needed to match this oscar data are much higher than any directly measured excess pressures. Also this data shows a frequency dependence for the viscosity parameter which does not follow the model.

The simple one degree of freedom system probably can be used to model the oscar swim bladder if an appropriate additional spring term (independent of frequency) can be found. The parameters used above, shear modulus and excess internal pressure, were not of a sufficient order of magnitude to predict the resonance frequency. Also a dominant viscous damping term can be used to determine Q if an appropriate mechanism (again independent of frequency) can be found.

The simple one degree of freedom system probably *cannot* be used to model the goldfish swim bladder. Since the swim bladder consists of two connected sacs, the mutual interaction between the two necessitates a more complex model using two degrees of freedom. The next step was to model the two chamber swim bladder of the goldfish as two coupled spherical air bubbles.

Two Resonant Air Bubbles

Shima (1971) developed a theory to calculate the natural frequencies of two spherical bubbles oscillating in water. His model included the effect of surface tension and ignored the effects of viscosity and fluid compressibility. For simplicity, the effect of surface tension will also be ignored in this application. The basic equations governing the motion of two bubbles are

$$\ddot{\xi}_1 + \frac{a_{2,0}^{\,2}}{d_{1,2}a_{1,0}}\ddot{\xi}_2 + \frac{1}{a_{1,0}^{\,2}}\frac{3\gamma p_0}{\rho}\xi_1 = 0 \qquad \text{(3-47a)}$$

$$\ddot{\xi}_2 + \frac{a_{1,0}^{\,2}}{d_{1,2}a_{2,0}}\ddot{\xi}_1 + \frac{1}{a_{2,0}^{\,2}}\frac{3\gamma p_0}{\rho}\xi_2 = 0 \qquad \text{(3-47b)}$$

where ξ_1, ξ_2, $a_{1,0}$, and $a_{2,0}$ are the displacements and radii of the two bubbles and $d_{1,2}$ is the distance between the centers of the two bubbles. These equations can be written in matrix form as

$$\begin{bmatrix} 1 & \frac{a_{2,0}^{\,2}}{d_{1,2}a_{1,0}} \\ \frac{a_{1,0}^{\,2}}{d_{1,2}a_{2,0}} & 1 \end{bmatrix} \begin{Bmatrix} \ddot{\xi}_1 \\ \ddot{\xi}_2 \end{Bmatrix} + \begin{bmatrix} \frac{1}{a_{1,0}^{\,2}} \frac{3\gamma p_0}{\rho} & 0 \\ 0 & \frac{1}{a_{2,0}^{\,2}} \frac{3\gamma p_0}{\rho} \end{bmatrix} \begin{Bmatrix} \xi_1 \\ \xi_2 \end{Bmatrix} = \begin{Bmatrix} 0 \\ 0 \end{Bmatrix}. \qquad (3\text{-}48)$$

Note that the coupling between the two is in the mass matrix. This can be more easily understood by considering the physical system, as shown in Figure 3-20. For the individual bubble, the spring is due to the compressible air within. This does not change upon introduction of other bubbles. The mass, however, is the mass of the surrounding fluid. Two bubbles oscillating in phase are having to displace the fluid mass between the two in the opposite direction, raising the effective mass and lowering the resonant frequency. In out of phase oscillation, the bubbles displace the fluid mass between the two in the same direction, reversing the effect.

From the governing equations, Shima determined the resonance frequencies to be

$$\omega_i = \frac{1}{a_{1,0}} \sqrt{\frac{3\gamma p_0}{\rho}} \sqrt{\frac{\left(1 + \frac{a_{2,0}^{\,2}}{a_{1,0}^{\,2}}\right) \pm \sqrt{\left(1 - \frac{a_{2,0}^{\,2}}{a_{1,0}^{\,2}}\right)^2 + 4\frac{a_{2,0}^{\,3}}{d_{1,2}^{\,2}a_{1,0}}}}{2\frac{a_{2,0}^{\,2}}{a_{1,0}^{\,2}}\left(1 - \frac{a_{1,0}a_{2,0}}{d_{1,2}^{\,2}}\right)}}. \qquad (3\text{-}49)$$

The resonance frequencies for a range of $a_{2,0} / a_{1,0}$ ratios for a fixed $d_{1,2}$ are shown in Figure 3-21 along with the resonance frequencies of the uncoupled individual bubbles. These values were calculated for the same 37.6 gram goldfish described earlier. Assuming equal volume swim bladders ($a_{2,0} / a_{1,0} = 1$), the resonance frequency for each uncoupled

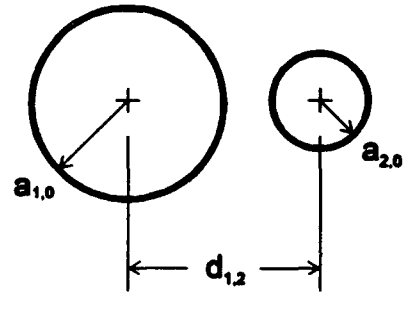

Figure 3-20. Geometry for the oscillation of two spherical bubbles, from Shima (1971).

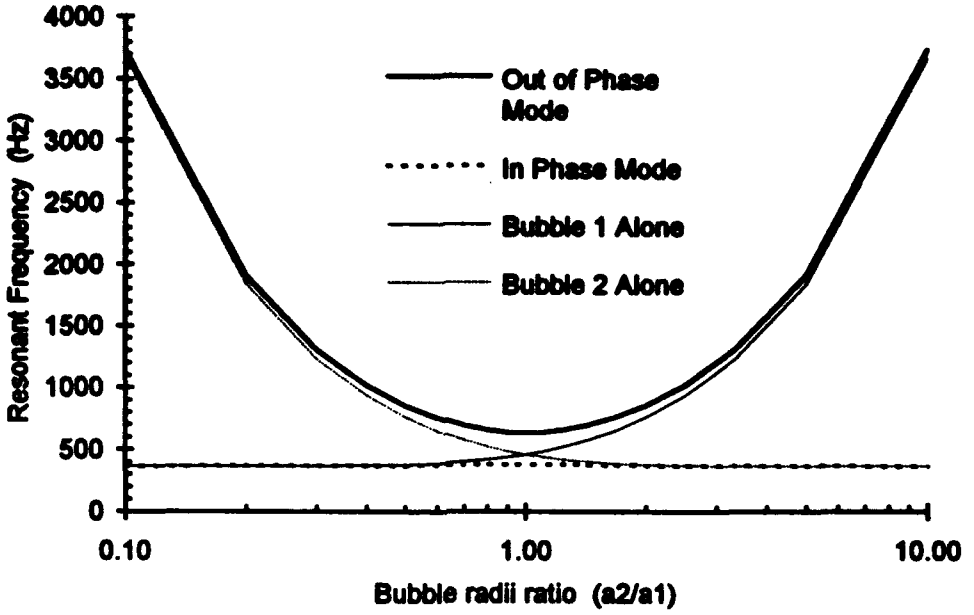

Figure 3-21. Calculated resonant frequencies for the in phase and out of phase modes for two coupled bubbles and the resonant frequencies of the individual bubbles as a function of the ratio of the bubble radii.

swim bladder was calculated using Equation 3-21 to be 462 Hz. For the coupled system, the resonance frequencies were 381 and 637 Hz. As the difference between the radii increases, the in phase resonance frequency for the coupled bubbles decreases and the out of phase increases. For all ratios, the in phase resonance for the coupled system was lower than the resonance of the larger bubble, and the out of phase was higher than the smaller bubble.

Zabolotskaya (1984) extended this analysis by adding the acoustic pressure, p, as a forcing function

$$\ddot{\xi}_1 + \frac{a_{2,0}^{\ 2}}{d_{1,2}a_{1,0}}\ddot{\xi}_2 + \frac{1}{a_{1,0}^{\ 2}}\frac{3\gamma p_0}{\rho}\xi_1 = -\frac{1}{\rho a_{1,0}}p \qquad (3\text{-}50a)$$

$$\ddot{\xi}_2 + \frac{a_{1,0}^{\ 2}}{d_{1,2}a_{2,0}}\ddot{\xi}_1 + \frac{1}{a_{2,0}^{\ 2}}\frac{3\gamma p_0}{\rho}\xi_2 = -\frac{1}{\rho a_{2,0}}p. \qquad (3\text{-}50b)$$

By assuming a harmonic solution and inverting the resultant impedance matrix, the displacement amplitudes as a function of frequency for the coupled bubbles were calculated to be

$$\xi_1 = \frac{\left(\omega_{2,0}^2 - \omega^2\right)\frac{p}{\rho a_{1,0}} + \omega^2 \frac{a_{1,0}^2}{d_{1,2} a_{2,0}} \frac{p}{\rho a_{2,0}}}{\left(\omega_{1,0}^2 - \omega^2\right)\left(\omega_{2,0}^2 - \omega^2\right) - \omega^4 \frac{a_{1,0} a_{2,0}}{d_{1,2}}} \tag{3-51a}$$

$$\xi_2 = \frac{\omega^2 \frac{a_{2,0}^2}{d_{1,2} a_{1,0}} \frac{p}{\rho a_{1,0}} + \left(\omega_{1,0}^2 - \omega^2\right)\frac{p}{\rho a_{2,0}}}{\left(\omega_{1,0}^2 - \omega^2\right)\left(\omega_{2,0}^2 - \omega^2\right) - \omega^4 \frac{a_{1,0} a_{2,0}}{d_{1,2}}}. \tag{3-51b}$$

where $\omega_{1,0}$ and $\omega_{2,0}$ are the resonance frequencies of the uncoupled bubbles. Equation 3-11 was then used to calculate the scattering cross section. Figures 3-22 and 3-23 show the response of the two bubbles for $a_{2,0} / a_{1,0}$ ratios of 0.50, 0.80, 0.95, and 1.00, representing the same 37.6 gram goldfish. Note that for moderate size differences, both the smaller and larger bubble shows twin peaks in their response curves.

Zhou (1992) took the mass coupled equations of Zabolotskaya (1984) and converted them to a stiffness coupled form, modeling the two chambered swim bladder as a two degree of freedom oscillator driven by harmonic motion of the base. Experimental measurements were performed on a two bubble system using NIVAMS, and the results were used to empirically determine the coupling stiffness term. Unfortunately, this conversion from mass coupling to stiffness coupling was unnecessary and obscures the physics of the problem.

When comparing the theoretical response to the goldfish data, two points can be made. First, the coupled two bubble model was able to mimic the general shape of the measured response curves. Second, though, the resonance frequencies predicted for the lower mode of the coupled system was below that of the larger bubble. The fish's measured swim bladder resonance was typically over twice the uncoupled resonance frequency [Figure 3-7].

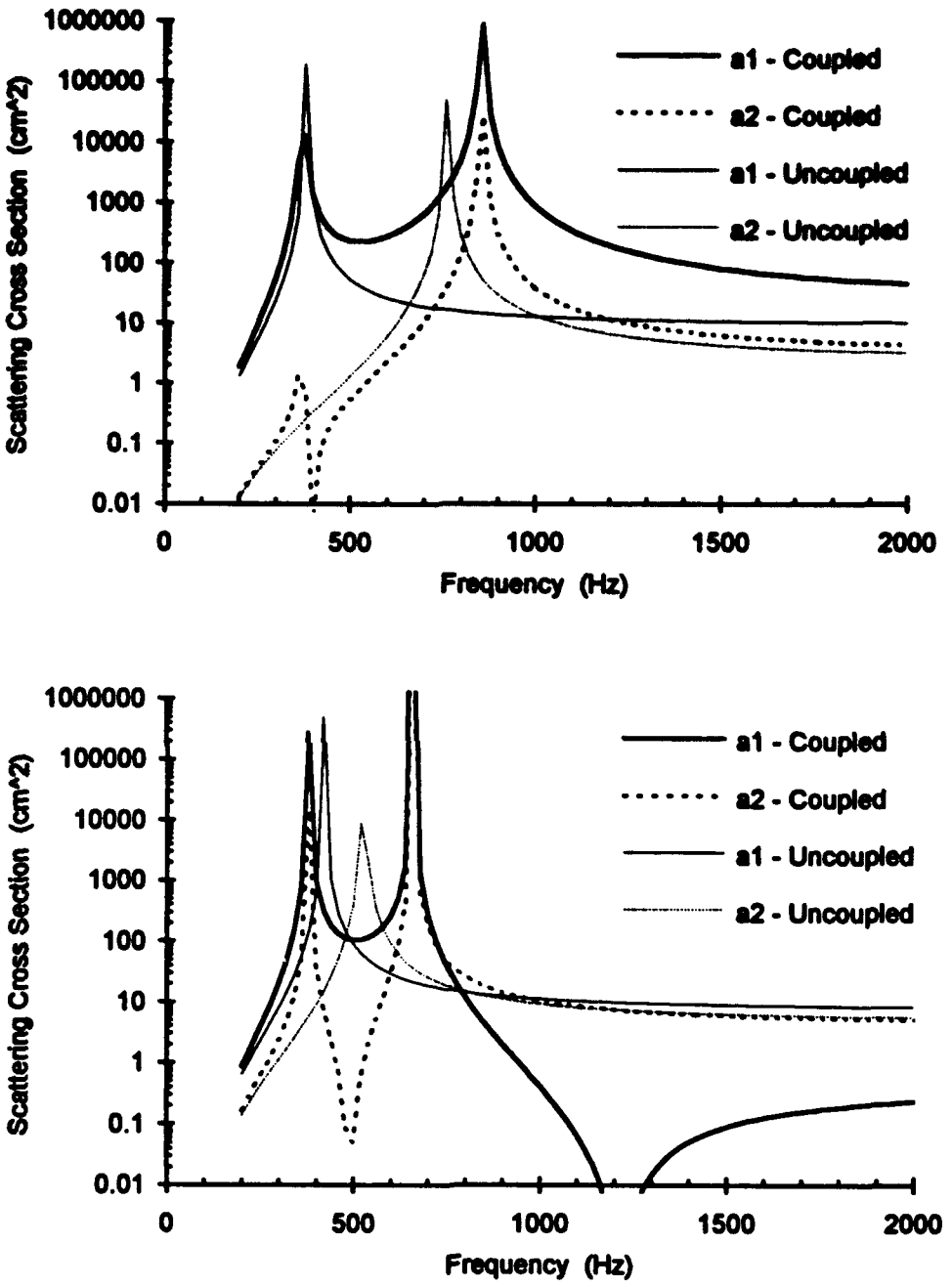

Figure 3-22. Calculated frequency response curves for a coupled and uncoupled pair of bubbles. In the top graph, the radii ratio, a2/a1, is 0.50 and the bottom is 0.80.

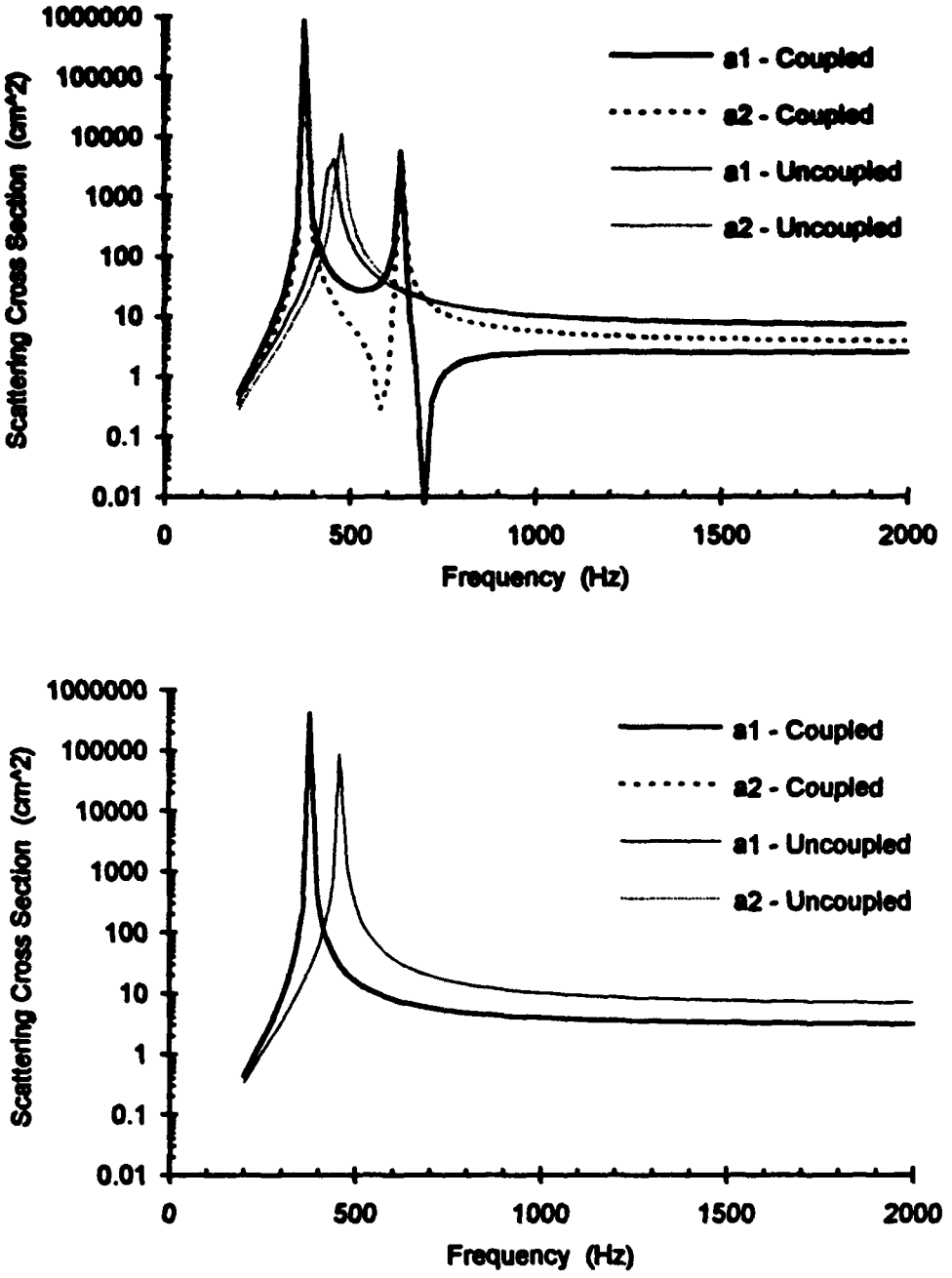

Figure 3-23. Calculated frequency response curves for a coupled and uncoupled pair of bubbles. In the top graph, the radii ratio, a2/a1, is 0.95 and the bottom is 1.00.

The important results from this data is that the swim bladders of oscars and goldfish do scatter significant amounts of sound. Also, for the single chambered swim bladder of the oscar, the frequency of greatest scattering for even a relatively small fish can be within the hearing range of many fish.

Chapter 4

Thresholds to Scattered Ambient Noise

The previous experiment demonstrated that the swim bladders of fish can be excellent scatterers of ambient noise. The next task of this thesis was to measure the ability of goldfish to detect this scattered ambient noise in the ambient noise field. To do this, an experimental apparatus (Scattered Ambient Noise Experiment Station) was devised to determine detection thresholds.

A preliminary study showed goldfish could detect simulated scattered ambient noise in an ambient noise masker (Rogers *et al.*, 1989). In this study, two goldfish (about 15 cm in length) were classically conditioned to suppress their heart rate upon presentation of an acoustic stimulus simulating the scattered noise. Otis *et al.* (1957) were the first to demonstrate classical heart rate conditioning in goldfish. Since then, this technique has been used to measure intensity thresholds and other discrimination capabilities in various fish (Buerkle, 1967, 1968; Chapman and Johnstone, 1974; Chapman and Sand, 1974; Offutt, 1971; Sand and Karlsen, 1986).

A spherical piezoelectric transducer simulated the noise scattered by the swim bladder of a fish. The scattered noise signal was simulated instead of having another live fish scatter the ambient noise to prevent detection through other sensory stimuli. If another fish had been used, it would have to have been surrounded by an acoustically transparent barrier impervious to potential visual, chemical, or hydrodynamic cues.

Two studies were made using SANES. The first measured the change in threshold with change in distance from the transducer to the observer. The goal was to determine the acoustic variable detected at threshold. The second measured the change in threshold with change in center frequency of the scatterer. The purpose was to determine the frequency characteristics at threshold. Then SANES was modified to use two spherical transducers to determine if the goldfish could discrimination scattered noise signals differing only in source direction. The results from these studies were then compared to similar work in the literature.

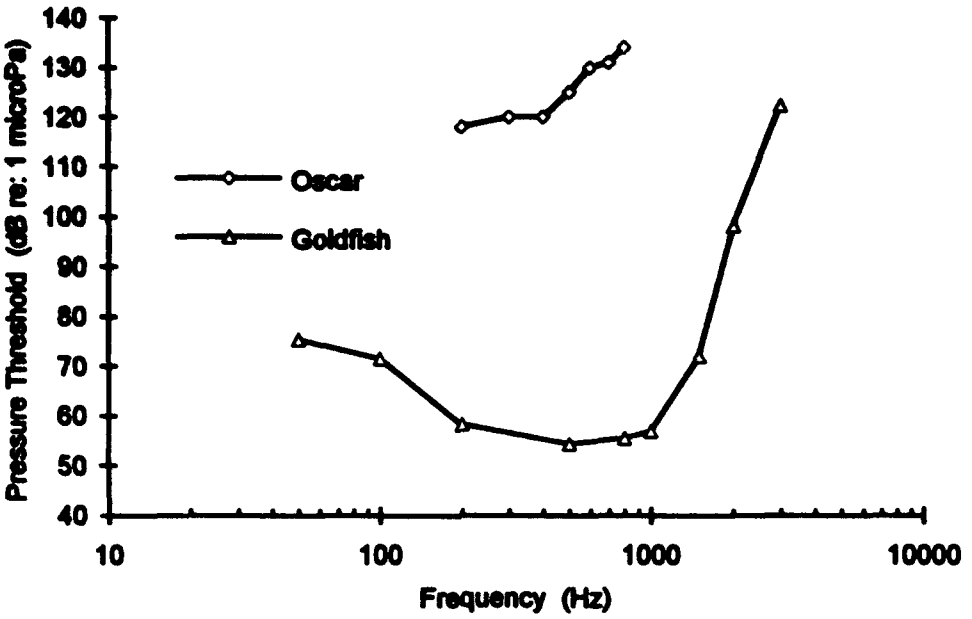

Figure 4-1. Sound pressure audiograms for the oscar (top) and the goldfish (bottom). Oscar audiogram is from Yan and Popper (1992) and goldfish from Jacobs and Tavolga (1967).

Unfortunately, not all fish species have been conditioned with electric shock, including cichlids (Yan and Popper, 1991). Oscars are in this family. Also recent behavioral tests using a positive reward technique discovered that sensitivity thresholds for the oscar, shown in Figure 4-1, are 60 to 80 dB higher than for the goldfish measured using the same technique (Yan and Popper, 1992). For these reasons, no attempt was made to measure detection thresholds for oscars using SANES.

Experimental Method - SANES

Figure 4-2 shows the final configuration for SANES used in measuring detection thresholds. A restrainer held the individual fish in a fixed location within a 388 liter glass aquarium (1.17 m x 0.72 m x 0.46 m). The restrainer, designed by Abrahamson (1988), consisted of two rings of high density Teflon™. One ring surrounded the head with the fish's eyes protruding through and allowed for normal respiratory movement of the gill covers. The other ring surrounded the fish's tail section near the anal fin to prevent the

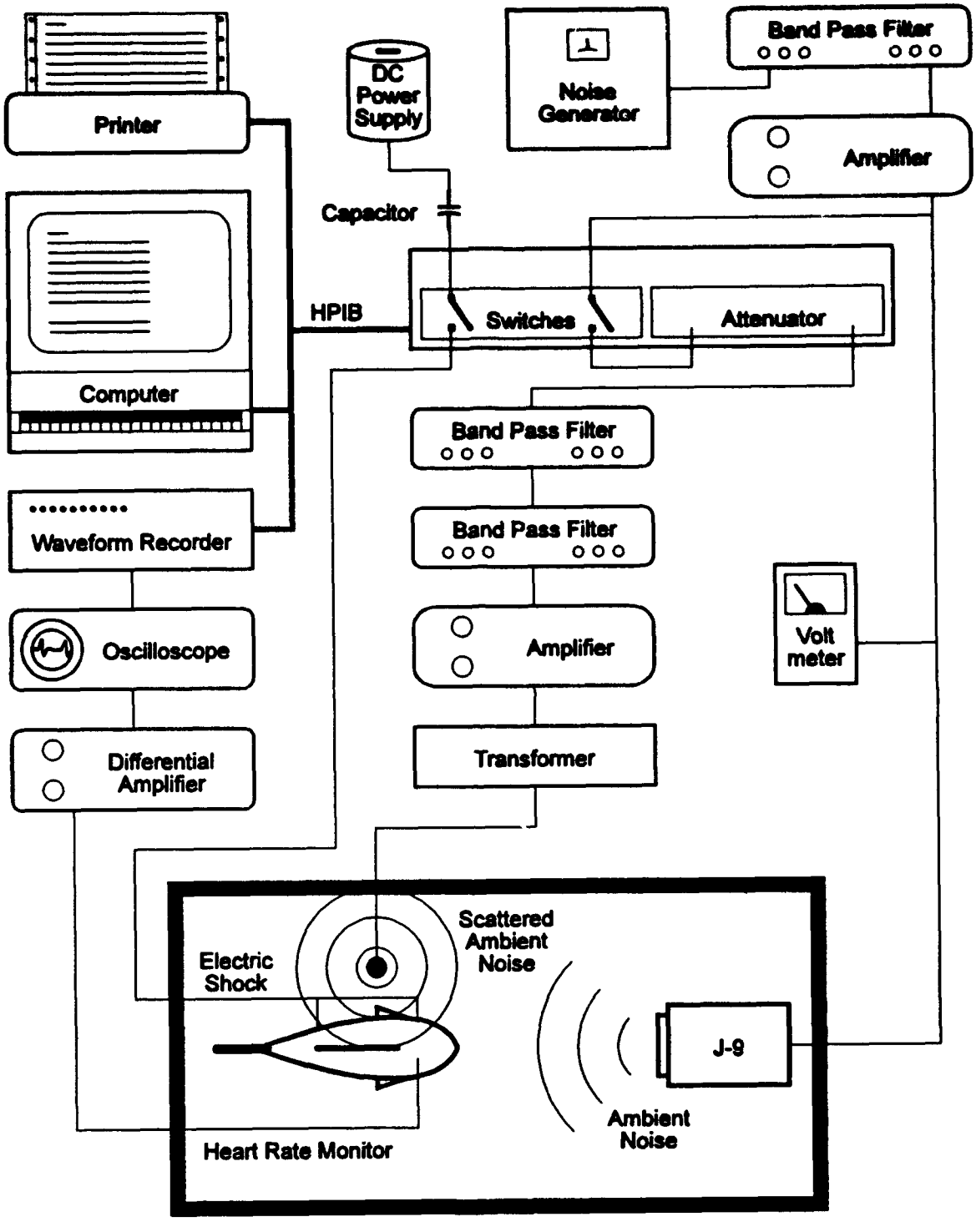

Figure 4-2. Scattered ambient noise experiment station (SANES).

fish from wriggling free. The aquarium rested on a table, supported by eight air-spring isolators (4.10/3.50 - 5 butyl inner tubes) to decouple the tank from floor vibrations. The table was placed on the carpeted floor of an environmental chamber intended to isolate the tank from airborne sound.

A USRD J-9 underwater transducer filled the aquarium with white noise (Brüel & Kjær 1405 noise generator) that had been band pass filtered between 200 and 1200 Hz (Wavetek 753A filter) and amplified (QSC 1400 amplifier). The simulated scattered signal mimicking the resonant swim bladder was the same white noise selectively attenuated (Wavetek 617 attenuator), bandpass filtered around the desired center frequency (Krohn-Hite 3100A filter and Wavetek 432 filter), and amplified (QSC 1400 amplifier). This filtered signal was impedance matched (Krohn-Hite MT-56R) and sent to a 19 mm dia. spherical piezoelectric transducer (proprietary). The transducer was positioned on the left side of the subject along a line 30 degrees caudal to a normal of the sagittal plane of the fish (Figure 4-3). Ranges along this imaginary line were measured from the center of the subject's ear to the center of the spherical transducer in the horizontal plane.

The heart activity of the fish was monitored using stainless steel electrodes implanted on both sides of the heart, using the technique as described in Roberts *et al.* (1973). The electrodes were fabricated from no. 8 stainless steel needles and coated with polyurethane except at the tips. Two were inserted through the ventral side of the fish, one on each side of the heart. The electrodes were adjusted in insertion depth for maximum signal-to-noise.

The ECG signal from the electrodes was amplified (Bak MDA-3 differential amplifier) monitored by an oscilloscope (Tektronics 2230), and sent to a waveform recorder (HP 5180A) for computer interfacing. The waveform recorder was used as a discriminator to determine the occurrence of heartbeats while the computer (HP 236) measured and recorded the intervals between heartbeats. The electrical stimulation was provided by the discharge of a capacitor (charged to 16-24 VDC) triggered to surface electrodes mounted in the rings near the head and the tail of the subject. The mild electric discharge through the fish's body caused a transient increase in the heartbeat interval.

The experiment was directed by the computer through the HPIB. The computer initiated the recording of the heart rate, switched on the conditioned stimulus,

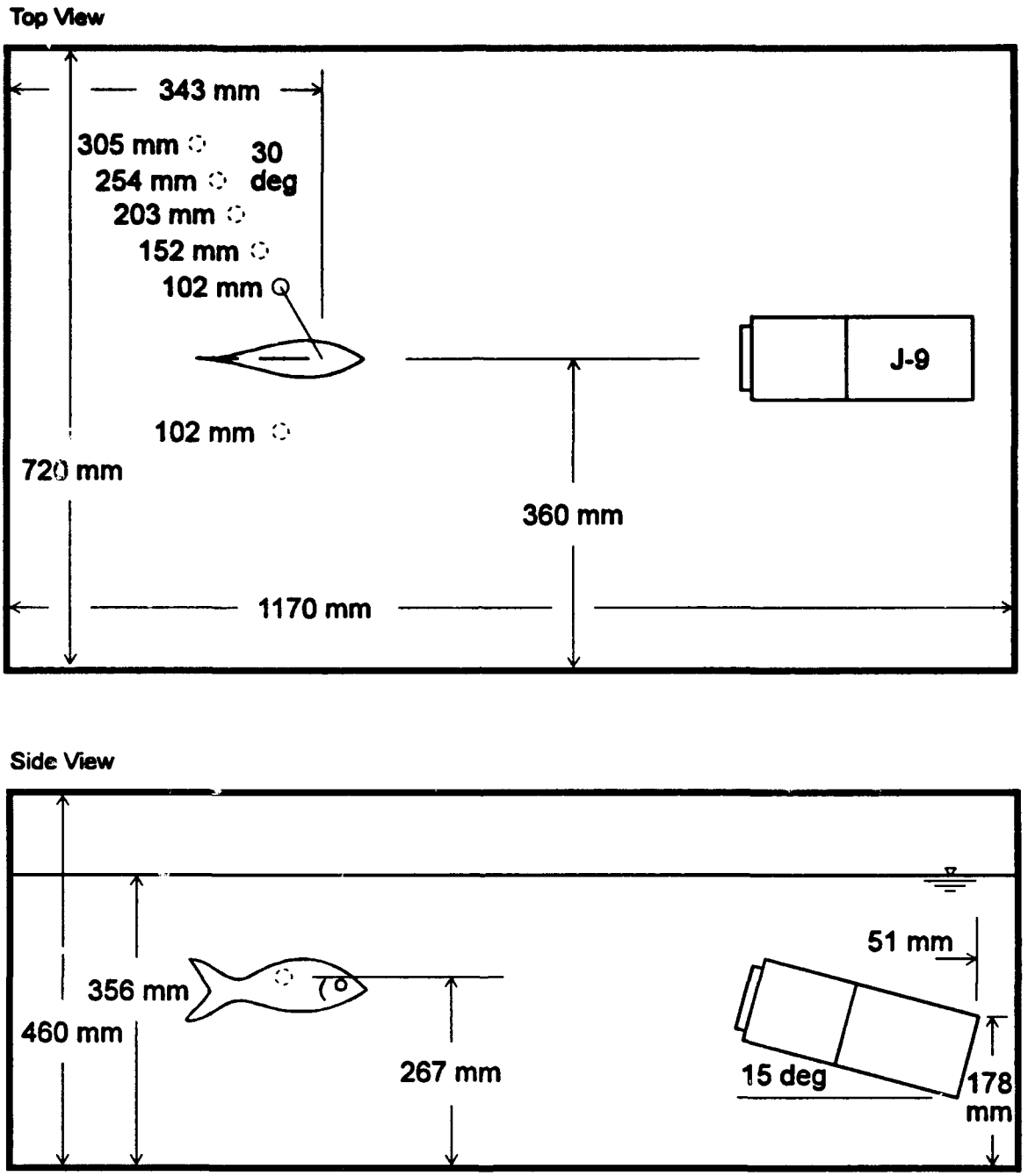

Figure 4-3. Position of the transducers and the fish in the test tank. The holders for the fish and the transducers are not shown. The range and center frequency studies used one spherical transducer on the left side of the subject. The directional discrimination study required identical transducers on both sides.

administered the shock, and determined the random time interval between trials. After each trial, data analysis determined the level of the stimulus for the next trial.

A conditioning or test trial began with the measurement of 10 heartbeat intervals to establish the current resting interval. On the eleventh heartbeat the conditioned stimulus (CS), the scattered ambient noise, was presented. On the next heartbeat an electric shock, the unconditioned stimulus (US), was paired with the termination of the CS. The time between trials was randomized between 1 and 3 minutes. Catch trials (no CS) were randomly interspersed to measure false alarms.

The subject was first trained with the CS at a 'loud' level until a consistent conditioned response (CR) was obtained. The detection criterion for the CR was defined as the heartbeat interval during the CS of at least 1.645 times the standard deviation longer than the mean of the resting heartbeat intervals. Detection and miss trials are illustrated in Figure 4-4. Thresholds were measured using a single staircase procedure with 3 dB increments in CS attenuation and calculated as the average of eight consecutive pass-fail transitions (Figure 4-5). After one threshold was determined, the CS was changed and the program repeated. One to four thresholds were measured in a given session. For the range study, the transducer was moved while for the center frequency study, the cutoff frequencies of the bandpass filters were set to the specified center frequency. Data for which the false alarm rate exceeded 25 percent was not used.

The sound pressure levels for the background, ambient, and scattered signals were measured by replacing the fish with a hydrophone (B&K 8103) positioned in the same location as the fish's ear. The background noise was measured using the spectrum analyzer with both the J-9 and the spherical projector disconnected. The ambient noise level produced by the J-9 was measured, then sound pressure levels for the scattered ambient noise were recorded as a function of range from the source to the hydrophone and as a function of center frequency of the scatterer. This data is shown in Appendix D.

Heavy filtering of the ambient noise signal helped reduce acoustical problem in the system. High pass filtering of the ambient noise at 200 Hz minimized tank wall resonances at low frequencies (below 100 Hz); low pass filtering at 1200 Hz minimized the volume resonance of the aquarium. Previous testing indicated that the principle volume mode of the tank was near 2000 Hz.

```
Trial number  42


I =   0   Etime =  1.51
I =   1   Etime =  4.55  Interval =   3.04
I =   2   Etime =  7.67  Interval =   3.12
I =   3   Etime = 10.81  Interval =   3.14
I =   4   Etime = 13.47  Interval =   2.66
I =   5   Etime = 16.67  Interval =   3.20
I =   6   Etime = 19.99  Interval =   3.32
I =   7   Etime = 23.54  Interval =   3.55
I =   8   Etime = 27.33  Interval =   3.79
I =   9   Etime = 30.27  Interval =   2.94
I =  10   Etime = 33.20  Interval =   2.93
I =  11 * Etime = 39.73  Interval =   6.53
Criterion =  3.702 PASSED at -27 dB on a Test trial


Trial number  43


I =   0   Etime =   .29
I =   1   Etime =  3.58  Interval =   3.29
I =   2   Etime =  6.64  Interval =   3.06
I =   3   Etime =  9.73  Interval =   3.09
I =   4   Etime = 12.68  Interval =   2.95
I =   5   Etime = 15.12  Interval =   2.44
I =   6   Etime = 18.14  Interval =   3.02
I =   7   Etime = 22.13  Interval =   3.99
I =   8   Etime = 25.17  Interval =   3.04
I =   9   Etime = 27.77  Interval =   2.60
I =  10   Etime = 31.68  Interval =   3.91
I =  11 * Etime = 34.71  Interval =   3.03
Criterion =  3.950 Failed at -30 dB on a Test trial
```

Figure 4-4. Examples of detection (number 42) and miss (number 43) trials. The criterion listed in the last line is 1.645 times the standard deviation plus the mean of the resting heartbeat intervals.

An attempt was made to study the change in threshold with change in bandwidth of the scattered signal. The nature of the output from the spherical transducer made this impossible. For a white noise voltage input, the sound pressure output was proportional to frequency squared. The filters available could not overcome this problem.

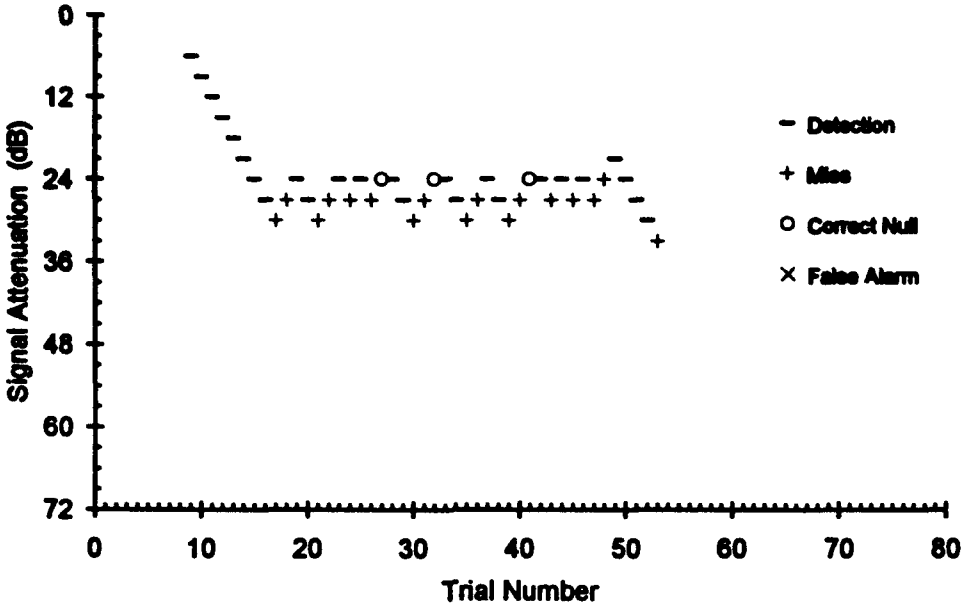

Figure 4-5. An example of a threshold measurement series. The threshold was calculated as the average of eight consecutive pass-fail transitions.

To investigate directional discrimination, SANES was modified to use two identical spherical projectors as shown in Figure 4-6. The first transducer was fixed on the left side along the same orientation used previously at a range of 10.2 cm. The second transducer was fixed on the right side symmetric to the first along the medial plane of the fish. Since the fish was located along the center line of the tank and the transducers placed symmetrically, then the only difference in the acoustic sources should have been direction.

The signal used was the 750 Hz center frequency noise. The switches split the noise signal after the attenuator and the second round of filtering. Identical filters, amplifiers (the L and R channels of the QSC 1400), transformers, and spherical transducers produced indistinguishable sound fields.

To determine directional discrimination, the program was changed. One transducer (right or left) continually pulsed scattered noise. Heartbeats were used as the trigger; one heartbeat switched the signal on, the next switched it off. To eliminate the

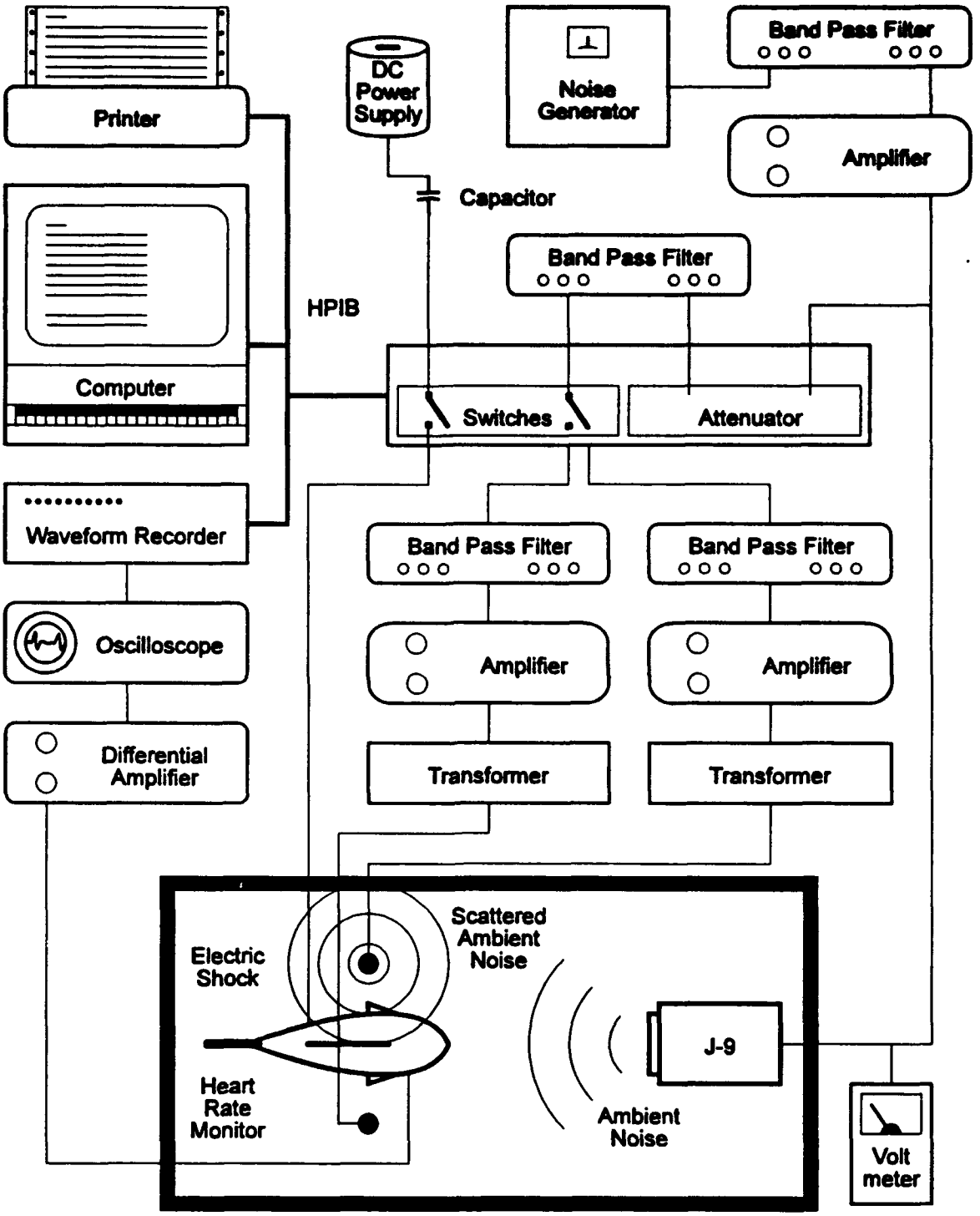

Figure 4-6. Scattered ambient noise experiment station modified for directional discrimination.

possibility of discrimination from intensity difference cues, the signal amplitude from pulse to pulse was varied randomly within a 12 dB range (3 dB steps). A conditioning trial began with the measurement of 10 heartbeat intervals (5 on, 5 off) to establish the current resting interval. On the eleventh heartbeat, the scattered noise was pulsed using the opposite transducer. On the next heartbeat, an electric shock coincided with the termination of the noise. Then pulses from the original transducer resumed. The time between trials was randomized between 1 and 3 minutes. The same detection criterion was used as before. The level of the signal used was at least 21 dB above the detection thresholds previously established .

The hydrophone was also used in the test of the system for transient clicks from the switched noise signals. Typically, photo conductive switches with long rise and fall times are used. SANES, however, used the computer controlled power relays switches (Wavetek 614) to drive reed type DIP switches (Magnecraft W171DIP-25) on the noise lines. Since transients are typically high frequency in nature, the filtering of this signal followed the switching eliminated this problem. The output from the hydrophone was pre-amplified (Ithaco 1201) and re-amplified through a boom box to headphones (Sony MDR-A10). An independent observer listening to the scattered noise did not report hearing turn-on or turn-off transients. At the fish's threshold, the observer was unable to detect the scattered noise signal. The observer was also unable to discriminate the different sources at the hydrophone in the directional study.

Experimental Results

Table 4-1 shows the number of data points collected for the two range studies (610 Hz and 750 Hz center frequency) and the center frequency study (15.2 cm range). All of the goldfish were approximately 15 cm in standard length (from the tip of the nose to the base of the caudal fin). Different masses indicate different subjects. The values for all of the data points are given in Appendix E in terms of signal level at threshold and signal-to-noise (S/N) measured as spectral density. Three data points for one subject overlap two of the studies. The 78.9 gram goldfish was used for both the range study at 750 Hz and the center frequency study.

The initial range study was made on five goldfish using a center frequency of 610 Hz. This was chosen to be near the center of the ambient noise band (200 - 1200 Hz).

Table 4-1. Number of successful threshold data points taken using SANES for the two range studies and the center frequency study. *Different masses indicate individual goldfish.*

Range Studies - 110 Data Points Total

610 Hz Center Frequency

	Centerline Distance from Transducer to Fish's Ear (Range)				
Mass of Fish	10.2 cm	15.2 cm	20.3 cm	25.4 cm	30.5 cm
76.8 g.	3	2	1	-	3
80.8 g.	3	1	3	2	3
90.3 g.	3	1	3	1	-
114.3 g.	4	-	3	3	-
118.9 g.	3	3	-	3	-

750 Hz Center Frequency

74.6 g.	3	3	3	3	3
77.2 g.	3	3	3	3	-
78.9 g.	1	3	-	2	2
80.2 g.	3	3	3	-	3
102.3 g.	3	3	3	3	3

Center Frequency Study - 42 Data Points Total

15.2 cm Range

	Center Frequency of Scattered Noise				
Mass of Fish	300 Hz	450 Hz	600 Hz	750 Hz	900 Hz
78.9 g.	3	3	4	3	4
82.2 g.	4	3	3	3	3
87.7 g.	2	-	3	1	3

The averages of the data points at each range for each subject are shown in Figure 4-7. The individual data points are shown in Appendix E - Table E-1 and Figures E-1 through E-5. The bottom graph is the same data in terms of signal density to noise density measured at 610 Hz. Since the noise density was independent of the location of the scattered noise transducer, the difference between the top and bottom data is a constant - 47.6 dB, which is equal to 20 times the logarithm of the noise density. A first order approximation for the data would be to assume that the pressure threshold for the individual goldfish was independent of range.

Later, the range study was repeated on five different goldfish using a center frequency of 750 Hz. The center frequency was changed to move away from the anomalous peak in the noise spectrum at 545 Hz. The averages of the data points at each range for each subject are shown in Figure 4-8. The individual data points are shown in Appendix E - Table E-2 and Figures E-6 through E-10. Again, the bottom graph is the same data in terms of signal density to noise density at 750 Hz. The difference for this data is about -48 dB. Again, it appears that there was no dependence on range for the pressure threshold. The dramatic differences between individuals was not present this time.

The center frequency study was performed on three goldfish, including one from the previous study, at a 15.2 cm range. This range was chosen to allow plenty of dynamic range for the scattered noise signal. The averages of the data points at each center frequency for each subject are shown in Figure 4-9. The individual data points are shown in Appendix E - Table E-3 and Figures E-11 through E-13.

One complication with interpreting the data from this study is that the simulated ambient noise density was not independent of frequency. Figure 4-10 shows measured simulated ambient noise density using 3 different bandwidths (BW). There is an anomalous peak at 545 Hz that is 20 dB above the noise level measured by the narrowest bandwidth. It's origin was never determined. The elevation of the data at 600 Hz was probably due to the proximity to the noise spike at 545 Hz in the ambient noise spectrum. Figure 4-11 shows the effect of bandwidth selection on the center frequency study data.

Attempts were made to condition the four goldfish from the range study at 750 Hz to discriminate between two sources differing only in location. None of the four fish could

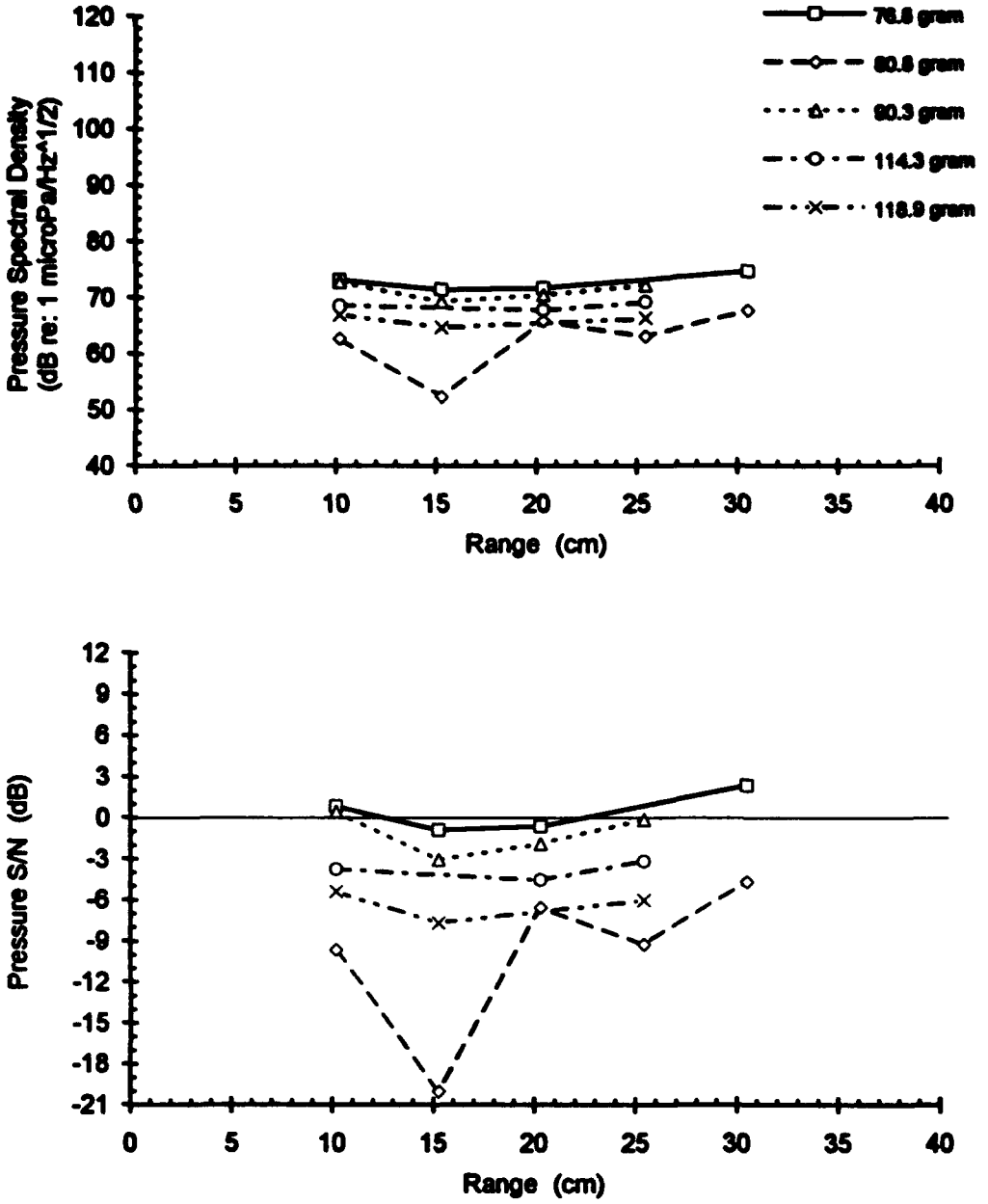

Figure 4-7. Data for the threshold versus range study using 610 Hz center frequency scattered noise.

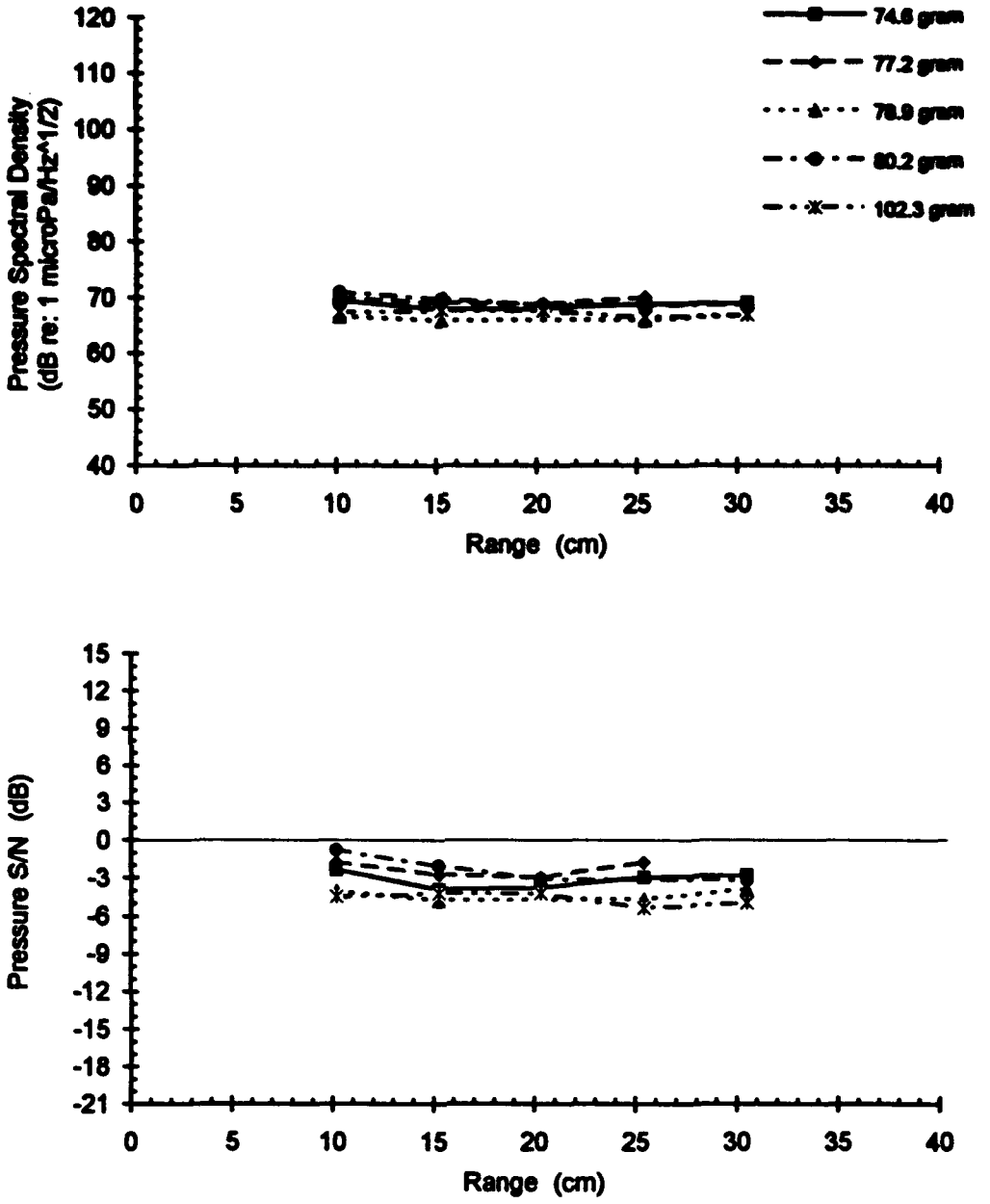

Figure 4-8. Data for the threshold versus range study using 750 Hz center frequency scattered noise.

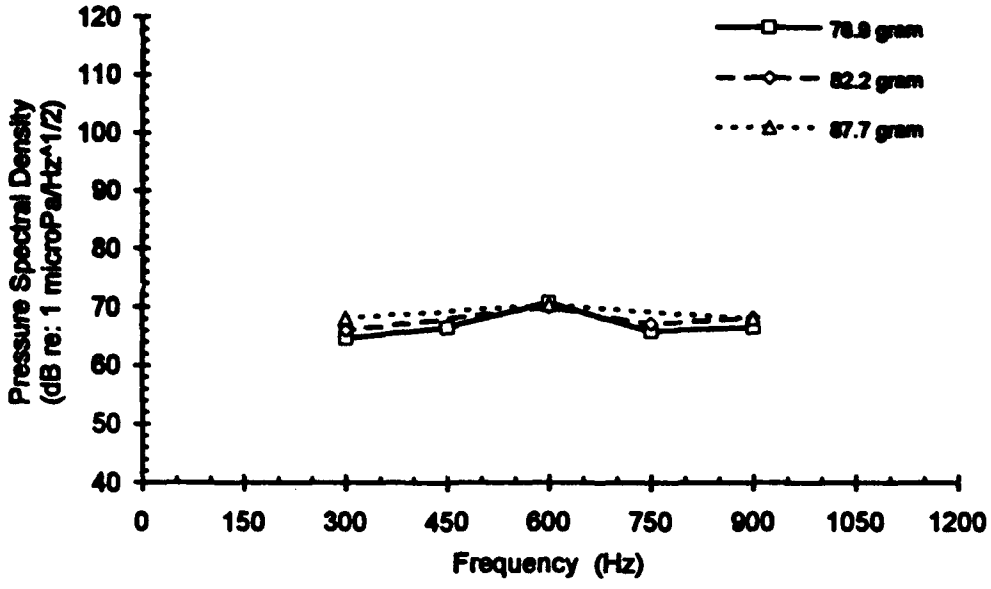

Figure 4-9. Data for the threshold versus center frequency study at a range of 15.2 cm.

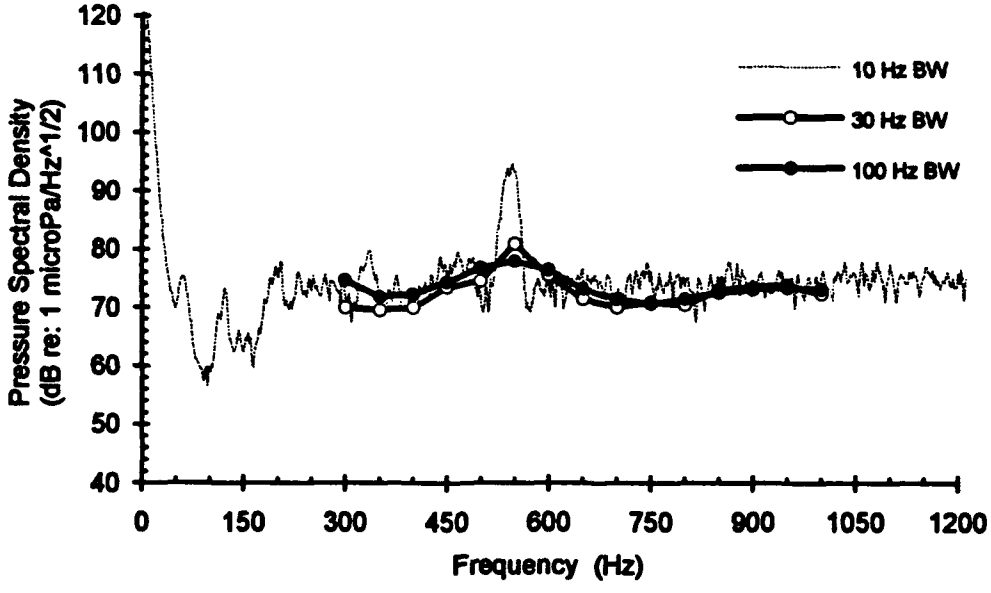

Figure 4-10. Ambient noise density for NIVAMS measured using different bandwidths. This plot is a combination of the data from Figures D-4 and D-5, with the 10 Hz BW data converted to pressure density.

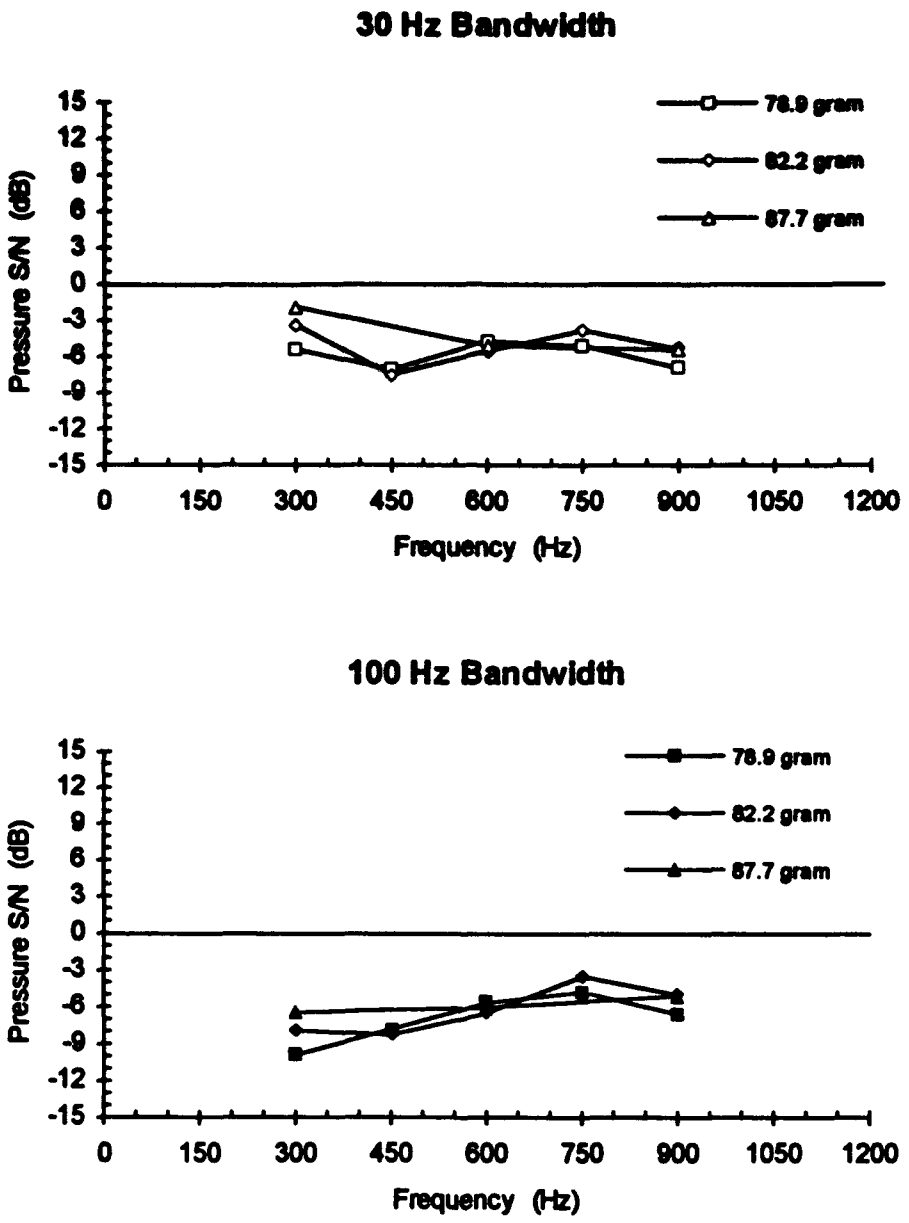

Figure 4-11. Data for the threshold versus center frequency study at a range of 15.2 cm using 30 Hz and 100 Hz bandwidths for the ambient noise.

be trained to discriminate between the two sources. An attempt on one subject consisted of first attempting to train the fish to discriminate the two sources (pulsed right side continuous, switch to left during trial); this failed. Then the fish was conditioned to respond to the transducer on the left (right side silent); this worked as usual. Then another attempt to train the fish to discriminate (same as first); this failed.

Comparison to Literature

The frequency dependence of the threshold indicates the presence of auditory filters. These filters restrict the bandwidth of the noise that interferes with the signal to be detected. If there were no filters, the detection could be a simple intensity discrimination across the entire hearing bandwidth. The signals used in this study was filtered noise with Q held constant. Therefore, as the center frequency of the signal increased, the bandwidth increased and the broadband intensity increased.

Fay (1974) examined the masking of tones by broadband noise in goldfish using a classical respiratory technique. Tonal thresholds were determined at 5 frequencies between 100 and 1200 Hz in quiet and under 3 noise levels [Figure 4-12]. Masking was found to be a linear function of noise level at all frequencies.

One way to compare the results from Fay (1974) to this study is in terms of critical masking ratios (CR). The CR estimates the noise bandwidth effective in masking a signal. For pure tone signals, the CR is the difference, in decibels, between the level of the signal at threshold and the level of the noise density. For the bandpass noise signals used here, the signal level is the product of the peak noise density and the bandwidth (at 6 dB down).

Figure 4-13 shows the critical ratios for the data from the center frequency study and the results from Fay (1974). In general, the data is consistent with the 3 dB per octave increase in the CR, although the CRs for the noise signals were 2 to 4 dB lower than the pure tones. This may be due to the coherence of the scattered noise signal to the ambient noise in this study.

Although supporting pressure detection at threshold, the inability of the goldfish to discriminate sources differing only in direction was surprising in reference to the available

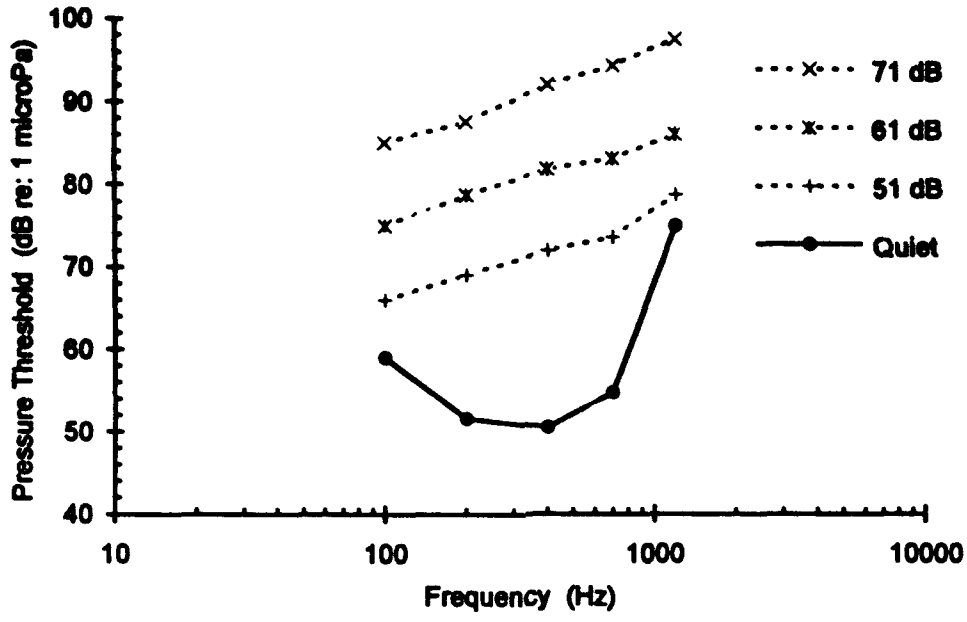

Figure 4-12. Thresholds for pure tone signals in broadband noise for the goldfish. The numbers represent the spectrum levels of the masking noise used. The quiet curve is the minimum detectable signal. (From Fay, 1974).

literature. Previous experiments have demonstrated directionality in the Mauthner cell response, directionality of the response of individual end organs, and the ability of another otophysan to discriminate sources differing only in location.

Moulton and Dixon (1967) demonstrated, using goldfish, that the Mauthner cell mediated escape reflex was directional in response to sound stimulus. But, the pressure threshold for the escape reflex was many orders of magnitude above the pressure threshold for hearing. A directional escape response doesn't require directional hearing at detection threshold.

Using whole body accelerations, Fay (1984a, 1988b) measured the directional sensitivity of single nerve fibers from the individual otolithic organs in the goldfish. Saccular fibers responded best to stimulus along a single axis. Utricular units responded best in the horizontal plane at a wide variety of azimuth angles. Lagena units tended to cluster in a vertical plane with a wide range of elevations. This data suggested to Fay that

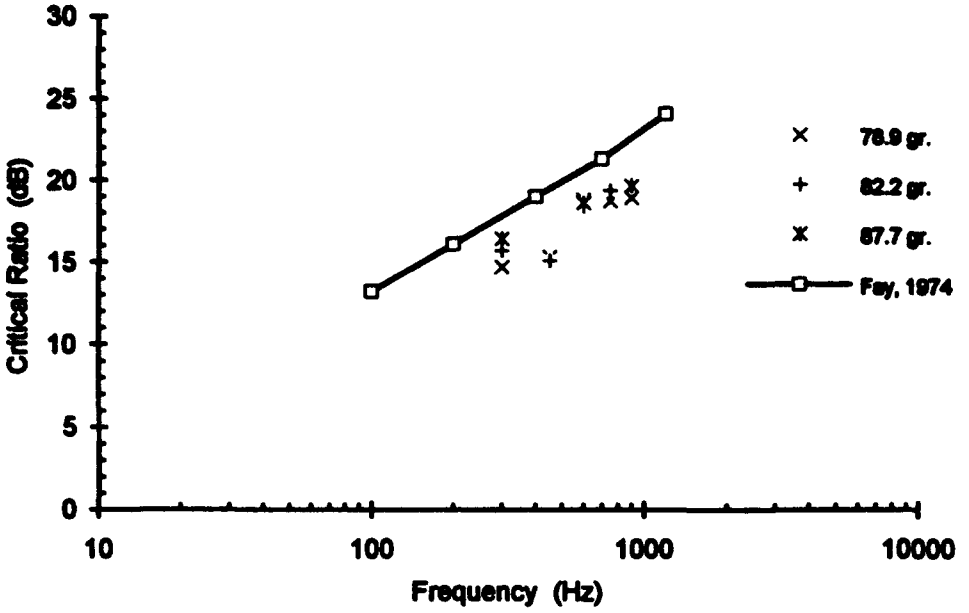

Figure 4-13. Critical ratios for the center frequency data and the pure tone data from Fay (1974).

the axis of particle motion was represented in the profiles of the most active fibers of the lagena. Also, the common directionality of the saccule fibers may be for coding the sound pressure waveform as it is transmitted from the swim bladder. For the 140 Hz stimuli, the best vibrational sensitivity for individual fibers was 25 to 35 dB higher than the best sensitivity using a sound pressure stimulus from a previous study (Fay, 1981). This suggests that sound pressure detection in the saccule occurs at lower levels than in the directional fibers of the lagena.

Schuijf *et al.* (1977) examined acoustic localization in an otophysan, the ide (*Leuciscus idus*). On a single subject, they demonstrated directional hearing for the coarse discrimination of bearings 180° apart using 75 Hz pure tones at 114 dB (re: 1 μPa) acoustic pressure. Unfortunately, the one subject disappeared after an act of willful hindering and additional subjects were not tested. In this study, the bearings were 120° apart.

The pressure detection at threshold is also interesting since the end organs of the ear are thought to be motion detectors. If the ambient noise is assumed omnidirectional,

then the time averaged magnitude of the acoustic particle displacement can be estimated from

$$\langle \xi_{noise} \rangle = \frac{\langle p_{noise} \rangle}{\sqrt{3\omega\rho_w c_w}}. \tag{4-1}$$

In the nearfield of the spherical transducer, the acoustic particle displacement of the signal was

$$\langle \xi_{signal} \rangle = \frac{\langle p_{signal} \rangle \left(1 + \frac{1}{(kr)^2}\right)^{1/2}}{\omega\rho_w c_w}. \tag{4-2}$$

where r is the range from the subject to the transducer. Therefore, the displacement signal to noise ratio, $SNR|_{displ}$, at the subject's ear was

$$SNR|_{displ} = SNR|_{press} \frac{1}{\sqrt{3}} \left(1 + \frac{1}{(kr)^2}\right)^{1/2} \tag{4-3}$$

dependent upon both center frequency and range. For the center frequency study at a 15.3 cm range, the displacement signal to noise is larger by a factor of 3.1 at 300 Hz to 1.2 at 900 Hz. For the range study at 750 Hz, the factor is 1.9 at 10.2 cm and 0.8 at 30.5 cm.

This study indicated that the goldfish is able to detect this scattered noise signal in the noise background. The next question is whether the measured range of detection can be useful to the fish.

Chapter 5

Biological Relevance

The first part of this research quantified the scattering of sound by the swim bladders of two species of fish. The second part measured the ability of the goldfish to detect ambient noise scattered as from a swim bladder in an ambient noise field. The next question asked is whether this detection could be relevant to the fish. To help answer this, the range of detection of a scattering swim bladder by another fish will be estimated and compared to some behavioral observations of predator-prey interactions.

The sound scattered by a fish's swim bladder using the simplest model is

$$p_{scat} = \frac{a_0}{r} p_{inc} \frac{\left(\frac{\omega}{\omega_0}\right)^2}{\left(\frac{\omega}{\omega_0}\right)^2 - 1 + i\frac{\omega}{\omega_0}\frac{1}{Q}} \tag{5-1}$$

where r is the distance from the scatterer to the receiver. At the resonance frequency, the magnitude reduces to

$$p_{scat} = \frac{a_0}{r} Q p_{inc}. \tag{5-2}$$

In this application, the incident pressure is the ambient noise, p_{amb}, and is assumed uniform over the entire volume of interest. The distance from the scatterer to the receiver is the range. Rearranging yields

$$\text{range} = a_0 Q \frac{p_{amb}}{p_{scat}}. \tag{5-3}$$

To determine the maximum detection range, the ratio of the scattered to ambient pressures used is the measured detection threshold signal-to-noise ratio ($SNR|_{press}$). The average for the five goldfish tested at 750 Hz was about -3.2 dB. The Q of the simulated scattered noise signal used in that study was about 5.6. Using those numbers, the detection range is

$$\text{range} = 8.1a_0. \qquad (5\text{-}4)$$

Since the detection range is proportional to the size of the swim bladder, a_0, the detection range is directly proportional to the length of the scattering fish. For the oscars, the ratio of body length to a_0 is about 10, so the detection range is on the order of the length of the scattering fish.

Enger *et al.* (1989) reports on the feeding behavior of a midwater predatory fish, the bluegill (*Lepomis macrochirus*), observed in daylight and in dark. In daylight, the bluegill rely mainly on vision to detect prey, initiating pursuit from distances of several body lengths and taking the prey within seconds. They tested bluegills, 12 to 15 cm in length, using 2.5 to 3.5 cm goldfish as prey.

Their feeding behavior differs in the dark, as observed under covert infrared illumination (Enger *et al.*, 1989):

> "The bluegills typically glided smoothly through the water, driven only by an occasional tail flip. Often, they calmly approached a live goldfish to strike from a short distance with great vigor - or to veer off slowly if the target had stopped moving. The eventual strike was so fast that on the video screen merely a sudden forward jerk and a sucking motion of the bluegill were seen, usually followed by only a glitter of scattered goldfish scales."

Their investigation was on the functions of the lateral line and inner ear in detecting moving prey. By using cobalt ions in the tank water, they were able to selectively block the function of the lateral line, but not the inner ear. The bluegills would approach prey from distances of at least 5 cm in apparently deliberate moves with and without a functional lateral line, but they would only attack goldfish from distances up to 2 cm when their lateral line was intact.

Note that these distances are much less than the 12 to 15 cm body length of the bluegills. If the goldfish is able to identify the predator in this range, then it might be able to avoid attack. If this is true, then detecting the scattered ambient noise is relevant.

Conclusions

The swim bladders of the oscars and goldfish tested scatter significant amounts of ambient noise. Also the frequency range of scattering is in the hearing range of many fish. The simple one degree of freedom system can be used to model the single swim bladder in the oscar if an appropriate additional spring term can be found. The more complex two degree of freedom system mimics the shape of the twin peak response curve of some goldfish, but the predicted resonance frequencies were low.

Goldfish are able to detect a filtered noise signal mimicking the scattering of a single swim bladder in a noise background. The detection pressure thresholds were independent of the distance to the source. This indicated that the goldfish detected the acoustic pressure at threshold. Pressure detection was confirmed when an attempt to condition goldfish to sources differing only in location failed. The detection pressure threshold was also independent of frequency when the bandpass width varied with center frequency. The calculated critical ratios were similar to those in Fay (1974).

The hypothesis examined in this thesis was that one fish could perceive nearby fish by recognizing the scattering of the ambient noise by the other's swim bladder. Although the goldfish was shown to be able to detect this kind of signal, this study did not show that the fish was able to use this information.

Future Work

As with all research, results lead to more questions and more work to address them. Areas of interest include the effect of the swim bladder on a fish's hearing, the inability of the goldfish to directionalize near threshold, and demonstration of the hypothesis of this thesis.

This research has dwelled on the detection of one fish's swim bladder by another fish. But what about the effect of swim bladder resonance on the one's own hearing? A previous study on the goldfish (Popper, 1974) indicated that swim bladder resonance frequencies were well above the frequencies of greatest sensitivity. The swim bladder resonance frequencies measured here fall at the upper end of the goldfish's hearing range. The oscar's resonance frequencies are well within its hearing range and show a well correlated shift with the oscar's mass. The question arises whether the volume of the swim

bladder affects the hearing ability of the fish. The one study on the effect of a fish's size on it's audiogram (Popper, 1971) was on goldfish, which showed no effect. But, Sand and Enger (1973) showed that swim bladder volume had an effect on an individual's saccular microphonic potentials in a cod. The measured swim bladder resonance frequency for the cod was well above it's hearing range (Sand and Hawkins, 1973) This type of study needs to be repeated on a species whose swim bladder resonates within it's hearing range.

The simple resonance model was able to predict the trends of the response of the single chambered swim bladder of the oscar, although the physical mechanisms responsible for the stiffness and damping need to be identified. The two chambered swim bladder of the goldfish needs a more complicated model, however. The measurements on both anterior and posterior swim bladders need to be made on subjects with known swim bladder sizes.

The effects on the frequency response of mutually interacting air bubbles poses an interesting effects on hearing. Zhou's (1992) experiments demonstrated that as two bubbles of different radii are brought closer together, the resonance frequency of one bubble gradually shows up in the response of the other, showing twin peaks. This means that it is possible that one single bladdered fish detects another, not by the scattered noise from the other fish, but by the mutual interaction of the two causing audible changes in it's own swim bladder, which is also scattering the ambient noise.

It also may be possible for a fish to hear the surface in a similar manner. Approaching the air-water interface causes the same change in resonance as approaching an identical out of phase source. This change in resonance frequency is separate from the change due to the decreasing ambient pressure with decreasing depth.

Another question of interest involves directional hearing in the otophysan goldfish. Moulton and Dixon (1967) demonstrated that the Mauthner cell mediated startle response in the goldfish is directional. In a preliminary test in this study, though, the goldfish could not directionalize sources at threshold. Lewis and Rogers (1994) have presented a hypothesis explaining how the startle response can be directional while the hearing is not. A study will soon be performed to test the hypothesis.

Appendix A

Relationship Between Scattering Cross-Section and Relative Motion

Previous theoretical models (Andreeva, 1964; Love, 1978) and experimental studies (McCartney and Stubbs, 1971; Sand and Hawkins, 1973; Lovik and Hovem, 1979) described the scattering of sound by the swim bladders of fish in terms of scattering cross-section. Results from previous experiments in this lab (Cox, 1987; Lewis *et al.*, 1991) were given in terms of relative motion. Appendix A shows the mathematical relationship between scattering cross-section and relative motion.

From Chapter 3 (Equation 3-11), the scattering cross-section for the data points could be calculated from

$$\sigma_s = \frac{4\pi a_0^2 (\omega \xi_{sb})^2}{\left(\frac{p_{inc}}{\rho_w c_w}\right)^2 \left[1 + \frac{1}{(ka_0)^2}\right]}. \qquad \text{(A-1)}$$

Since $ka_0 << 1$ (the diameter of the swim bladder is much smaller than the wavelength of sound in the frequency range of interest), this reduces to

$$\sigma_s = \frac{4\pi a_0^2}{\left(\frac{p_{inc}}{\rho_w c_w}\right)^2} (\omega \xi_{sb})^2 (ka_0)^2$$

$$= \left[4\pi a_0^2 \left(\frac{\rho_w a_0}{p_{inc}}\right)^2\right] (\omega^2 \xi_{sb})^2. \qquad \text{(A-2)}$$

As the incident pressure was relatively constant (see Figure 3-3), this results in saying that the scattering cross-section is proportional to swim bladder acceleration squared.

Relative motion, as defined in Cox (1987), is given by

$$\text{Relative motion} = \frac{v_{sb}}{\sqrt{v_x^2 + \left(\frac{p_{inc}}{\rho_w c_w}\right)^2}}, \tag{A-3}$$

where the x direction is along the axis of the low frequency sound projector. Using the one-dimensional Euler's equation,

$$v_x = \frac{\Delta p_{inc}}{\rho_w \omega \ell} \tag{A-4}$$

relative motion can be expressed in measurable quantities as

$$\text{Relative motion} = \frac{v_{sb}}{\sqrt{\left(\frac{\Delta p_{inc}}{\rho_w \omega \ell}\right)^2 + \left(\frac{p_{inc}}{\rho_w c_w}\right)^2}}. \tag{A-5}$$

If the first term in the denominator dominates, then

$$\text{Relative motion} = \left[\frac{\rho_w \ell}{\Delta p_{inc}}\right](\omega v_{sb}) \tag{A-6}$$

so relative motion goes as the acceleration of the swim bladder surface. Therefore, the scattering cross-section is proportional to relative motion squared. To check this, the relative magnitudes of the two terms under the radical are compared in Figure A-1. For frequencies below 1700 Hz, v_x dominates, so scattering cross-section and relative motion are showing the same relationship. Note that the incident sound field, and thus this conclusion, was dependent on the geometry of the tank, the location of the J-9, and the position of the focal point of the ultrasonic transducers.

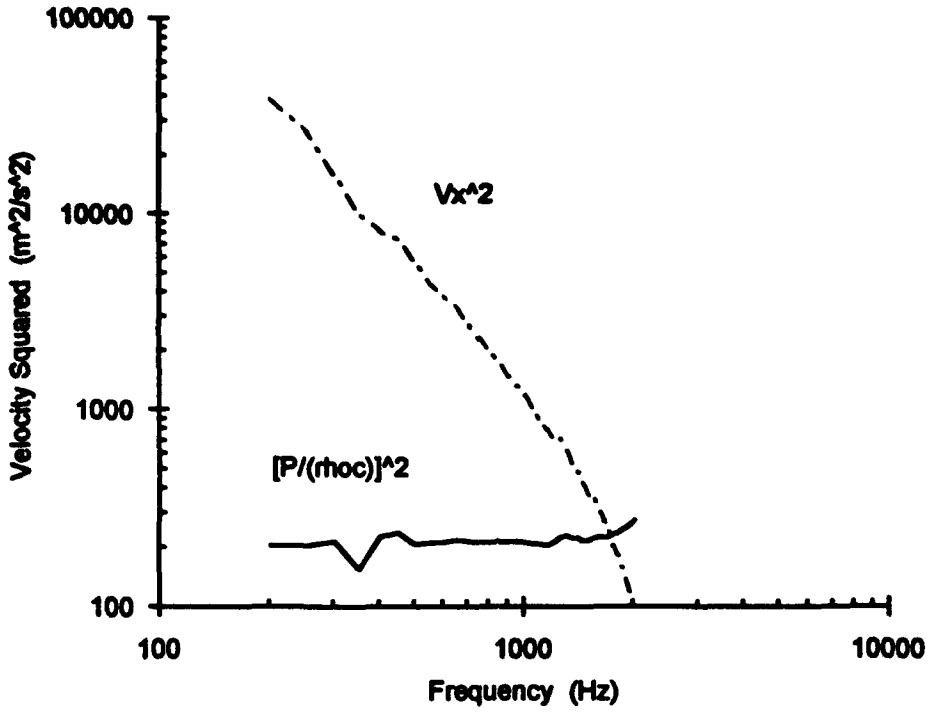

Figure A-1. Comparison of the squares of the acoustic particle velocity (solid line) and the particle velocity due to the incompressible flow in the nearfield of the J-9 (dashed line).

Appendix B

Swim Bladder Response of Goldfish

Appendix B contains the goldfish swim bladder data collected from 1987 to 1991 by Thomas Lewis, Joey Lloyd, David Rogers, and Steve Flanagan using the NIVAMS as described in Chapter 3. Table B-1 consists of the parameters describing the responses in the chronological order that the data was taken for both the anterior and posterior swim bladders. The file name corresponds to a set of frequency sweeps for a given fish on a given day. The file extension identifies separate sweeps. The masses of the fish are unique - different masses correspond to different fish, identical masses are the same fish. For example, data was taken on a specific goldfish of mass 33.1 grams on 4 different days (GF0420TL, GF0423J1, GF0428TL, and GF0507TL). On the first day, 3 frequency sweeps were taken (.PL1, .PL2, and .PL3).

A star (*) in the next column , labeled 2?, indicates that twin peaks were found in the frequency response. Data with more than one peak indicates that a more complex model was needed than the single degree of freedom used. Therefore, these sweeps were not analyzed further. Of the 22 goldfish tested, two showed consistent twin peak response of their anterior swim bladder (48.9 gram and 58.8 gram). For the posterior swim bladder of the five goldfish measured, two showed twin peaks (32.2 gram and 37.6 gram), but not consistently.

The single peak data was then fit to a generalized form of the scattering cross-section,

$$\sigma_s = \frac{4\pi a^2}{\left[\left(\frac{\omega_0}{\omega}\right)^2 - 1\right]^2 + \frac{\omega_0^{\,2}}{Q^2\omega^2}}, \qquad \text{(B-1)}$$

using a three parameter (a, ω_0, and Q) non-linear least squares curve fit. The first parameter, a, characterizes the size of the scatterer and acts as a scaling function. The resonant frequency, ω_0, locates the natural frequency of the system. The quality factor,

Q, is a measure of the bandwidth of the peak. The final column, OK?, indicates a subjective assessment of whether the best fit curve follows the trend of the data points. Parameters from curves that did not were not used in further analysis.

Figures B-1 to B-29 are the plots of the data for each fish on each day, shown in order of increasing mass. Anterior swim bladder measurements are shown first, then posterior measurements.

Table B-1. Goldfish swim bladder data.

File Name	.Ext	Mass (g)	2?	a (m)	Res. Freq. (Hz)	Q	OK?
GF0420TL	.PL1	33.1		0.0013	1320.0	1.425	
	.PL2			0.0012	1233.5	1.268	
	.PL3			0.0013	1416.0	1.428	
GF0423J1	.PL1	33.1		0.0011	1085.0	2.488	
	.PL2			0.0009	1073.1	2.973	
GF0423J2	.PL1	26.1					no
GF0428TL	.PL1	33.1		0.0011	1258.2	2.378	
GF0430JL	.PL1	26.1					no
	.PL2						no
	.PL3						no
	.PL4						no
GF0506TL	.PL1	43.1		0.0010	1042.8	2.524	
	.PL2			0.0010	1149.4	2.898	
	.PL3			0.0009	1155.3	3.058	
	.PL4			0.0010	1191.1	2.364	
GF0507JL	.PL1	22.6					no
	.PL2						no
	.PL3						no
	.PL4						no
	.PL5						no
GF0507TL	.PL1	33.1					no
	.PL2			0.0012	1289.3	1.970	
GF0513TL	.PL1	22.6					no
GF0514JL	.PL1	39.5		0.0011	992.4	2.001	
GF0515TL	.PL1	43.1		0.0011	1149.7	2.288	
	.PL2			0.0010	1292.6	2.867	
	.PL3			0.0011	1313.4	2.502	
	.PL4			0.0011	1257.8	2.107	
GF0727DR	.PL1	52.0		0.0021	622.8	2.088	
GF0729DR	.PL1	36.0		0.0018	1019.1	1.733	
GF0729D2	.PL1	14.8					no
GF0731DR	.PL1	35.0		0.0016	1395.0	1.994	
GF0731D2	.PL1	48.9		0.0021	706.0	1.543	
GF0731D3	.PL1	52.0		0.0020	723.2	4.128	
GF0801DR	.PL1	36.0		0.0023	915.2	1.428	
	.PL2			0.0022	935.8	1.751	
	.PL3			0.0022	1015.1	1.754	

File Name	.Ext	Mass (g)	2?	a (m)	Res. Freq. (Hz)	Q	OK?
GF0801D2	.PL1	14.8		0.0014	1244.4	1.870	
GF0802DR	.PL1	48.9	*				no
	.PL2		*				no
	.PL3		*				no
	.PL4		*				no
GF0803DR	.PL1	52.0		0.0019	794.3	2.240	
GF0803D2	.PL1	36.0		0.0022	987.6	1.770	
	.PL2			0.0020	958.5	2.296	
GF0806DR	.PL1	52.0		0.0017	919.6	3.129	
	.PL2			0.0015	896.5	4.244	
	.PL3			0.0017	91[illegible]7	3.065	
GF0806D2	.PL1	14.8		0.0012	1214.4	2.437	
	.PL2			0.0012	1219.3	2.582	
GF0807DR	.PL1	48.9	*				no
	.PL2		*				no
	.PL3		*				no
GF0807D2	.PL1	35.0		0.0018	1381.9	1.324	
GF0808DR	.PL1	14.8		0.0007	1226.1	4.018	
GF0808D2	.PL1	52.0		0.0014	783.7	2.925	
GF0809DR	.PL1	35.0		0.0009	1388.1	3.210	
	.PL2			0.0009	1435.1	3.333	
	.PL3			0.0012	1238.3	2.252	
	.PL4			0.0012	1092.6	1.572	
GF0810DR	.PL1	14.8		0.0008	1220.6	2.920	
	.PL2			0.0009	1092.9	1.572	
GF0829DR	.PL1	99.0		0.0015	708.4	2.220	
	.PL2			0.0013	667.2	2.685	
	.PL3			0.0013	650.5	2.384	
GF0911SF	.PL1	35.0		0.0014	1018.4	2.374	
	.PL2			0.0012	1023.0	2.932	
GF0913SF	.PL1	35.0		0.0013	1268.0	2.357	
GF0917SF	.PL1	36.0		0.0016	1116.5	2.100	
	.PL2			0.0015	1138.5	2.168	
GF0921SF	.PL1	58.8	*				no
	.PL2		*				no
	.PL3		*				no
GF0317TL	.PL1	39.8		0.0014	717.6	2.975	
GF0317T2	.PL1	57.1		0.0014	833.4	2.516	

File Name	.Ext	Mass (g)	2?	a (m)	Res. Freq. (Hz)	Q	OK?
GF0318TL	.PL1	2.2					no
	.PL2						no
	.PL3						no
GF0318T2	.PL1	19.4		0.0013	1287.2	1.626	
	.PL2			0.0012	1340.5	1.800	
	.PL3			0.0013	1332.5	1.423	
GF0319TL	.PL1	28.4		0.0015	1176.7	1.243	
	.PL2			0.0015	1157.8	1.223	
	.PL3			0.0016	1086.1	1.050	
	.PL4			0.0016	993.7	0.947	
	.PL5			0.0017	672.1	0.619	
GF0320TL	.PL1	39.8		0.0017	1041.8	1.373	
	.PL2			0.0018	905.2	1.077	
GF0326TL	.PL1	57.1		0.0014	504.6	2.896	
	.PL2			0.0014	497.5	2.431	
	.PL3			0.0014	530.9	2.966	
GF0328TL	.PL1	46.5		0.0015	623.5	1.477	
GF0330TL	.PL1	50.0		0.0015	952.0	1.747	
	.PL2			0.0014	960.6	1.808	
	.PL3			0.0014	977.4	1.896	
	.PL4			0.0014	973.0	1.770	
	.PL5			0.0014	979.0	1.779	
GF0404TL	.PL1	32.1		0.0012	1249.8	1.793	
	.PL2			0.0012	1038.6	1.503	
GF0409TL	.PL1	32.2		0.0012	1040.8	2.546	
	.PL2			0.0012	1041.5	2.619	
	.PL3			0.0012	1048.5	2.660	
GF0416TL	.PL1	37.6		0.0015	1228.3	1.980	
	.PL2			0.0015	1231.0	1.847	
	.PL3			0.0015	1232.4	1.812	
	.PL4			0.0016	1211.6	1.762	
Posterior							
GF0318T2	.PL4	19.4		0.0011	1292.0	1.230	
	.PL5			0.0012	1290.8	1.133	
	.PL6			0.0010	1376.5	1.805	
GF0319TL	.PL6	28.4		0.0008	1052.1	1.368	
	.PL7			0.0008	1101.2	1.503	
	.PL8			0.0009	1029.9	1.393	

File Name	.Ext	Mass (g)	2?	a (m)	Res. Freq. (Hz)	Q	OK?
GF0330TL	.PL6	50.0		0.0009	1092.3	2.313	
	.PL7			0.0009	1090.9	2.233	
	.PL8			0.0010	1076.2	2.182	
	.PL9			0.0009	1079.1	2.358	
	.PL0			0.0009	1081.2	2.494	
GF0409T2	.PL1	32.2	*				no
	.PL2		*				no
	.PL3		*				no
GF0410TL	.PL1	32.2	*				no
	.PL2		*				no
GF0410T2	.PL1	32.2					no
	.PL2		*				no
	.PL3		*				no
GF0416T2	.PL1	37.6	*				no
	.PL2		*				no
	.PL3		*				no
	.PL4		*				no
	.PL5						no
GF0417TL	.PL1	37.6		0.0010	1121.5	3.129	
	.PL2			0.0009	1111.9	3.223	
	.PL3			0.0010	1010.3	2.363	
	.PL4			0.0010	952.9	2.039	
	.PL5			0.0010	1098.3	3.048	
	.PL6			0.0010	1106.7	3.004	
GF0417T2	.PL1	37.6	*				no
	.PL2		*				no
	.PL3		*				no
	.PL4		*				no
	.PL5		*				no
	.PL6		*				no

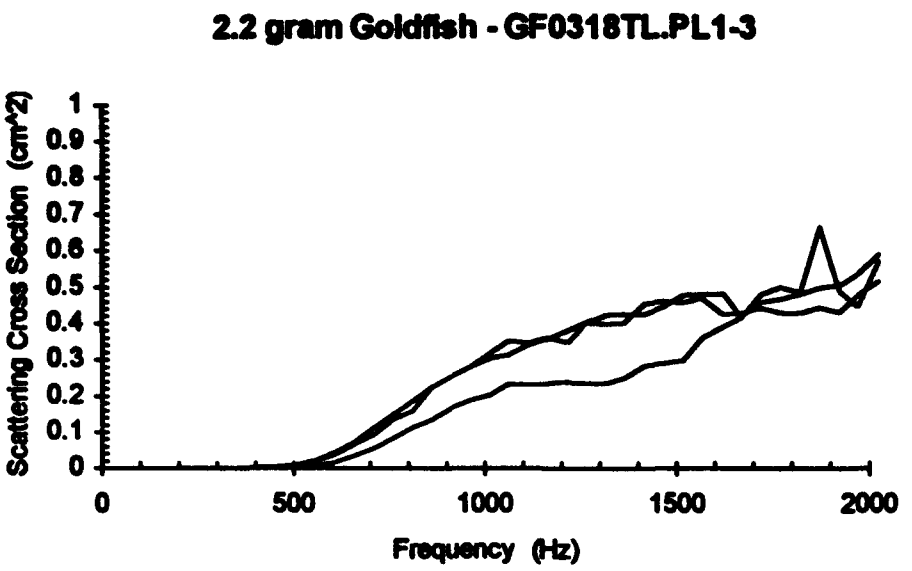

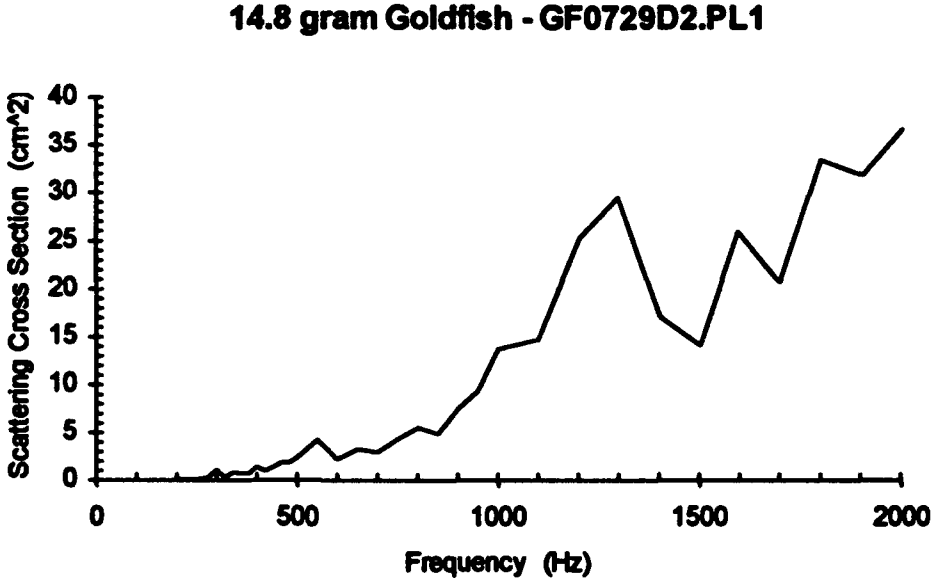

Figure B-1. Swim bladder frequency response of a 2.2 gram and a 14.8 gram goldfish.

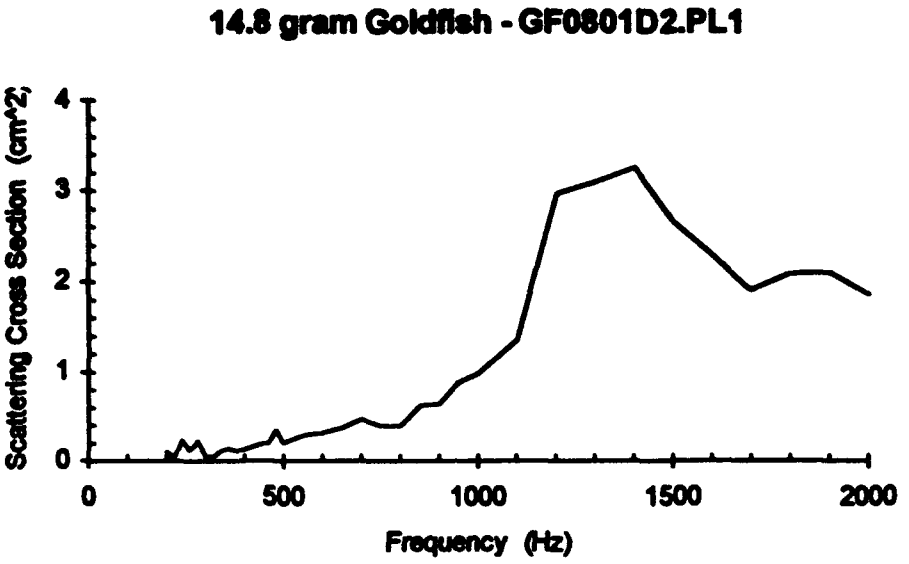

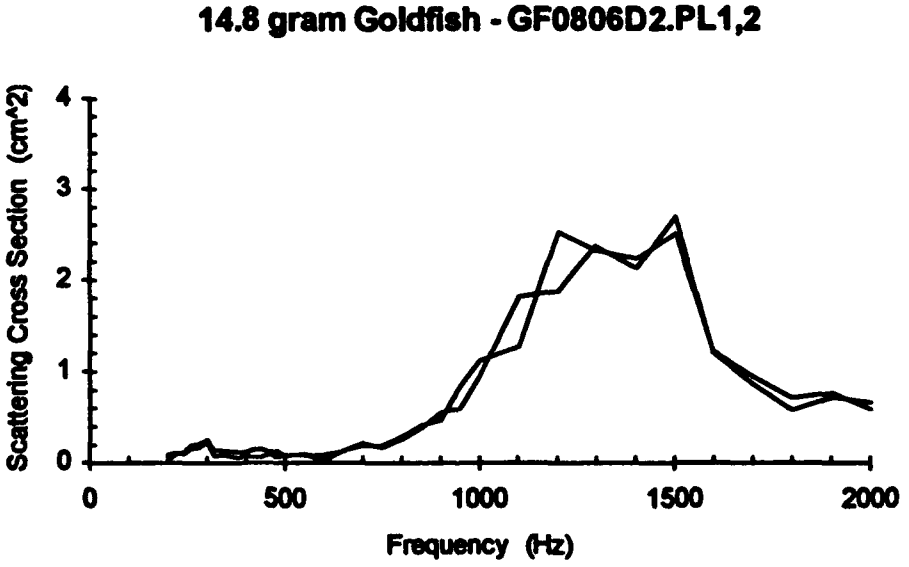

Figure B-2. Swim bladder frequency response of a 14.8 gram goldfish.

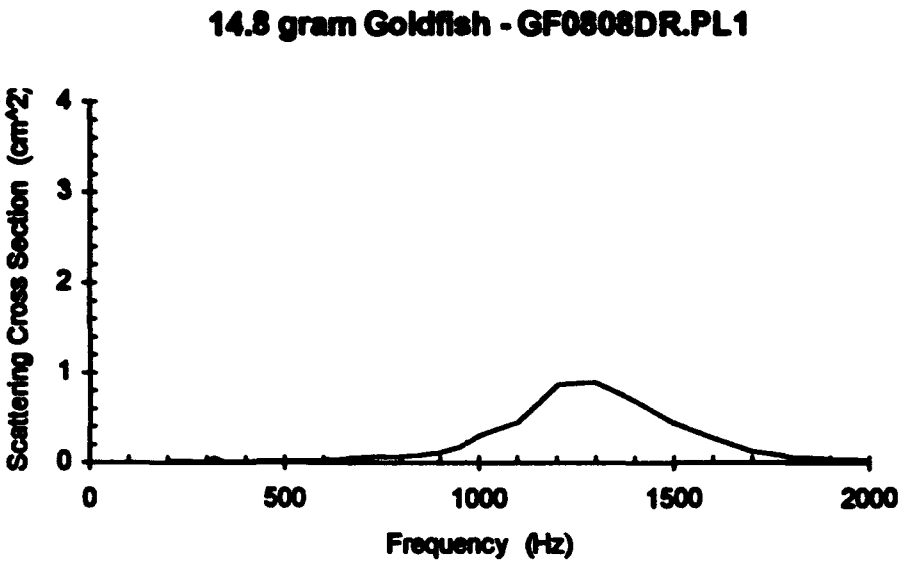

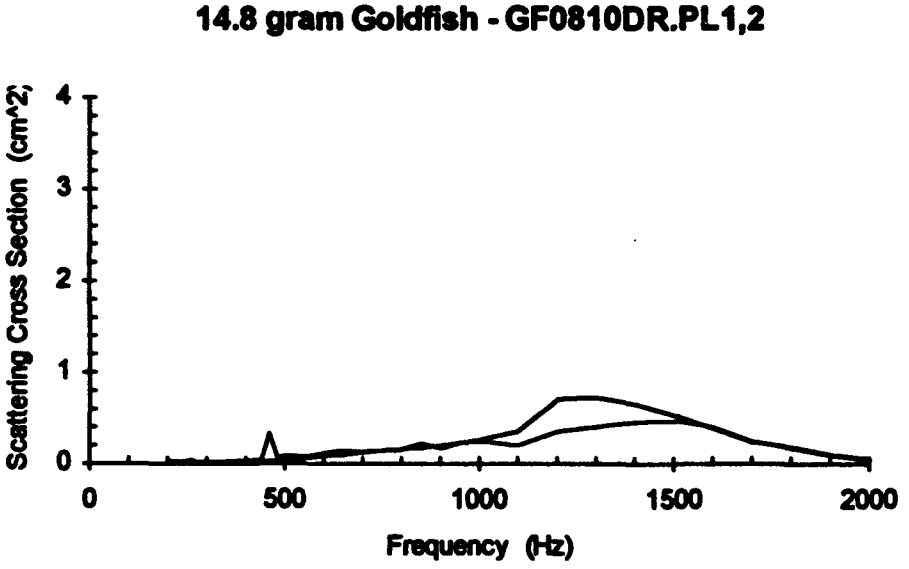

Figure B-3. Swim bladder frequency response of a 14.8 gram goldfish.

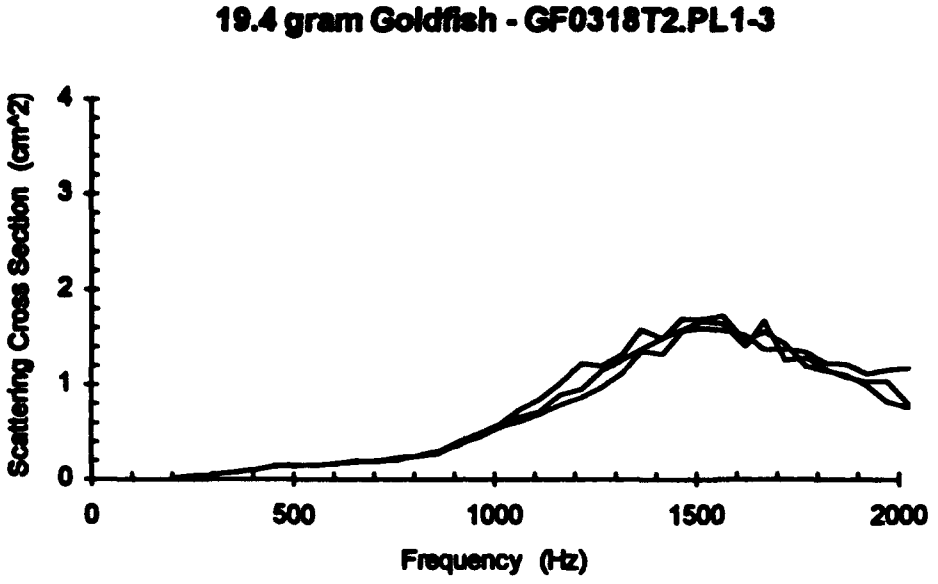

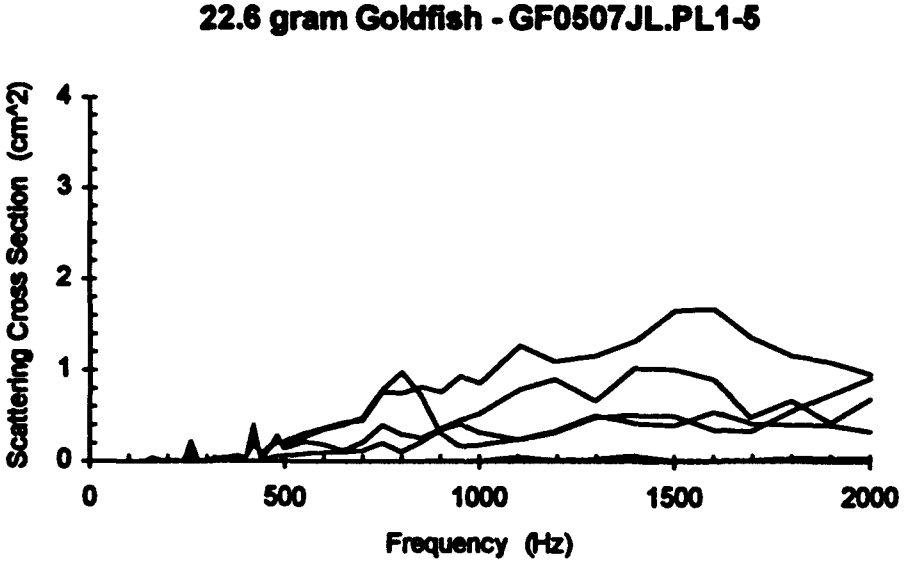

Figure B-4. Swim bladder frequency response of a 19.4 gram and a 22.6 gram goldfish.

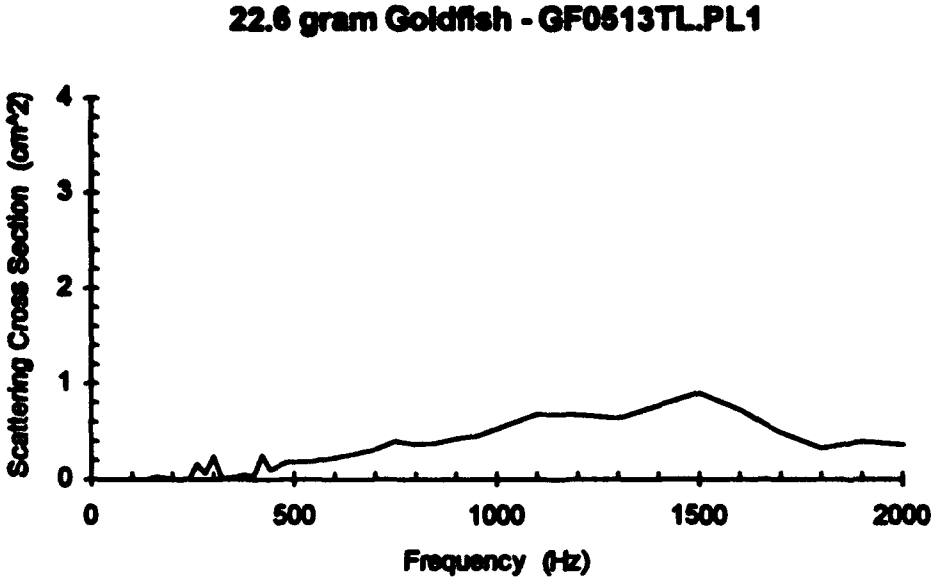

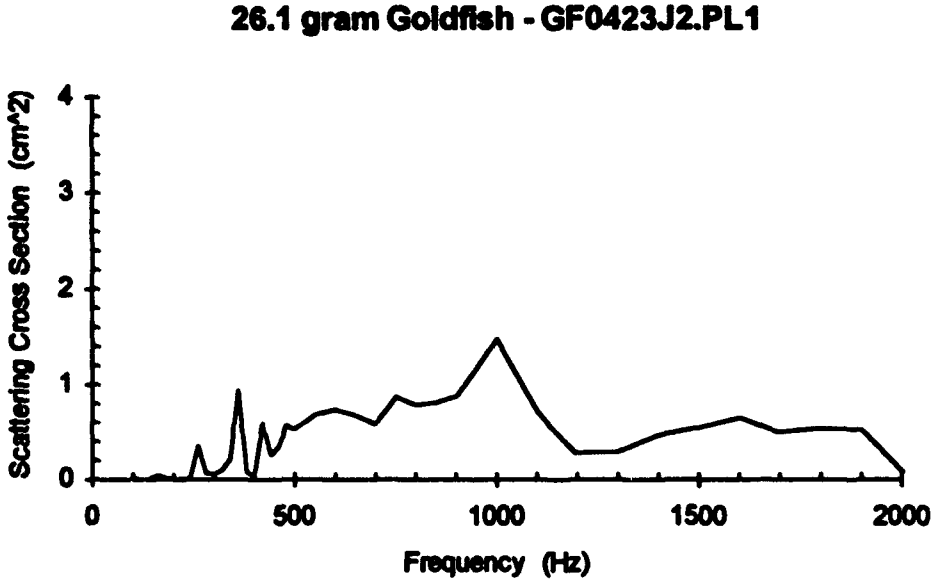

Figure B-5. Swim bladder frequency response of a 22.6 gram and a 26.1 gram goldfish.

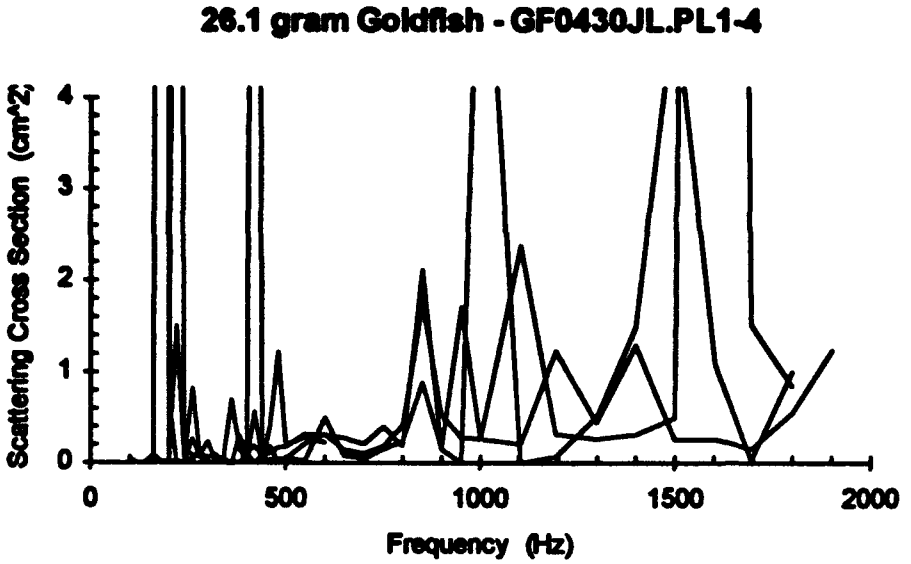

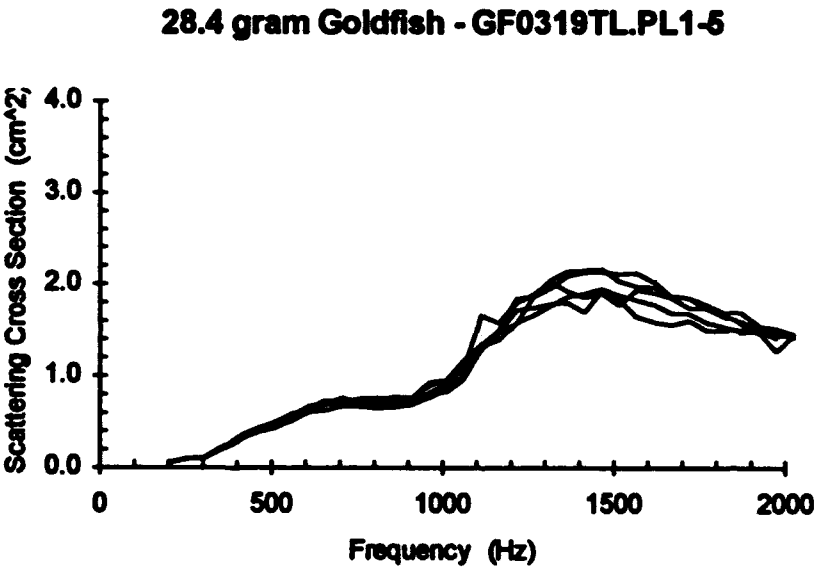

Figure B-6. Swim bladder frequency response of a 26.1 gram and a 28.4 gram goldfish.

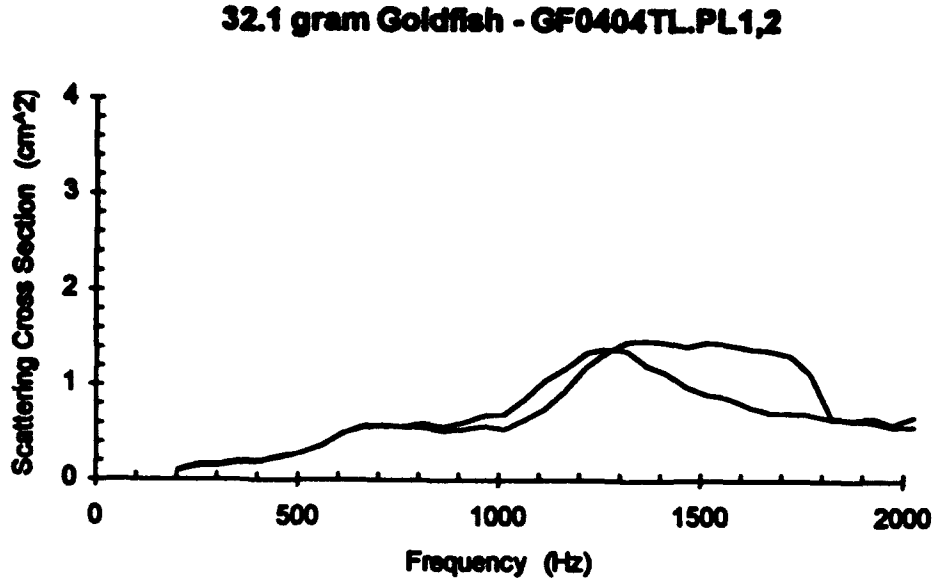

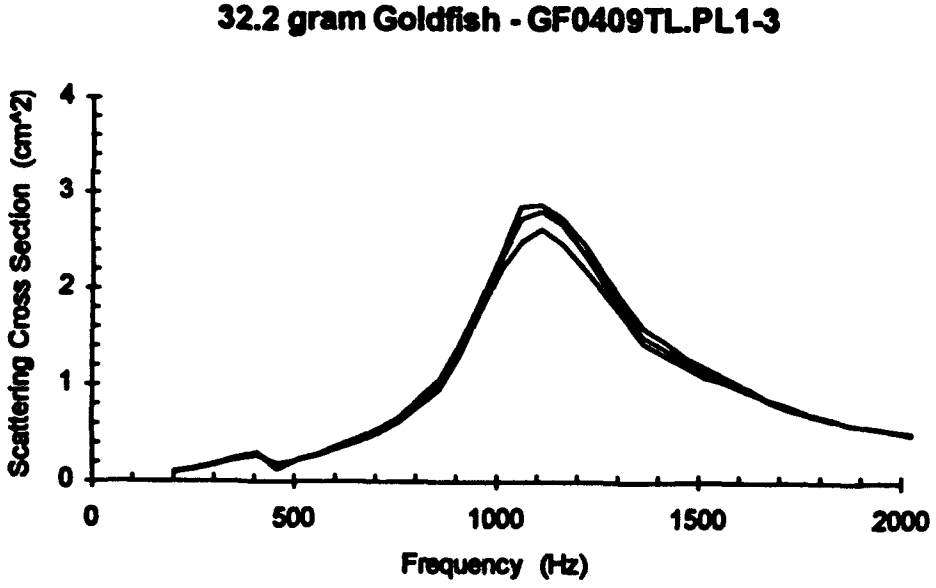

Figure B-7. Swim bladder frequency response of a 32.1 gram and a 32.2 gram goldfish.

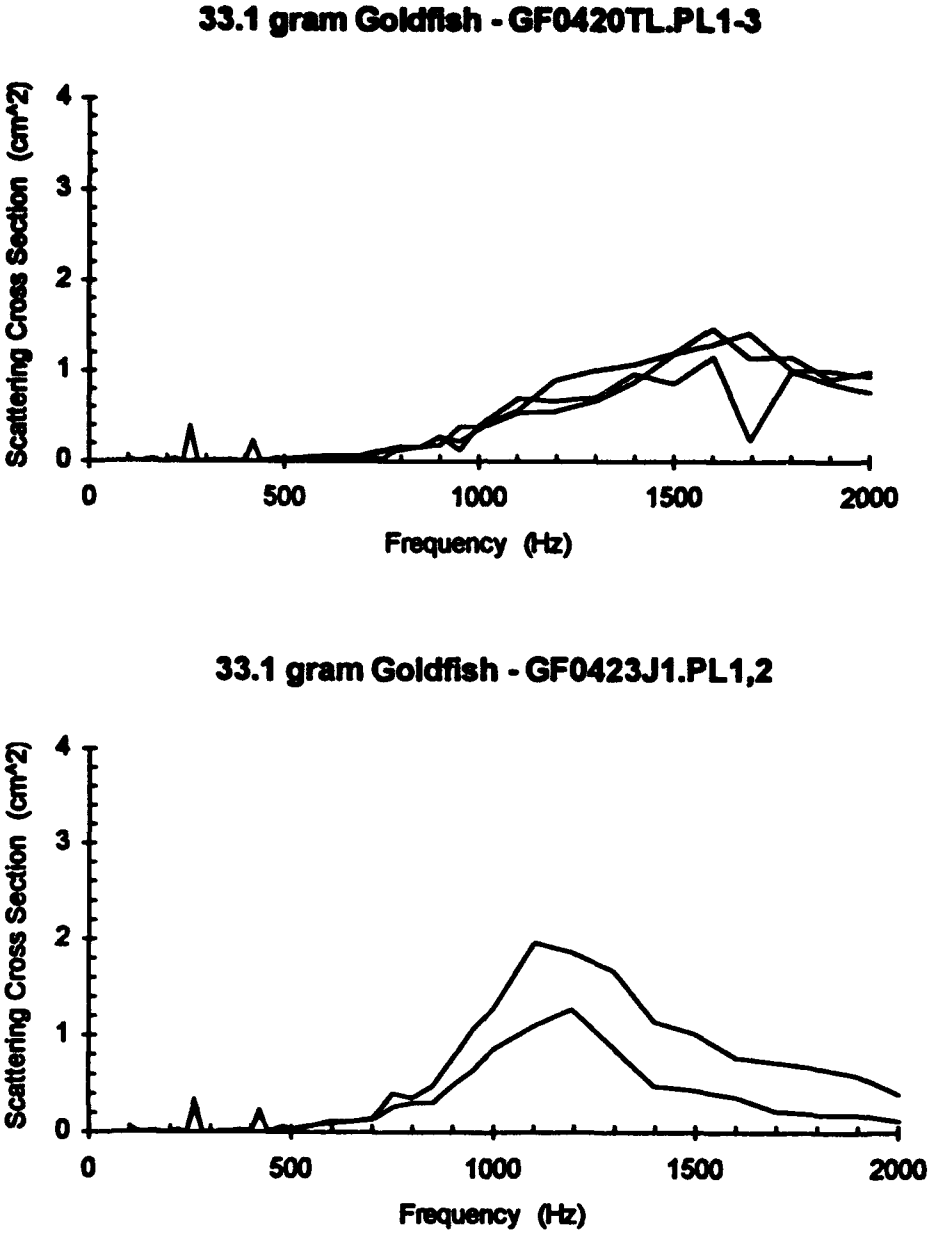

Figure B-8. Swim bladder frequency response of a 33.1 gram goldfish.

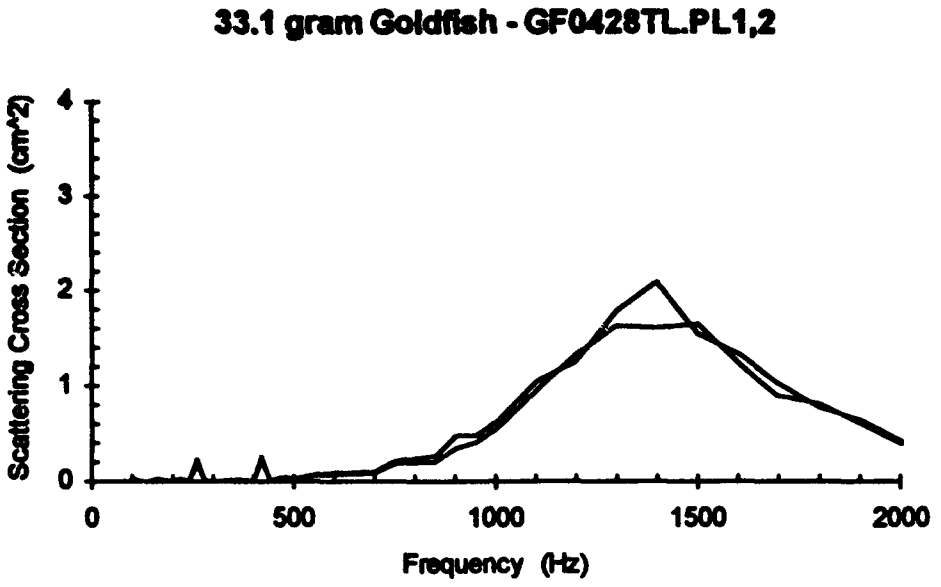

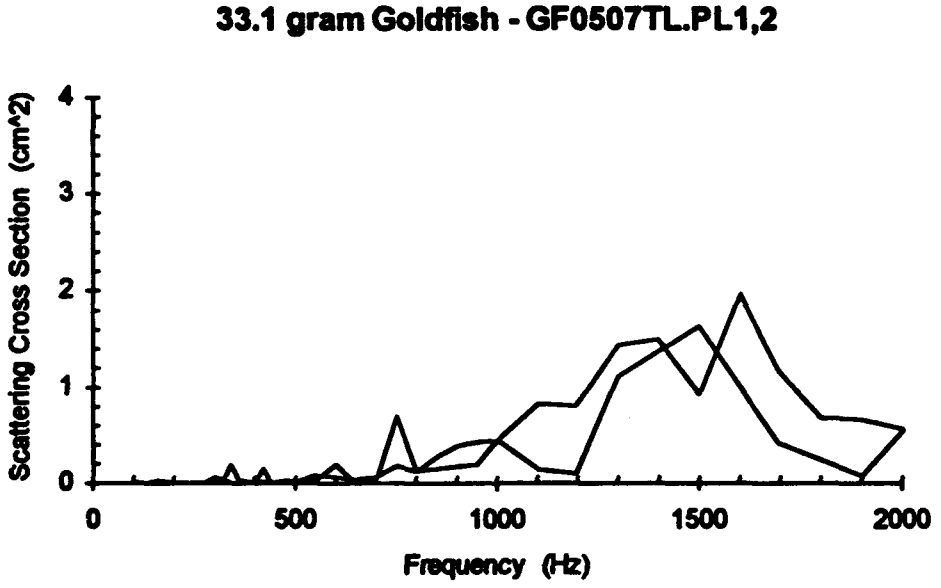

Figure B-9. Swim bladder frequency response of a 33.1 gram goldfish.

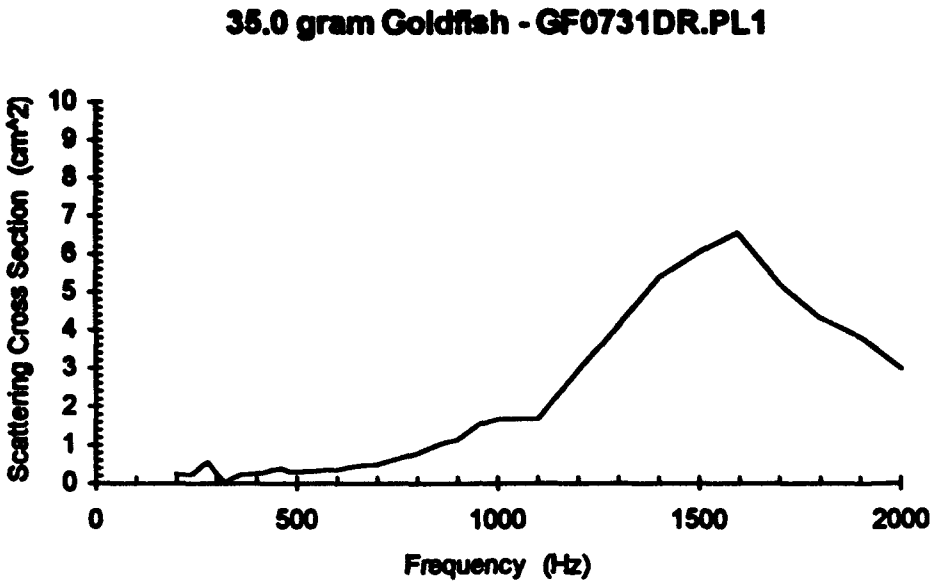

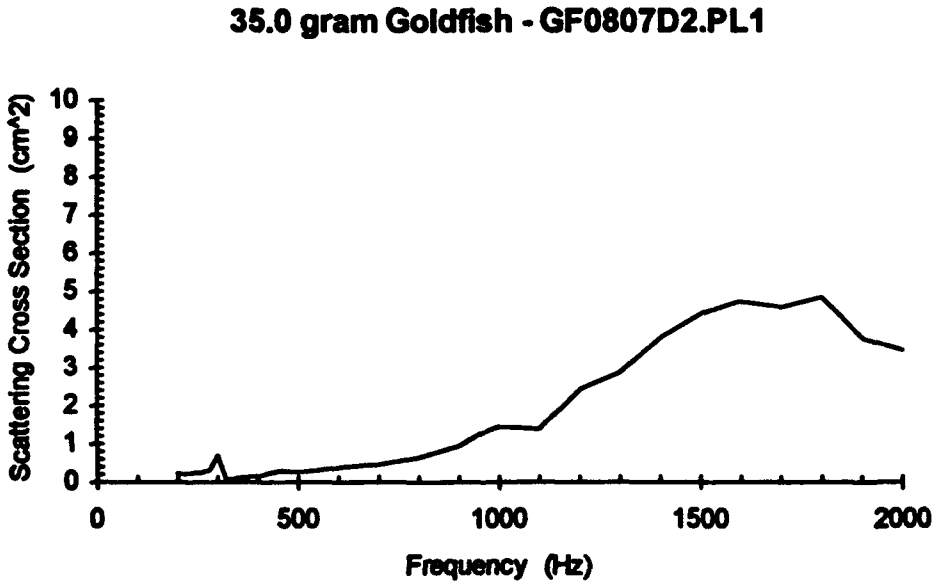

Figure B-10. Swim bladder frequency response of a 35.0 gram goldfish.

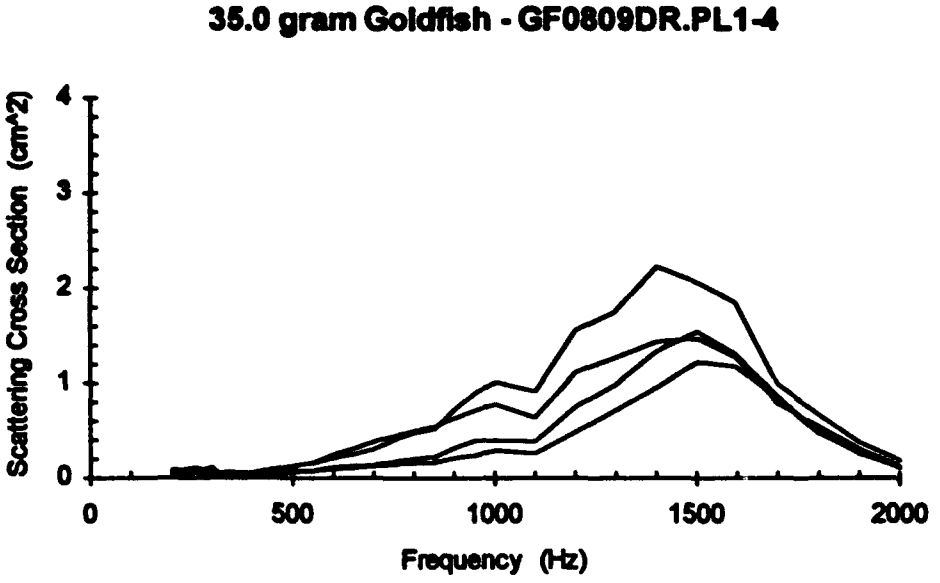

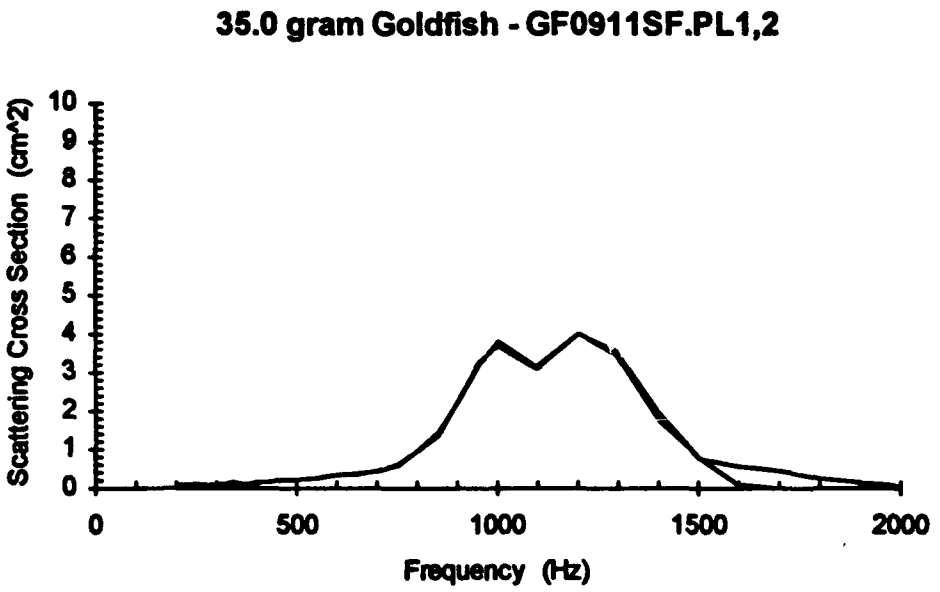

Figure B-11. Swim bladder frequency response of a 35.0 gram goldfish.

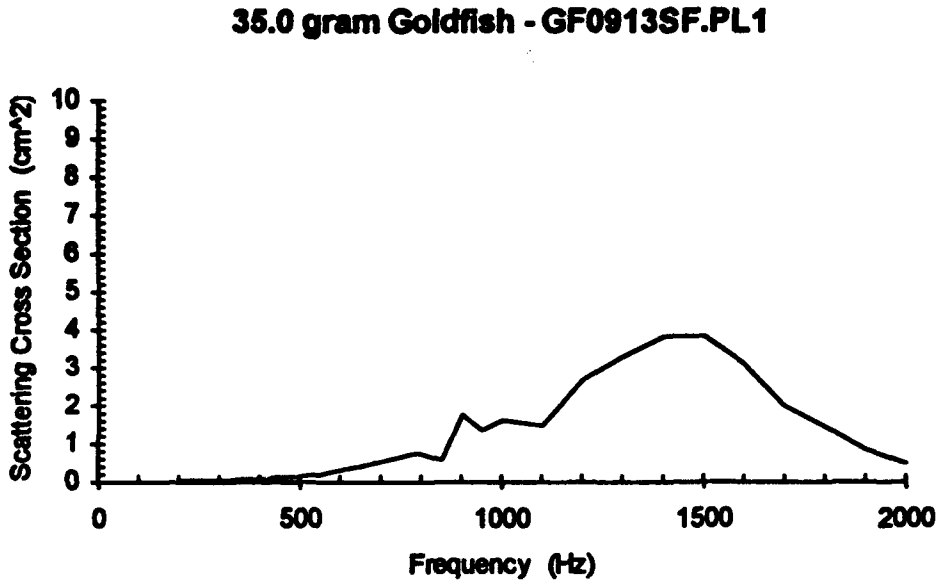

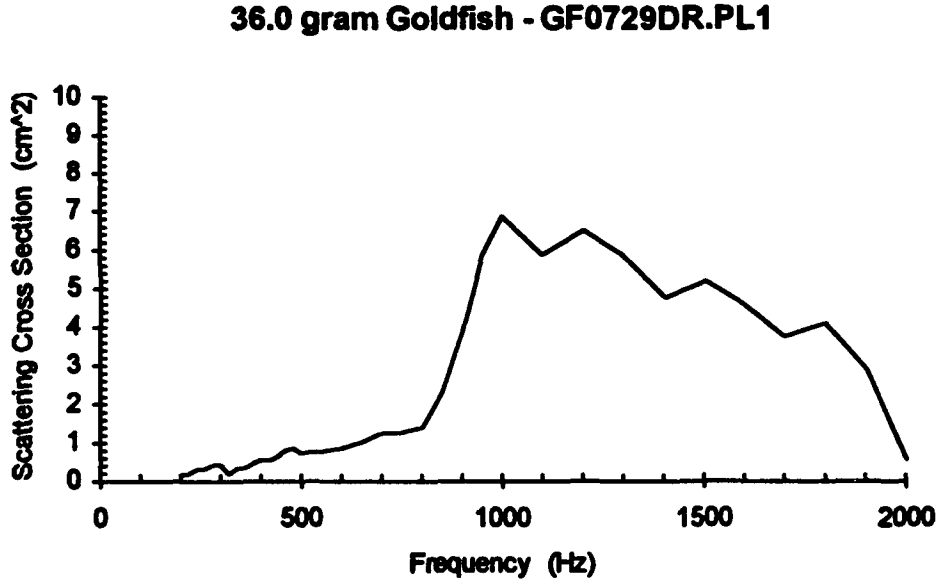

Figure B-12. Swim bladder frequency response of a 35.0 and a 36.0 gram goldfish.

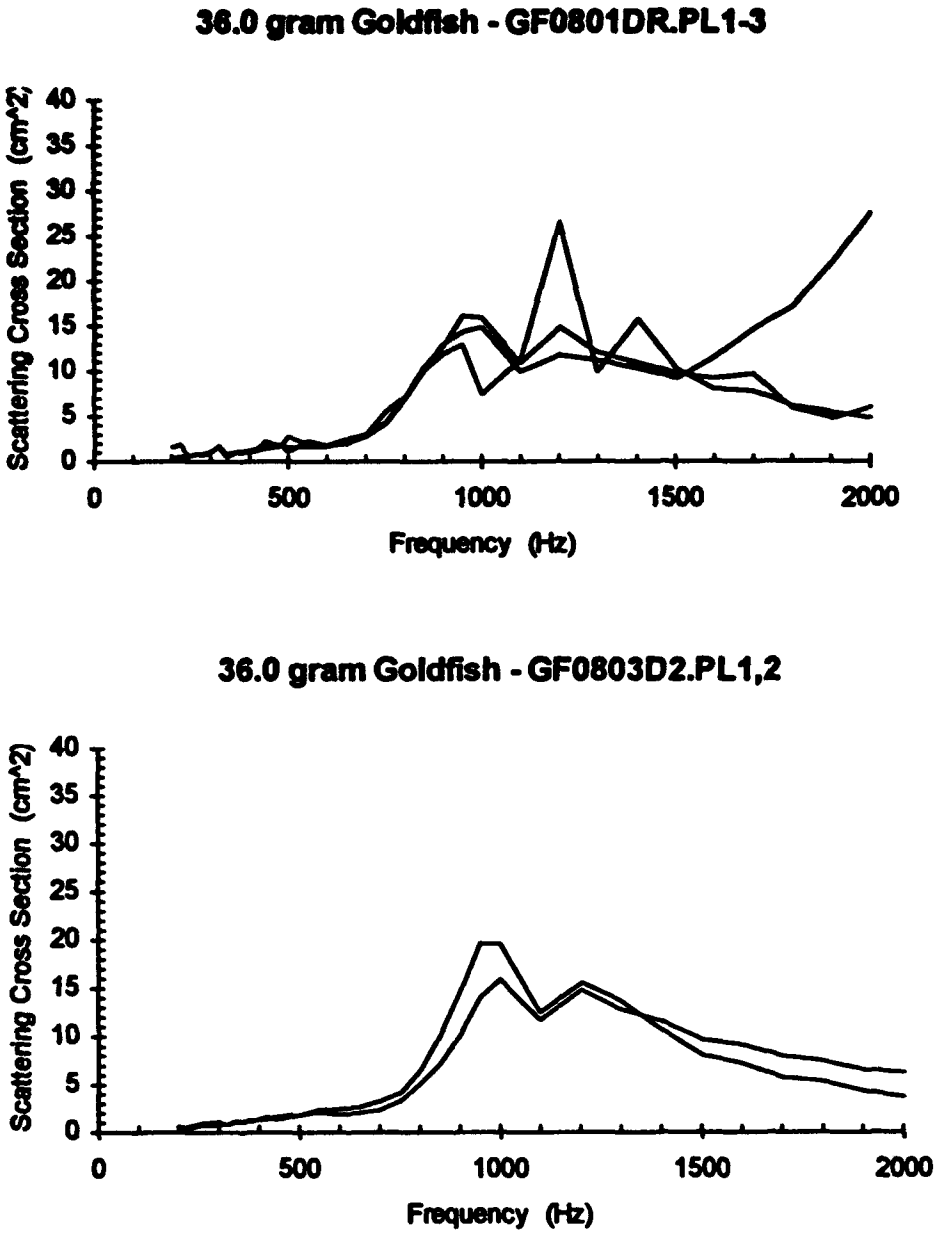

Figure B-13. Swim bladder frequency response of a 36.0 gram goldfish.

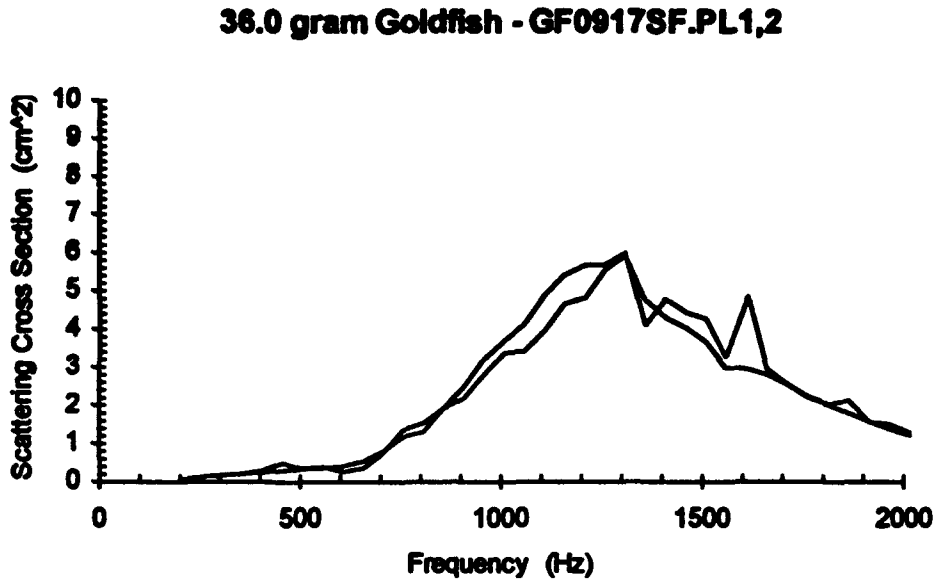

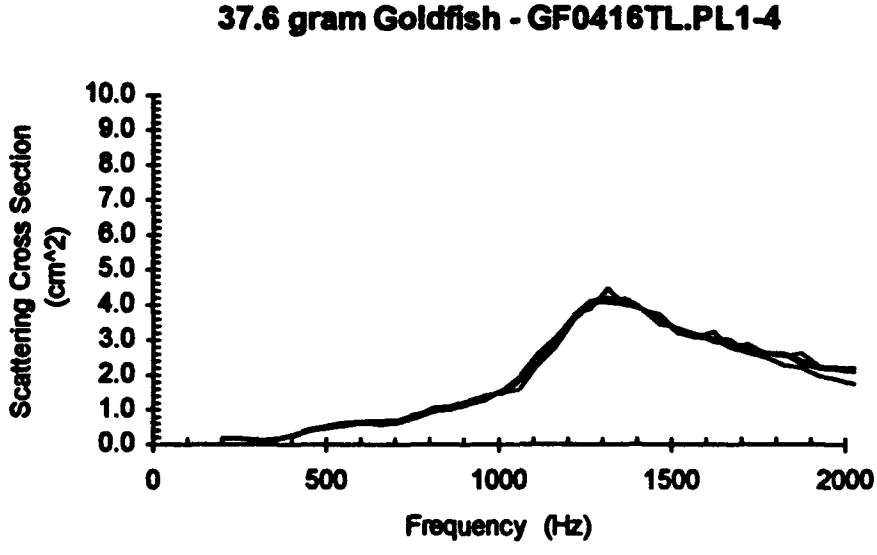

Figure B-14. Swim bladder frequency response of a 36.0 gram and a 37.6 gram goldfish.

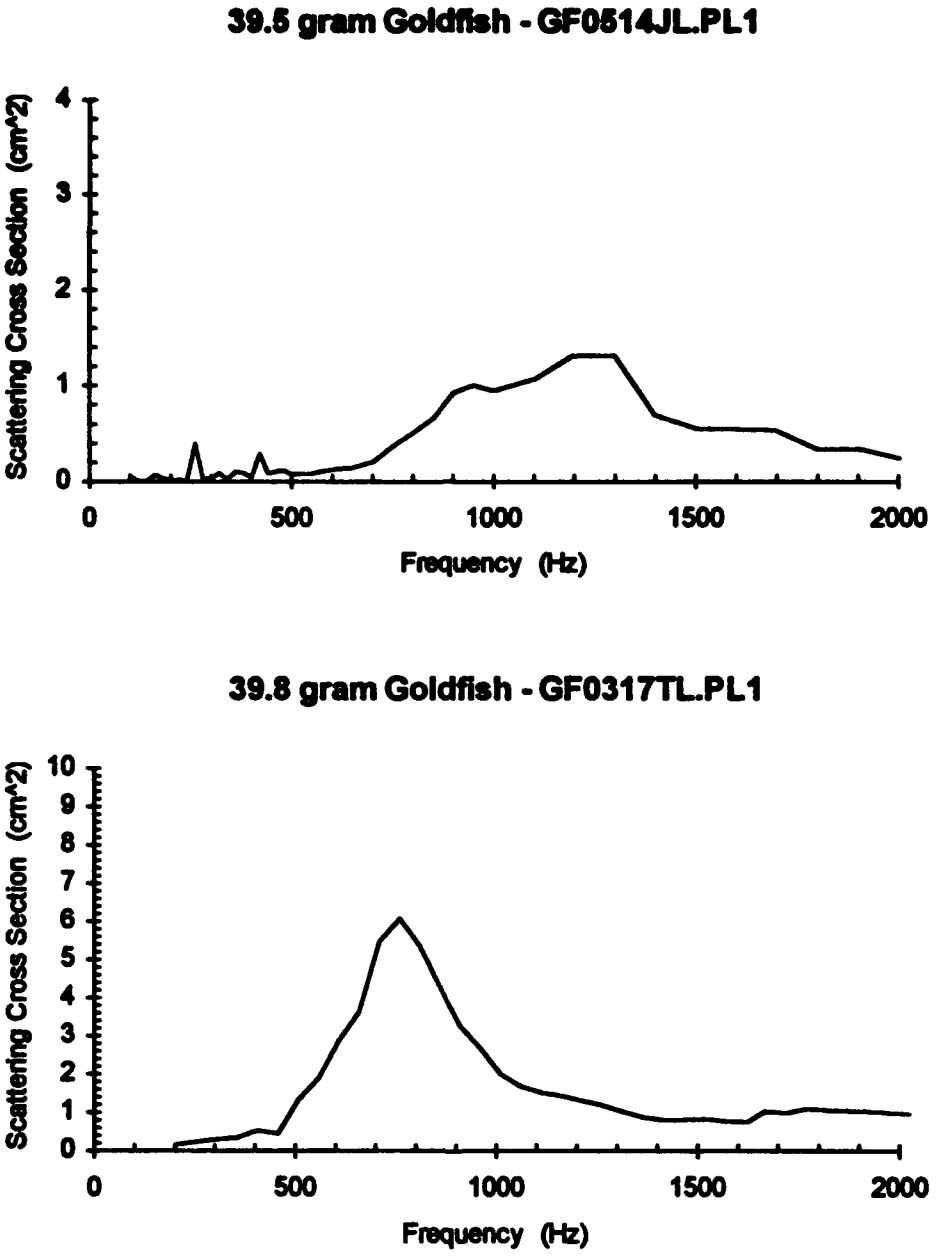

Figure B-15. Swim bladder frequency response of a 39.5 gram and a 39.8 gram goldfish.

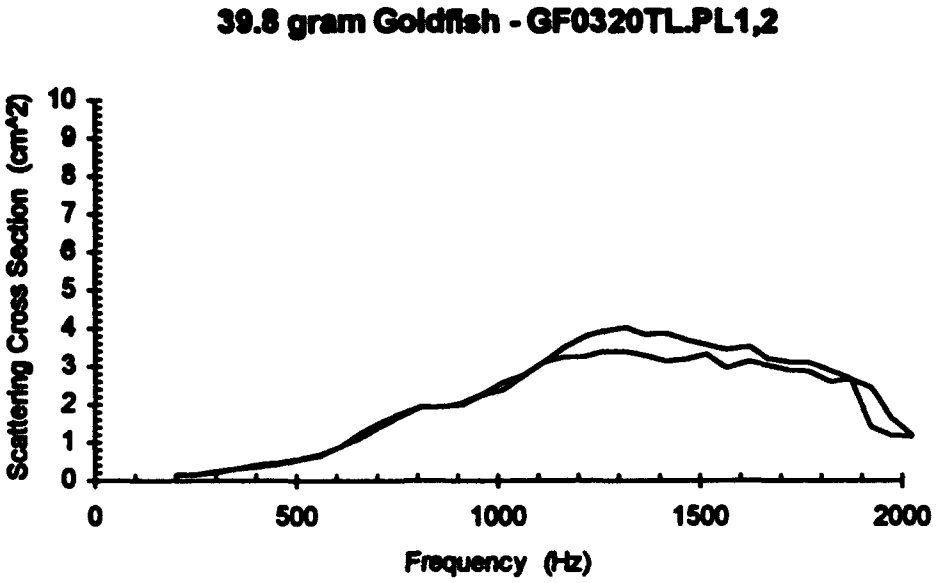

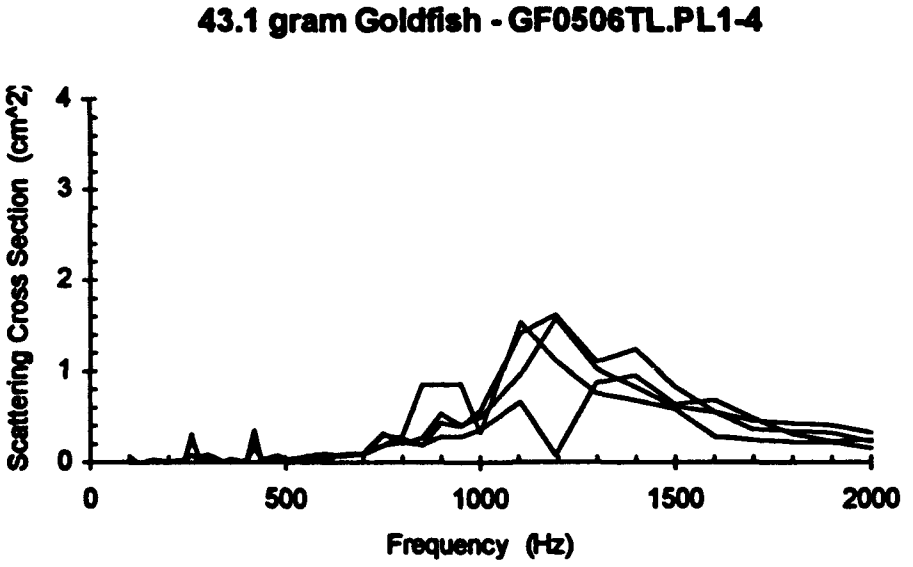

Figure B-16. Swim bladder frequency response of a 39.8 gram and a 43.1 gram goldfish.

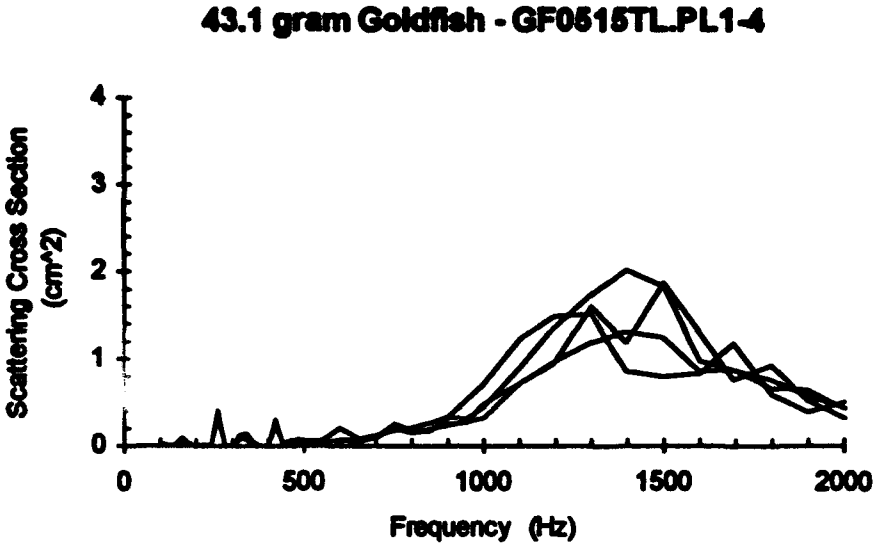

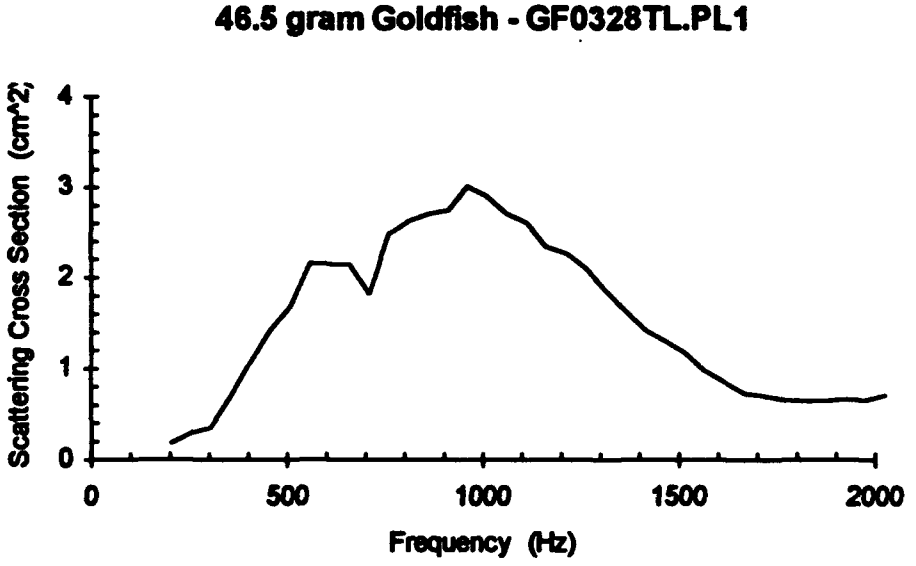

Figure B-17. Swim bladder frequency response of a 43.1 and a 46.5 gram goldfish.

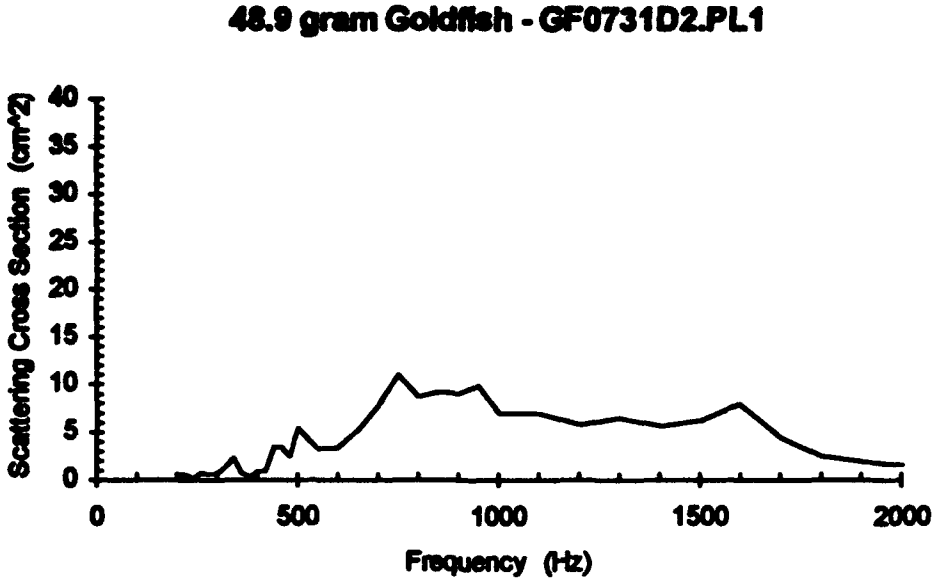

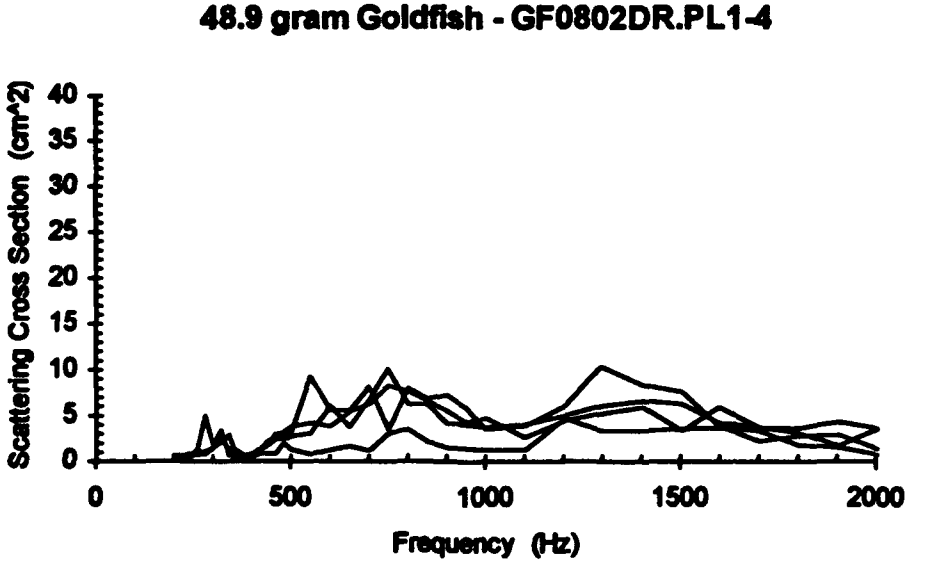

Figure B-18. Swim bladder frequency response of a 48.9 gram goldfish.

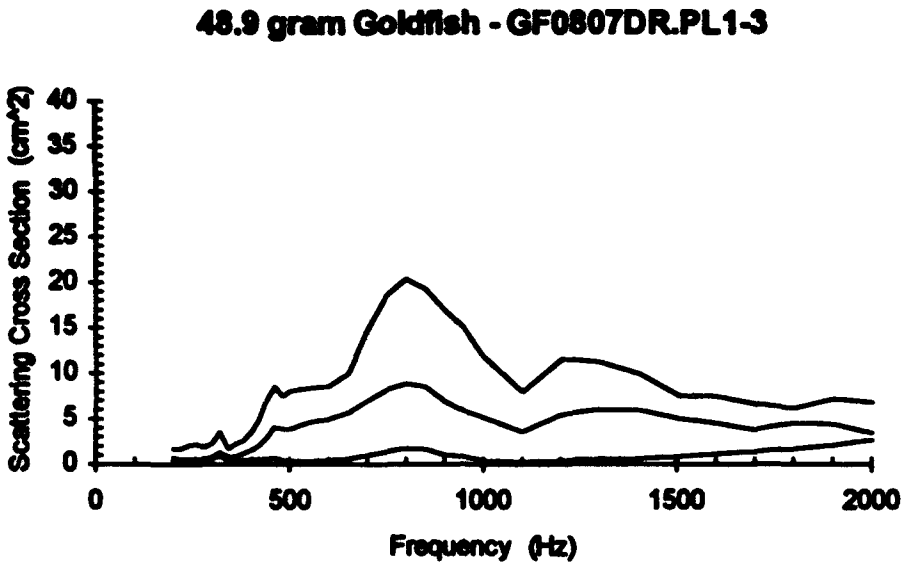

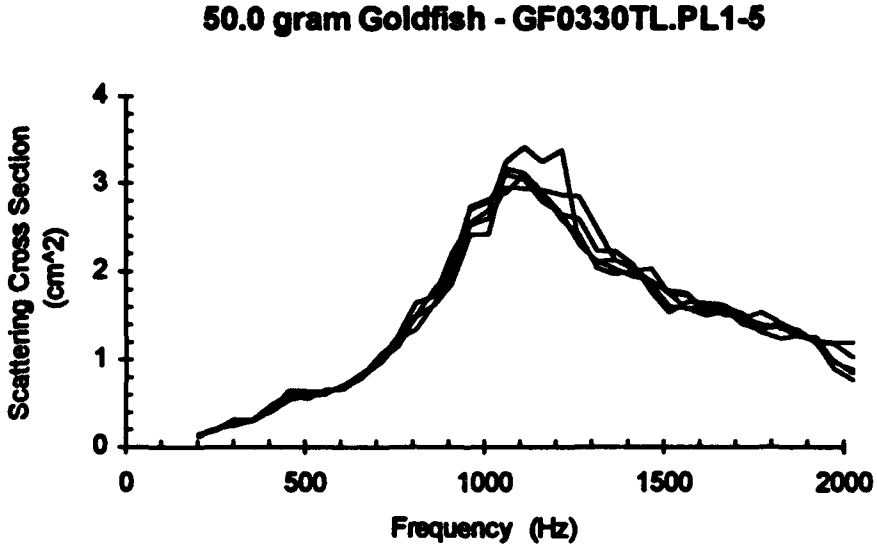

Figure B-19. Swim bladder frequency response of a 48.9 and a 50.0 gram goldfish.

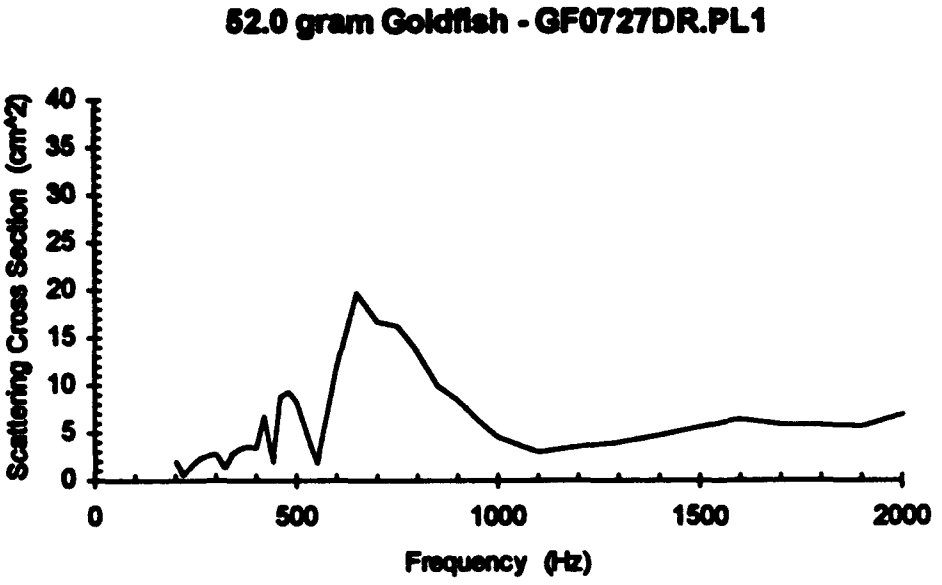

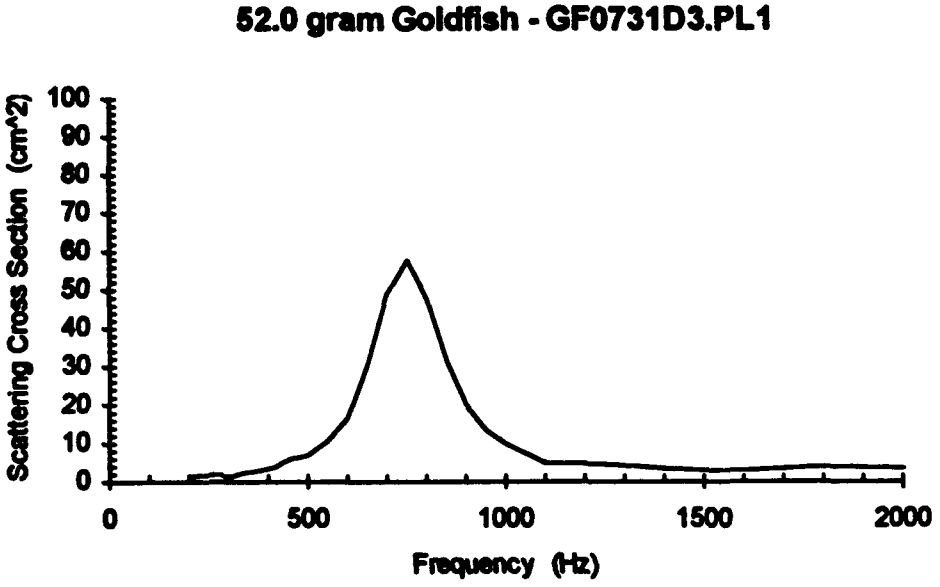

Figure B-20. Swim bladder frequency response of a 52.0 gram goldfish.

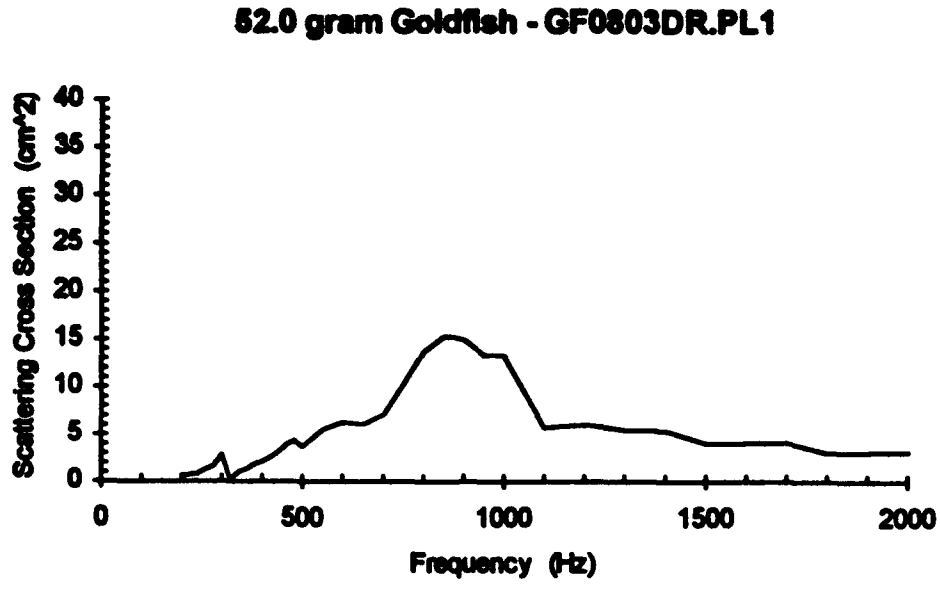

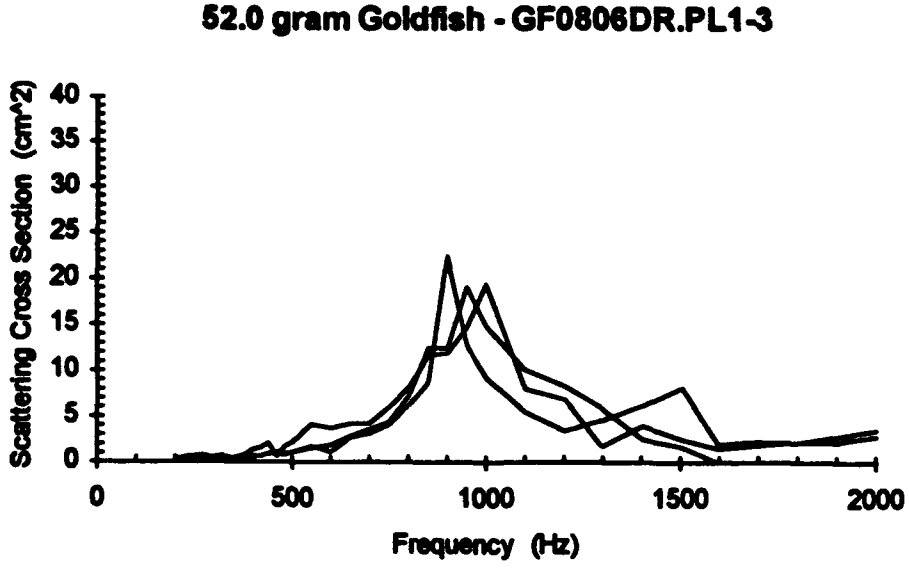

Figure B-21. Swim bladder frequency response of a 52.0 gram goldfish.

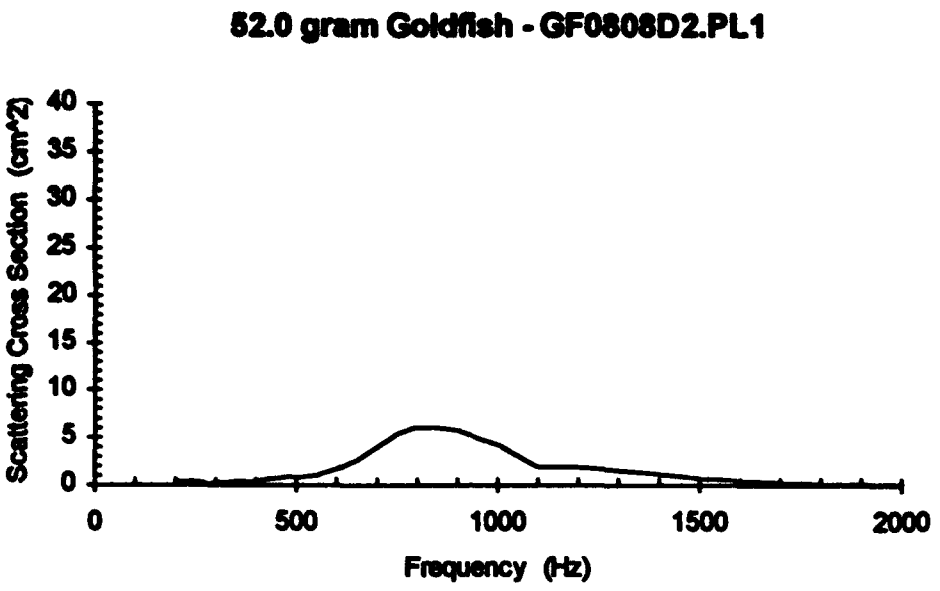

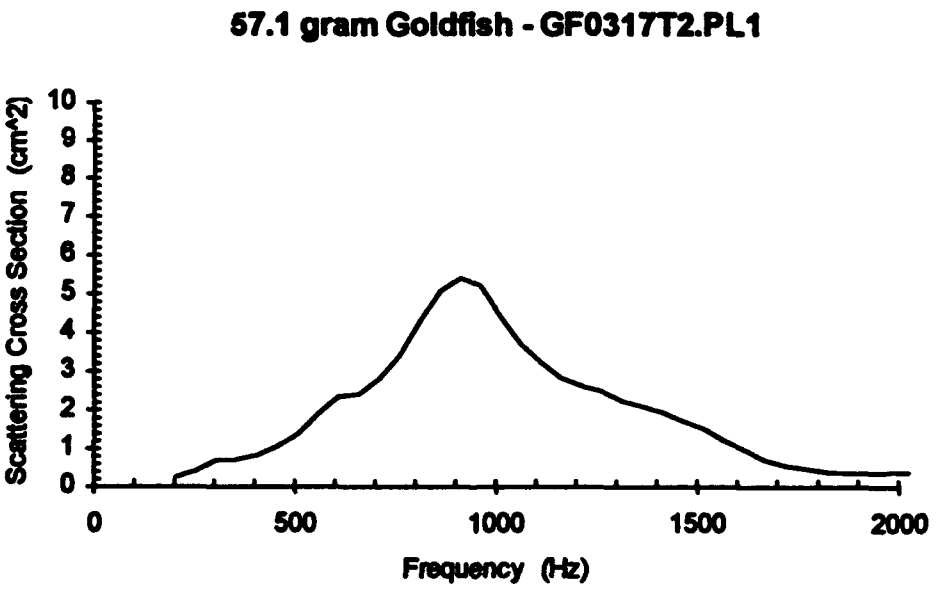

Figure B-22. Swim bladder frequency response of a 52.0 and a 57.1 gram goldfish.

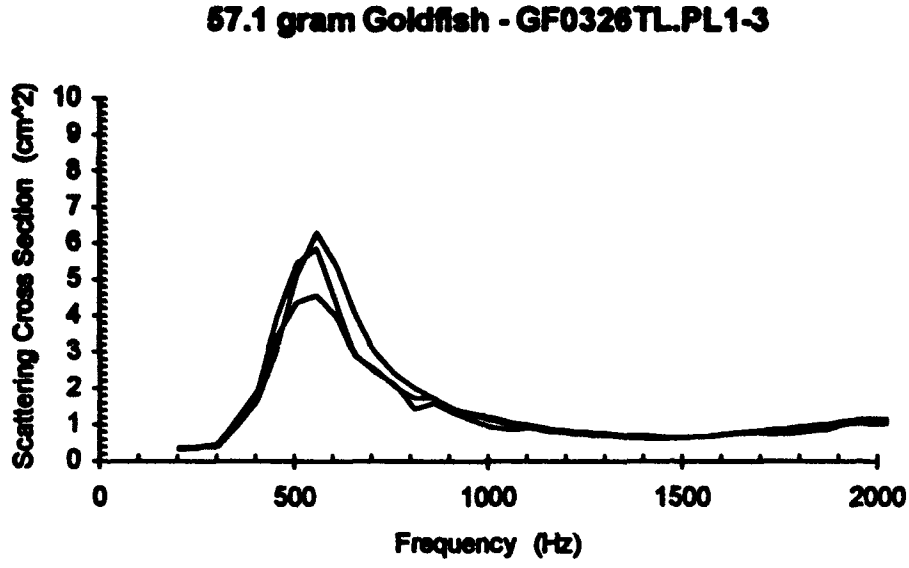

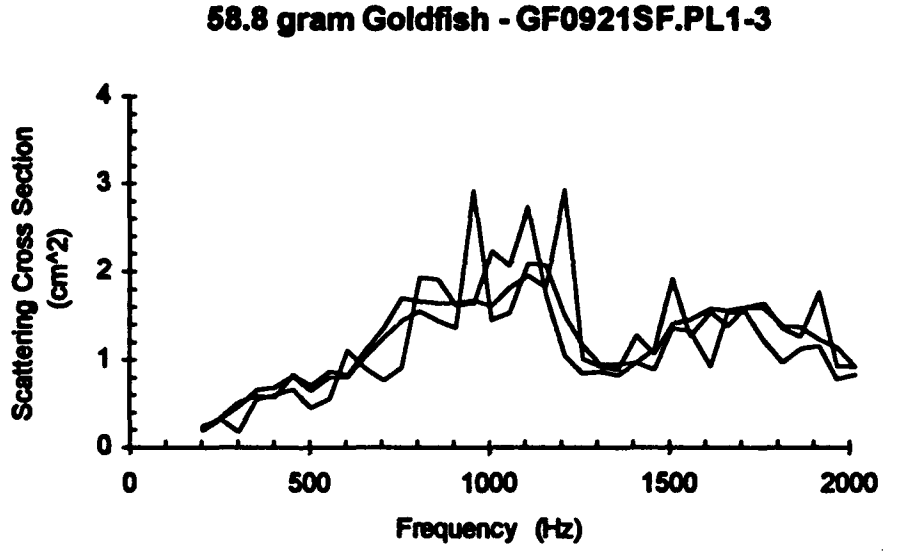

Figure B-23. Swim bladder frequency response of a 57.1 and a 58.8 gram goldfish.

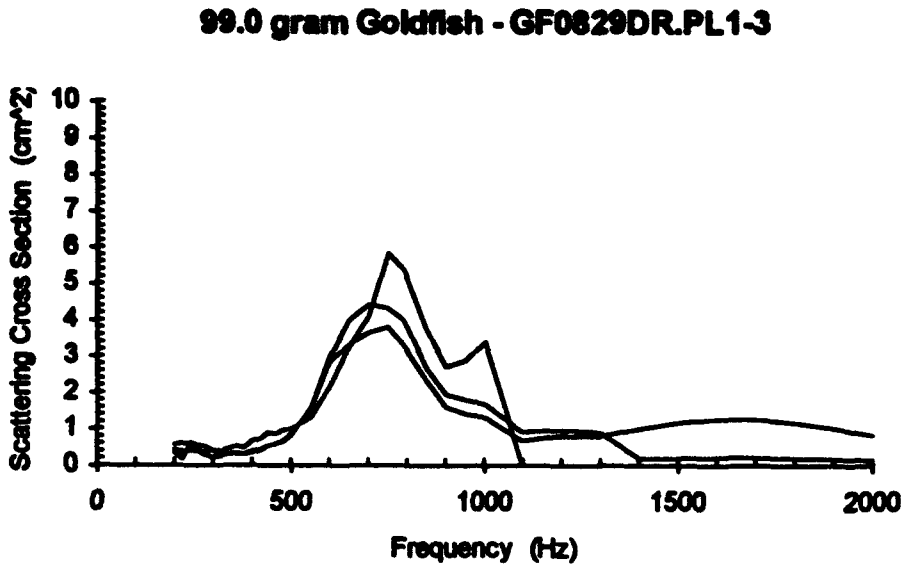

Figure B-24. Swim bladder frequency response of a 99.0 gram goldfish.

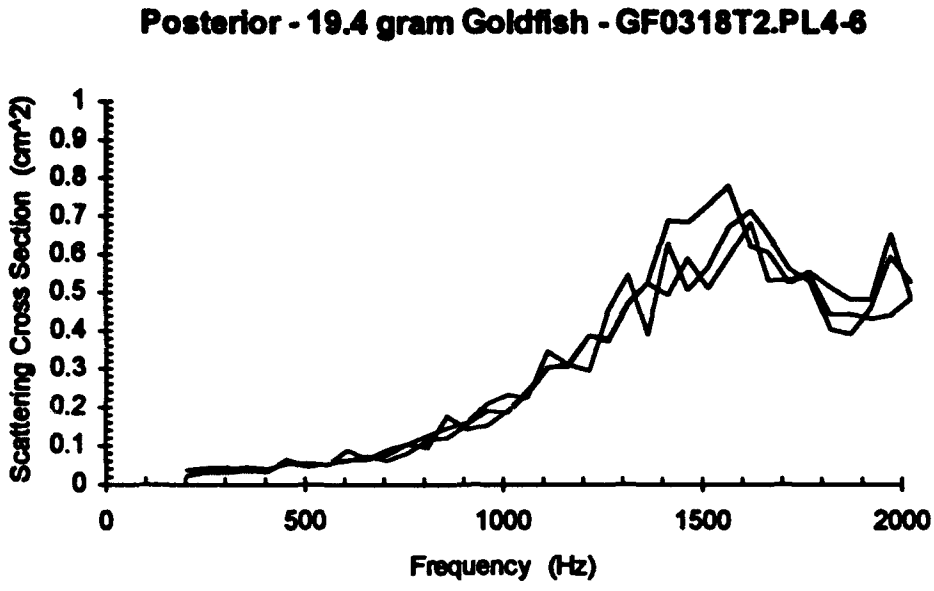

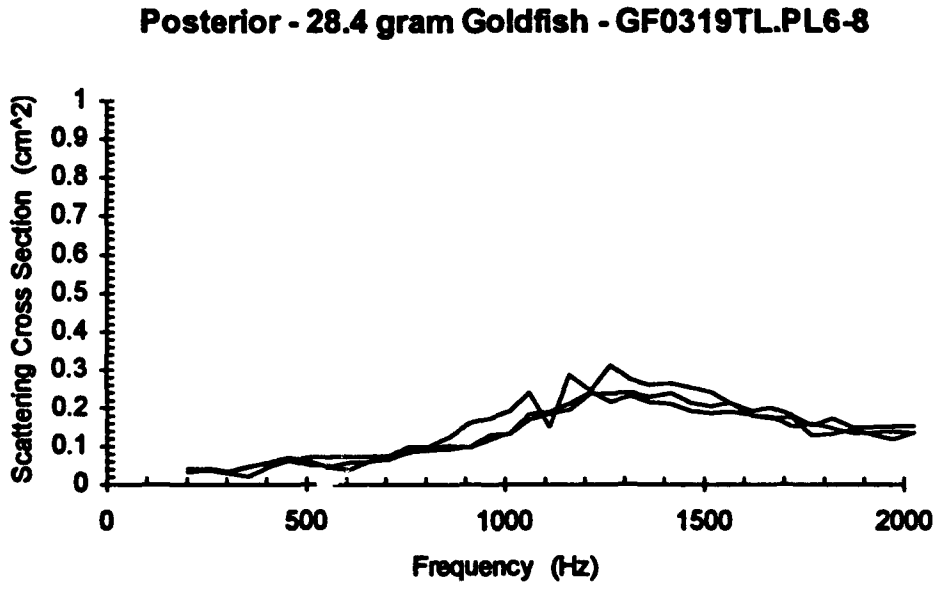

Figure B-25. Posterior swim bladder frequency response of a 19.4 and a 28.4 gram goldfish.

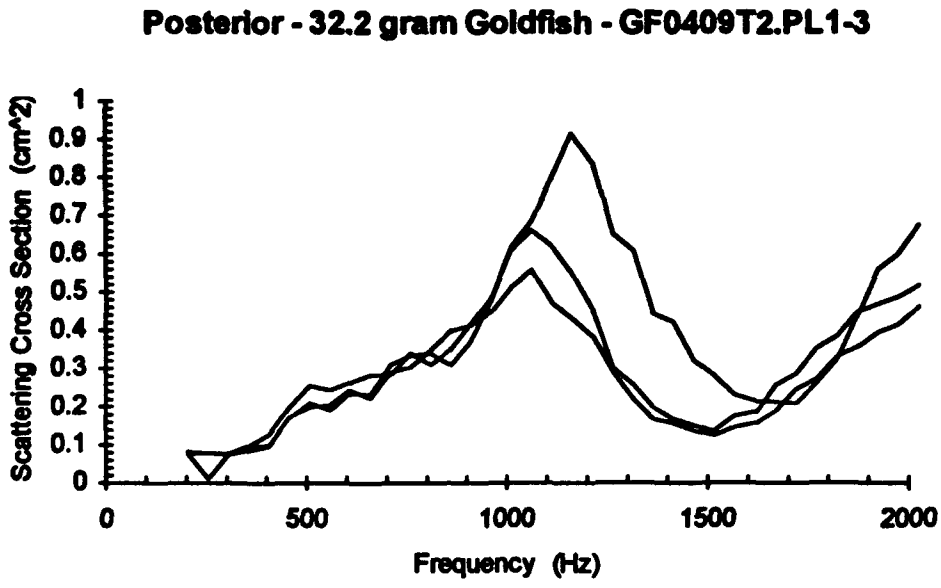

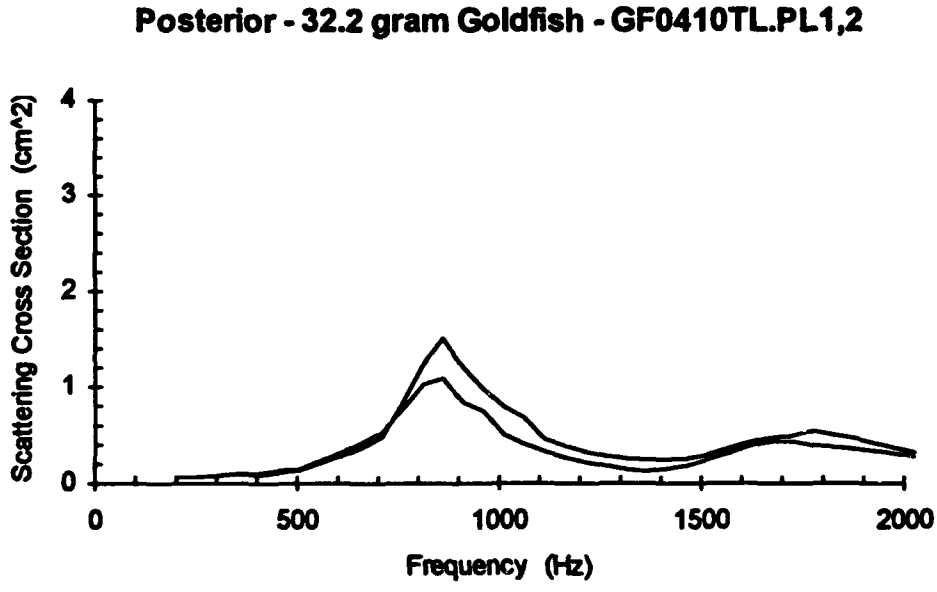

Figure B-26. Posterior swim bladder frequency response of a 32.2 gram goldfish.

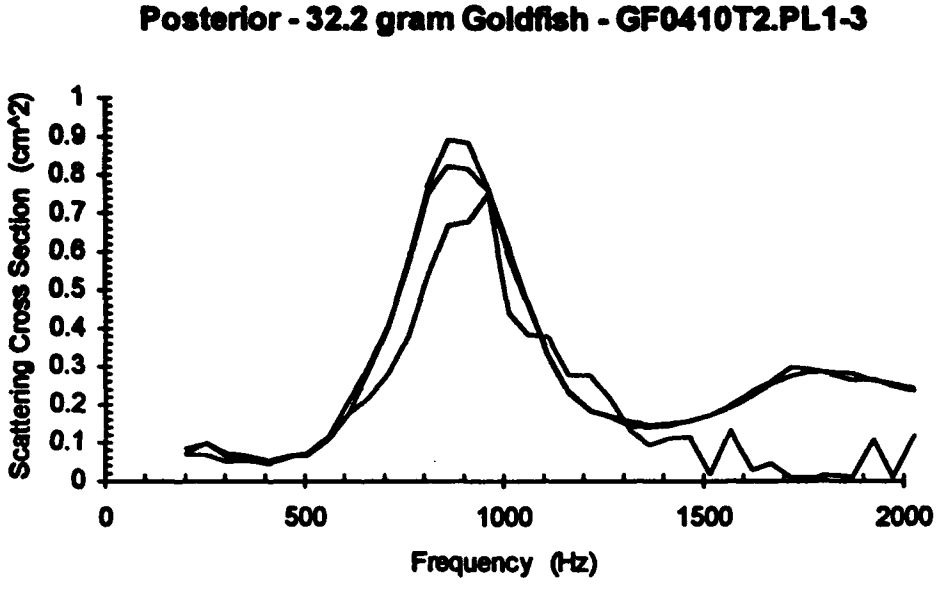

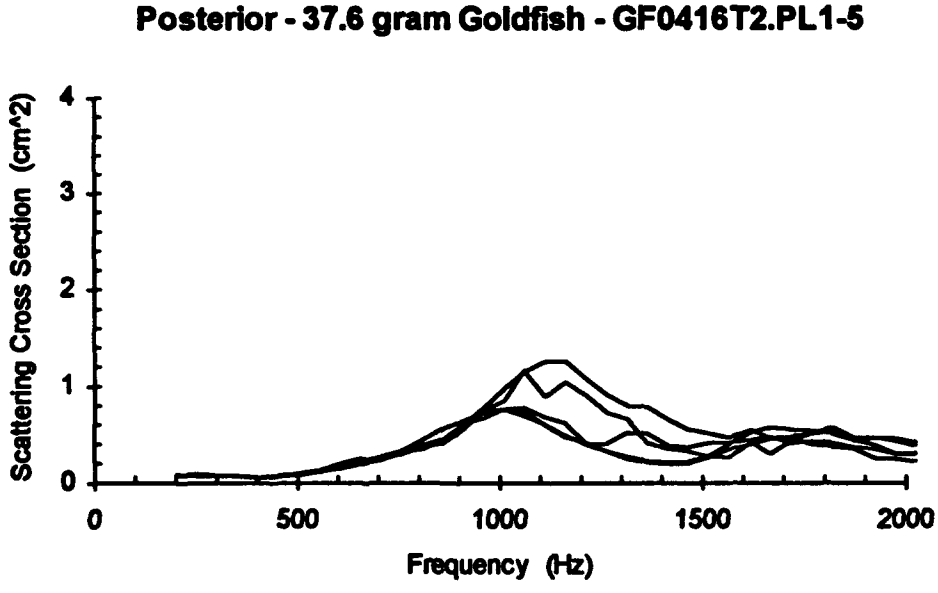

Figure B-27. Posterior swim bladder frequency response of a 32.2 and a 37.6 gram goldfish.

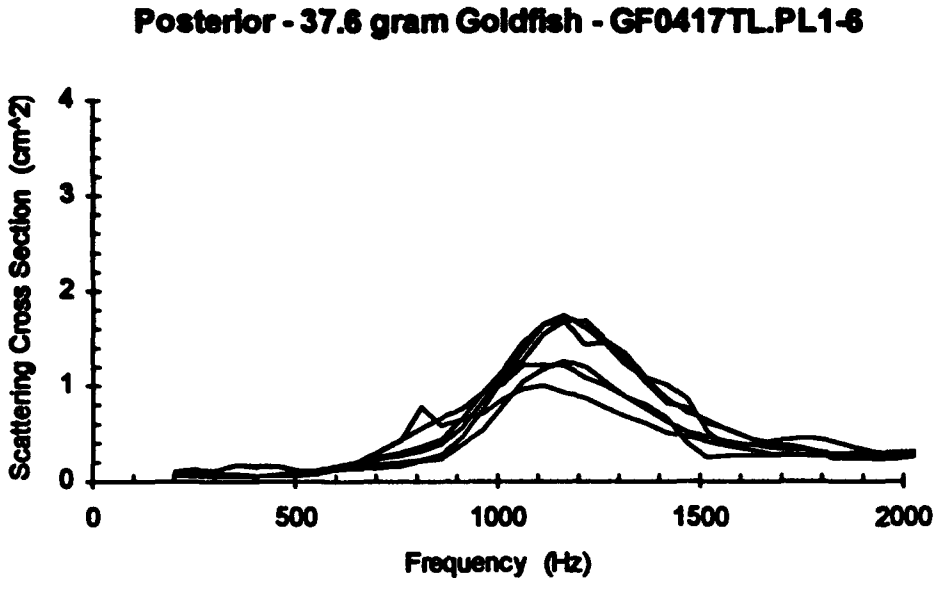

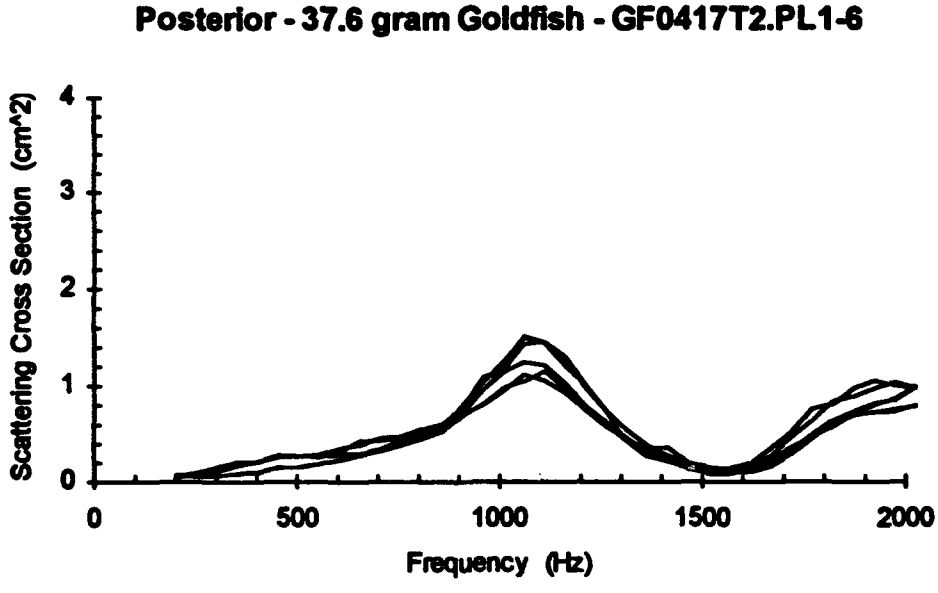

Figure B-28. Posterior swim bladder frequency response of a 37.6 gram goldfish.

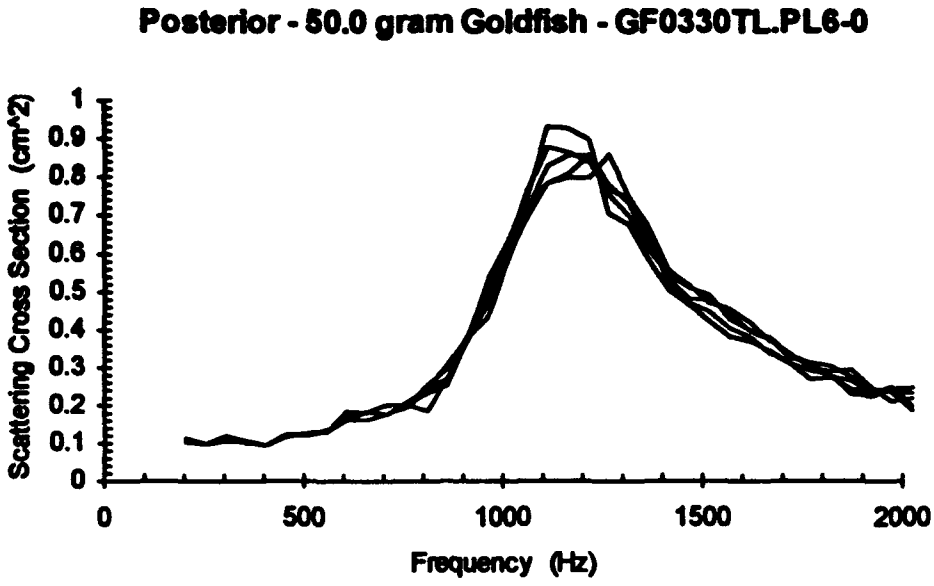

Figure B-29. Posterior swim bladder frequency response of a 50.0 gram goldfish.

Appendix C

Swim Bladder Response of Oscars

Appendix C contains the oscar swim bladder data collected from 1989 to 1991 by David Rogers, Steve Flanagan, Thomas Lewis, and Wen Zhou using the NIVAMS as described in Chapter 3. Table C-1 consists of the parameters describing the responses in the chronological order that the data was taken. The file name corresponds to a set of frequency sweeps for a given fish on a given day. The file extension identifies separate sweeps. The masses of the fish are unique - different masses correspond to different fish, identical masses are the same fish.

The data was fit to a generalized form of the scattering cross-section,

$$\sigma_s = \frac{4\pi a^2}{\left[\left(\frac{\omega_0}{\omega}\right)^2 - 1\right]^2 + \frac{\omega_0^{\,2}}{Q^2\omega^2}}, \qquad \text{(C-1)}$$

using a three parameter (a, ω_0, and Q) non-linear least squares curve fit. The first parameter, a, characterizes the size of the scatterer and acts as a scaling function. The resonant frequency, ω_0, locates the natural frequency of the system. The quality factor, Q, is a measure of the bandwidth of the peak. The final column, OK?, indicates a subjective assessment of whether the best fit curve follows the trend of the data points. Parameters from curves that did not were not used in further analysis. Figures C-1 to C-29 are the plots of the data for each fish on each day, shown in order of increasing mass.

Table C-1. Oscar swim bladder data.

File Name	.Ext	Mass (g)	a (m)	Res. Freq. (Hz)	Q	OK?
OS0828DR	.PL1	25.0				no
	.PL2		0.0016	526.2	3.682	
	.PL3					no
OS0920SF	.PL1	63.3	0.0021	475.6	3.713	
	.PL2					no
OS0307TL	.PL1	12.9	0.0017	601.9	3.365	
	.PL2		0.0018	601.7	3.117	
OS0308TL	.PL1	13.8				no
OS0420TL	.PL1	6.2	0.0022	894.8	4.168	
OS0421TL	.PL1	15.4	0.0019	644.9	3.812	
	.PL2		0.0018	681.5	3.596	
OS0422TL	.PL1	37.4	0.0019	529.1	3.746	
	.PL2		0.0019	550.4	3.868	
OS0423TL	.PL1	184.4	0.0021	258.9	3.891	
OS011	.PL1	14.1	0.0016	545.2	2.530	
OS021	.PL1	34.3	0.0020	449.3	4.133	
	.PL2		0.0020	438.9	4.340	
OS031	.PL1	53.8	0.0023	394.9	5.076	
	.PL2		0.0022	382.7	5.078	
	.PL3		0.0025	406.1	3.836	
OS041	.PL1	57.5	0.0021	384.1	3.842	
	.PL2		0.0022	396.1	3.369	
	.PL3		0.0022	400.1	3.329	
OS051	.PL1	37.4				no
	.PL2					no
OS061	.PL1	13.8	0.0017	642.2	3.771	
	.PL2		0.0017	606.6	3.432	
OS071	.PL1	41.7	0.0022	558.5	3.614	
	.PL2		0.0023	578.3	3.179	
OS081	.PL1	45.4	0.0021	444.2	3.791	
OS091	.PL1	38.0	0.0025	502.7	2.964	
OS101	.PL1	42.9	0.0018	438.7	3.071	
OS111	.PL1	6.5	0.0016	791.2	4.353	
OS121	.PL1	16.9	0.0020	565.9	4.236	
OS141	.PL1	11.4	0.0018	625.4	4.164	
OS151	.PL1	12.3	0.0019	673.4	3.745	
OS161	.PL1	35.4	0.0022	498.3	3.067	
OS171	.PL1	16.1	0.0019	569.1	4.180	
OS181	.PL1	9.1	0.0016	705.1	4.437	

File Name	.Ext	Mass (g)	a (m)	Res. Freq. (Hz)	Q	OK?
OS191	.PL1	6.7	0.0017	745.1	4.388	
OS201	.PL1	6.9	0.0016	750.6	5.022	
OS211	.PL1	7.8	0.0018	750.7	4.888	
OS221	.PL1	7.5	0.0016	781.8	3.535	
OS231	.PL1	48.6	0.0023	389.6	5.002	
OS241	.PL1	27.2	0.0024	539.1	4.332	
OS251	.PL1	21.9	0.0024	567.3	4.189	

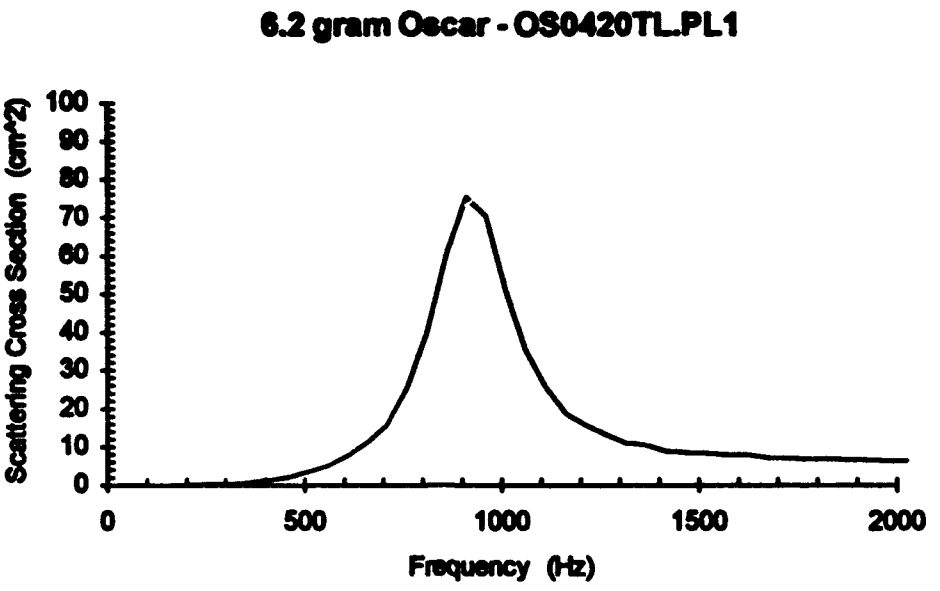

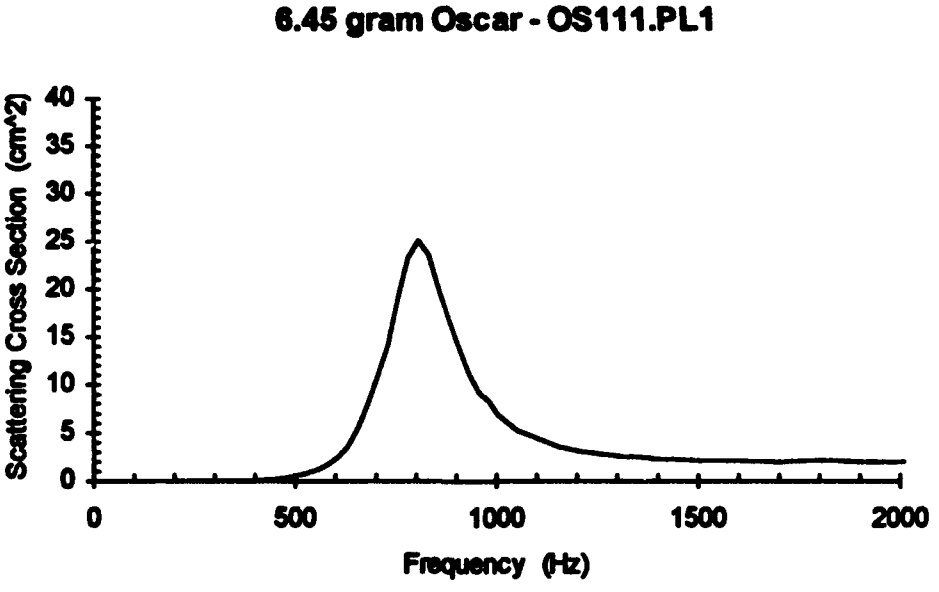

Figure C-1. Swim bladder frequency response of a 6.2 gram and a 6.45 gram oscar.

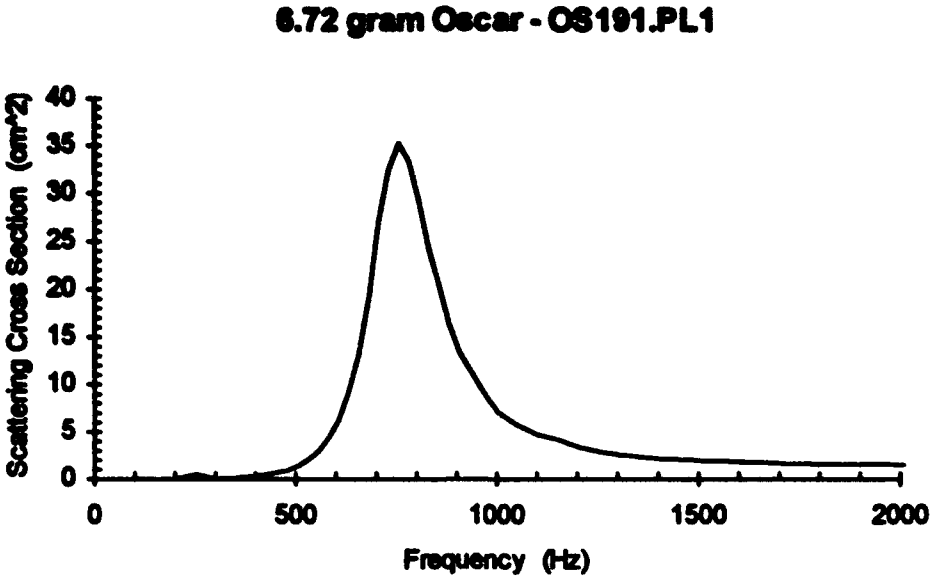

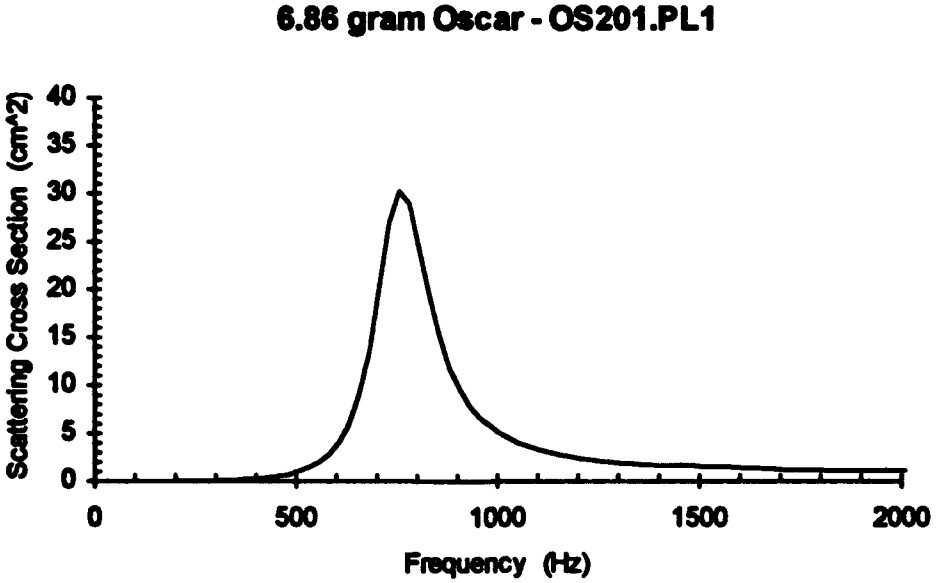

Figure C-2. Swim bladder frequency response of a 6.72 gram and a 6.86 gram oscar.

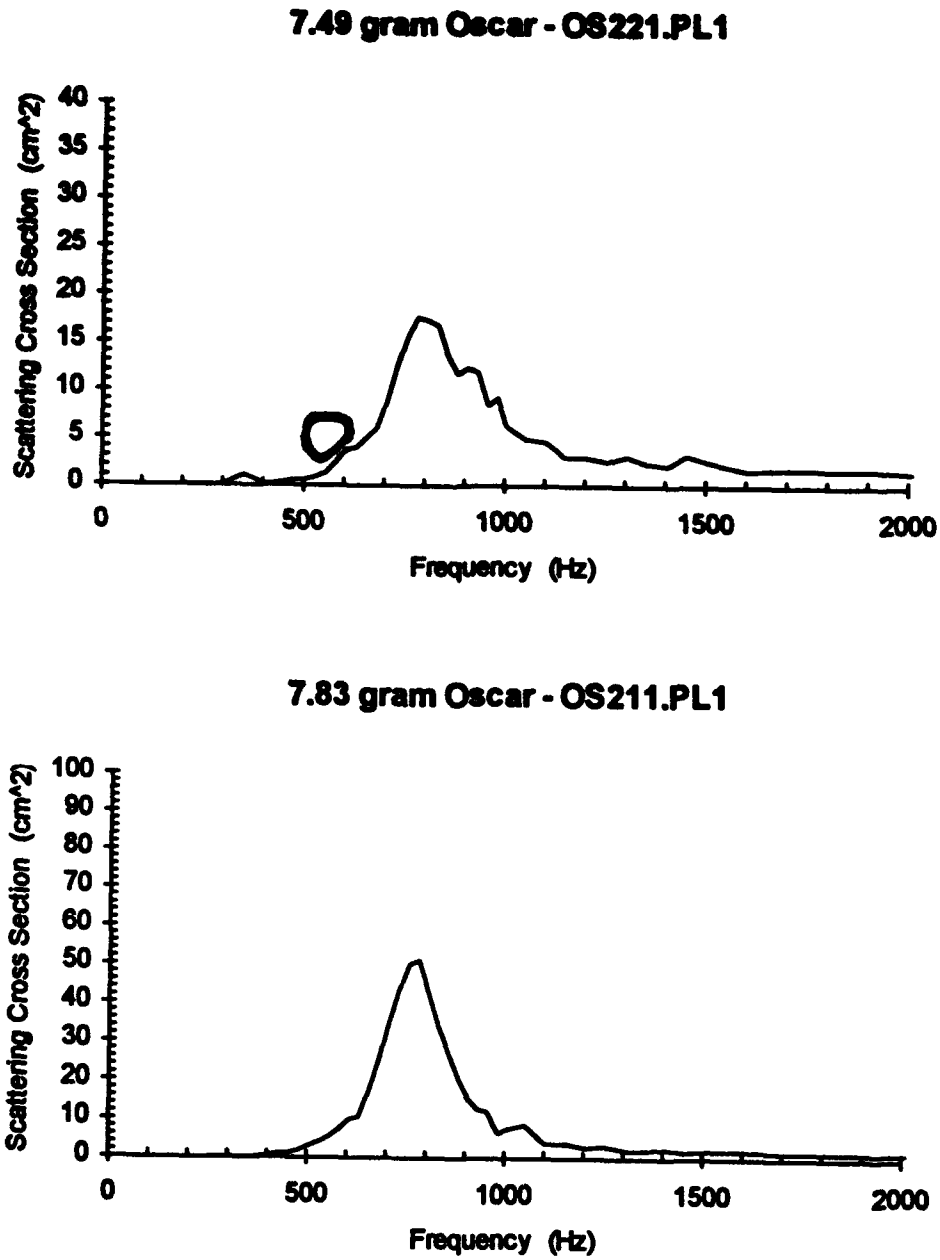

Figure C-3. Swim bladder frequency response of a 7.49 gram and a 7.83 gram oscar.

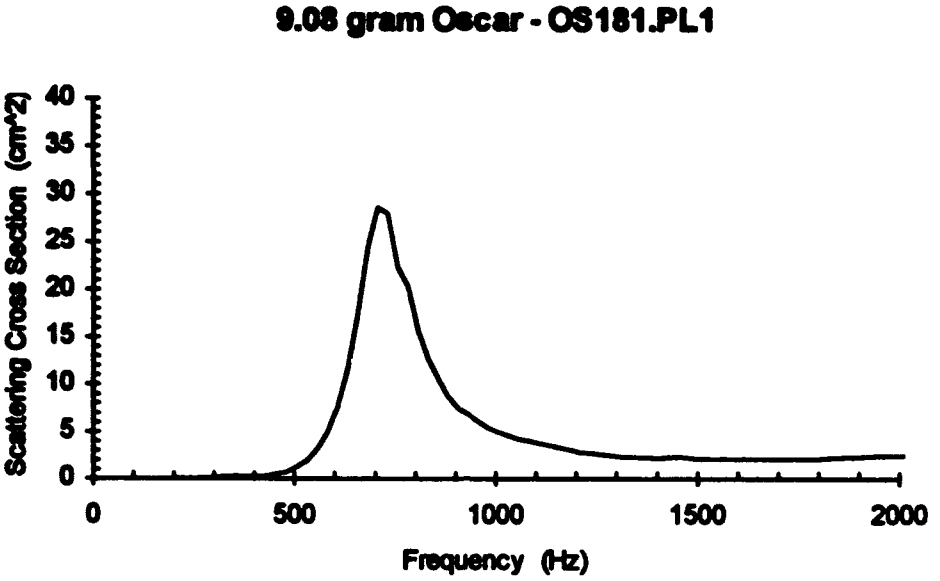

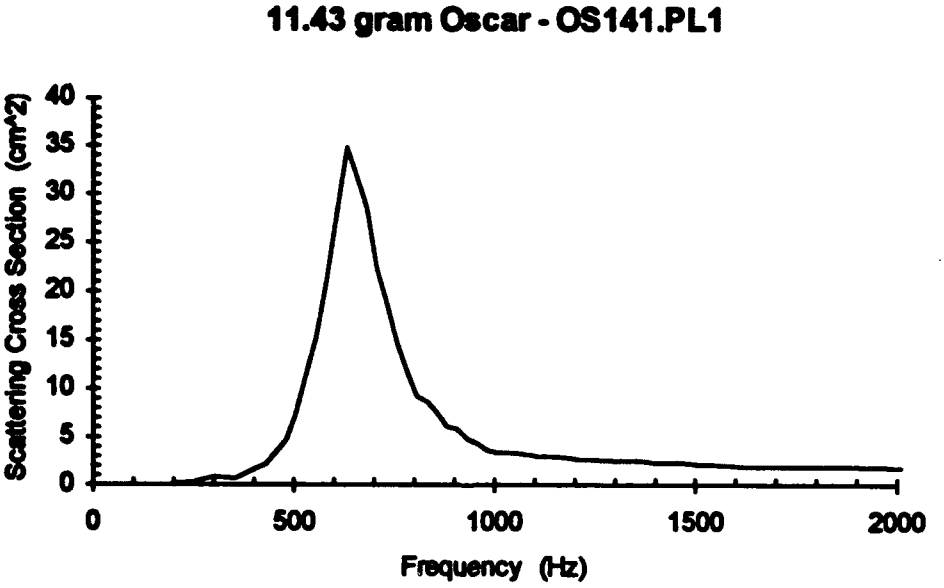

Figure C-4. Swim bladder frequency response of a 9.08 gram and a 11.43 gram oscar.

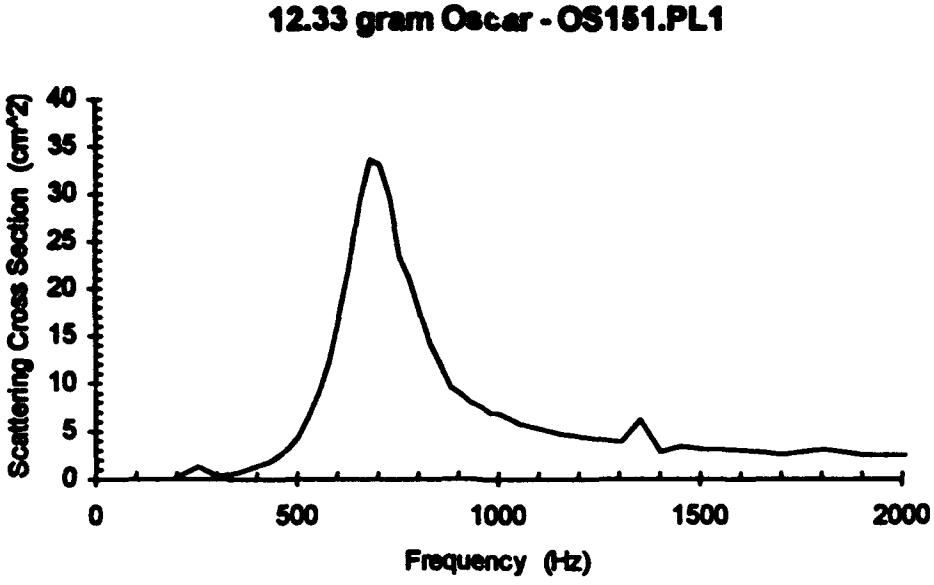

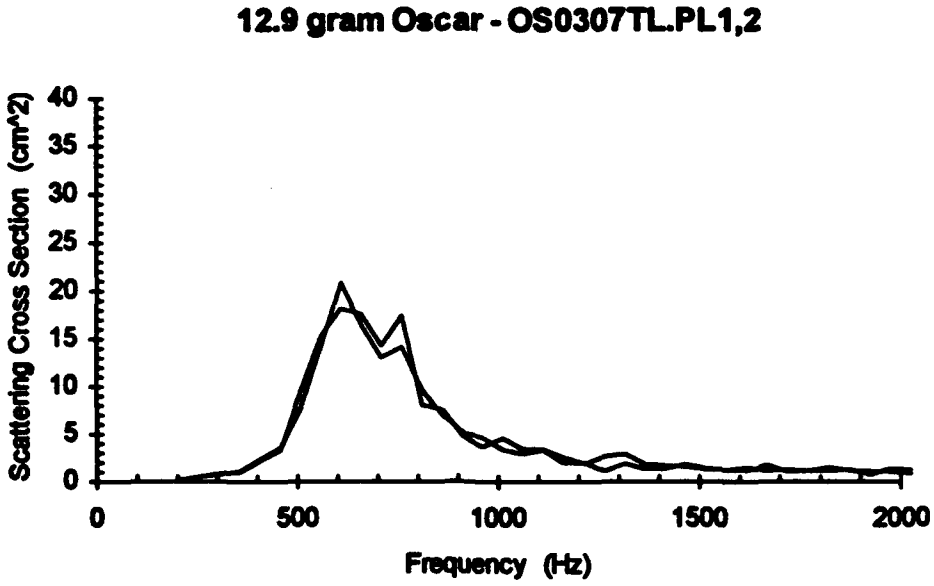

Figure C-5. Swim bladder frequency response of a 12.33 gram and a 12.9 gram oscar.

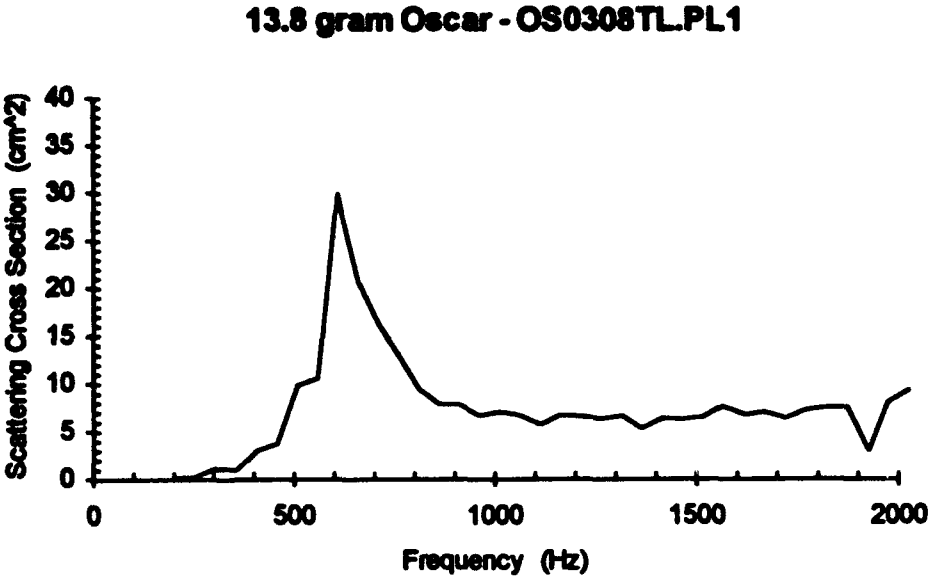

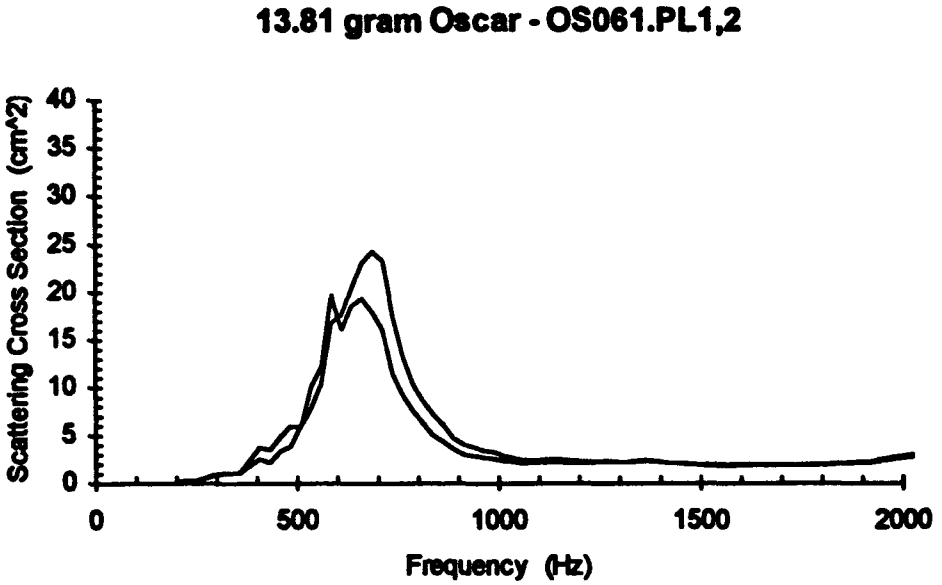

Figure C-6. Swim bladder frequency response of a 13.8 gram and a 13.81 gram oscar.

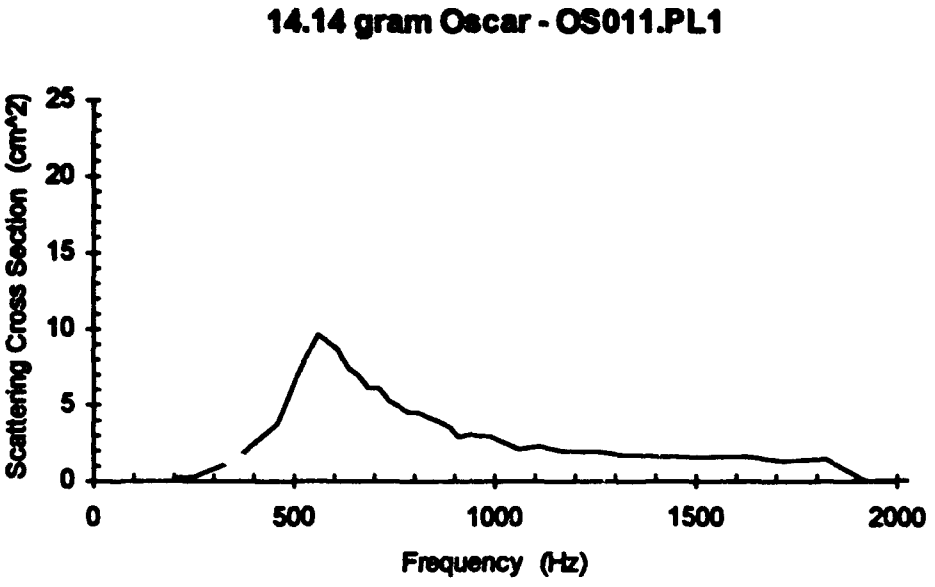

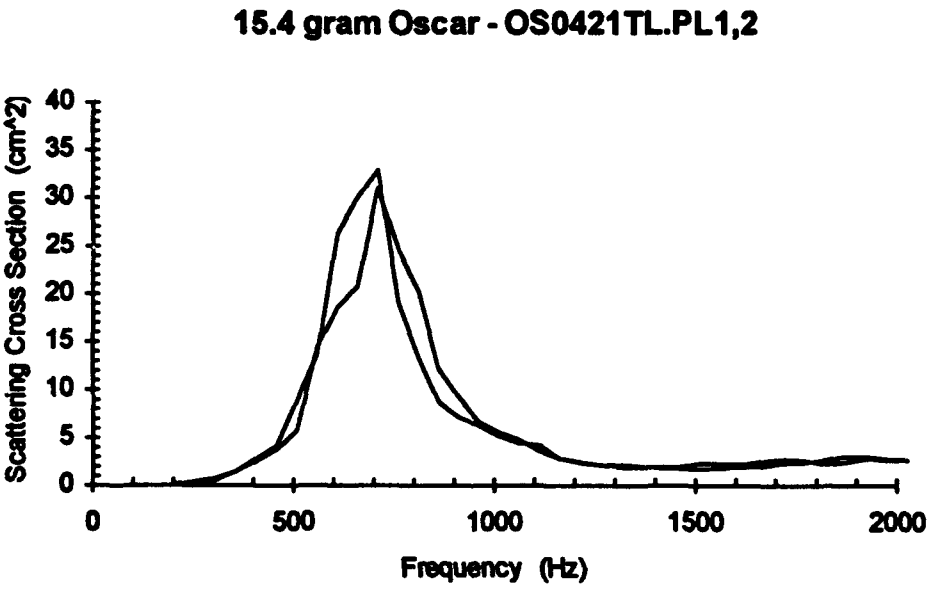

Figure C-7. Swim bladder frequency response of a 14.14 gram and a 15.4 gram oscar.

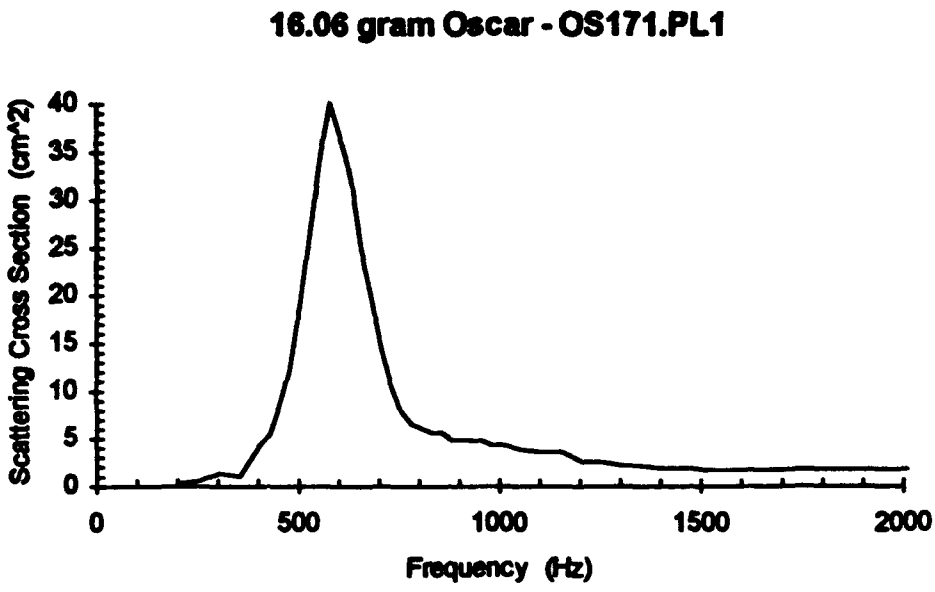

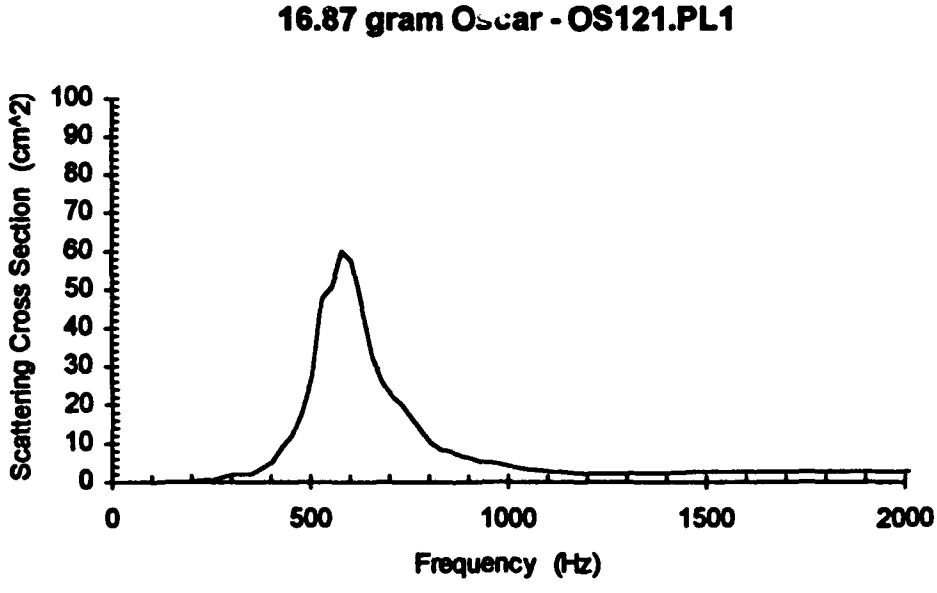

Figure C-8. Swim bladder frequency response of a 16.06 gram and a 16.87 gram oscar.

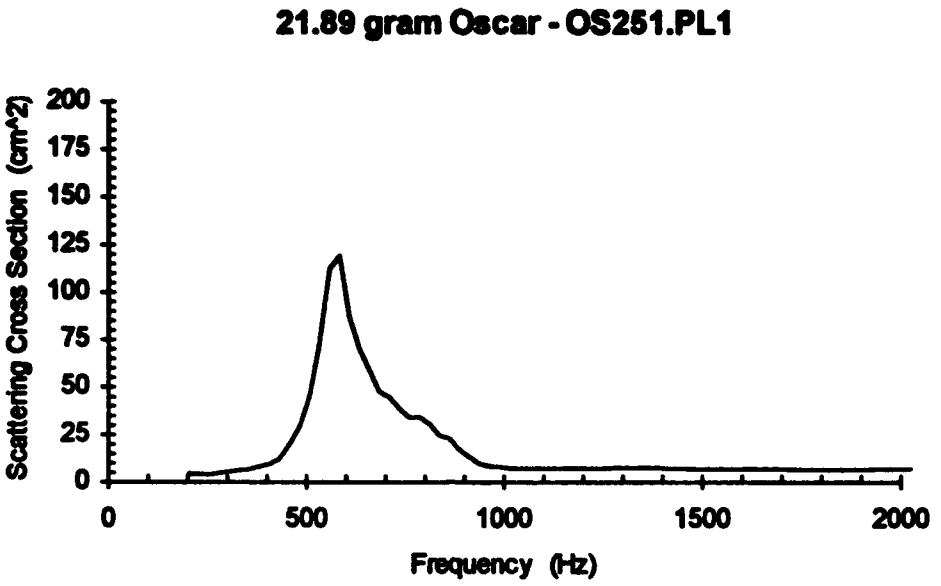

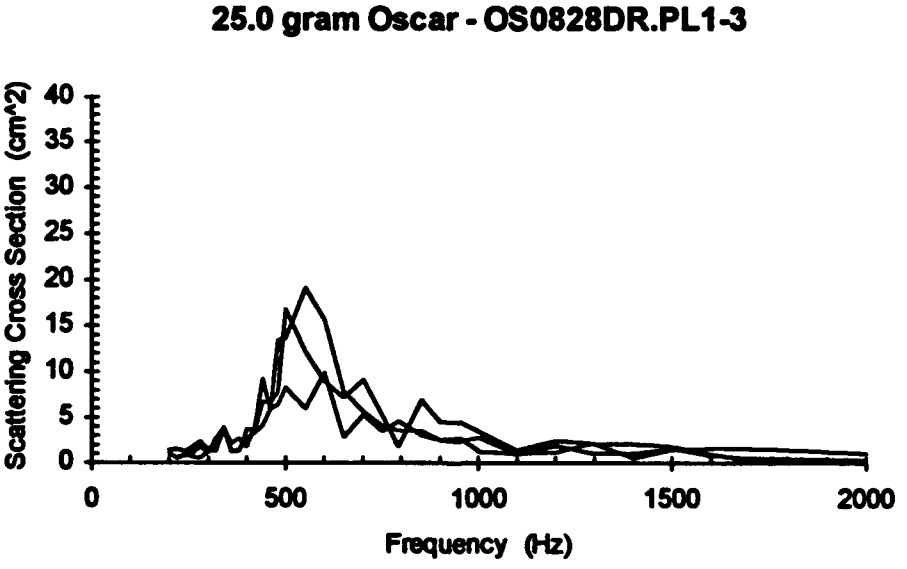

Figure C-9. Swim bladder frequency response of a 21.89 gram and a 25.0 gram oscar.

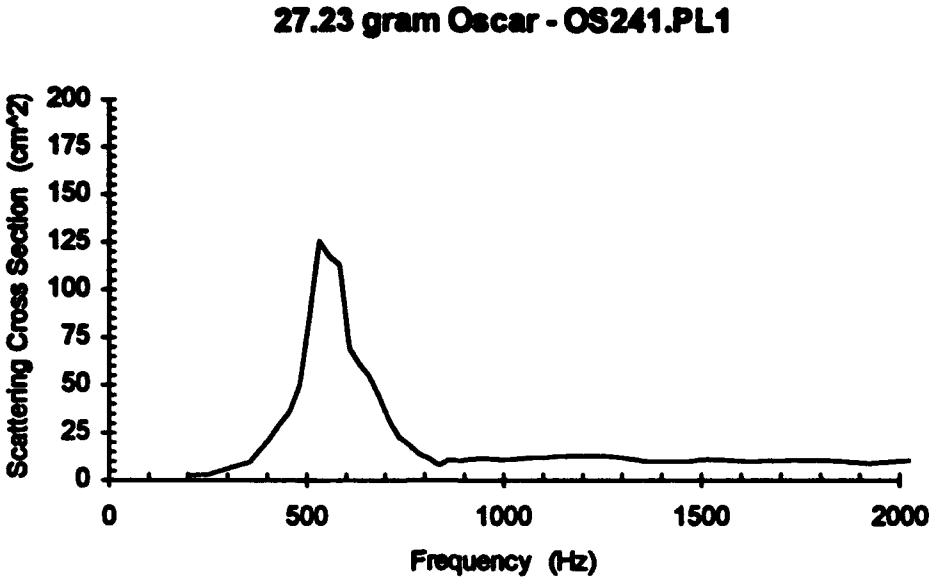

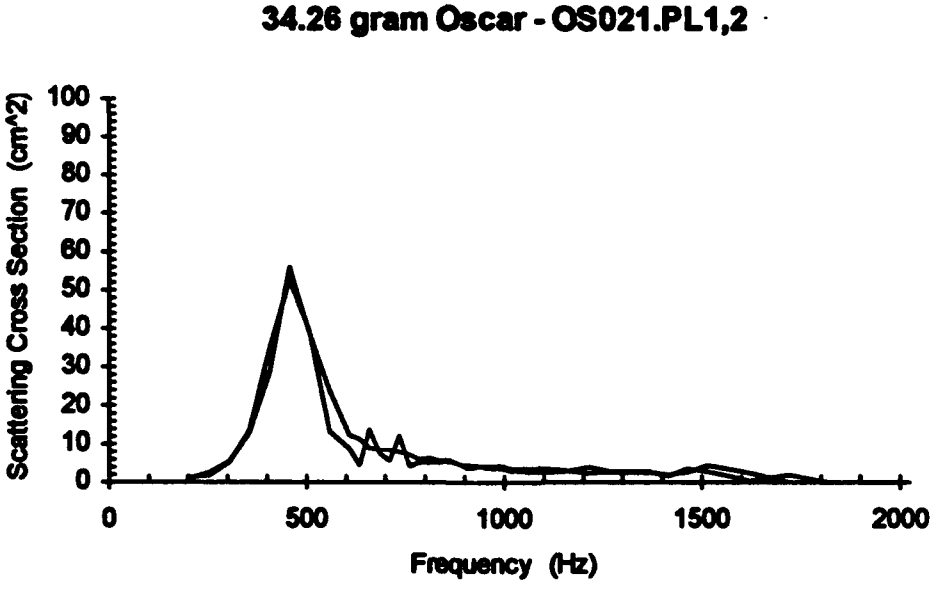

Figure C-10. Swim bladder frequency response of a 27.23 gram and a 34.26 gram oscar.

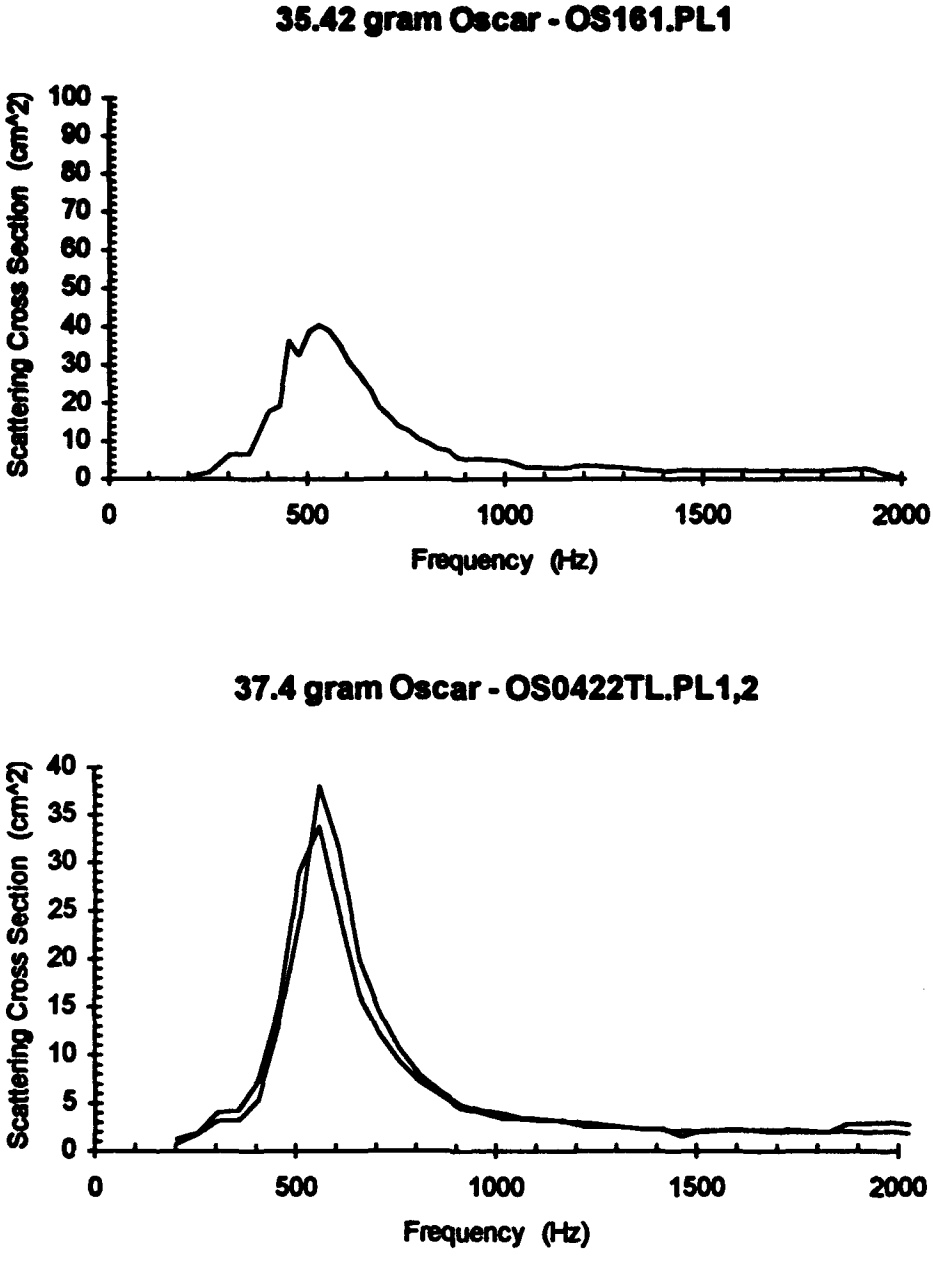

Figure C-11. Swim bladder frequency response of a 35.42 gram and a 37.4 gram oscar.

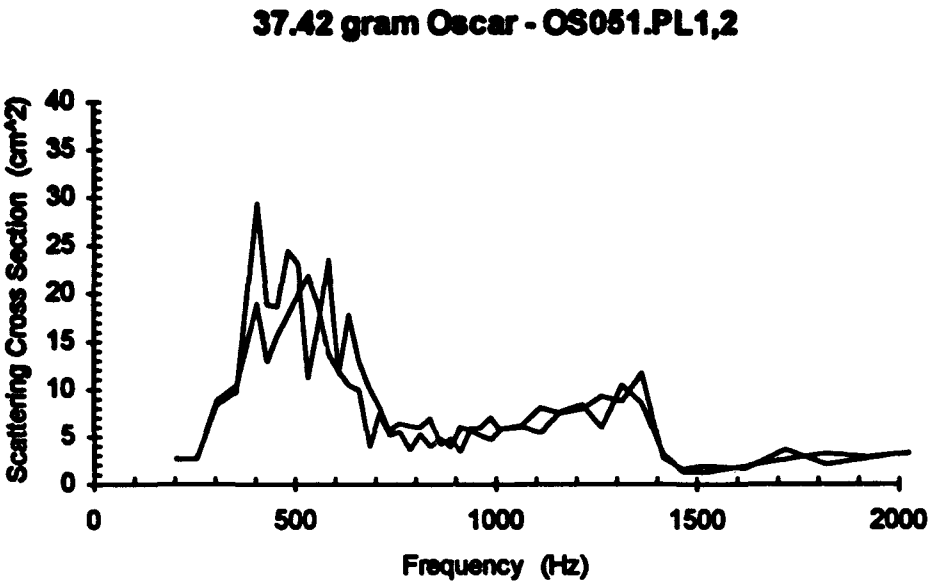

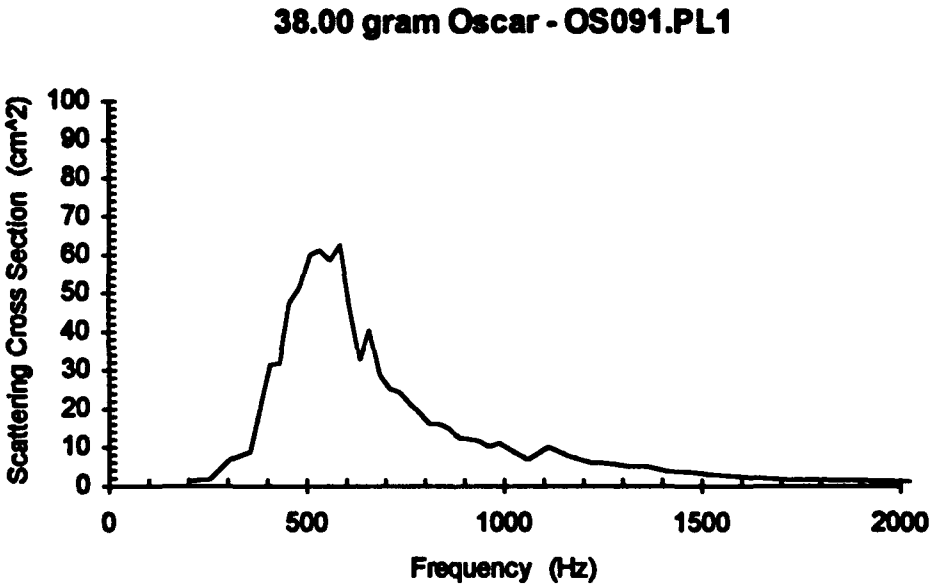

Figure C-12. Swim bladder frequency response of a 37.42 gram and a 38.00 gram oscar.

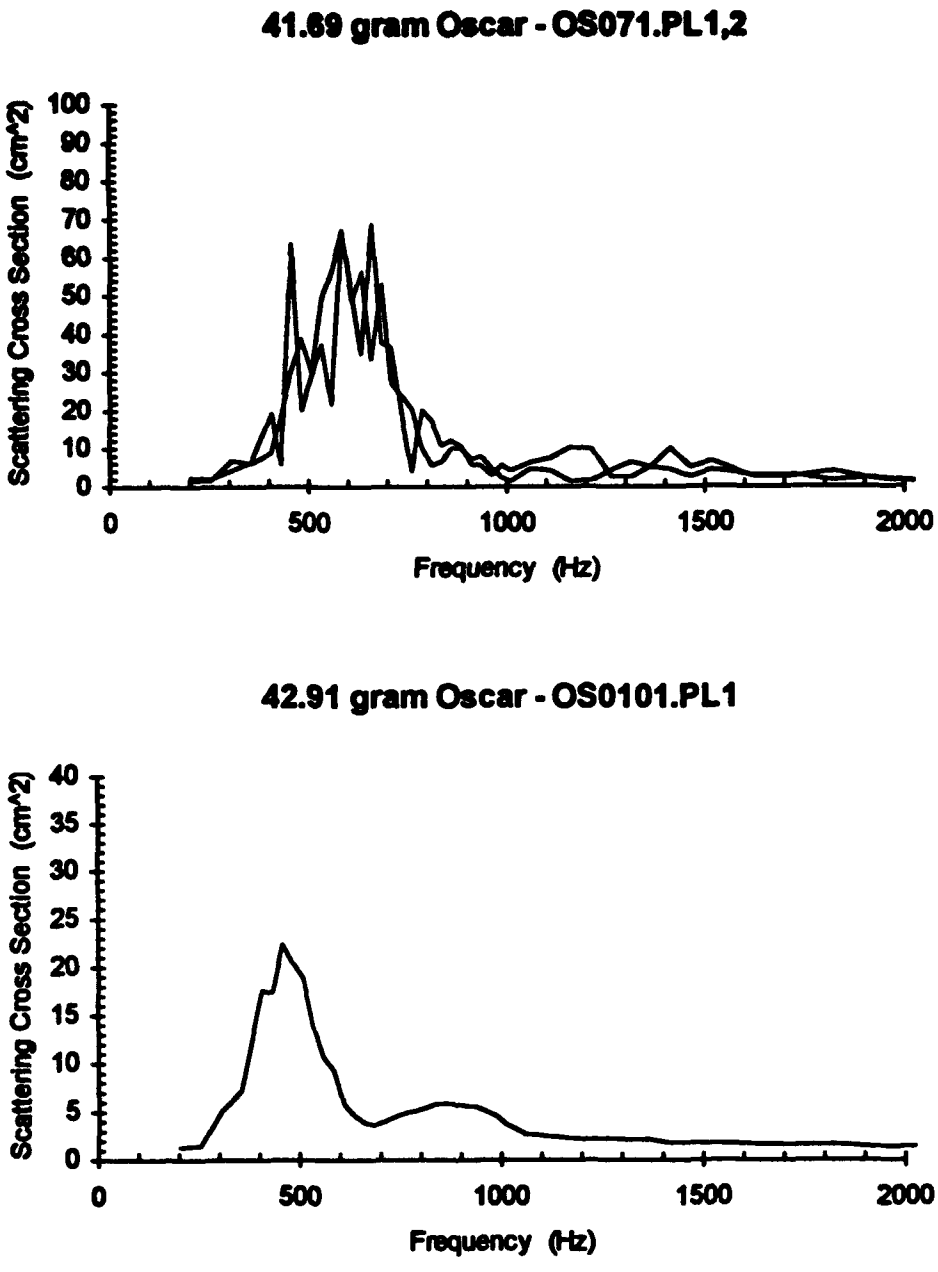

Figure C-13. Swim bladder frequency response of a 41.69 gram and a 42.91 gram oscar.

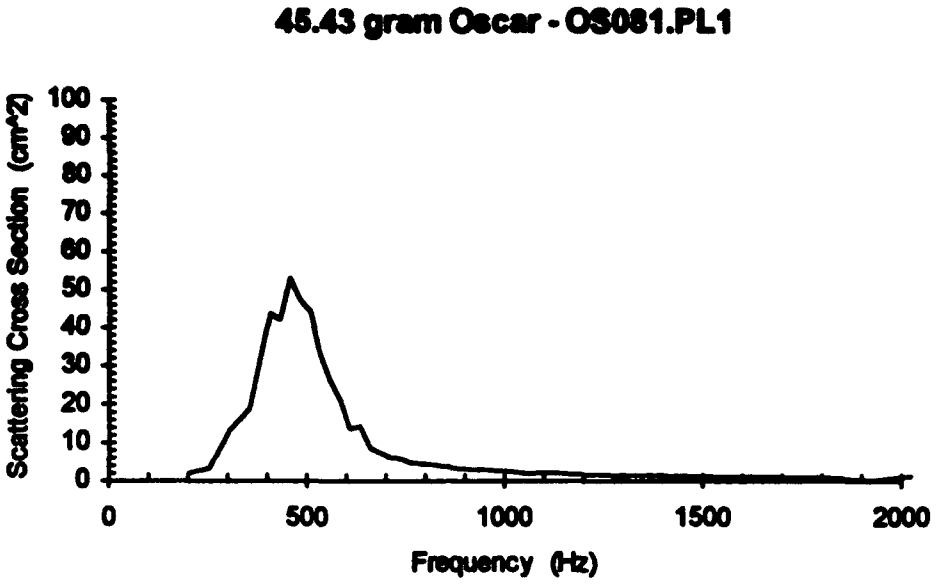

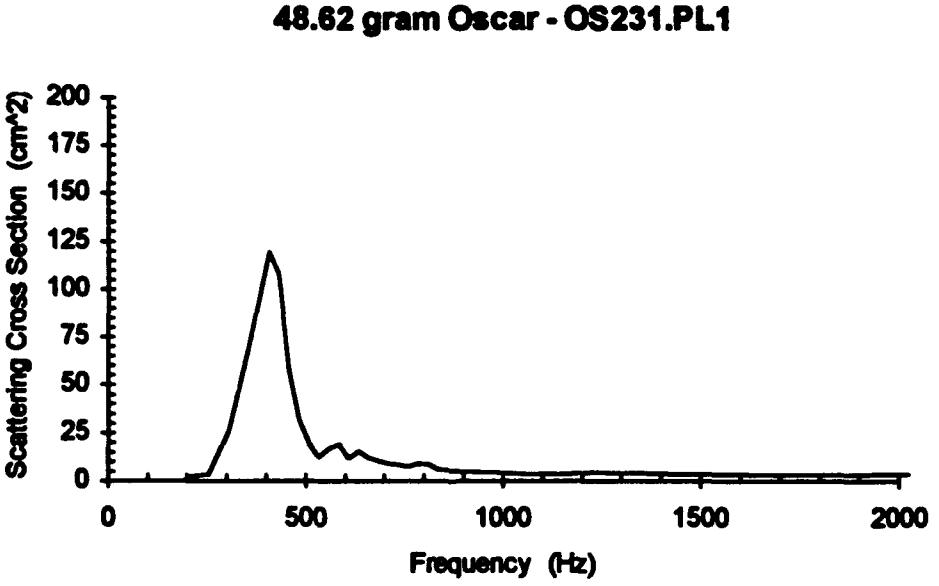

Figure C-14. Swim bladder frequency response of a 45.43 gram and a 48.62 gram oscar.

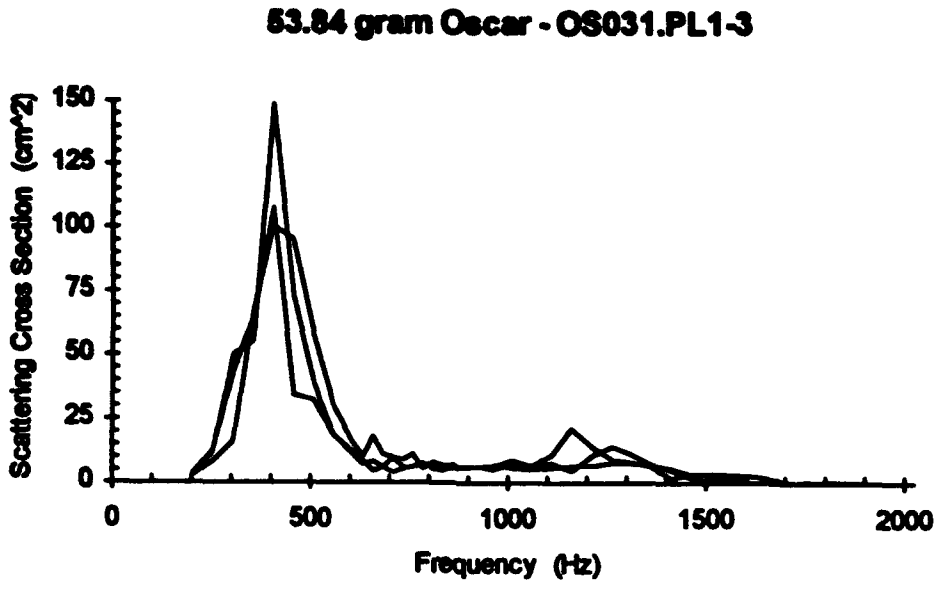

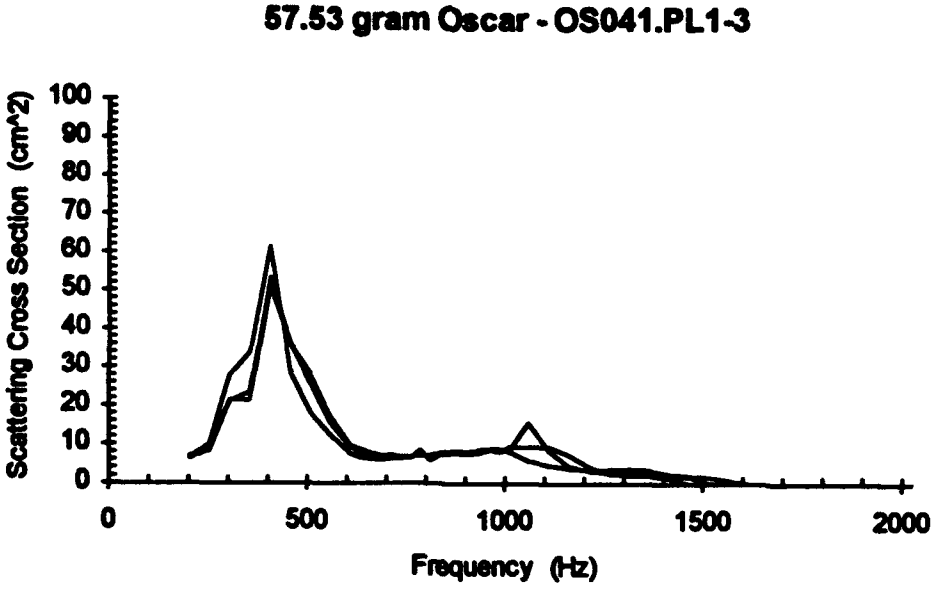

Figure C-15. Swim bladder frequency response of a 53.84 gram and a 57.53 gram oscar.

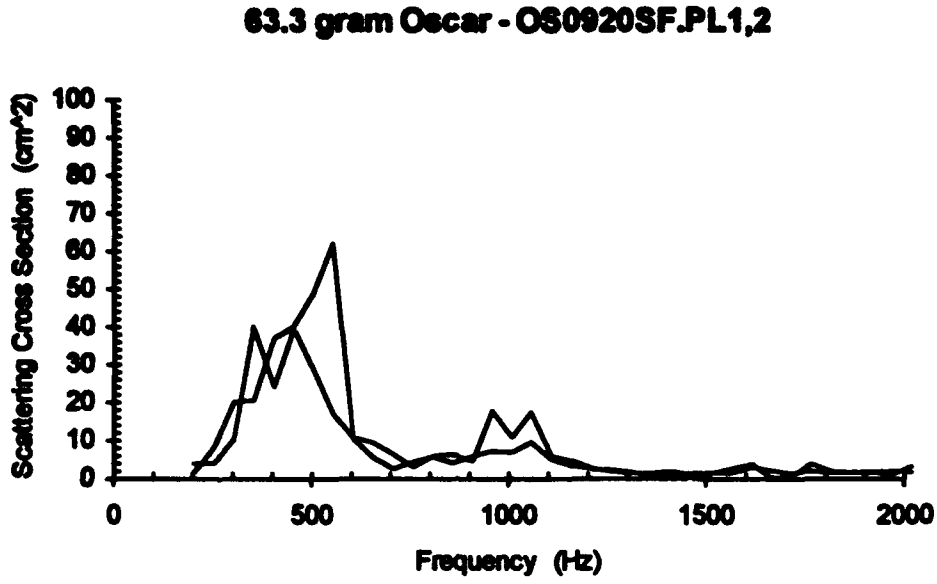

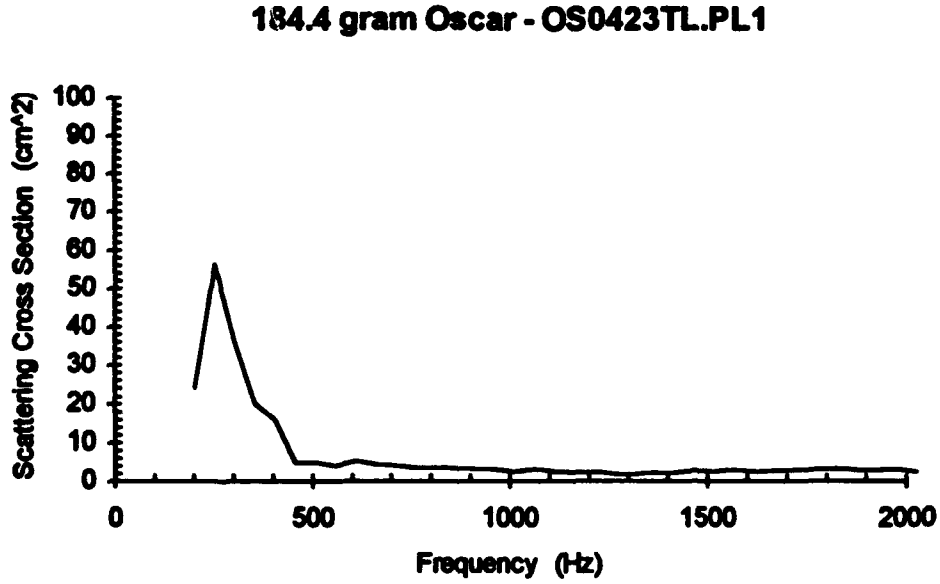

Figure C-16. Swim bladder frequency response of a 63.3 gram and a 184.4 gram oscar.

Appendix D

Calibration Curves for the

Simulated Scattered Ambient Noise

Appendix D contains the frequency response and calibration curves for the SANES. The sound pressure levels for the background, ambient, and scattered ambient noise were measured by replacing the fish with a hydrophone (B&K 8103) positioned in the same location as the fish's ear. The background noise was measured with both the J-9 and the spherical projector disconnected. The ambient noise level produced by the J-9 was measured, then sound pressure levels for the scattered ambient noise were recorded as a function of range from the source to the hydrophone and as a function of center frequency of the scatterer.

Two types of measurements were made using the spectrum analyzer (HP 3585A). Automatic frequency sweeps collected data representing the signal level within a specified bandwidth around the data point frequency. This output was in volts. Also manual measurements at specific frequencies were made using the NOISE LVL function. This function uses 100 independent readings to provide a direct reading of the noise spectral density normalized to a 1 Hz bandwidth, in volts per root Hz. Therefore, this function automatically averaged the signal over time and bandwidth. These were converted to pressure (μPa) and pressure spectral density ($\mu Pa / \sqrt{Hz}$), respectively, using a measured sensitivity factor for the hydrophone.

The graphs in Figures D-1 to D-4 show 1001 points which represent the sound pressure level within 10 Hz bandwidths. The data shown is the average of 5 independent frequency sweeps. The asymptote as frequency approaches zero is an artifact of the spectrum analyzer. The low frequency peaks at 60, 120, and 180 Hz are line voltage noise. The origin for the peaks at 545 Hz in the ambient and background noise curves was not determined.

Since scattered pressure squared is proportional to scattering cross section, the quality factors for the simulated scattered noise signals were determined by fitting the data to the generalized form of the scattering cross-section,

$$\sigma_s = \frac{4\pi a^2}{\left[\left(\frac{\omega_0}{\omega}\right)^2 - 1\right]^2 + \frac{\omega_0^2}{Q^2\omega^2}}, \qquad \text{(D-1)}$$

using the same three parameter (a, ω_0, and Q) non-linear least squares curve fit as before.

Figure D-1 represents the scattered, ambient, and background noise for the first study of scattered ambient noise threshold versus range with the scattered noise centered at 610 Hz at a given range. Scattered noise levels at different ranges differed only by their maximum amplitude. Figures D-2 through D-4 are scattered and ambient noise levels for the threshold versus center frequency with the center of the spherical transducer located 15.2 cm from the center of the fish's ear. In the second study on threshold versus range using a center frequency of 750 Hz, the frequency response curve for the scattered noise is shown in Figure D-3 (bottom). Figure D-5 is the same sound field as the bottom graph of Figure D-3 but measured using the NOISE LVL function. Since the noise level was not truly flat, changing the bandwidth changed the measured values.

Figure D-6 are the calibration curves for the studies of scattered noise versus range using a 610 Hz and 750 Hz center frequency while Figure D-7 is for the scattered noise versus center frequency study, showing the magnitude of the peak of the frequency response curves. The data points were collected using the NOISE LVL function. Note how better behaved the calibration curves are at 750 Hz as compared to 610 Hz. Whether this is due to the peak at 545 Hz is unknown.

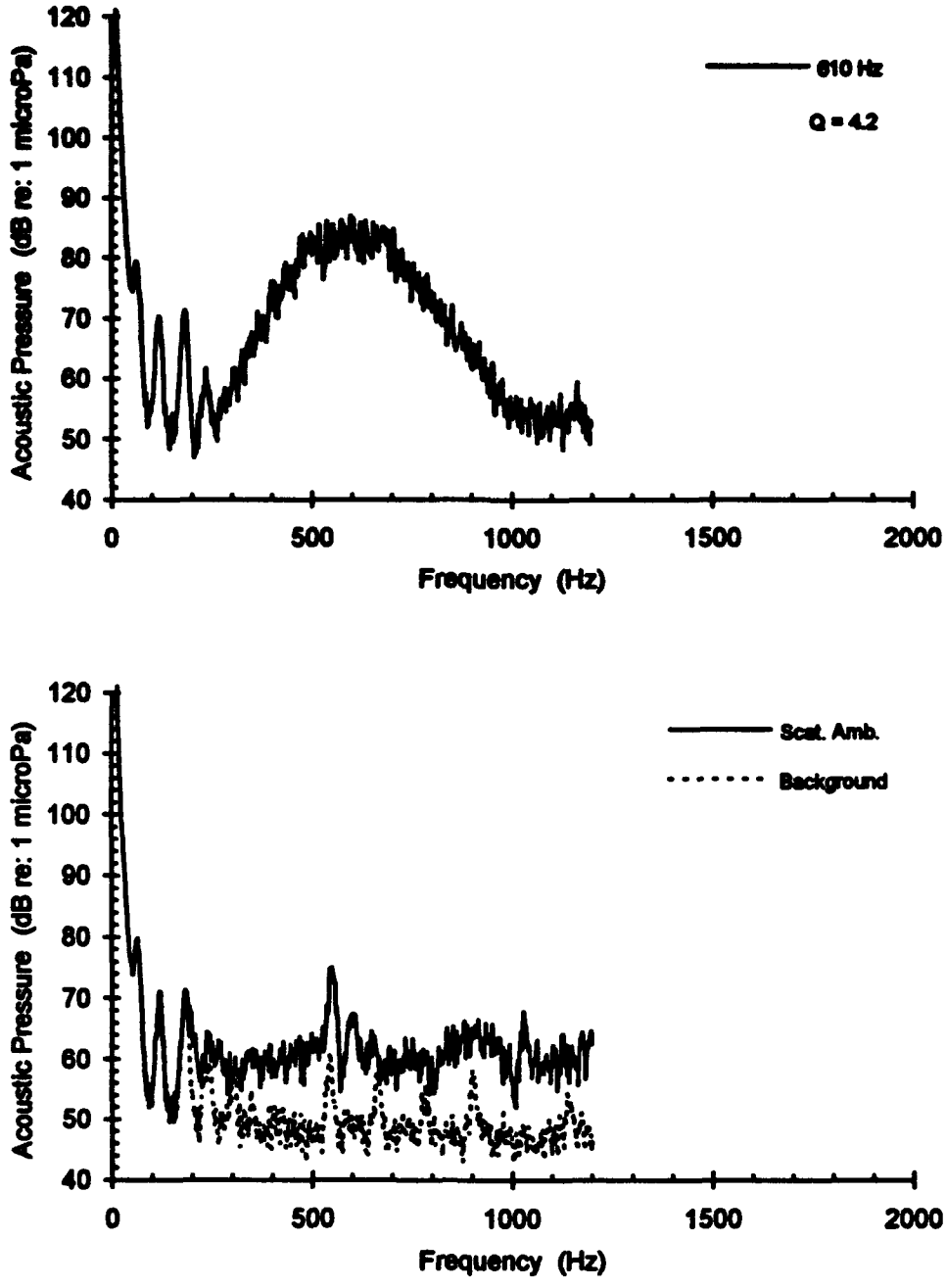

Figure D-1. Frequency response curves for SANES from the study of threshold versus range. The top graph is the simulated scattered noise centered at 610 Hz. The lower graph shows the simulated ambient noise and the background noise.

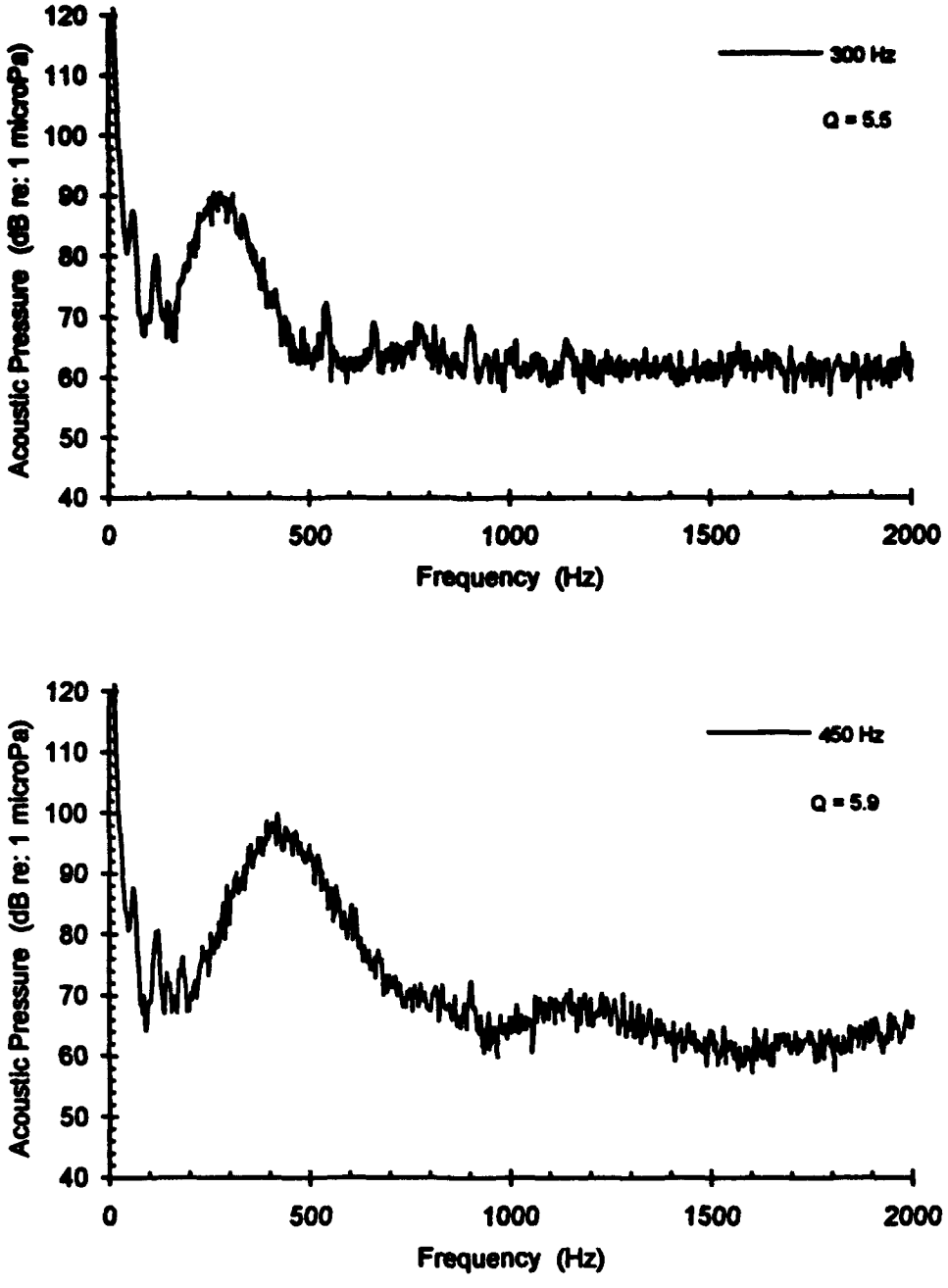

Figure D-2. Frequency response curves for SANES from the study of threshold versus center frequency. The top graph is the simulated scattered noise centered at 300 Hz; the bottom at 450 Hz.

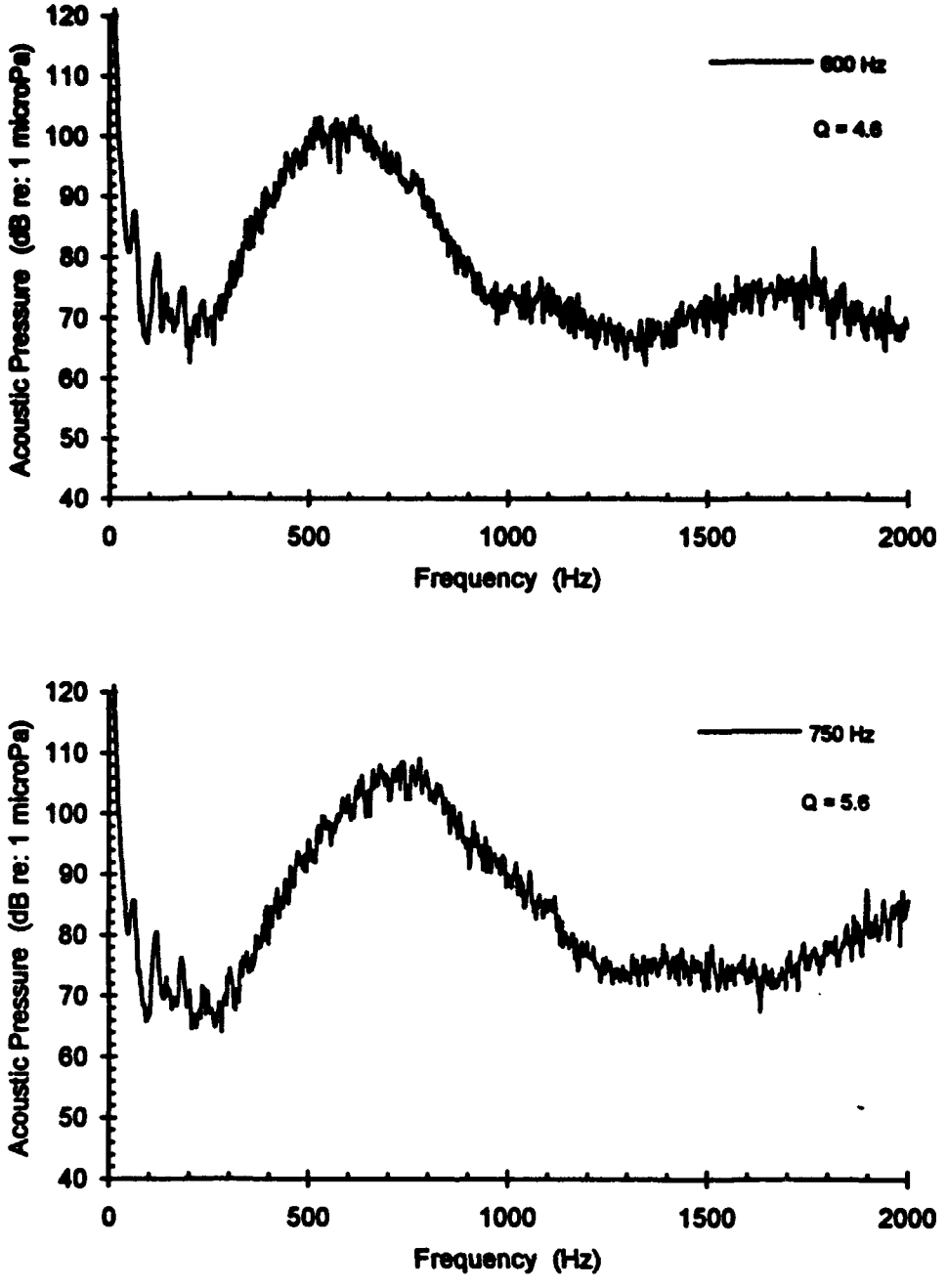

Figure D-3. Frequency response curves for SANES from the study of threshold versus center frequency. The top graph is the simulated scattered noise centered at 600 Hz; the bottom at 750 Hz.

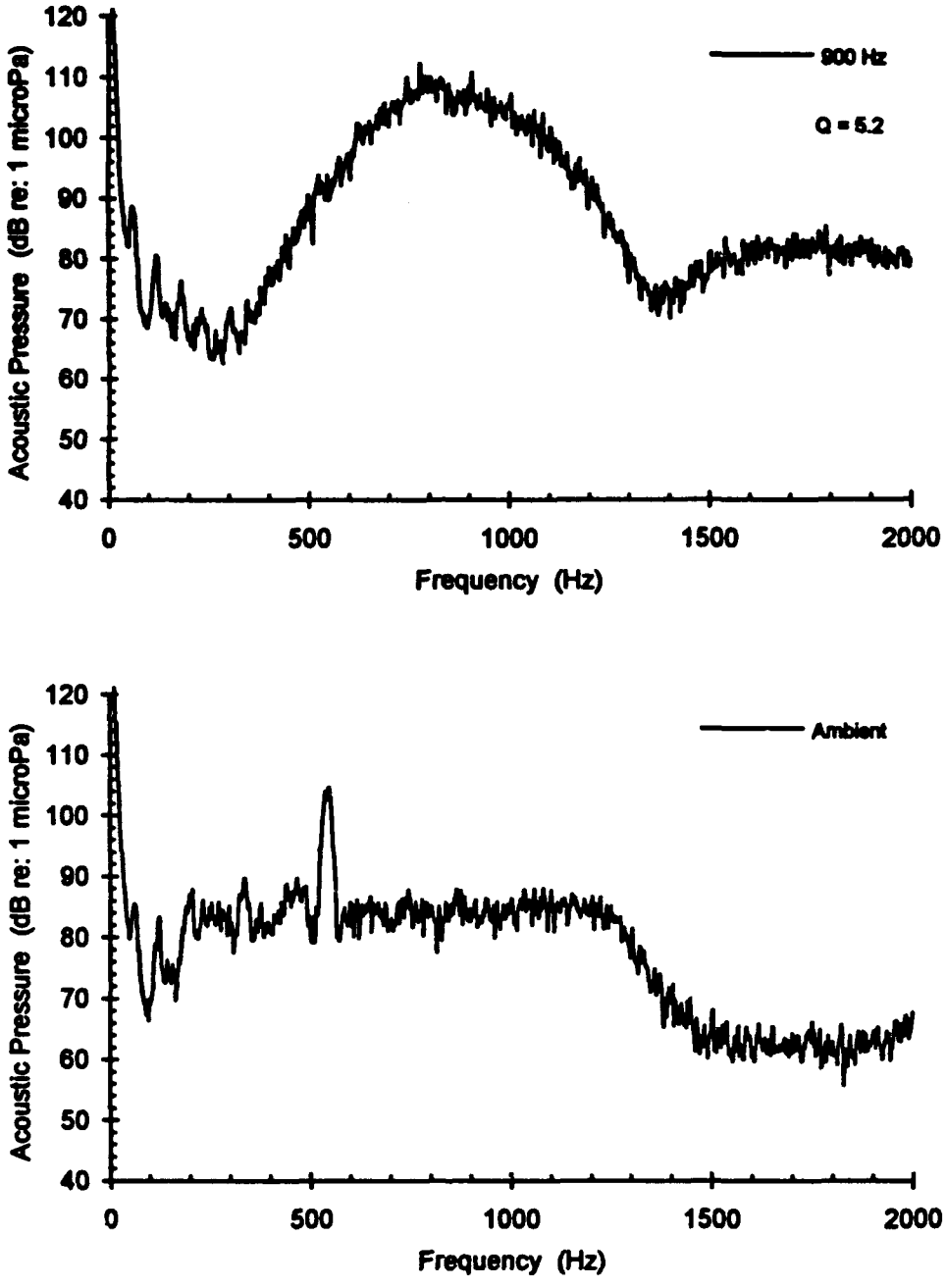

Figure D-4. Frequency response curves for SANES from the study of threshold versus center frequency. The top graph is the simulated scattered noise centered at 900 Hz; the bottom is the simulated ambient noise.

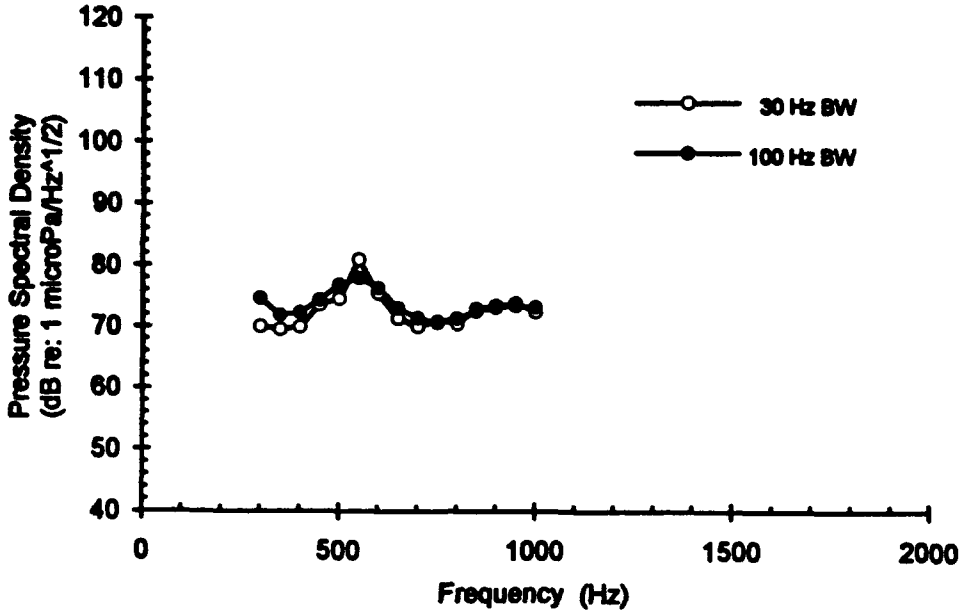

Figure D-5. Ambient noise levels for SANES from the study of threshold versus center frequency measured using the NOISE LVL function of the spectrum analyzer. The two different curves represent the use of different filter bandwidths.

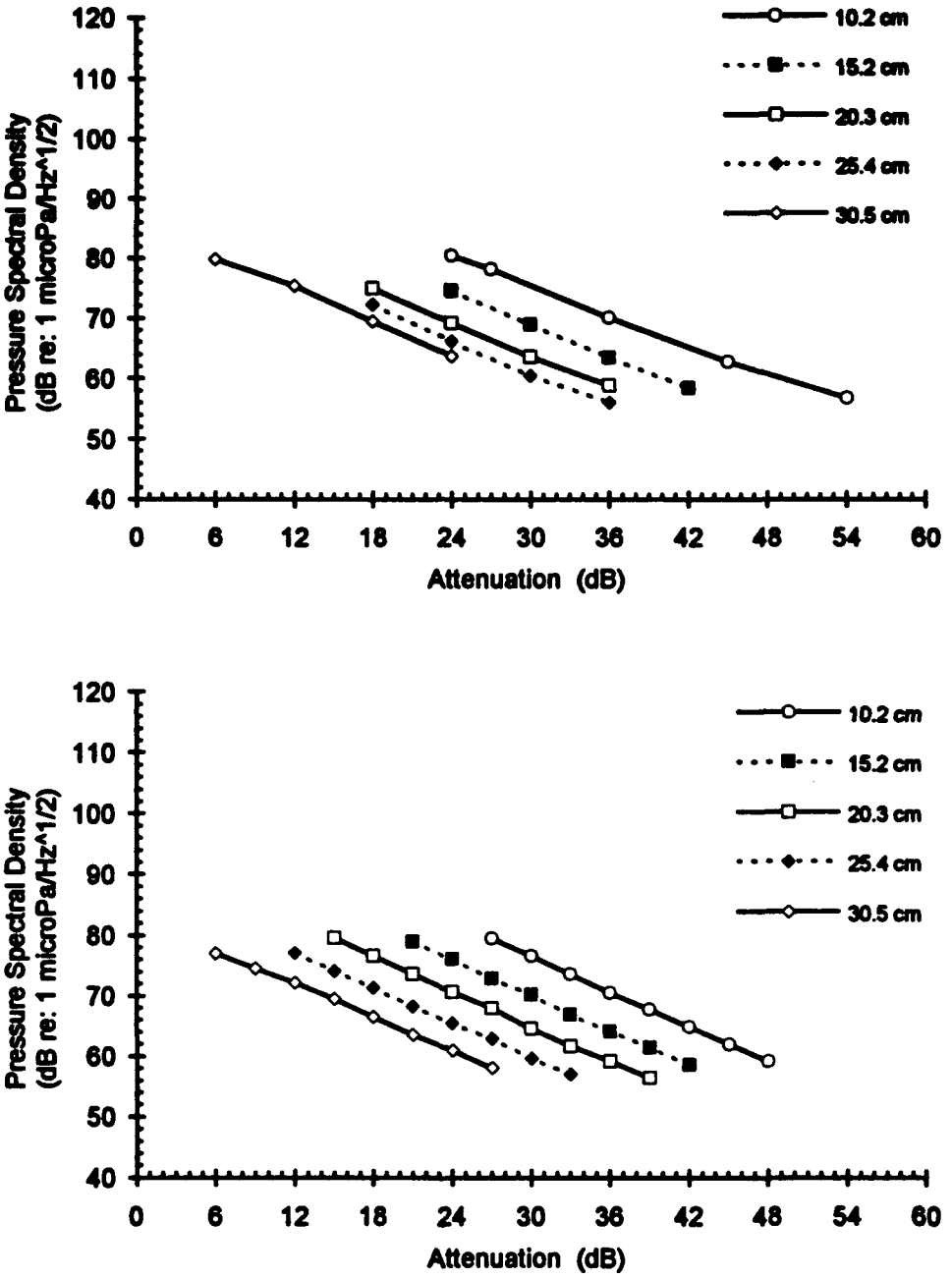

Figure D-6. Calibration curves for scattered ambient noise as a function of signal attenuation for the five discrete ranges at 610 Hz (top) and 750 Hz (bottom) center frequency. The data points indicate the magnitude at the peak of the frequency response.

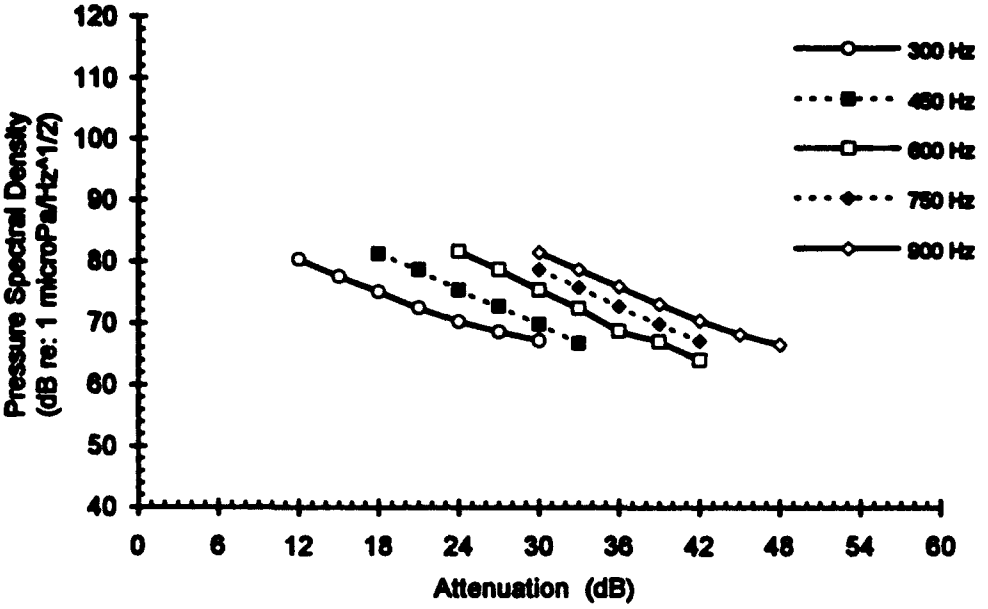

Figure D-7. Calibration curves for scattered ambient noise as a function of signal attenuation for the five center frequencies at a 15.2 cm range. The data points indicate the magnitude at the peak of the frequency response.

Appendix E

Scattered Ambient Noise Thresholds for Goldfish

Appendix E contains the data from the studies measuring thresholds of scattered ambient noise in an ambient noise field. Three studies were performed. Tables E-1 and E-2 contain the data for the threshold versus range studies using fixed center frequencies of 610 Hz and 750 Hz respectively. Table E-3 contains the data for the threshold versus center frequency for a fixed range of 15.2 cm.

The data points are given in units of pressure spectral density ($\mu Pa / \sqrt{Hz}$), indicating the magnitude at the peak of the scattered noise. The top graphs are given in dB of the same units. These can be converted to overall signal level by adding 10 times the log of the bandwidth of the scattered noise. The bandwidth can be obtained from Appendix D by multiplying the center frequency by the Q. The lines in the range studies are the averages of all the data points for that subject. In the center frequency study, the lines connect the averages at each center frequency.

The bottom graphs in Figures E-1 to E-10 represent the ratio of the pressure spectral density of the scattered noise to the ambient noise at the center frequency. The ambient noise level is, of course, independent of the location of the spherical transducer. But, the ambient noise level is a function of frequency. The bottom graphs in Figures E-11 to E-13 represent the pressure spectral density to noise ratio using the data from Figure D-5. Again, since the noise was not uniform, the results depended upon the bandwidth chosen.

Table E-1. Threshold data taken using SANES for the range study using a 610 Hz center frequency for the scattered noise. Different masses indicate individual goldfish. The data points are in units of pressure spectral density (μ $\sqrt{\ }$), indicating the magnitude of the peak of the scattered noise.

Range Study - 610 Hz Center Frequency

Mass of Fish	Centerline Distance from Transducer to Fish's Ear (Range)				
	10.2 cm	15.2 cm	20.3 cm	25.4 cm	30.5 cm
76.8 g.	5678	4052	3880	-	5520
	3701	3449			4299
	4301				6504
80.8 g.	2011	417	3416	861	2972
	1115		1000	2008	1583
	984		1463		2749
90.3 g.	2691	2925	3488	4109	-
	6317		3880		
	4140		2708		
114.3 g.	3540	-	2440	3398	-
	1919		2673	2465	
	3002		2289	2806	
	2358				
118.9 g.	3863	1275	-	1990	-
	1376	1785		1831	
	1469	2104		2428	

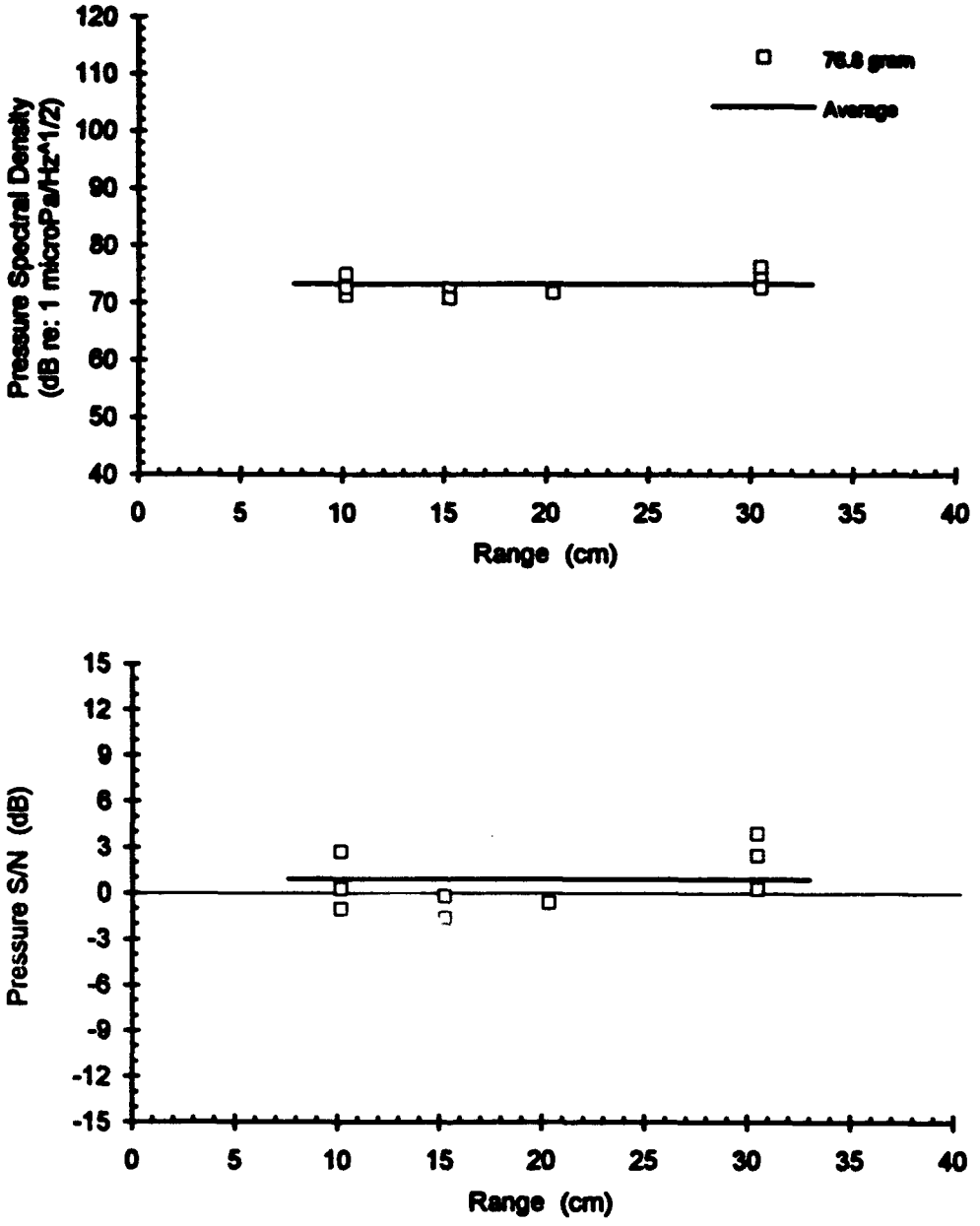

Figure E-1. Measured thresholds of scattered ambient noise centered at 610 Hz versus range for a 76.8 gram goldfish. The top graph is in terms of pressure spectral density. The bottom is in terms of pressure spectral density signal-to-noise.

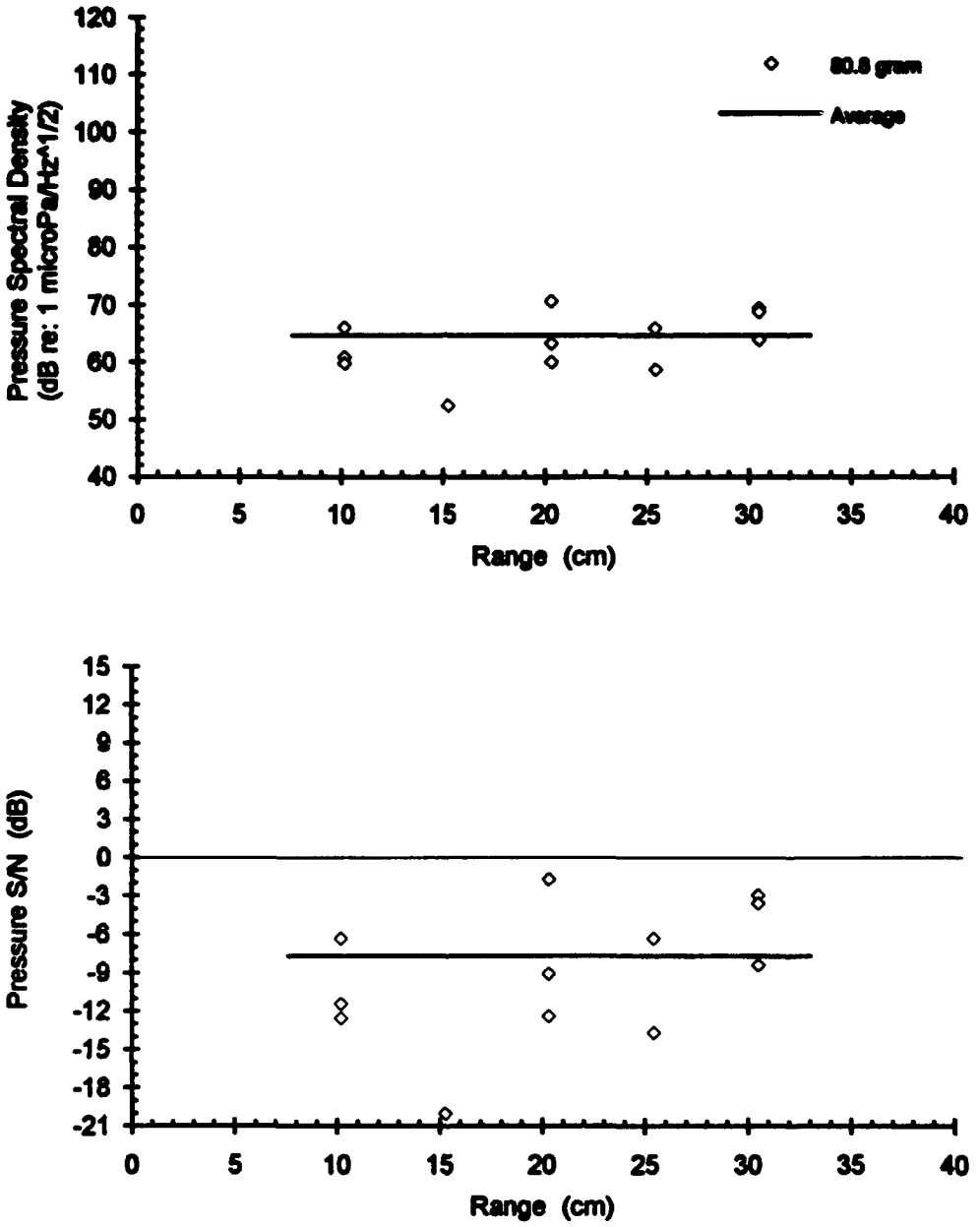

Figure E-2. Measured thresholds of scattered ambient noise centered at 610 Hz versus range for a 80.8 gram goldfish. The top graph is in terms of pressure spectral density. The bottom is in terms of pressure spectral density signal-to-noise.

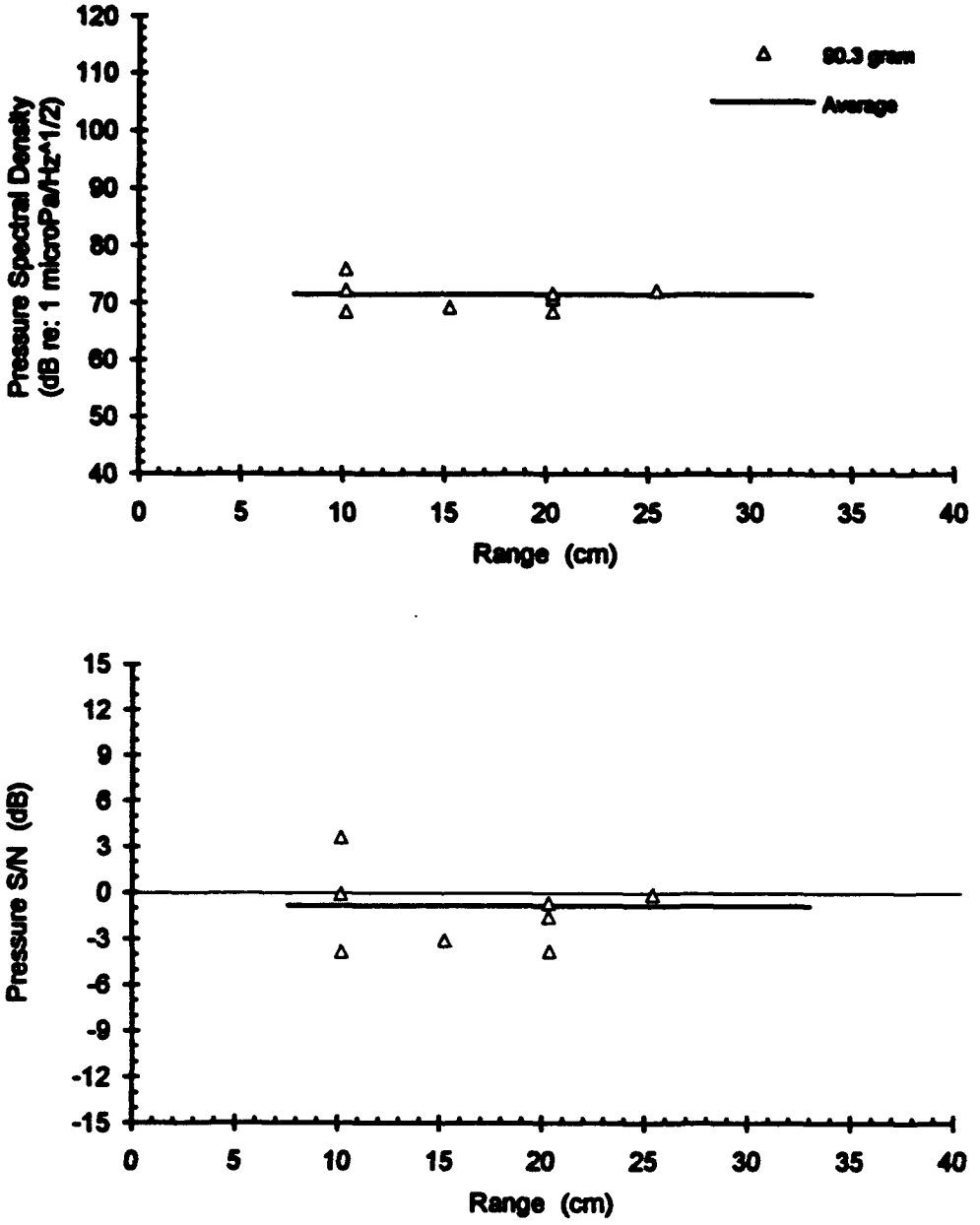

Figure E-3. Measured thresholds of scattered ambient noise centered at 610 Hz versus range for a 90.3 gram goldfish. The top graph is in terms of pressure spectral density. The bottom is in terms of pressure spectral density signal-to-noise.

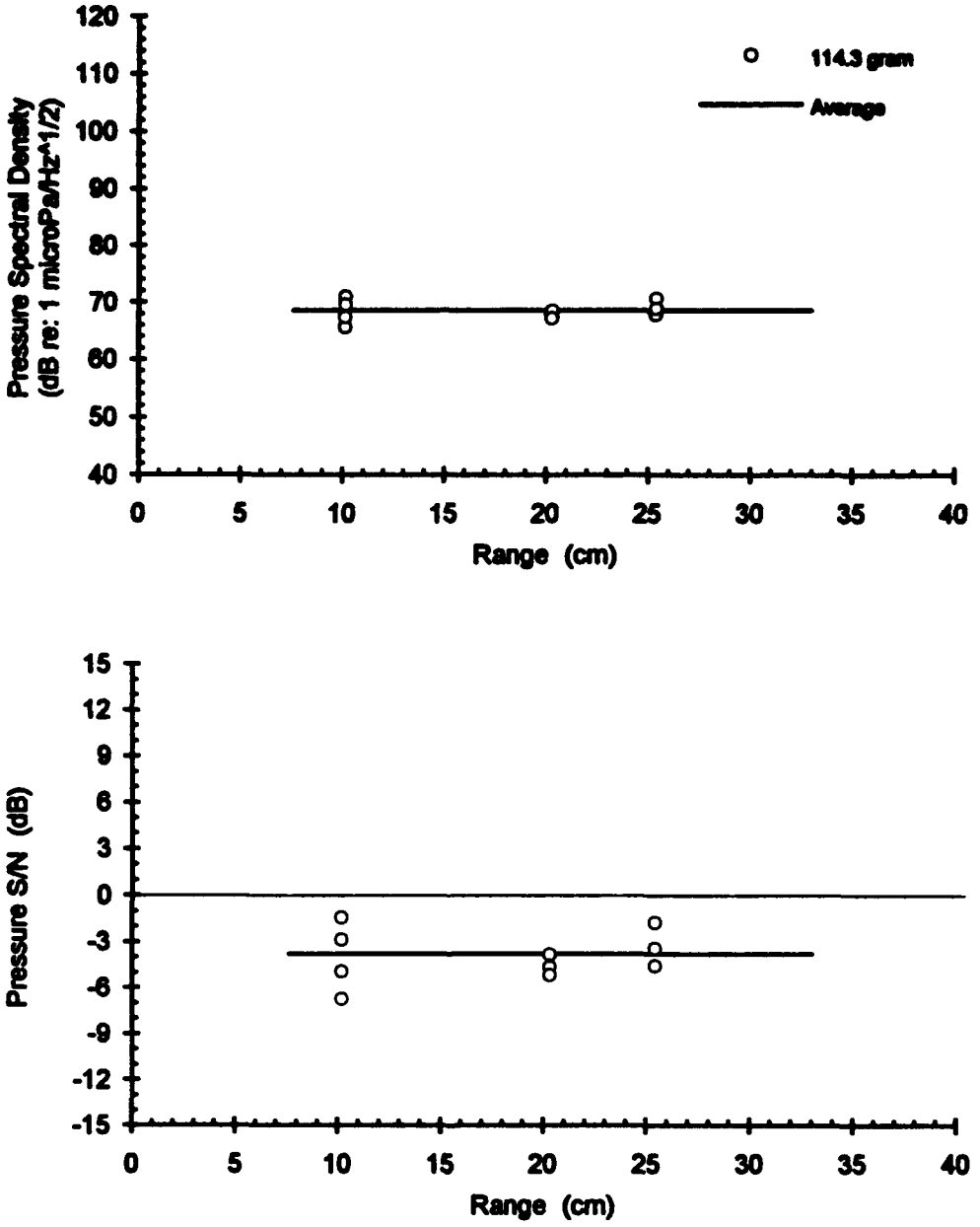

Figure E-4. Measured thresholds of scattered ambient noise centered at 610 Hz versus range for a 114.3 gram goldfish. The top graph is in terms of pressure spectral density. The bottom is in terms of pressure spectral density signal-to-noise.

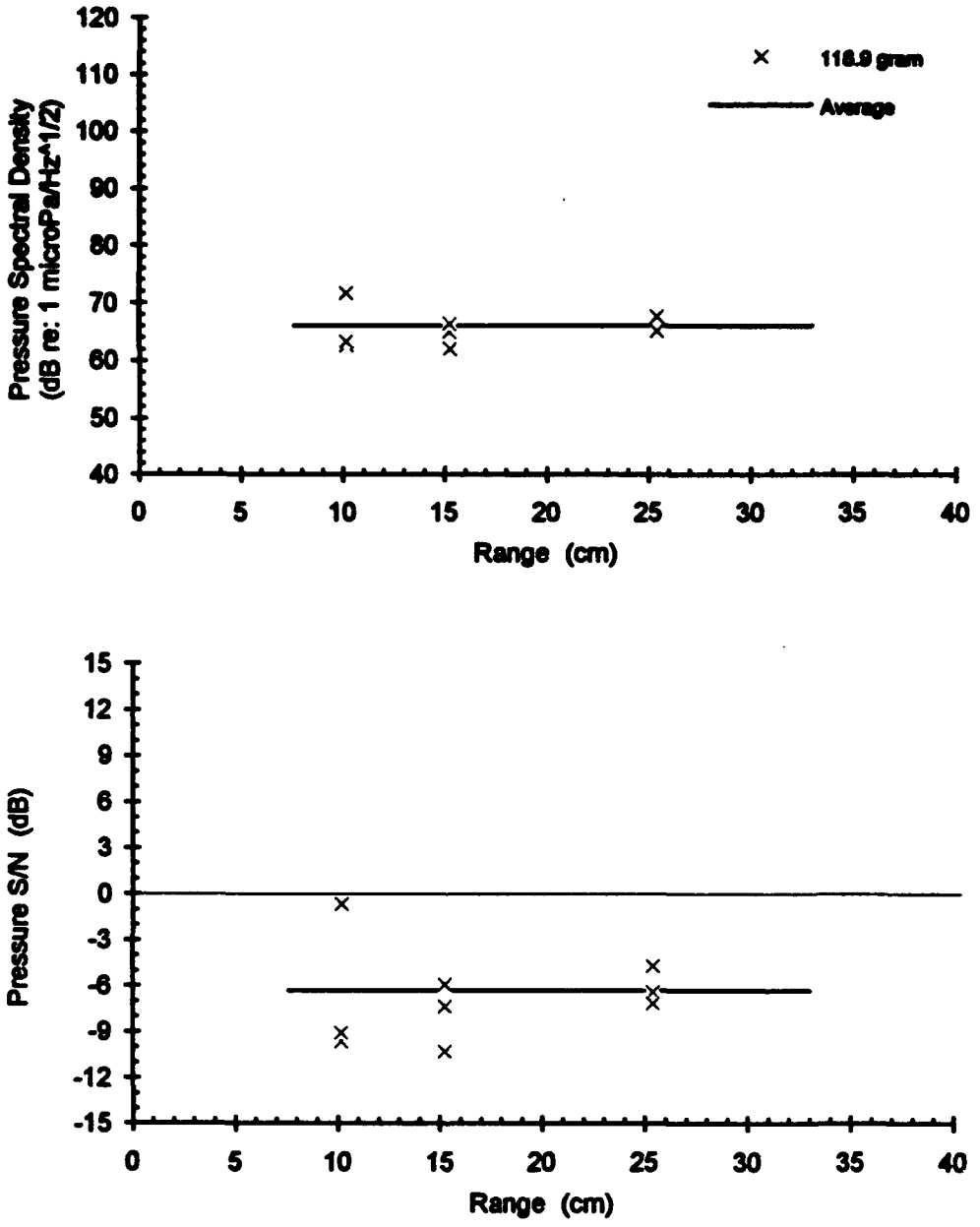

Figure E-5. Measured thresholds of scattered ambient noise centered at 610 Hz versus range for a 118.9 gram goldfish. The top graph is in terms of pressure spectral density. The bottom is in terms of pressure spectral density signal-to-noise.

Table E-2. Threshold data taken using SANES for the range study using a 750 Hz center frequency for the scattered noise. Different masses indicate individual goldfish. The data points are in units of pressure spectral density ($\mu Pa / \sqrt{Hz}$), indicating the magnitude of the peak of the scattered noise.

Range Study - 750 Hz Center Frequency

	Centerline Distance from Transducer to Fish's Ear (Range)				
	10.2 cm	15.2 cm	20.3 cm	25.4 cm	30.5 cm
Mass of Fish					
74.6 g.	2410	2727	2305	2916	2707
	2830	2015	2651	2259	2707
	3675	2727	2620	3183	3081
77.2 g.	2022	3718	1945	3275	-
	3379	2183	2261	3608	
	4180	2646	4125	2694	
78.9 g.	2149	1766	-	1754	2202
		2247		2252	2171
		1902			
80.2 g.	3822	3162	2410	-	3049
	4180	3440	3233		3112
	2694	2646	2559		1977
102.3 g.	2516	2884	2348	2125	2246
	2052	2113	2050	2282	2300
	2442	2212	2800	1936	2090

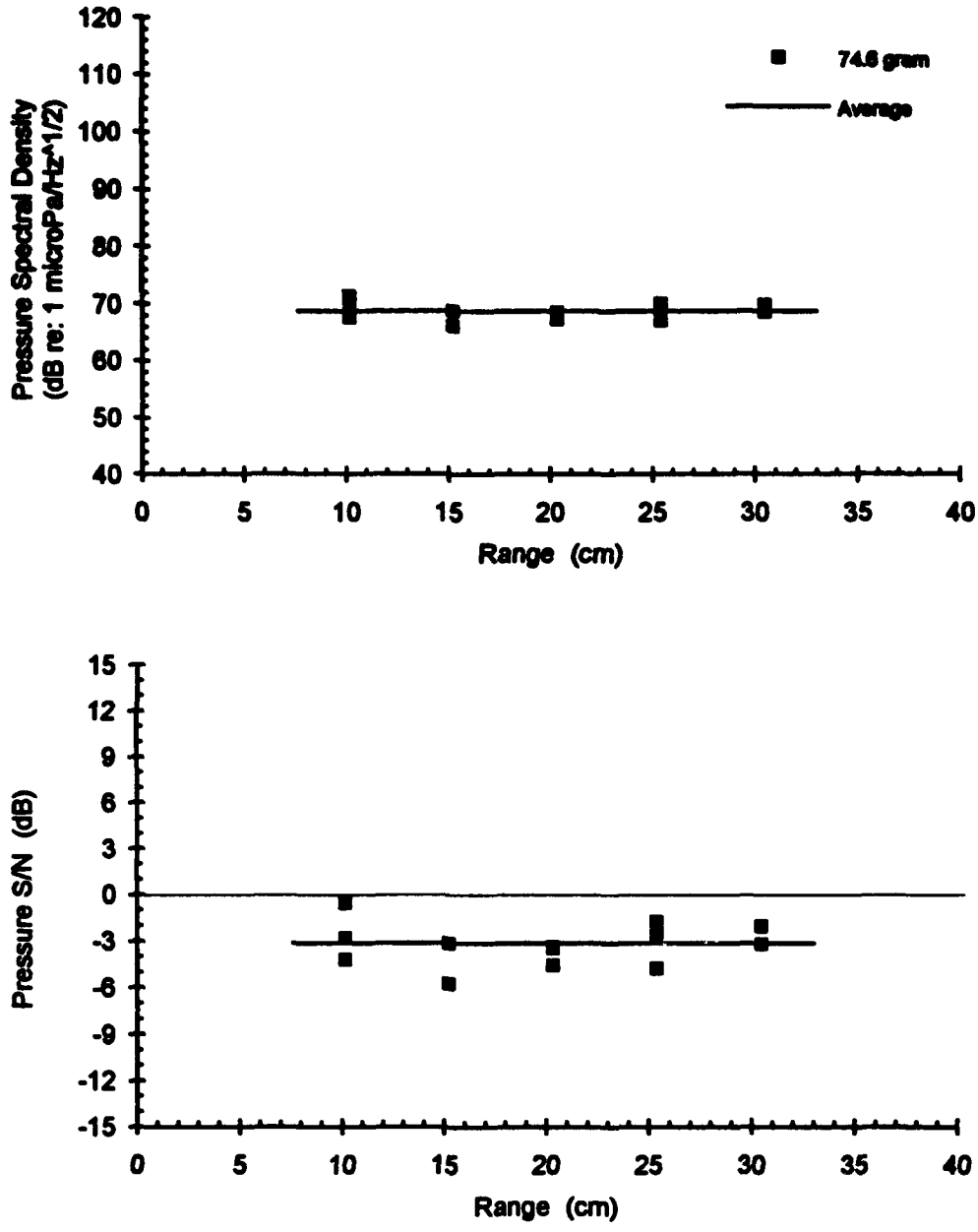

Figure E-6. Measured thresholds of scattered ambient noise centered at 750 Hz versus range for a 74.6 gram goldfish. The top graph is in terms of pressure spectral density. The bottom is in terms of pressure spectral density signal-to-noise.

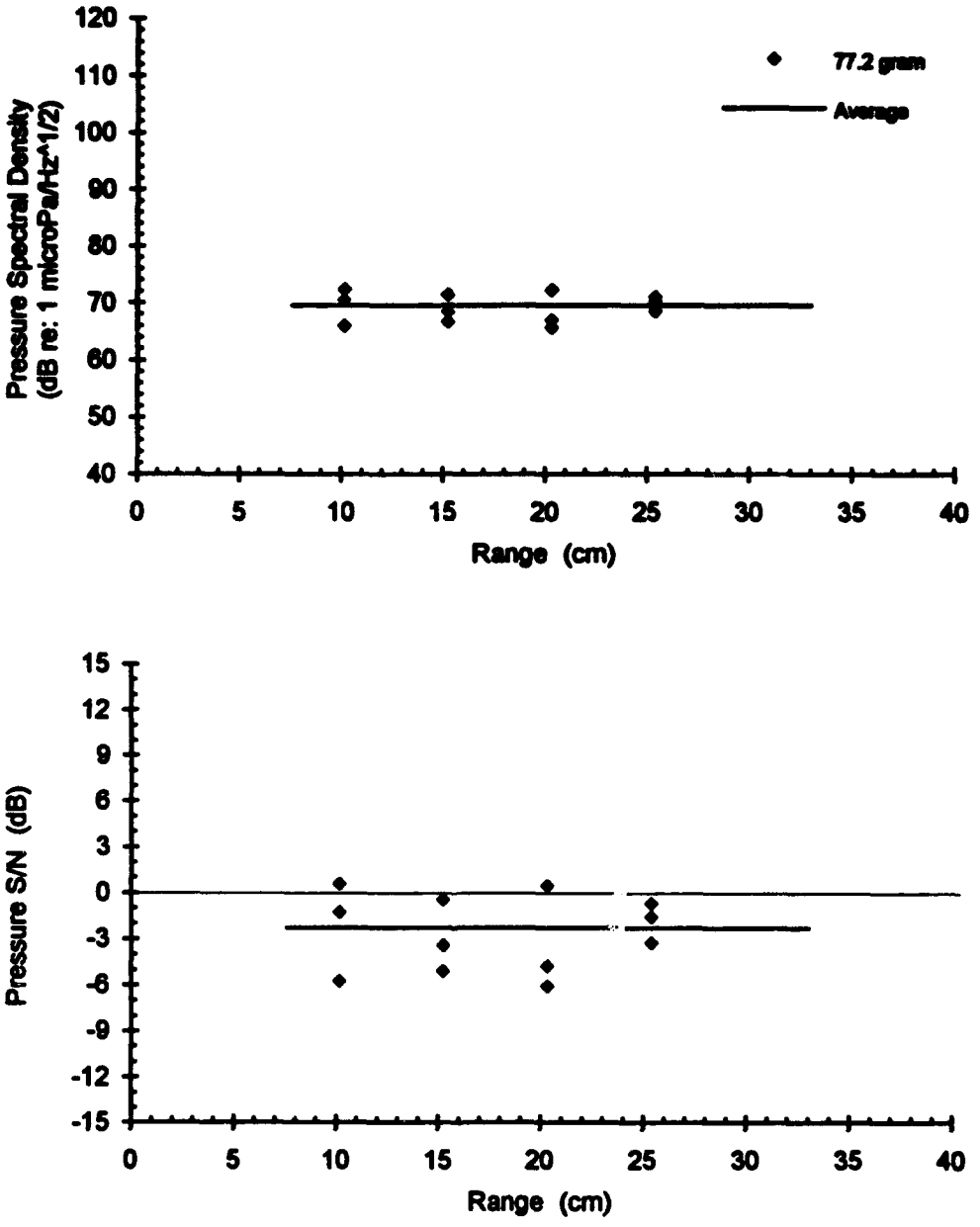

Figure E-7. Measured thresholds of scattered ambient noise centered at 750 Hz versus range for a 77.2 gram goldfish. The top graph is in terms of pressure spectral density. The bottom is in terms of pressure spectral density signal-to-noise.

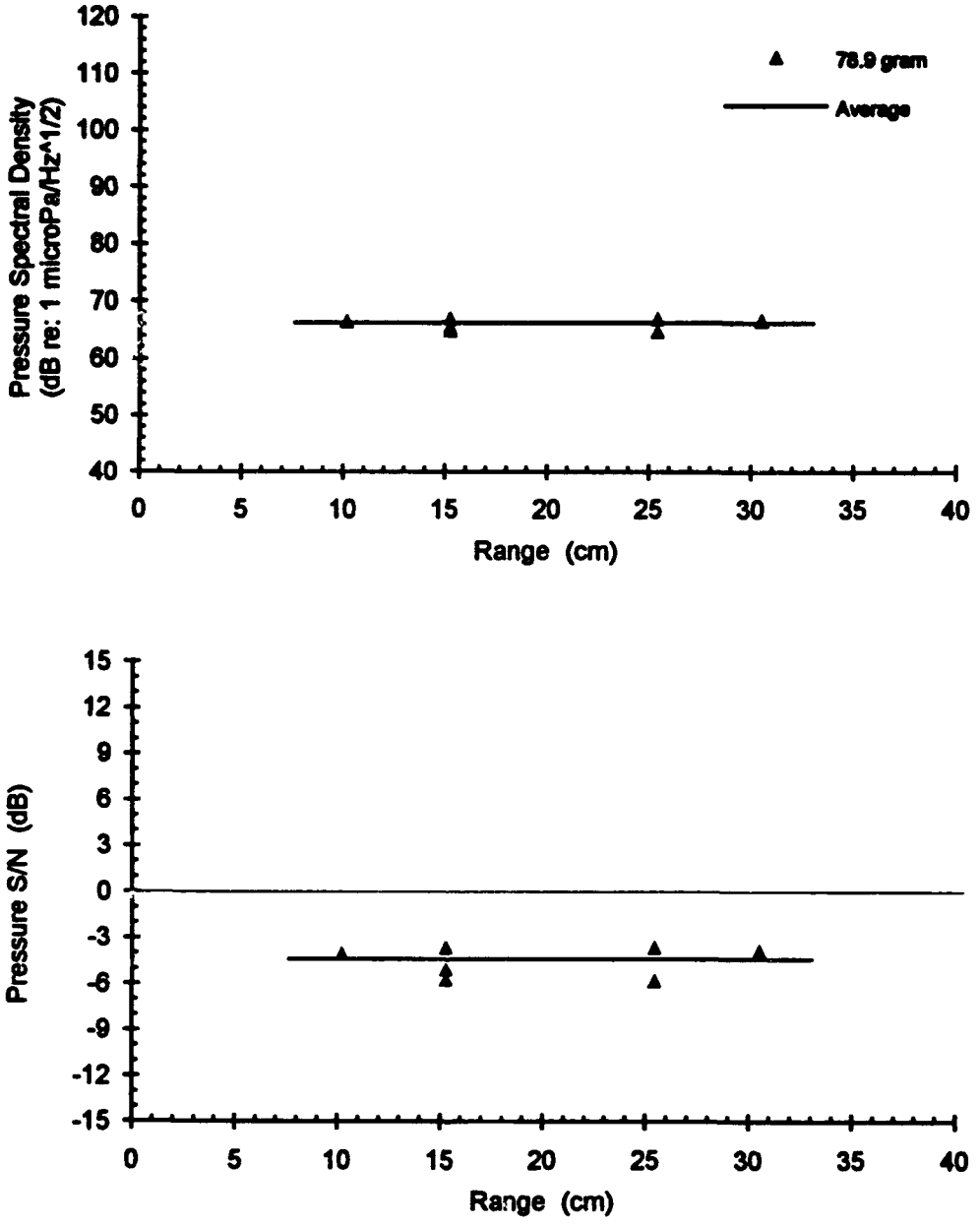

Figure E-8. Measured thresholds of scattered ambient noise centered at 750 Hz versus range for a 78.9 gram goldfish. The top graph is in terms of pressure spectral density. The bottom is in terms of pressure spectral density signal-to-noise.

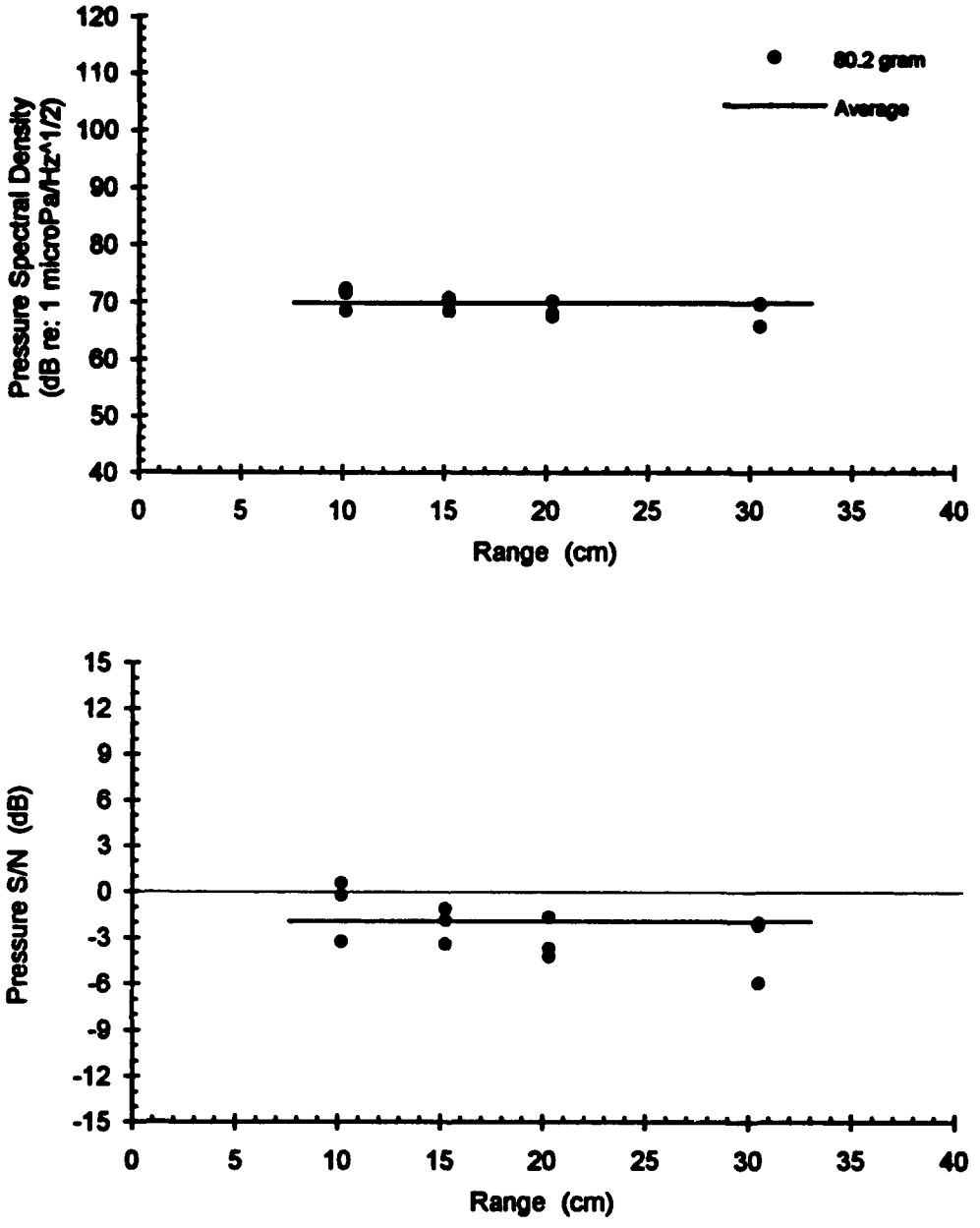

Figure E-9. Measured thresholds of scattered ambient noise centered at 750 Hz versus range for a 80.2 gram goldfish. The top graph is in terms of pressure spectral density. The bottom is in terms of pressure spectral density signal-to-noise.

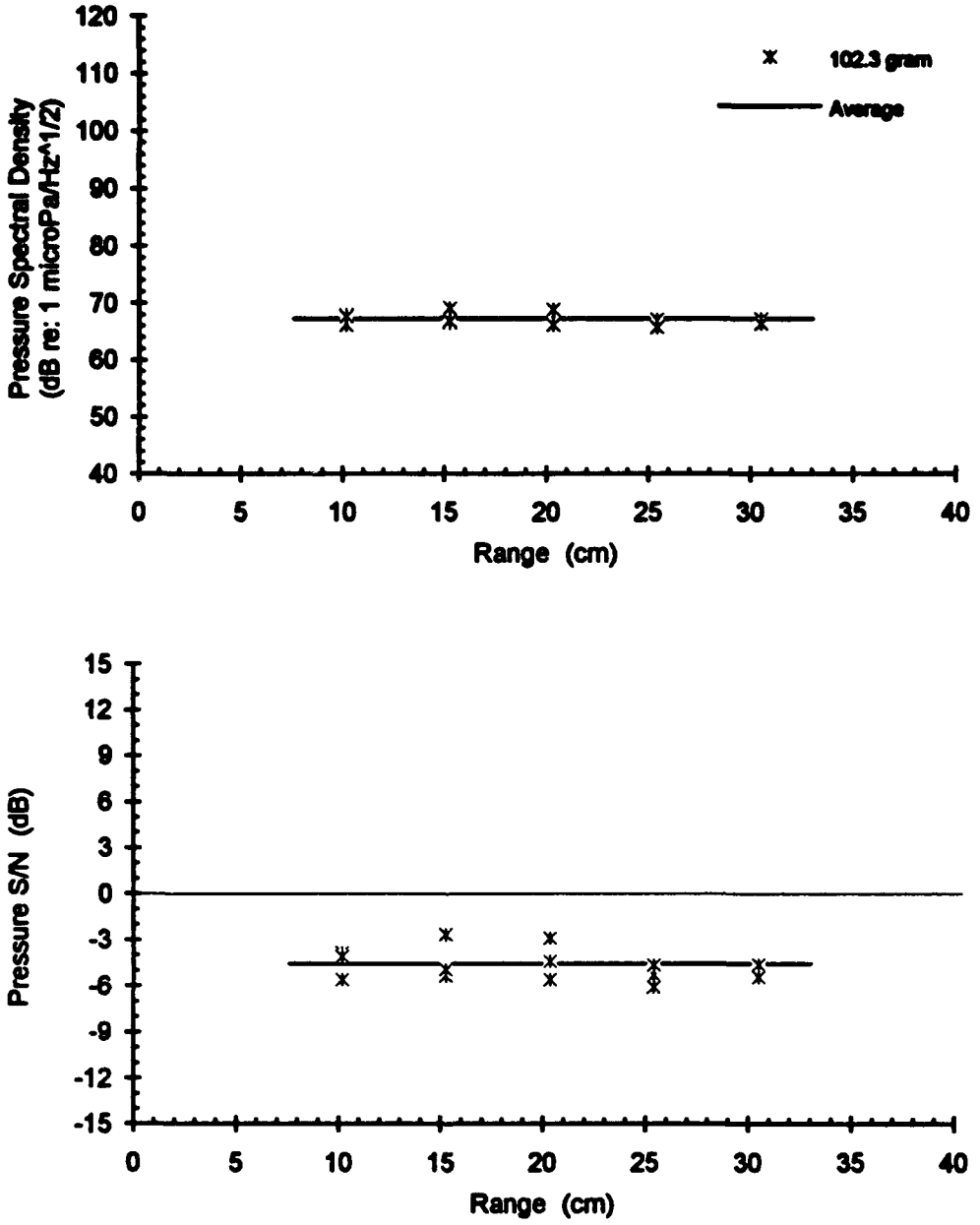

Figure E-10. Measured thresholds of scattered ambient noise centered at 750 Hz versus range for a 102.3 gram goldfish. The top graph is in terms of pressure spectral density. The bottom is in terms of pressure spectral density signal-to-noise.

Table E-3. Threshold data taken using SANES for the center frequency study using a 15.2 cm range for the spherical transducer. Different masses indicate individual goldfish. The data points are in units of pressure spectral density ($\mu Pa / \sqrt{Hz}$), indicating the magnitude of the peak of the scattered noise.

Center Frequency Study - 15.2 cm Range

	Center Frequency of Scattered Noise				
	300 Hz	450 Hz	600 Hz	750 Hz	900 Hz
Mass of Fish					
78.9 g.	2020	1965	2936	1766	2514
	1630	2778	3457	2247	1540
	1520	1613	4287	1903	1998
			3218		2453
82.2 g.	2589	2051	3059	2053	3077
	2098	2119	3892	2438	2363
	1832	1879	2516	2342	2242
	2176				
87.7 g.	2252	-	3117	3563	2363
	2904		3356		3331
			3497		1877

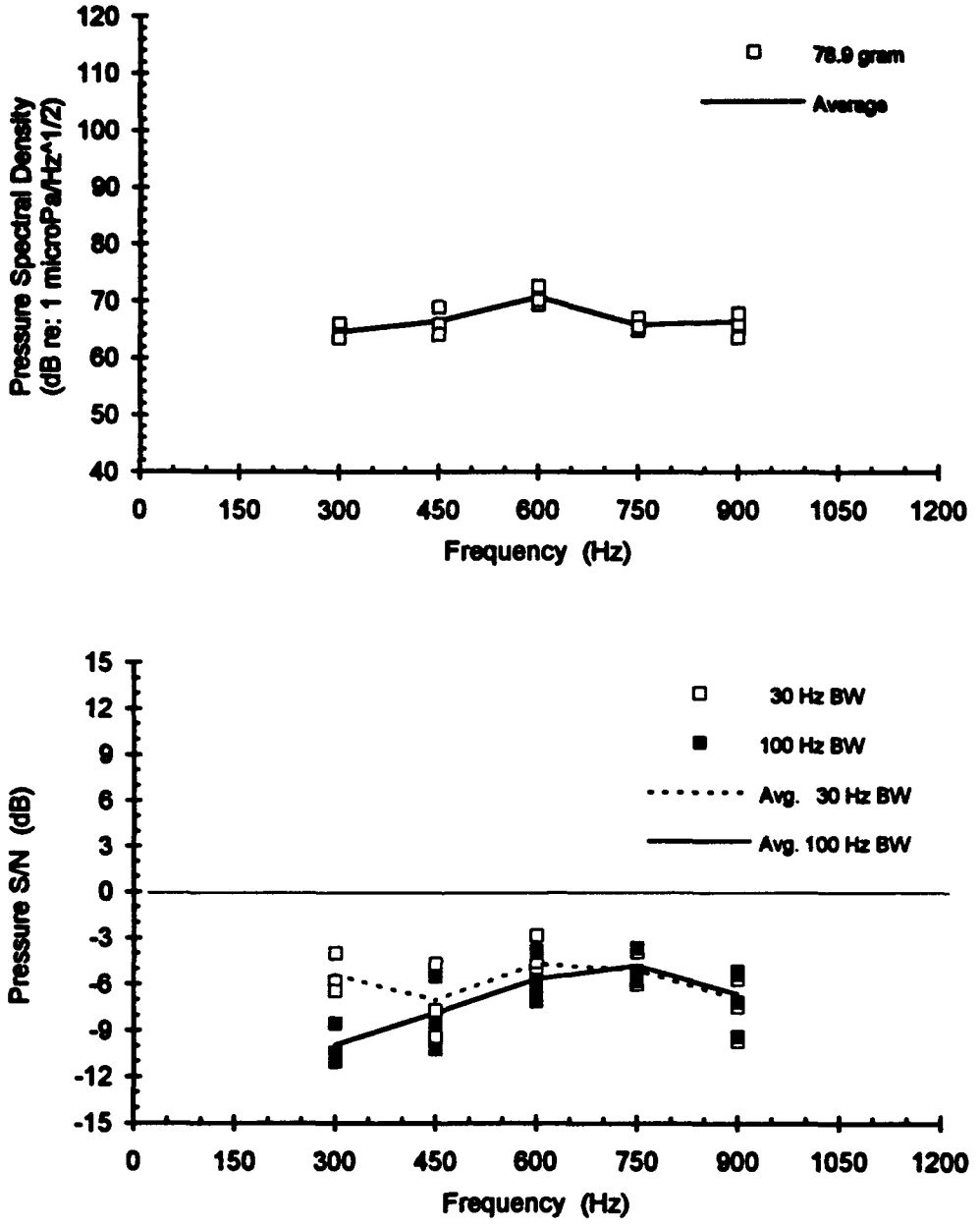

Figure E-11. Measured thresholds of scattered ambient noise versus center frequency of the scatterer for a 78.9 gram goldfish. The top graph is in terms of pressure spectral density. The bottom is in terms of pressure spectral density signal-to-noise.

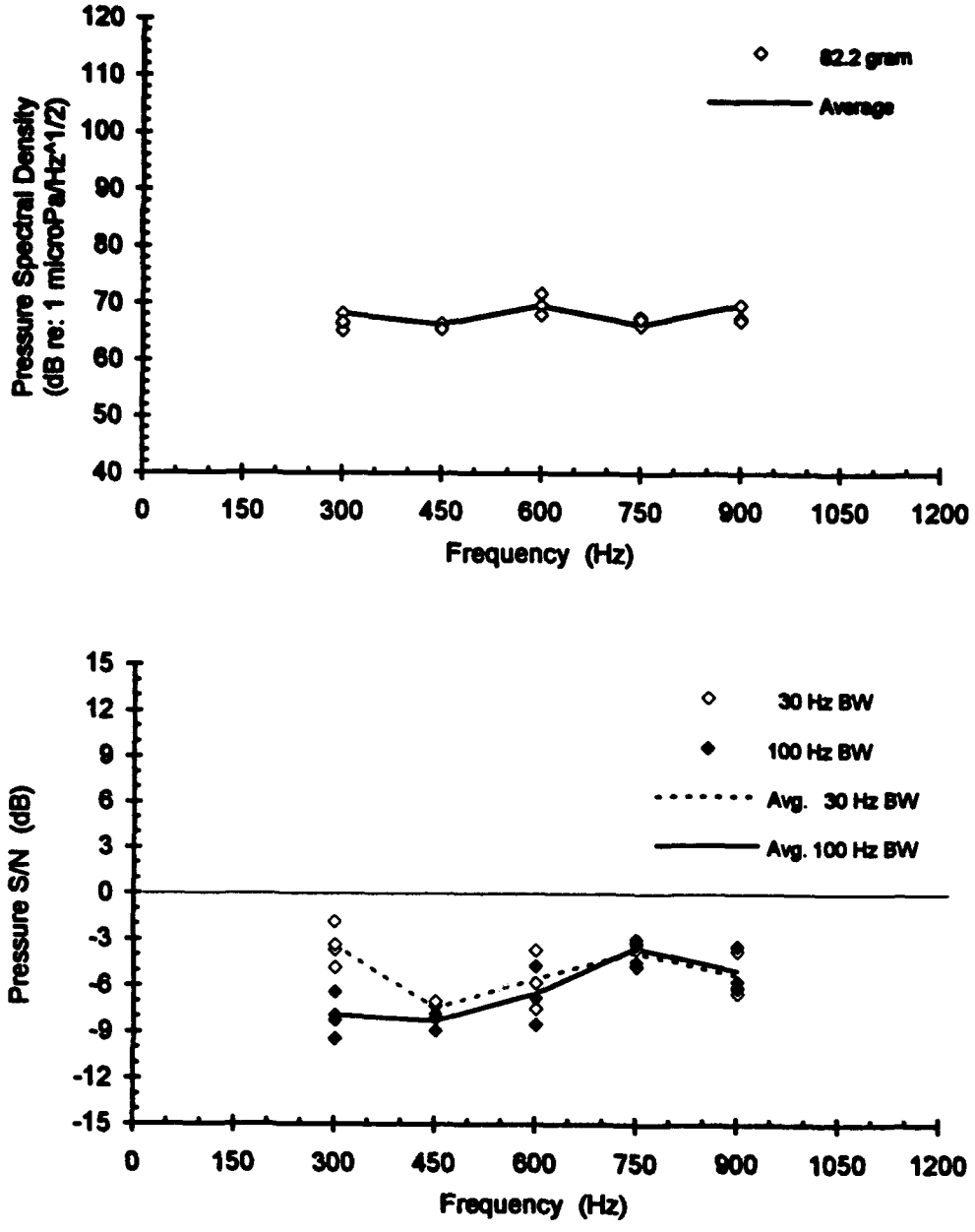

Figure E-12. Measured thresholds of scattered ambient noise versus center frequency of the scatterer for a 82.2 gram goldfish. The top graph is in terms of pressure spectral density. The bottom is in terms of pressure spectral density signal-to-noise.

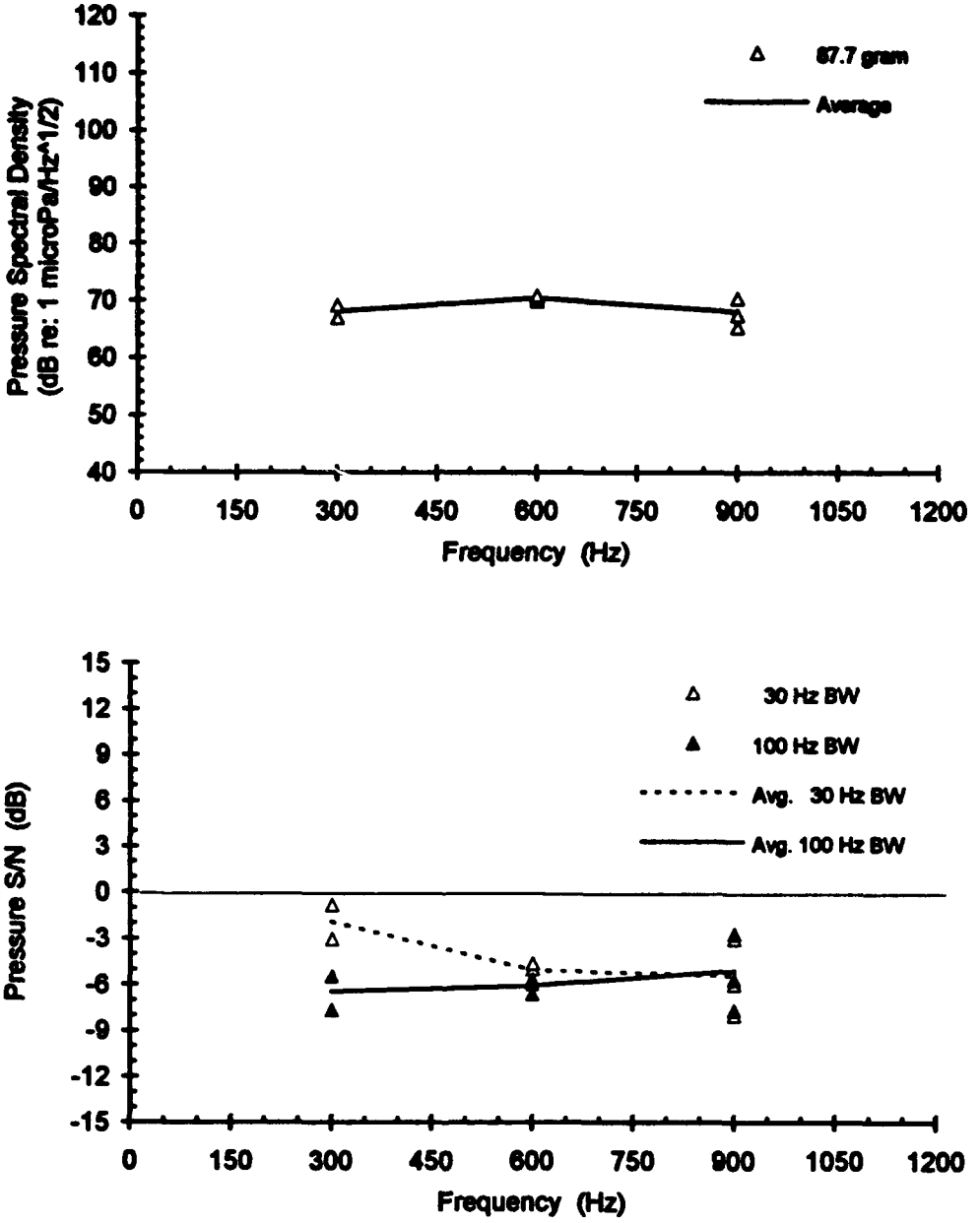

Figure E-13. Measured thresholds of scattered ambient noise versus center frequency of the scatterer for a 87.7 gram goldfish. The top graph is in terms of pressure spectral density. The bottom is in terms of pressure spectral density signal-to-noise.

Bibliography

Abrahamson, S. (1987). "Automated psycho-acoustic experimental station," Masters thesis, George W. Woodruff School of Mechanical Engineering, Georgia Institute of Technology, Atlanta, GA.

Alexander, R.McN. (1959a). "The densities of Cyprinidae," J. Exp. Biol. 36, 333-340.

Alexander, R.McN. (1959b). "The physical properties of the isolated swimbladder in Cyprinidae," J. Exp. Biol. 36, 341-346.

Alexander, R.McN. (1959c). "The physical properties of the swimbladder in intact Cypriniformes," J. Exp. Biol. 36, 315-332.

Alexander, R.McN. (1959d). "The physical properties of the swimbladders of fish other than Cypriniformes," J. Exp. Biol. 36, 347-355.

Alexander, R.McN. (1961). "The physical properties of the swimbladders of some South American Cypriniformes," J. Exp. Biol. 38, 403-410.

Alexander, R.McN. (1966). "The physical aspects of swimbladder function," Biol. Rev. 41, 141-172.

Andreeva, I.B. (1964). "Scattering of sound by air bladders of fish in deep sound-scattering ocean layers," Sov. Phys. Acoust. 10, 17-20.

Bigelow, H.B. (1904). "The sense of hearing in the goldfish, *Carassius auratus* L.," Amer. Nat. 38, 275-284.

Blaxter, J.H.S., E.J. Denton, and J.A.B. Gray (1981). "Acoustico-lateralis systems in clupeid fishes," in *Hearing and Sound Communication in Fishes*, edited by W.N. Tavloga, A.N. Popper, and R.R. Fay (Springer-Verlag, New York), pp. 39-59.

Brekhovskikh, L. and Yu. Lysanov (1982). *Fundamentals of Ocean Acoustics* (Springer-Verlag, Berlin).

Buerkle, U. (1967). "An audiogram of the Atlantic cod, *Gadus morhua* L.," J. Fish. Res. Bd. Canada 24, 2309-2319.

Buerkle, U. (1968). "Relation of pure tone thresholds to background noise level in the Atlantic cod (*Gadus morhua*)," J. Fish Res. Bd. Canada 25, 1155-1160.

Buerkle, U. (1969). "Auditory masking and the critical bands in the Atlantic cod (*Gadus morhua*)," J. Fish. Res. Bd. Canada 26, 1113-1119.

Buwalda, R.J.A. and J. van der Steen (1979). "The sensitivity of the cod sacculus to directional and non-directional sound stimuli," Comp. Biochem. Physiol. 64A, 467-471.

Chapman, C.J. and A.D.F. Johnstone (1974). "Some auditory discrimination experiments on marine fish," J. Exp. Biol. 61, 521-528.

Chapman, C.J. and O. Sand (1974). "Field studies of hearing in two species of flatfish *Pleuronectes platessa* (L.) and *Limanda limanda* (L.) (Family Pleuronectidae)," Comp. Biochem. Physiol. 47A, 371-385.

Clay, C.S. and H. Medwin (1977). *Acoustical Oceanography* (John Wiley & Sons, New York).

Coombs, S. and A.N. Popper (1982). "Comparative frequency selectivity in fishes: Simultaneously and forward-masked psychophysical tuning curves," J. Acoust. Soc. Am. 71, 133-141.

Cox, M. (1987). "An experimental investigation of the mechanics of the peripheral auditory system in goldfish," Ph.D. thesis, George W. Woodruff School of Mechanical Engineering, Georgia Institute of Technology, Atlanta, GA.

Cox, M. and P.H. Rogers (1986). "Ultrasonic measurements of vibrational amplitudes of auditory organs in fish," in *Advances in Test Measurements - Volume 23* (Instrument Society of America, Research Triangle Park), 337-350.

Cox, M. and P.H. Rogers (1987). "Automated noninvasive motion measurement of auditory organs in fish using ultrasound," J. Vib. Acoust. Str. Reliab. in Dsgn. 109, 55-59.

Dijkgraaf, S. (1960). "Hearing in bony fishes," Proc. Roy. Soc. Lond. Ser. B 152, 51-54.

Dusenbery, D.B. (1992). *Sensory Ecology* (W.H. Freeman, New York).

Enger, P.S., A.J. Kalmijnn and O. Sand (1989). "Behavioral investigations on the function of the lateral line and inner ear in predation," in *The Mechanosensory Lateral Line: Neurobiology and Evolution*, edited by S. Coombs, P. Gorner, and H. Munz (Springer-Verlag, New York), pp. 575-587.

Fay, R.R. (1969). "Behavioral audiogram for the goldfish," J. Aud. Res. 9, 112-121.

Fay, R.R. (1974). "Masking of tones by noise for the goldfish (*Carassius auratus*)," J. Comp. Physiol. Psychol. 87, 708-716.

Fay, R.R. (1978). "Sound detection and sensory coding by the auditory systems of fishes," in *The Behavior of Fish and Other Aquatic Animals*, edited by D. Mostofsky (Academic Press, New York), pp. 197-231.

Fay, R.R. (1981). "Coding of acoustic information in the eighth nerve," in *Hearing and Sound Communication in Fishes*, edited by W.N. Tavloga, A.N. Popper, and R.R. Fay (Springer-Verlag, New York), pp. 189-221.

Fay, R.R. (1984a). "The goldfish ear codes the axis of acoustic particle motion in three dimensions," Science 225, 951-953.

Fay, R.R. (1984b). "Temporal processing by the auditory system of fishes," in *Time Resolution in Auditory Systems*, edited by A. Michelsen (Springer-Verlag, Berlin), pp. 28-57.

Fay, R.R. (1988a). *Hearing in Vertebrates: A Psychophysics Databook* (Hill-Fay Associates, Winnetka, IL).

Fay, R.R. (1988b). "Peripheral mechanisms for spatial hearing in fishes," in *Sensory Biology of Aquatic Animals*, edited by J. Atema, R.R. Fay, A.N. Popper, and W.N. Tavolga (Springer-Verlag, New York), pp. 711-731.

Fay, R.R. and S. Coombs (1983). "Neural mechanisms in sound detection and temporal summation," Hear. Res. 10, 69-92.

Fay, R.R. and A.N. Popper (1974). "Acoustic stimulation of the ear of the goldfish (*Carassius auratus*)," J. Exp. Biol. 61, 243-260.

Fay, R.R. and A.N. Popper (1980). "Structure and function in teleost auditory systems," in *Comparative Studies of Hearing in Vertebrates*, edited by A.N. Popper and R.R. Fay (Springer-Verlag, New York), pp. 1-42.

Fay, R.R. and T.J. Ream (1985). "Acoustic response and tuning in saccular nerve fibers of the goldfish (*Carassius auratus*)," J. Acoust. Soc. Am. 79, 1883-1895.

Fay, R.R., W.A. Yost, and S. Coombs (1983). "Psychophysics and neurophysiology of repetition noise processing in a vertebrate auditory system," Hear. Res. 12, 31-55.

Flock, A. (1971). "Sensory transduction in hair cells," in *Handbook of Sensory Physiology, Vol. I*, edited by W.R. Lowenstein (Springer-Verlag, Berlin), pp. 396-441.

Gee, J.H., K. Machniak, and S.M. Chalanchuk (1974). "Adjustment of buoyancy and excess internal pressure of swimbladder gases in some North American freshwater fishes," J. Fish. Res. Board Can. 31, 1139-1141.

Hawkins, A.D. (1981). "The hearing abilities of fish," in *Hearing and Sound Communication in Fishes*, edited by W.N. Tavloga, A.N. Popper, and R.R. Fay (Springer-Verlag, New York), pp. 109-133.

Hawkins, A.D. and O. Sand (1977). "Directional hearing in the median vertical plane by the cod," J. Comp. Physiol. 122, 1-8.

Jacobs, D.W. and W.N. Tavolga (1967). "Acoustic intensity limens for the goldfish," Anim. Behav. 15, 324-335.

Jones, F.R.H. and N.B. Marshall (1953). "The structure and functions of the teleostean swimbladder," Biol. Rev. 28, 16-83.

Kamil, A.C. (1988). "Behavioral ecology and sensory biology," in *Sensory Biology of Aquatic Animals*, edited by J. Atema, R.R. Fay, A.N. Popper, and W.N. Tavolga (Springer-Verlag, New York), pp. 189-201.

Lebedeva, L.P. (1965). "Measurement of the dynamic complex shear modulus of animal tissue," Sov. Phys. Acoust. 11, 163-165.

Lewis, T.N. and P.H. Rogers (1992). "Detection of scattered ambient noise by fish," J. Acoust. Soc. Am. 91, 7PP1.

Lewis, T.N. and P.H. Rogers (1994). "Directional hearing in the goldfish (*Carassius auratus*)," J. Acoust. Soc. Am. 95.

Lewis, T.N., P.H. Rogers, D.B. Rogers, and S.N. Flanagan (1991). "Frequency response of the swimbladders of fish," J. Acoust. Soc. Am. 89, 7AB6.

Lewis, T.N., P.H. Rogers, and W.X. Zhou (1992). "Scattered ambient noise as an auditory stimulus for fish," *Proceedings of the 14th International Congress on Acoustics*, edited by Peizi Li (S. Hirzel Verlag, Stuttgart), Vol. 4, I4-1.

Love, R.H. (1978). "Resonant acoustic scattering by swimbladder-bearing fish," J. Acoust. Soc. Am. 64, 571-580.

Lovik, A. and J.M. Hoven (1979). "An experimental investigation of the swimbladder resonance in fishes," J. Acoust. Soc. Am. 66, 850-854.

Lowenstein, O. (1971). "The labyrinth," in *Fish Physiology, Vol. 5: Sensory Organs*, edited by W.S. Hoar and D.S. Randell (Academic Press, New York), pp. 207-240.

McCartney, B.S. and A.R. Stubbs (1971). "Measurements of the acoustic target strengths of fish in dorsal aspect, including swimbladder resonance," J. Sound Vib. 15, 397-420.

Minnaert, M. (1933). "On musical air-bubbles and the sound of running water," Phil. Mag. 26, 235-248.

Moulton, J.M. and R.H. Dixon (1967). "Directional hearing in fishes,"in *Marine Bio-Acoustics, Volume 2*, edited by W.N. Tavolga (Pergamon, Oxford), pp. 187-232.

Myrberg, A.A., Jr. and R.J. Riggio (1985). "Acoustically mediated individual recognition by a coral reef fish (*Pomacentrus partitus*)," Anim. Behav. 33, 411-416.

Offutt, G.C. (1971). "Response of the tautog (*Tautoga onitis*, Teleost) to acoustic stimuli measured by classical conditioning the heart rate," Conditional Reflex 6, 205-214.

Otis, L.S., J.A. Cerf, and G.J. Thomas (1957). "Conditioned inhibition of respiration and heart rate in the goldfish," Science 126, 263-264.

Parvulescu, A. (1967). "The acoustics of small tanks," in *Marine Bio-Acoustics, Volume 2*, edited by W.N. Tavolga (Pergamon, Oxford), pp. 7-13.

Pierce, A.D. (1981). *Acoustics: An Introduction to Its Physical Principles and Applications*, (McGraw-Hill, New York).

Platt, C. (1977). "Hair cell distribution and orientation in goldfish otolith organs," J. Comp. Neur. 172, 283-298.

Platt, C. (1983). "The peripheral vestibular system in fishes," in *Fish Neurobiology, Vol. 1: Brainstem and Sense Organs*, edited by R.G. Northcutt and R.E. Davis (Univ. Mich. Press, Ann Arbor, MI), pp. 89-124.

Platt, C. and A.N. Popper (1981). "Fine structure and function of the ear," in *Hearing and Sound Communication in Fishes*, edited by W.N. Tavloga, A.N. Popper, and R.R. Fay (Springer-Verlag, New York), pp. 3-38.

Platt, C., A.N. Popper, and R.R. Fay (1989). "The ear as a part of the octavolateralis system," in *The Mechanosensory Lateral Line*, edited by S. Coombs, P. Gorner, and H. Munz (Springer-Verlag, New York), pp. 633-651.

Poggendorf, D. (1952). "The absolute threshold of hearing of the bullhead (*Amiurus nebulosus*) and contributions to the physics of the Weberian apparatus of the ostariophysi," Zeitschr. Vergleich. Physiol. 34, 222-257.

Popper, A.N. (1971a). "The effect of size on auditory capacities of the goldfish," J. Aud. Res. 11, 239-247.

Popper, A.N. (1971b). "The morphology of the Weberian ossicles of two species of the genus *Astyanax* (Ostariophysi: Characidas)," J. Morph. 133, 179-188.

Popper, A.N. (1974). "The response of the swim bladder of the goldfish (*Carassius auratus*) to acoustic stimuli," J. Exp. Biol. 60, 295-304.

Popper, A.N. (1977). "A scanning electron microscopic study of the sacculus and lagena in the ears of fifteen species of teleost fishes," J. Morphol. 153, 397-418.

Popper, A.N. (1983). "Organization of the inner ear and auditory processing," in *Fish Neurobiology, Vol. 1: Brainstem Sense Organs*, edited by R.G. Northcutt and R.E. Davis (Univ. Mich. Press, Ann Arbor, MI), pp. 125-178.

Popper, A.N. and S. Coombs (1980). "Auditory mechanisms in teleost fishes," Amer. Sci. 68, 429-440.

Popper, A.N. and S. Coombs (1982). "The morphology and evolution of the ear in actinopterygian fishes," Am. Zool. 22, 311-328.

Popper, A.N. and R.R. Fay (1984). "Sound detection and processing by teleost fish: a selective review," in *Comparative Physiology of Sensory Systems*, edited by L. Bolis, R.D. Keynes, and S.H.P. Maddrell (Cambridge Univ. Press, Cambridge), pp. 67-101.

Popper, A.N., C. Platt, and W.M. Saidel (1982). "Acoustic functions in the fish ear," Trends in Neurosci. 5, 276-280.

Popper, A.N., P.H. Rogers, W.M. Saidel, and M. Cox (1988). "Role of the fish ear in sound processing," in *Sensory Biology of Aquatic Animals*, edited by J. Atema, R.R. Fay, A.N. Popper, and W.N. Tavloga (Springer-Verlag, New York), pp. 687-710.

Roberts, M.G., D.E. Wright, and G.E. Savage (1973). "A technique for obtaining the electrocardiogram of fish," Comp. Biochem. Physiol. 44A, 665-668.

Rogers, P.H. (1986). "What are fish listening to? - a possible answer," J. Acoust. Soc. Am. Suppl. 1 79, S22.

Rogers, P.H. and M. Cox (1987). "Biomechanics of the acoustico-lateralis system in fish," Research Proposal to the Office of Naval Research, College of Engineering, Georgia Institute of Technology, Atlanta, GA.

Rogers, P.H. and M. Cox (1988). "Underwater sound as a biological stimulus," in *Sensory Biology of Aquatic Animals*, edited by J. Atema, R.R. Fay, A.N. Popper, and W.N. Tavolga (Springer-Verlag, New York), pp 131-149.

Rogers, P.H., T.N. Lewis, M.J. Willis, and S. Abrahamson (1989). "Scattered ambient noise as an auditory stimulus for fish," J. Acoust. Soc. Am. Suppl. 1 85, N9.

Rogers, P.H., A.N. Popper, M.C. Hastings, and W.M. Saidel (1988). "Processing of acoustic signals in the auditory system of bony fish," J. Acoust. Soc. Am. 83, 338-349.

Saidel, W.N. and A.N. Popper (1983). "Spatial organization in the saccule and lagena of a teleost: Hair cell patterns and innervation," J. Morphol. 177, 301-317.

Sand, O. (1974). "Directional sensitivity of microphonic potentials from the perch ear," J. Exp. Biol. 60, 881-899.

Sand, O. and P.S. Enger (1973). "Evidence for an auditory function of the swimbladder in the cod," J. Exp. Biol. 59, 405-414.

Sand, O. and A.D. Hawkins (1973). "Acoustic properties of the cod swim bladder," J. Exp. Biol. 58, 797-820.

Sand, O. and H.E. Karlsen (1986). "Detection of infrasound by the Atlantic cod," J. Exp. Biol. 125, 197-204.

Schellart, N.A.M. and A.N. Popper (1992). "Functional aspects of the evolution of the auditory system of actinopterygian fish," in *Comparative Evoutionary Biology of Hearing*, edited by D.B. Webster, R.R. Fay, and A.N. Popper (Springer-Verlag, New York), pp. 295-322.

Schuijf, A. and R.J.A. Buwalda (1980). "Underwater localization - a major problem in fish acoustics," in *Comparative Studies of Hearing in Vertebrates*, edited by A.N. Popper and R.R. Fay (Springer-Verlag, New York), pp. 43-77.

Schuijf, A. and A.D. Hawkins (1983). "Acoustic distance discrimination by the cod," Nature 302, 143-144.

Shima, A. (1971). "The natural frequencies of two spherical bubbles oscillating in water," J. Basic Engng., Trans. ASME 93, 426-432.

Strasberg, M. (1953). "The pulsation frequency of nonspherical gas bubbles in liquids," J. Acoust. Soc. Am. 25, 536-537.

Tavolga, W.N. (1964). "Sonic characteristics and mechanisms in marine fishes," in *Marine Bio-Acoustics*, edited by W.N. Tavolga (Pergamon, Oxford), pp. 195-211.

Tavolga, W.N. (1967). "Masked auditory thresholds in teleost fishes," in *Marine Bio-Acoustics, Volume 2*, edited by W.N. Tavolga (Pergamon, Oxford), pp. 233-245.

Tavolga, W.N. (1974). "Signal/noise ratio and the critical band in fishes," J. Acoust. Soc. Am. 55, 1323-1333.

Urick, R.J. (1967). *Principles of Underwater Sound for Engineers* (McGraw-Hill, New York).

van Bergeijk, W.A. (1967). "The evolution of vertebrate hearing," in *Contributions to Sensory Physiology*, edited by W.D. Neff (Academic Press, New York), pp. 1-49.

von Frisch, K. (1938). "The sense of hearing in fish," Nature 141, 8-11.

Weston, D.E. (1967). "Sound propagation in the presence of bladder fish," in *Underwater Acoustics, Vol. 2*, edited by V.M. Albers (Plenum, New York), pp. 55-88.

White, F.M. (1986). *Fluid Mechanics, Second Edition* (McGraw-Hill, New York).

Yan, H.Y. and A.N. Popper (1991). "An automated positive reward method for measuring acoustic sensitivity in fish," Behav. Res. Meth. Instru. & Compu. 23, 351-356.

Yan, H.Y. and A.N. Popper (1992). "Auditory sensitivity of the cichlid fish *Astronotus ocellatus* (Cuvier)," J. Comp. Physiol. A 171, 105-109.

Zabolotskaya, E.A. (1984). "Interaction of gas bubbles in a sound field," Sov. Phys. Acoust. 30, 365-368.

Zhou, W.X. (1992). "Twin-peak resonance of swimbladder in fish," Master's thesis, George W. Woodruff School of Mechanical Engineering, Georgia Institute of Technology, Atlanta, Georgia.